ADVANCES IN UV-WRITTEN FIBRE BRAGG GRATINGS

LORNA ANNE EVERALL

Doctor of Philosophy

ASTON UNIVERSITY

December 1998

ASTON UNIVERSITY

ADVANCES IN UV-WRITTEN FIBRE BRAGG GRATINGS

LORNA ANNE EVERALL

Doctor of Philosophy

December 1998

ABSTRACT

This thesis presents details on the advances made in the fabrication and application of UV-written in-fibre gratings. The basic concepts behind wave propagation in an optical fibre are introduced and the mechanisms responsible for the ability to write gratings in optical fibre are discussed. A number of techniques for the fabrication of in-fibre gratings are presented, including the phase mask method, which has been utilised for the majority of devices presented here.

The experimental work begins with fundamental work on the characterisation of in-fibre gratings, examining some of the parameters and techniques used in the assessment of the device quality. This includes measurement of the UV-induced refractive index change in both hydrogen-loaded and un-loaded fibres. Also presented is a detailed study on the optimisation of in-fibre Bragg gratings using the technique of apodisation, where the induced refractive index is profiled to improve the spectral characteristics of the grating. The study was conducted for gratings placed under length constraints, since many applications require packaged devices or ultra-short 'point' gratings.

The main body of experimental work is concerned with the fabrication and application of gratings written in optical fibre. A number of different types of bandpass filter have been fabricated, using both uniform and pre-chirped phase masks, and have been tested in different sensing and WDM systems. These novel fabrication techniques have made it possible to produce Moiré, phase shifted and concatenated devices in a simple, yet flexible manner.

Other devices investigated include chirped gratings for use as dispersion compensators in high-bit-rate communication systems. Results from a standard fibre transmission experiment, incorporating such a grating as a dispersion compensating element, are presented.

The final section of work details the fabrication of long period gratings, using a technique that requires no phase or amplitude mask. These devices have found use as wavelength-to-amplitude converters in strain and temperature interrogation systems.

KEY WORDS

Optical Fibre, Bragg grating, Long period grating, Chirped grating, Bandpass filters

To my family and friends, especially Darren and Andy.

You believed in me, even when I doubted myself.

ACKNOWLEDGEMENTS

I would like to acknowledge some of the many people who have, in their own individual ways, contributed to this thesis.

Firstly, I would like to thank my supervisor, Ian Bennion, for the much needed support, encouragement and sheer entertainment that he provided during my three years at Aston. Acknowledgement also goes to NORTEL for the CASE studentship they provided and in particular to my external supervisors, Kevin Byron and Howard Rourke, for their interest and ideas. I must acknowledge all those in the Electronic Engineering department at Glasgow University, especially Xuefeng Liu, who provided most of the phase masks used in this work. Thanks to all the members of the Photonics Research Group -both past and present- who have all helped me at one time or another. Special thanks go to John Williams, Lin Zhang and Kate Sugden, who managed to carefully guide me through three years of experimental mayhem; especially John who proved himself to be a sage on all things electronic, photonic and aerobic. Also to Bert Biggs who provided endless technical support.

During the past three years I have been lucky enough to collaborate with many excellent researchers. These include the partners in the ACTS PHOTOS project, who accepted my devices for packaging and testing. A special mention goes to Alessandro Iocco from EPFL, who designed and tested the tunable filter prototype detailed Section 3.5.4. Also to Francesco Pozzi (from SIRTI) and Frank Bruyere (from Alcatel) who respectively packaged and tested the multiwavelength filter, for the WDM work in Section 5.4.3. The apodisation work was carried out with the help and humour of Karen Chisholm; and Richard Fallon provided the strain sensing results on the long period grating (in addition to providing the warped sense of humour and unforgettable laugh). Thanks to you both. Section 4.5 details the use of a Bragg grating as a chromatic dispersion compensating element. These results are provided courtesy of Paul Harper and others working in the 'main' laboratory at Aston.

Finally, I would like to acknowledge those of you who have had the misfortune to make my acquaintance over the past three years. Without the smiles you gave me, this would not have been possible. Thank you.

CONTENTS

LIST OF FIGURES

1. IN-FIBRE GRATINGS

1.1 Introduction to Fibre Gratings

In today's society, fibre optics is universally accepted, having been integrated into everyday applications without people appreciating the impact they have on their lives. One of the simplest applications is in the direct transmission of images and illumination to places which have a limited physical space. A seemingly endless number of applications, including dentists' drills, endoscopes, and high power industrial lasers used for cutting and drilling, all utilise fibre optics. Optical fibre is also helping cope with the high demands which are being placed on global communication systems whilst the world experiences an 'information explosion'; high-speed fibre optic communication networks are vital for the successful introduction of services such as Internet access and audio and video transmission.

As customer expectations increase, more pressure is placed on the systems and their components to be faster and better than their predecessors. The many recent advances in fibre optics, particularly in fibre gratings as we know them today, have been born from these expectations. The key advantage of fibre gratings over other competing technologies is that they can be directly integrated into fibre-optic systems, acting as replacements for bulk optical devices. In addition to this, fibre gratings have low insertion loss, high extinction and potentially low cost. The as-yet fully unleashed potential which gratings have has excited a great deal of interest from research groups and industrial laboratories throughout the world in recent years. Research in the fibre grating field has developed sufficiently to allow its transfer into commercial systems. Many companies are now looking at gratings for use in routing, filtering and in high-capacity telecommunications networks, and also as optical sensing transducer elements in a multitude of optical sensing systems.

The aim of this chapter is to provide a general introduction to fibre gratings and to place the research presented in this thesis in relation to that being carried out in the rest of the world. Section 1.2 provides a historical overview of the research field, highlighting some of the fundamental technological advances which have provided the foundations for the work contained within this thesis. Section 1.3 provides an overview of the novel work described in this thesis, offering an insight into the topics that will be presented in subsequent chapters.

1.2 Historical Overview

The principle on which the transmission of light in an optical fibre depends, that of total internal reflection, has been known since the nineteenth century. Despite this, the field of fibre optics did not really expand until the 1950's when a cladding layer was incorporated into previously unclad glass fibre designs. This revolutionised the field and led to the standard optical fibre in use today. At that point in time optical fibre was still exceedingly lossy, typically ~1000dB/km, which severely limited any practical application. In 1970, the situation changed dramatically when Kapron *et al*, from Corning, managed to reduce this loss to ~20dB/km [1], heralding the dawn of the fibre communication era. By 1979 further advances in the fabrication technology resulted in the loss being reduced to about 0.2 dB/km, in the 1550nm wavelength region [2]. The availability of such low loss fibre allowed the propagation of optical signals over large distances and transformed the fields of optical fibre communication and sensing.

Concurrent with the improvements in the characteristics of optical fibre was the first demonstration of permanent in-fibre gratings, by Hill *et al* [3,4] in 1978, at the Canadian Communications Research Centre, Ottowa. It was reported that intense Argon-ion laser radiation, at a wavelength of 488nm, was coupled into a germania-doped fibre and after several minutes an increase in the intensity of the reflected light was observed. This reflection grew until almost all the light was reflected back from the fibre. By strain and temperature tuning the fibre grating it was concluded that a narrowband Bragg grating had been produced along the 1m length of fibre.

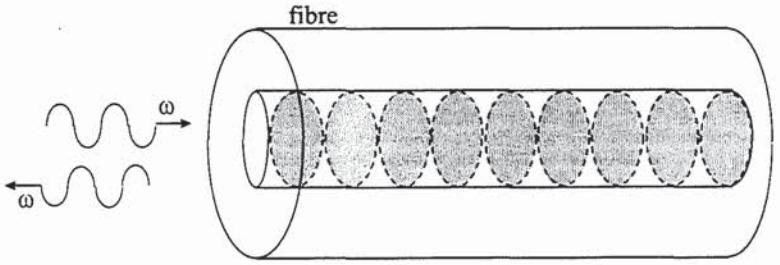

Figure 1.1: A periodic modulation in the refractive index of the fibre induced by a standing wave pattern of light, frequency ω, reflecting back from the end of the fibre

The change in the transmission characteristics of the optical fibre was believed to be initiated by a standing wave interference pattern, set up between the incident light and the small (~4%) far-end reflection (see Figure 1.1). It was presumed that a periodic refractive index change, corresponding to the pattern formed by the standing wave, was induced in the fibre via some mechanism of photosensitivity. The spatial

modulation in refractive index acted as a grating which reflected light at the same wavelength as the writing source. This meant that the applications for such gratings were restricted to those requiring gratings at this single writing-source wavelength. Although this phenomenon generated a great deal of academic attention at the time, serious outside interest into the field of Bragg gratings did not arise until 1989.

It was Meltz and Morey [5] who rekindled this interest by proposing that fibre gratings could be formed by the exposure of two beams of ultra-violet light, through the side of the cladding glass. This work followed on from that done by Lam and Garside [6] who recognised that the underlying effect for the fabrication of in-fibre filters was based on a modification of the core refractive index, which remained even after the laser light was removed. This was found to be more efficient if it was made a one-photon process, by using UV light, at a wavelength of 254nm, rather than the two-photon process which Hill had observed. Meltz and Morey experimentally confirmed this when they demonstrated grating fabrication using two intersecting UV-beams, of wavelength 244nm (Figure 1.2). Using an interferometric arrangement, gratings were formed at a wavelength which was dependent on the period of the interference maxima, set by the angle between the two beams, and the wavelength of the UV radiation, rather than by the visible radiation launched into the core of the fibre. This transverse holographic technique is possible since the fibre cladding is relatively transparent to UV light whereas the core is highly absorbing. This fabrication arrangement proved to be flexible and the grating-formation was found to be significantly more efficient.

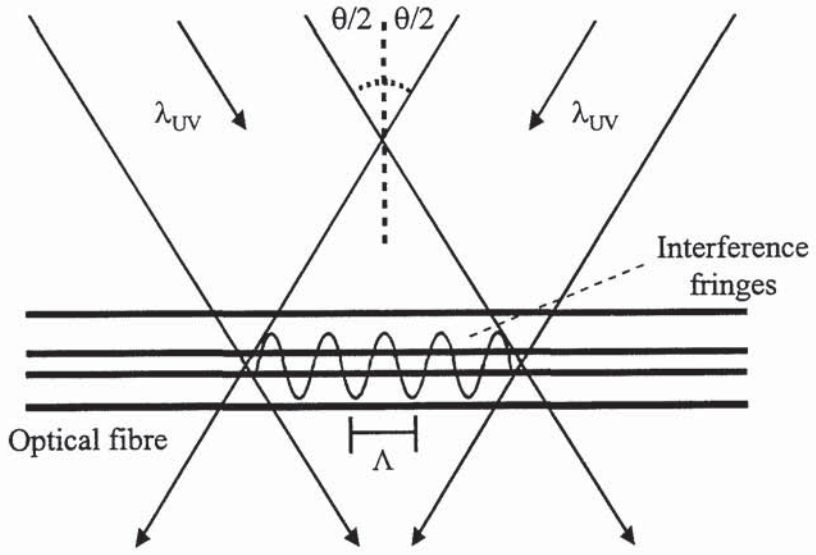

Figure 1.2: The transverse holographic technique, which utilises interfering UV beams to produce a periodic modulation in the refractive index of the fibre core

This holographic fabrication technique was later extended by Kashyap *et al* [7] to allow the fabrication of gratings at wavelengths around 1500nm, which is an important spectral region for devices having application in fibre optic communications and optical sensors.

Historically, these two techniques introduced the most significant advances in grating fabrication, although since that time there have been numerous alternative techniques reported [8,9,10]. The popularity of these techniques diminished with the introduction of the phase mask fabrication technique, by Hill *et al* [11] in 1993. This technique generated a great deal of interest within the Bragg grating community, since it greatly simplified the grating manufacturing process and had the ability to produce high performance devices. It is this technique that has attracted the attention of commercial institutions around the world and has stimulated the establishment of companies fabricating gratings and phase masks.

As illustrated in Figure 1.3, the phase mask is simply a flat plate of silica which is transparent to UV light, and has a periodic surface relief structure etched upon it. UV light which is incident normal to the phase mask is diffracted by the periodic etching of the mask. Generally, most of the light is contained in the 0, +1 and -1 diffracted orders. The phase mask corrugations are designed so that the zero order is suppressed, to typically less than 5%, with approximately 40% of the total light intensity in each of the +1 and -1 orders. The two ± 1 diffracted orders interfere, inducing a periodic refractive index modulation in the optical fibre, which is placed directly behind the fibre. In this case, the wavelength at which the grating is written depends on the periodicity of the phase mask pattern, where the resultant grating has half the period of the phase mask.

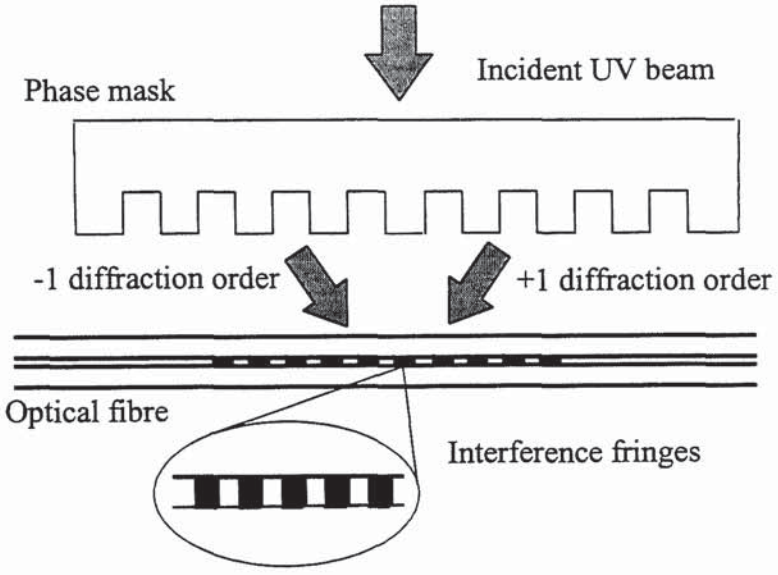

Figure 1.3: In-fibre grating fabrication by the UV exposure of a phase mask

The phase mask technique has many benefits, compared to the holographic technique. It offers easier alignment of the fibre, reduced stability requirements in the set-up and lower coherence requirements on the UV laser, allowing gratings to be written with an excimer laser. By exposing several fibres at the same time, multiple gratings can be written and fabrication reproducibility is guaranteed since it largely depends on the phase mask, which produces a consistent interference pattern. These factors have combined to reduce the unit cost of each grating and make grating-based devices a commercial reality.

The successful acceptance which phase mask fabricated Bragg gratings have received from outside the academic environment has encouraged further research into the fabrication of more novel grating structures for a wider range of applications. This was the impetus for the work contained in this thesis. Using the phase mask fabrication technique as a starting point, it has been possible to write many new and interesting grating structures, including apodised, chirped, phase shifted, Moiré and sampled gratings. Such gratings are nonuniform, either in period or in the amplitude of the induced refractive index change.

One reason for a nonuniform grating design is to reduce the unwanted sidelobes that are apparent in uniform-grating spectra and to tailor the grating reflection profile to approximate the 'top-hat' function which is desired in applications such as dense wavelength-division multiplexing. This process is called 'apodisation'. Chirping the period of the grating produces a nonuniform device which has broadband dispersive properties and is therefore useful as a dispersion compensating element. The addition of a discrete phase shift in an otherwise periodic structure opens up a narrow passband in the reflection profile of the grating, and such a structure finds application in distributed feedback lasers. The superposition of two gratings of slightly different period produces an effective 'beating' effect in the overall induced refractive index modulation. This modulation has a slowly varying envelope that incorporates a rapidly varying component and induces a number of passbands to open up within the grating reflection profile. The resulting devices are categorised as Moiré gratings. Another type of grating is a sampled grating, which has a much larger periodic superstructure, in which the coupling strength or grating period is varied with a period much larger than the nominal value.

The variety of in-fibre Bragg grating devices that can now be fabricated has led to their employment in a wide range of applications, many of them not considered previously. The diversity of the applications is so large that it is not possible to do justice to them all within the scope of this chapter. Instead the intention is to provide an idea of the range of applications in which gratings are used, and to direct the reader to other sources of information for a more detailed explanation.

- **Narrowband Bragg reflectors**, for use as filters in telecommunications, represent one of the most obvious applications for gratings [12] [13]. Since fibre gratings can be fabricated with reflectivities up to ~100% and bandwidths ranging from several nanometers down to picometers, they offer great flexibility in design for narrowband reflectors in fibre and semiconductor lasers.

- **All-fibre lasers** can be constructed using fibre Bragg gratings as wavelength selective resonator mirrors, with doped fibre such as erbium or neodymium, as the gain medium [14] [15] [16] [17]. Such lasers are versatile since the pump semiconductor laser may be directly integrated by splicing the external fibre grating cavity to the all-fibre laser, thus making it a compact and simple system.

- **Chromatic dispersion** in high-bit-rate fibre transmission systems can cause significant signal distortion, leading to system penalties. Compensation of this dispersion can be achieved by passing the signal through a device whose dispersion is equal, but opposite in sign, to that of the transmission fibre [18] [19] [20] [21]. Chirped fibre Bragg gratings can achieve these specifications, offering large, constant dispersion over broad bandwidths.

- Bragg gratings appear to have unlimited potential as **sensing devices** [22] [23] [24] [25], since the Bragg reflection wavelength is sensitive to many environmental parameters, such as strain, temperature, pressure and vibration. Fibre sensors offer a significant number of advantages, over conventional electro-mechanical sensor systems, such as their electrically passive operation, immunity to electro-magnetic interference, high sensitivity and multiplexing capabilities. There has been considerable interest in the use of Bragg grating arrays for quasi-distributed embedded sensing in composite materials, creating so-called 'smart structures'. Here, the grating array is embedded into the material to allow the real-time monitoring of parameters such as strain, temperature and vibration, from which the health of the structure can be assessed. Other sensing configurations, such as grating-based chemical sensors, pressure sensors and accelerometers have been demonstrated.

- Optical fibre communication systems employing **wavelength division multiplexing/demultiplexing** techniques require low-loss, compact, stable components for use as wavelength selective channel dropping or inserting filters. All-fibre components, incorporating Bragg gratings, have proved themselves capable of achieving these requirements at potentially low-cost and a number of configurations, including optical circulators connected to Bragg gratings, have been reported [26] [27] [28]. Other interferometric approaches have been pursued, including a grating-coupled Mach-Zehnder, which have ensured low-loss and reduced complexity.

- The advent of **erbium-doped fibre amplifiers** (EDFA) had a huge effect on the design and manufacture of communication systems. Both Bragg and long-period gratings have found application for gain flattening, residual pump rejection and pumping efficiency improvement, ensuring improved EFDA performance [29] [30] [31].
- Fibre gratings can be written with slight birefringence, using a UV beam that is polarised along the fibre diameter. In this way the two orthogonal polarisations will have slightly different peak wavelengths. This effect has been used to produce **polarisation-mode converters** [32] [33].
- A more recent application which has emerged is that in **microwave photonics**. Interest has been shown in the use of passive optical fibre components for a number of microwave processing functions [34] [35]. The small feature size which gratings can achieve makes them desirable elements for operation at higher modulating frequencies, where electronic wideband processing is difficult.

From the range of applications discussed here, it may fairly be said that research and development in the area of fibre gratings has exploded in recent years. Work on the development of fibre grating technology is being carried out at numerous academic and industrial institutions throughout Europe, America, Australia and Asia. The high level of interest in the area has led to workshops, conferences, topical meetings and special issue publications devoted to the technology. This section has been designed to give a brief introduction to Bragg grating technology and the related applications of gratings. Further information can be found in the selection of excellent review papers that have been published. Bennion *et al* [36] offer a thorough tutorial-review paper on the fundamentals of UV-written in-fibre Bragg gratings. Other general introductory papers include those written by Hill *et al* [37] and Russell *et al* [38]. In Erdogan's review paper, detailed information on the spectral characteristics that can be achieved by gratings is provided [39]. For general information on some of the applications for gratings, Giles [40] and Kersey *et al* [41] have written excellent review papers on lightwave and sensing applications, respectively.

1.3 Thesis Overview

This thesis is concerned with the fabrication and characterisation of various in-fibre devices and investigates a number of potential applications for such novel structures.

The key innovations presented within this thesis include:

- Extensive characterisation work on fundamental grating fabrication principles
- A novel apodisation technique for spectrally shaping Bragg gratings

- New information on the parameter trade-offs for apodised Bragg gratings
- Some of the first work on chirped phase-mask fabricated gratings, including the first report on chirped, phase-mask fabricated multi-passband Moiré gratings
- A novel technique for the fabrication of long-period gratings

It is firstly necessary to provide some background information on the subject of in-fibre gratings, which will allow the fundamental concepts concerning gratings to be introduced. Chapter 2 deals with this, introducing the theory behind wave propagation in an optical fibre and the mechanisms which are responsible for the ability to write gratings in optical fibre. Also detailed in Chapter 2 are some of the various techniques reported for the fabrication of in-fibre gratings, including the phase mask and point-by-point technique, which have both been used in the work contained within this thesis. More emphasis has been placed on detailing the phase mask technique, since the majority of gratings presented in this thesis have been fabricated using this method.

Chapter 3 details a number of techniques and parameters used in the characterisation of in-fibre gratings. This work is of great importance since, once a grating has been fabricated, it is crucial to assess how successful the technique has been in achieving the desired specification. Included in this chapter are experiments on the measurement of the refractive index change induced in the core of an optical fibre when it is exposed to UV-radiation. Methods of characterising the phase mask, as well as the grating, are also detailed. One technique that can greatly improve the spectral characteristics of a grating is that of apodisation, whereby the induced refractive index modulation in the fibre core can be 'shaped' by introducing an additional modulation profile. The spectral characteristics of the resulting grating depend on the particular apodisation profile used. Chapter 3 contains a detailed study on the optimisation of in-fibre Bragg gratings using a variety of apodisation profiles. A comparison of the experimental and theoretical results is presented. This work provides important new information on the trade-offs that exist between grating parameters in order to optimise a device.

Chapters 4 to 6 contain the main body of experimental work on the fabrication of in-fibre devices. Each chapter concentrates on one particular type of in-fibre device, detailing novel experimental fabrication techniques and confirming these results with the aid of theoretical modelling. Throughout this thesis, the fundamental grating fabrication and characterisation work has been greatly enhanced by the possibility of collaborations, both with other members within this research group and also with other research groups world-wide. Although all the devices described have many potential applications, the concluding sections of Chapters 4 to 6 contain collaborative work, assessing the value of each device for one particular application.

Chapter 4 details work on the fabrication of dispersion compensators, for implementation in high-bit-rate communications systems. A number of different fabrication techniques are compared, including some of the first work using chirped phase masks, and the resulting devices are fully characterised. In order to gain an appreciation of the quality of these devices, it was possible to incorporate one in a pulse propagation experiment and the results concerning its implementation are included. As an extension of this, further experimental work on the compensation of higher orders of dispersion was carried out and the first results of gratings specifically designed and fabricated for quadratic dispersion compensation are presented.

Chapter 5 investigates different methods for the fabrication of bandpass filters, for use in sensing and WDM applications. One type of resonator, a Moiré, has been fabricated using both uniform period and chirped phase masks. The novel methods of fabrication made it possible to produce specifically designed multipassband structures, for application in WDM systems. Other resonating structures detailed within this chapter include phase shifted gratings, where a single or multiple phase shift is incorporated into the mask itself, producing a number of interesting grating profiles. In addition to providing an insight into the shaping of transmission filters, this work aids with the understanding of the effect that stitch errors have on phase mask fabricated gratings. As part of a European collaborative project, multipassband filters have been fabricated by the concatenation of apodised gratings, to form a filter for incorporation in a wavelength division multiplexing system. The collaborative enabled this device to be packaged and tested by other groups to examine its success in meeting the WDM system requirements.

The final experimental chapter is concerned with long period gratings, which are made without the need for a mask of any description. The fabrication technique detailed is a particularly simple yet flexible one, which allows gratings of any periodicity to be fabricated. The simplicity and low-cost of the fabrication system make it very attractive to grating manufacturers. A number of these devices have been implemented into a novel interrogation system for strain and temperature sensing and these results are also presented.

Chapter 7 summarises the findings of the work presented in this thesis and considers the future for in-fibre gratings and Chapter 8 contains the appendices. A listing of the 27 publications resulting from this work is given in Chapter 9.

---

1 F.P. Kapron, D.B. Keck, R.D. Maurer, 'Radiation losses in glass optical waveguides', *Appl. Phys. Lett.*,**17**, (10), 1970, pp.423-425

2 T. Miya, Y. Terunuma, T. Hosaka, T. Miyashita, 'Ultimate low-loss single mode fibre at 1.55μm', *Electron. Lett.*, **15**, (4), 1979, pp.106-108

3 K.O. Hill, Y. Fujii, D.C. Johnson, B.S. Kawasaki, 'Photosensitivity in optical fibre waveguides: Application to reflection filter fabrication', *Appl. Phys. Lett.*, **32**, (10), 1978, pp.647-649

4 B.S. Kawasaki, K.O. Hill, D.C. Johnson, Y. Fujii, 'Narrow-band Bragg reflectors in optical fibres', *Opt. Lett.*, **3**, 1978, pp.66-68

5 G. Meltz, W.M. Morey, W.H. Glenn, 'Formation of Bragg gratings in optical fibers by a transverse holographic method', *Opt. Lett.*, **14**, (15), 1989, pp.823-825

6 D.K.W. Lam, B.K. Garside, 'Characterisation of single mode optical fibre filters', *Appl. Opt.*, **20**, (3), 1981, pp.440-445

7 R. Kashyap, J.R. Armitage, R. Wyatt, S.T. Davey, D.L. Williams, 'All-fibre narrowband reflection gratings at 1500nm', *Electron. Lett.*, **26**, (11), 1990, pp.730-732

8 R. Kashyap, J.R. Armtiage, R.J. Campbell, D.L. Williams, G.D. Maxwell, B.J. Ainslie, C.A. Millar, 'Light-sensitive optical fibres and planar waveguides', *BT Technol. J.*, **11**, (2), 1994, pp.150-158

9 Q. Zhang, D.A. Brown, L. Reinhart, T.F. Morse, 'Simple prism-based scheme for fabricating Bragg gratings in optical fibres', *Opt. Lett.*, **19**, (23), 1994, pp.2030-2032

10 H. Patrick, S.L. Gilbert, 'Growth of Bragg gratings produced by continuous-wave ultraviolet light in optical fibre', *Opt. Lett.*, **18**, (18), 1993, pp.1484-1486

11 K.O. Hill, F. Bilodeau, B. Malo, D.C. Johnson, J. Albert, 'Bragg gratings fabricated in monomode photosensitive optical fibre by UV exposure through a phase mask', *Appl. Phys. Lett.*, **62**, (10), 1993, pp.1035-1037

12 D.M. Bird, J.R. Armitage, R. Kashyap, R.M.A. Fatah, K.H. Cameron, 'Narrow line semiconductor laser using fibre grating', *Electron. Lett.*, **27**, (13), 1991, pp.1115-1116

13 K.O.Hill, D.C. Johnson, F. Bilodeau, S. Faucher, 'Narrow-bandwidth optical waveguide transmission filters', *Electron. Lett.*, **23**, (9), 1987, pp.465-466

14 J-L. Archambault, S.G. Grubb, 'Fibre gratings in lasers and amplifiers', *J. Lightwave Technol.*, **15**, (8), 1997, pp.1378-1390

15 M. Hofer, M.H. Ober, R. Hofer, M.E. Fermann, G. Sucha, D. Harter, K. Sugden, I. Bennion, C.A.C. Mendonca, T.H. Chiu, 'High power neodymium soliton fibre laser that uses a chirped fibre grating', *Opt. Lett.*, **20**, (16), 1995, pp.1701-1703

16 G.A. Ball, W.W .Morey, 'Continuously tunable single-mode erbium fibre laser', *Opt. Lett.*, **17**, 1992, pp.420-422

17 S.V. Chernikov, R. Kashyap, P.F. McKee, J.R. Taylor, 'Dual frequency all fibre grating laser source', *Electron Lett.*, **29**, (12), 1993, pp.1089-1091

18 F. Ouellette, J-F. Cliché, S. Gagnon, 'All-Fiber devices for chromatic dispersion compensation based on chirped distributed resonant coupling dispersion compensation', *J. Lightwave Technol.*, **12**, (10), 1994, pp.1728-1737

19 K.O. Hill, F. Bilodeau, B. Malo, T. Kitagawa, S. Theriault, D.C. Johnson, J. Albert, K. Takiguchi, 'Chirped in-fibre Bragg gratings for compensation of optical-fibre dispersion', *Opt. Lett.*, **19**, (17), 1994, pp.1314-1316

20 J.A.R. Williams, I. Bennion, K. Sugden, N.J. Doran, 'Fibre dispersion compensation using a chirped in-fibre Bragg grating', *Electron. Lett.*, **30**, (12), 1994, pp.985-986

21 K. Ennser, M.N. Zervas, R.I. Laming, 'Optimization of linearly chirped grating dispersion compensation systems', *Opt. Fibre Technol.*, **3**, 1997, pp.120-122

22 Y-J. Rao, 'In-fibre Bragg grating sensors', *Meas. Sci. Technol.*, **8**,1997, pp.355-375

23 R.W. Fallon, L. Zhang, A. Gloag, I. Bennion, 'Identical broadband chirped grating interrogation technique for temperature and strain sensing', *Electron. Lett.*, **33**, (8), 1997, pp.705-707

24 A.D. Kersey, 'A review of recent developments in fibre optics sensor technology', *Optic. Fibre Technol.*, **2**, 1996, pp.291-317

25 *12th International Conf. On Optic. Fibre Sensors, (OFC '97) Tech. Digest,* **16**, 1997

26 F. Bakhti, P. Sansonetti, C. Sinet, L. Garsca, L. Martineau, S. Lacroix, X. Daxhelet, F. Gonthier, 'Optical add/drop multiplexer based on UV-written Bragg grating in a fused 100% coupler', *Electron. Lett.*, **33**, (9), 1997, pp.803-804

27 S.S. Orlov, A. Yariv, S. Van Essen, 'Coupled-mode analysis of fibre-optic add-drop filters for dense wavelength division multiplexing', *Opt. Lett.*, **22**, (10), 1997, pp.688-690

28 V. Mizrahi, T. Erdogan, D.J. DiGiovanni, P.J. Lemaire, W.M. MacDonald, S.G. Kosinski, S. Cabot, J.E. Sipe, 'Four channel fibre grating demultiplexer', *Electron. Lett.*, **30**, (10), 1994, pp.780-781

29 A.M. Vengsarkar, J.R. Pedrazzani, J.B. Judkins, P.J. Lemaire, N.S. Bergano, C.R. Davidson, 'Long period fibre grating based gain equalizers', *Opt. Lett.*, **21**, (5), 1996, pp.336-338

30 J.F. Massicott, S.D. Willson, J.R. Armitage, R. Kashyap, D. Williams, R.A. Lobbett, '1480nm pumped erbium doped fibre amplifier with all optical automatic gain control', *Electron. Lett.*, **30**, (12), 1994, pp.962-964

31 M.C. Farries, C.M. Ragdale, D.C.J. Reid, 'Broadband chirped fibre Bragg filters for pump rejection and recycling in erbium doped fibre amplifiers', *Electron. Lett.*, **28**, (5), 1992, pp.487-489

32 K.O. Hill, F. Bilodeau, B. Malo, D.C. Johnson, 'Birefringent photosensitivity in monomode optical fibre: application to external writing of rocking filters', *Electron. Lett.*, **27**, (17), 1991, pp.1548-1550

33 K.O. Hill, B. Malo, K.A. Vineberg, F. Bilodeau, D.C. Johnson, I. Skinner, 'Efficient mode conversion in telecommunication fibre using externally written gratings', *Electron. Lett.*, **26**, (16), 1990, pp.1270-1271

34 J. Marti, J.M. Fuster, R.I. Laming, 'Experimental reduction of chromatic dispersion effects in lightwave microwave/ millimeter-wave transmissions using tapered linearly chirped fibre gratings', *Electron. Lett.*, **33**, (13), 1997, pp.1170-1171

35 W. Zhang, J.A.R. Williams, L.A. Everall, I. Bennion, 'Fibre optic radio frequency notch filter with linear and continuous tuning by using a chirped fibre grating', *Electron. Lett.*, **34**, (18), 1998, pp.1770-1771

36 I. Bennion, J.A.R. Williams, L. Zhang, K. Sugden, N.J. Doran, 'UV-written in-fibre Bragg gratings', *Opt. Quantum Electron.*, **28**, 1996, pp.93-135

37 K.O. Hill, G. Meltz, 'Fiber Bragg grating technology fundamentals and overview', *J. Lightwave Technol.*, **15**, (8), 1997, pp.1263-1276

38 P.St.J. Russell, J-L. Archambault, L. Reekie, 'Fibre Gratings', *Physics World*, 1993, pp.41-46

39 T. Erdogan, 'Fibre grating spectra', *J. Lightwave Technol.*, **15**, (8), 1997, pp.1277-1294

40 C.R.Giles, 'Lightwave applications of fibre Bragg gratings', *J. Lightwave Technol.*, **15**, (8), 1997, pp.1391-1404

41 A.D. Kersey, M.A. Davis, H.J, Patrick, M. LeBlanc, K.P. Koo, C.G. Askins, M.A. Putnam, E.J. Friebele, 'Fibre grating sensors', *J. Lightwave Technol.*, **15**, (8), 1997, pp.1442-1463

2. BACKGROUND

2.1 Chapter Overview

This chapter is designed to introduce some of the issues which need to be addressed when designing and fabricating Bragg gratings. Section 2.2 gives a brief introduction into in-fibre Bragg gratings with details of some of the grating modelling techniques available. Although the processes responsible for the photosensitivity utilised in Bragg grating fabrication are not wholly understood, there are several possible models which are universally acknowledged and these are discussed. Also covered in this chapter are fundamental issues, such as the effect which varying the type of fibre or fabrication technique has on the optimisation of grating design.

All of the work contained within this thesis is concerned with the fabrication and subsequent characterisation of in-fibre gratings. Therefore, in this chapter, a number of the most notable grating fabrication techniques are introduced, along with full details of the techniques utilised in the work contained within this thesis.

2.2 In-Fibre Bragg Gratings

A fibre Bragg grating is a periodic perturbation in the effective refractive index along the length of the fibre core, which is formed by the UV exposure of the fibre core to an interference pattern. In its simplest case the grating can be represented as a uniform sinusoidal modulation in the refractive index in the core of the fibre, *n(z)*, where

$$n(z) = n_{core} + \delta n\left[1 + V\cos\left(\frac{2\pi z}{\Lambda}\right)\right]$$

Equation 2-1

where n_{core} is the refractive index in the core of the fibre prior to exposure, δn is the amplitude of the induced refractive index change, Λ is the period of the modulation and V is the UV fringe visibility.

For a forward propagating wave incident on the Bragg grating, a narrow band of wavelengths is diffracted by successive coherent scattering from the periodic index perturbations. The strongest interaction occurs at the Bragg wavelength, λ_B given by

$$\lambda_B = 2n_{eff}\Lambda$$

Equation 2-2

where λ_B is the Bragg wavelength, n_{eff} is the effective refractive index in the core of the fibre and Λ is the grating period. In the simplest case of contradirectional coupling, the incident wave is coupled to a backward propagating wave and is therefore reflected.

It is possible to evaluate the expected reflection and transmission characteristics which are produced from such uniform periodic structures using coupled mode theory [1,2]. Obviously, with the fabrication techniques currently available, grating fabrication is not limited to the production of uniform structures alone and chirped, tapered and phase-shifted structures can all be easily written. There are several techniques available for the theoretical analysis of the spectra resulting from these non-uniform structures. Hill [3] detailed a method of evaluation based on the iteration of a pair of coupled mode integral equations. Kogenik [4] showed that the coupled mode equations can be reduced to a single second-order Riccati differential equation, where the non-uniformity of the structure is represented by a tapering in the coupling strength (i.e. the depth of corrugation) and by a chirp in the period of the structure. Other methods [5,6,7] replaced the non-uniform grating by a series of short uniform structures which could be characterised by a transfer matrix. Using such a technique, the overall response of the structure can be calculated by numerical matrix multiplication.

2.3 Coupled-Mode Theory

Coupled mode theory is one approach to obtaining an approximate solution for the propagation of electromagnetic radiation in a periodic layered medium. As such, it a useful tool for modelling how a Bragg grating affects wave propagation in an optical fibre [8,9]. The optical properties of a periodic medium can be described by its dielectric tensor, ε. For a periodically varying medium, such as a Bragg grating, coupled-mode theory treats the periodic variation of the dielectric tensor as a perturbation that couples the unperturbed normal modes of the structure. This type of analysis usually assumes that the difference between the refractive index of the core and cladding is very small. Also assumed is that there is no absorption loss and the propagating modes do not couple significantly to the TE and TM radiation modes.

Yariv *et al* [10] drew an analogy between the coupling between unperturbed modes due to the dielectric perturbation and a transition between the eigenstates of an atom under the influence of a time-dependent perturbation. The conditions at which

coupling can take place can be determined by the method of variation of constants. This approach consists of expressing the electric field vector of the electromagnetic wave as an expansion in the normal modes of the unperturbed dielectric structure. Here, the assumption is made that the dielectric perturbation is weak, so that the variation of the mode amplitudes is slow. Such an approach results in a set of coupled linear differential equations for the change in amplitude of the ath mode, A_a given by

$$\frac{d}{dz}A_a = -i\frac{\beta_a}{|\beta_a|}\sum_b\sum_m \kappa_{ab}^{(m)} A_b e^{i\left(\beta_a-\beta_b-m\frac{2\pi}{\Lambda}\right)z}$$

Equation 2-3

where $\kappa_{ab}^{(m)}$ is the coupling coefficient between the ath and bth modes due to the mth Fourier component of the dielectric perturbation. Although, in practise, an infinite number of mode amplitudes are involved, near the resonant condition only two modes are strongly coupled. This resonant coupling condition is also known as the phase matching condition, and is given by

$$\beta_a - \beta_b - m\frac{2\pi}{\Lambda} = 0$$

Equation 2-4

where β_a and β_b are the propagation constants for the two modes being coupled, m is an integer and Λ is the period.

The second condition for significant mode coupling is that the coupling coefficient, $\kappa_{ab}^{(m)}$, must not equal zero. This condition depends on the wave characteristics, such as their polarisation.

Assuming that coupling only takes place between two modes, 1 and 2, then Equation 2-3 becomes

$$\frac{d}{dz}A_1 = -i\frac{\beta_1}{|\beta_1|}\kappa_{12}^{(m)} A_2 e^{i\Delta\beta z}$$

$$\frac{d}{dz}A_2 = -i\frac{\beta_2}{|\beta_2|}\kappa_{21}^{(-m)} A_1 e^{-i\Delta\beta z}$$

Equation 2-5

where these equations describe the coupling between the two modes. The signs of the factors $\frac{\beta_1}{|\beta_1|}$ and $\frac{\beta_2}{|\beta_2|}$ in the coupled equations (Equation 2-5) determine the behaviour

of the coupling, since they depend on the direction of propagation of the coupled modes. The coupling can therefore be either contradirectional or codirectional.

2.3.1 Contradirectional Coupling

When the coupled modes are propagating in opposite directions, for example if $\beta_1 > 0$ and $\beta_2 < 0$, then the signs of the factors $\frac{\beta_1}{|\beta_1|}$ and $\frac{\beta_2}{|\beta_2|}$ become 1 and -1 respectively. The coupled equations of Equation 2-5 then become

$$\frac{dA_1}{dz} = -i\kappa_{12}^{(m)} A_2 e^{i\Delta\beta z}$$

$$\frac{dA_2}{dz} = i\kappa_{12}^{(m)*} A_1 e^{-i\Delta\beta z}$$

Equation 2-6

where A_1 and A_2 are the complex amplitudes of the normalised modes.

Figure 2.1 represents this contradirectional coupling case. For first order diffraction, which usually dominates in a fibre grating, m=1, such that Equation 2-4 becomes $\Delta\beta = \frac{2\pi}{\Lambda}$ [11]. The negative β values, in Figure 2.1, describe modes that propagate in the -z direction. Regions representing bound core modes ($n_{cl} < n_{eff} < n_{co}$) and those representing cladding modes ($1 < n_{eff} < n_{cl}$) are also shown.

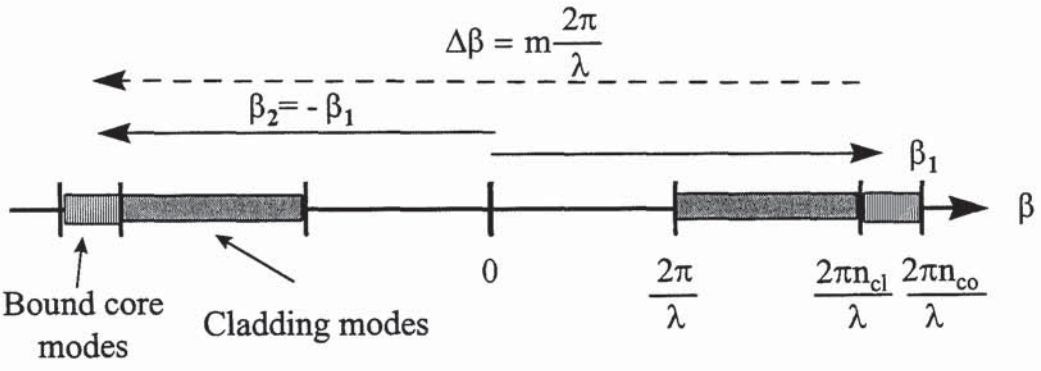

Figure 2.1: Contradirectional coupling in a fibre grating, represented in terms of propagation vectors [12]

Since A_1 and A_2 are the complex amplitudes of the normalised modes then it can be deduced that $|A_1|^2$ and $|A_2|^2$ represent the power carried by modes 1 and 2 respectively. The coupled mode equations, given in Equation 2-6, are consistent with the conservation of energy, which can be expressed as

$$\frac{d}{dz}\left(|A_1|^2 - |A_2|^2\right) = 0$$

Equation 2-7

The solution of Equation 2-6 for the contradirectional case is usually taken to be subject to certain boundary conditions: It is assumed that light is incident at z=0 on the perturbation region, which occurs between z=0 and z=L. The boundary conditions are therefore that the amplitude of the incident wave A_1 at z=0, is $A_1(0)=1$ and that A_2 the amplitude of the reflected wave, at z=L is $A_2(L)=0$. The general solution to Equation 2-6 then becomes

$$A_1(z)e^{i(\Delta\beta/2)z} = A_2(0)\frac{i\kappa_{12}e^{i(\Delta\beta/2)z}}{-(\Delta\beta/2)\sinh(SL) + iS\cosh(SL)}\sinh\left[S(z-L)\right]$$

$$A_2(z)e^{-i(\Delta\beta/2)z} = A_2(0)\frac{e^{-i(\Delta\beta/2)z}}{-(\Delta\beta/2)\sinh(SL) + iS\cosh(SL)}$$

$$\times\left\{\frac{\Delta\beta}{2}\sinh\left[S(z-L)\right] + iS\cosh\left[S(z-L)\right]\right\}$$

Equation 2-8

where $S = \sqrt{\kappa^2 - \left(\Delta\beta/2\right)^2}$, $\kappa \equiv |\kappa_{12}|$ and Λ is the periodicity of the structure.

A complete power exchange for contradirectional coupling only occurs when the phase-matching condition is satisfied, such that $\Delta\beta=0$. The solution of Equation 2-8 is:

$$A_1(z) = A_2(0)\left(\frac{\kappa_{12}}{\kappa}\right)\left(\frac{\sinh\left[\kappa(z-L)\right]}{\cosh\left(\kappa L\right)}\right)$$

$$A_2(z) = A_2(0)\left(\frac{\cosh\left[\kappa(z-L)\right]}{\cosh\left(\kappa L\right)}\right)$$

Equation 2-9

As was stated earlier, Bragg reflection is a typical example of contradirectional coupling, and so coupled mode theory is often used to examine the optical properties from a Bragg grating. Figure 2.2 shows a section of an optical fibre, having a typical periodic modulation in the refractive index, to which this coupled mode theory can be applied. Also shown is a plot of the mode powers $|A_2(z)|^2$ and $|A_1(z)|^2$ for this

contradirectional case, where the phase matching condition is satisfied. For large arguments of the cosh and sinh functions in Equation 2-9, the incident mode power drops off exponentially along the perturbation region. This is due to the reflection of power into the backward travelling mode, A_2.

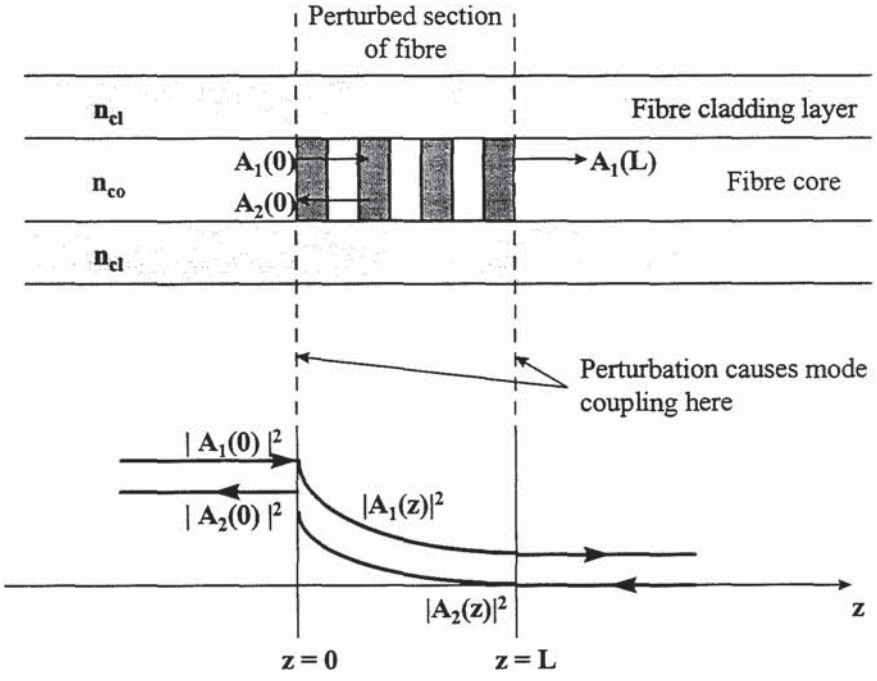

Figure 2.2: (Top) A section of fibre incorporating a Bragg grating (Bottom) The incident and reflected intensities inside the section [10]

The reflectivity of the Bragg reflector is defined as

$$R = \left| \frac{A_2(0)^2}{A_1(0)^2} \right|$$

Equation 2-10

and is given, according to Equation 2-8, by

$$R(L,\lambda) = \frac{\kappa^2 \sinh^2(SL)}{(\Delta\beta/2)^2 \sinh^2(SL) + S^2 \cosh^2(SL)}$$

for $\kappa^2 > (\Delta\beta/2)^2$

$$R(L,\lambda) = \frac{\kappa^2 \sin^2(QL)}{(\Delta\beta/2)^2 - \kappa^2 \cos^2(QL)}$$

for $\kappa^2 < (\Delta\beta/2)^2$

Equation 2-11

where $Q = \sqrt{\left(\Delta\beta/2\right)^2 - \kappa^2}$.

Using these equations it is possible to examine the reflection characteristics of a uniform period Bragg grating. Figure 2.3 plots out the reflectance, R against ΔβL, which is the amount of detuning from the central grating resonance peak, for increasing values of κL. It can be seen that as κL increases, the reflectivity of the grating also increases and the central resonance peak broadens. Thus for strong gratings the bandwidth is largely dependent on the coupling coefficient and these gratings exhibit broader bandwidths.

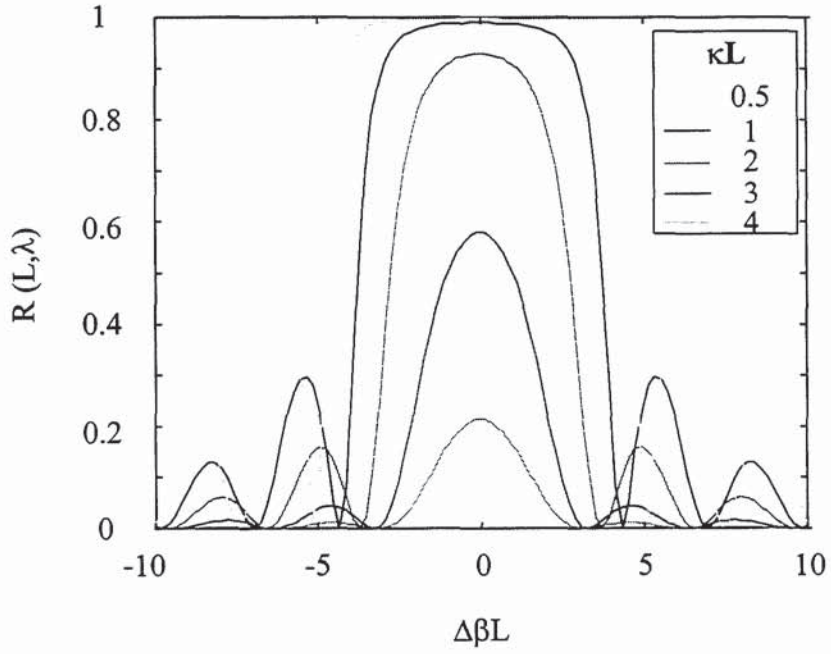

Figure 2.3: A graph showing reflectance, R, against ΔβL for a periodic grating with different values of κL (κL=0.5,1,2,3,4)

The maximum reflectivity occurs when the Bragg condition is met, i.e. $\Delta\beta = 0$, so that $m\lambda = 2n_{eff}\Lambda \equiv \lambda_B$. Equation 2-11 therefore becomes:

$$R_{max} = \tanh^2(\kappa L)$$

Equation 2-12

Figure 2.4 shows the transmission profile of a typical Bragg grating, fabricated in boron-germainum co-doped fibre using the phase mask fabrication technique, which will be detailed later in the chapter. The grating was uniform in period and had a length of 2mm. The resulting spectral profile was measured to have a bandwidth of 0.75nm and a reflectivity of 79%.

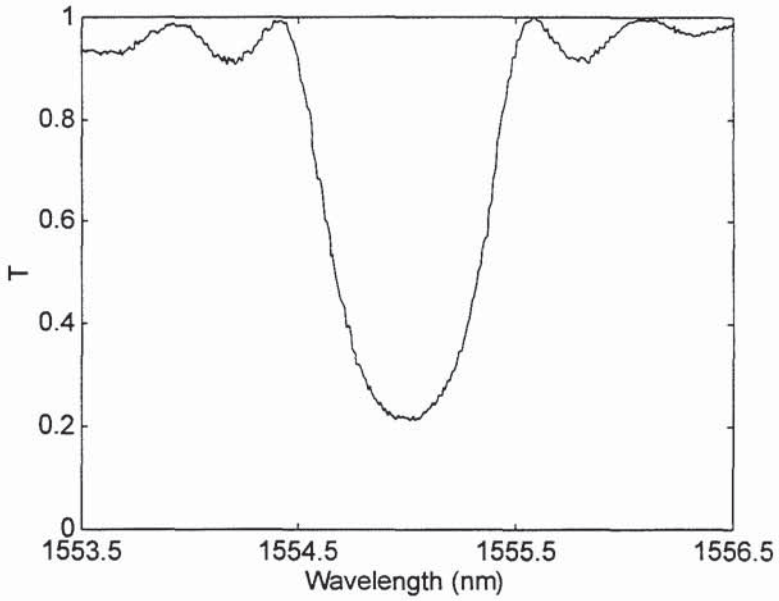

Figure 2.4: Transmission profile of a 2mm long uniform period Bragg grating

2.3.2 Codirectional Coupling

When the coupled modes are propagating in the same direction, +z for example, then the factors $\frac{\beta_1}{|\beta_1|}$ and $\frac{\beta_2}{|\beta_2|}$ of Equation 2-5 both become equal to 1. These coupled equations therefore become

$$\frac{dA_1}{dz} = -i\kappa_{12}^{(m)} A_2 e^{i\Delta\beta z}$$

$$\frac{dA_2}{dz} = -i\kappa_{12}^{(m)*} A_1 e^{-i\Delta\beta z}$$

Equation 2-13

Considering the modes propagating in an optical fibre, then for the case of codirectional coupling, light from the guided fundamental mode is coupled to the forward propagation cladding modes and the diffracted and incident waves both propagate in the same direction, as illustrated in Figure 2.5.

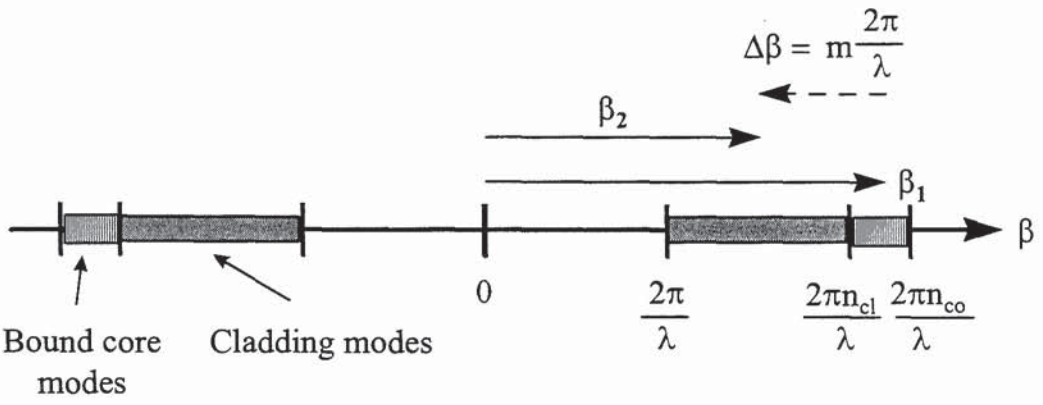

Figure 2.5: Core-to-cladding mode coupling from a fibre grating, represented in terms of propagation constants [12]

The phase matching condition between the guided mode and the forward propagating cladding modes, of order m is given by

$$\Delta\beta = \beta_1 - \beta_2^{(m)} = \frac{2\pi}{\Lambda^{(m)}}$$

Equation 2-14

where $\Lambda^{(m)}$ is the grating periodicity required to couple the fundamental mode to the mth cladding mode. The wavelength at which the coupling takes place therefore depends on the periodicity Λ and the difference in effective refractive indices of the two modes.

The coupled mode equations, given in Equation 2-13, are again consistent with the conservation of energy, $|A_1|^2$ and $|A_2|^2$ represent the power carried by modes 1 and 2 respectively, so that

$$\frac{d}{dz}\left(|A_1|^2 + |A_2|^2\right) = 0$$

Equation 2-15

The general solution of the codirectional coupled mode equations, Equation 2-13, can be obtained by an integration from 0 to z and from this, the spectral dependence of a grating transmission can be derived (see Appendix 8.1 for the full derivation). The ratio of the power coupled into the mth cladding mode to the initial power contained in the guided LP_{01} mode is then given by the expression

$$\left|t_m(\lambda)\right|^2 = 1 - \frac{\sin^2\left[\kappa L\sqrt{1+\frac{(\Delta\beta/2)^2}{\kappa^2}}\right]}{1+\left(\frac{\Delta\beta/2}{\kappa}\right)^2}$$

Equation 2-16

where $\Delta\beta$ is the phase matching condition given by Equation 2-14, κ is the coupling strength of the grating, which is proportional to the UV induced index change, and L is the grating length.

For codirectional coupling at a given wavelength, $\Delta\beta$ is small, as shown in Figure 2.5, which results in a large grating periodicity. This is typically in the order of hundreds of micrometers and, as such, the devices are described as 'long period' gratings. The transmission profile for a typical long period grating is shown in Figure 2.6. The grating, which was written in boron-germanium co-doped fibre, had a periodicity of 500μm and a total length of 1.1cm. This resulted in four clear loss peaks appearing within the wavelength range illuminated by the light source.

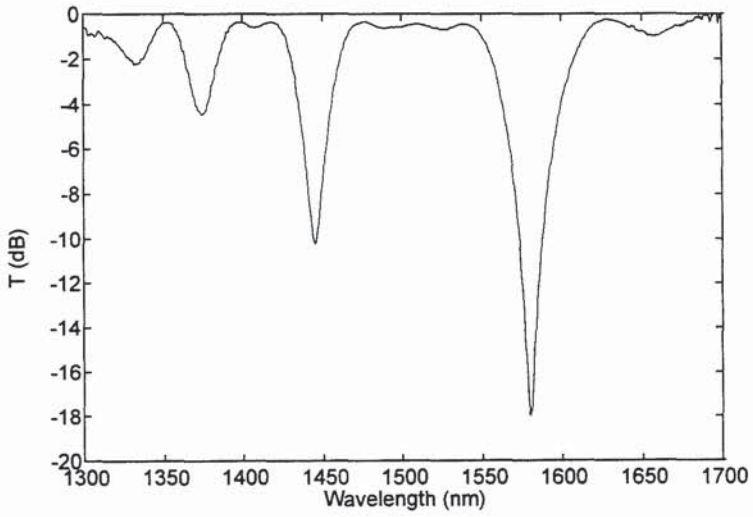

Figure 2.6: The transmission profile of a typical long period grating, written with period 500μm and length 1.1cm

2.4 Photosensitivity

The fabrication of in-fibre Bragg gratings relies on a UV-induced permanent refractive index change. Although Bragg gratings are now widely available, the precise origins of the refractive index change which produces such gratings is still not yet fully

understood and a number of mechanisms have been suggested [13]. A large body of evidence suggests that the mechanism for photo-induced refractive index change arises due to defects associated with oxygen deficiencies in the chemical structure of the fibre, referred to as the colour-centre model [14,15,16]. Other work proposes the thermoelectric stress relaxation of the glass network [17] or structural rearrangement of the glass matrix [18], possibly densification [19]. The stress relief model, proposed by Sceats *et al* [17] suggests that the UV-induced bond breaks allowing the relaxation of stress arising from the expansion coefficient mismatch and the drawing process. From the photoelastic relation [20] an index change is deduced, although Fonjallaz *et al* proved that if this process is operating then it is not dominant [21].

2.4.1 Colour Centre Model

The basis of the mechanism for the colour centre model is the ionisation of a GeO deficiency centre that exhibits an absorption band centred at 240nm. Hand and Russell [22] examined the photoinduced refractive index change in a germanosilicate fibre exposed to a 488-nm Argon Ion laser and related it to a two-photon absorption process. The presence of Ge atoms within a fibre core leads to the formation of oxygen-deficient bonds, such as Si-Ge, Si-Si and Ge-Ge, and these act as defects within the silica. Single-photon absorption of 244nm radiation from an excimer laser, or two-photon absorption of 488nm radiation from an Argon ion laser, provides the energy required to break these bonds. Electrons are released and subsequently trapped at the hole-defect sites to form colour centres - Ge(1) and Ge(2) in the absorption bands 281nm and 213nm respectively. This redistribution of electrons modifies the absorption bands in the visible UV spectrum.

The resulting change in the absorption spectrum produces an associated change in the refractive index of the fibre, which is described by the Kramers-Kronig relation [23]. Since the index change can only occur in regions of the fibre core where the UV light has been absorbed, a periodic UV intensity variation can be transferred into the fibre.

The colour centre model explains photoinduced refractive index changes up to $\sim 10^{-4}$ but experimental refractive index changes greater than 10^{-3} have been achieved [24]. This has led to the continuation of research into the photosensitivity of fibre in order to account for the higher refractive index changes achieved.

2.4.2 Densification

Another mechanism contributing to the photosensitivity of fibre is based on the re-structuring of the molecular structure of the glass matrix, leading to compaction [21,25]. Cordier *et al* [26] presented evidence to support the densification model,

using electron microscopy to examine UV-induced gratings written in a fibre preform. This work identified microstructural changes which were attributed to densification resulting from strain relaxation induced by the creation of the GeE' centres. Using a separate technique, Poumellec *et al* [27] came to the same conclusion. In this case, scanning light interferometry was used to perform 3D imaging analysis of the preform topography. The model used assumed that the UV-induced periodic corrugations resulted from both permanent and elastic strains. Such a model seems to account for both the large refractive index change and also the localisation of the UV- induced birefringence along the grating wavevector. It should be noted that the above results were achieved using fibre preforms, which are then be pulled into optical fibre of more typical dimensions, and the pulling process itself will introduce defects into the glass structure.

2.5 Hydrogenation

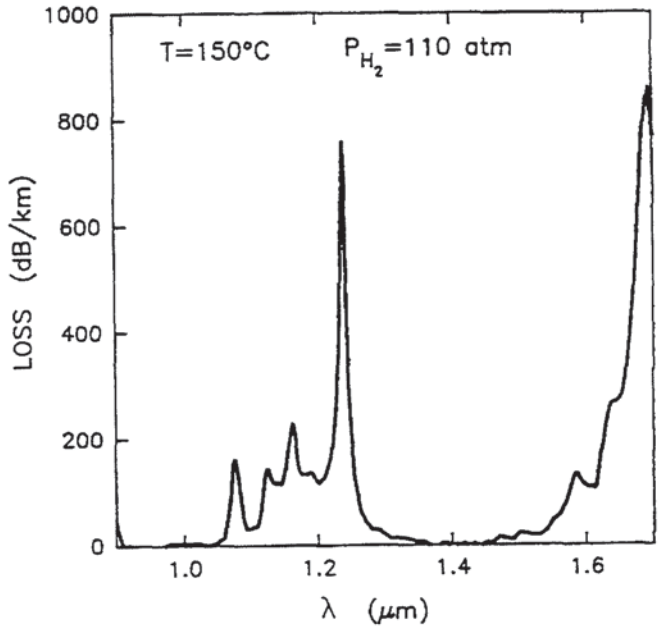

Figure 2.7: Loss increases due to molecular hydrogen dissolved in a single-mode fibre at a pressure of 110 atm and a temperature of 150°C [32]

In order to increase the maximum achievable refractive index change in the fibre there have been several techniques reported [28,29,30]. Lemaire *et al* [31] proposed a method based on the treatment of the fibre by high temperature hydrogen loading, prior to UV-irradiation. It is still unclear why the technique of hydrogen loading increases the photosensitivity of the material, since there is no apparent absorption increase near 240nm due to the loading. On exposing the treated material to UV-radiation, it is postulated that the hydrogen molecules dissociate, forming Si-OH and

Ge-OH groups as well as oxygen deficient centres, thus increasing the refractive index change. Figure 2.7 shows the molecular hydrogen loss increase in a GeO_2 doped fibre which has been exposed to hydrogen at a pressure of 110 atmospheres and a temperature of 150°C.

In order for hydrogen loading to be carried out, fibres are placed into a hydrogenation chamber and for the work contained in this thesis the chamber was a thin tube. Once inside, the fibre is then subjected to hydrogen at a pressure of 120-150 bar, at room temperature, for a time period of up to several weeks, when they are considered to be saturated by the hydrogen [32]. The equilibrium solubility of hydrogen in fused silica fibre is given as ~116ppm (where 1ppm is defined as 10^{-6} moles of H_2 per mole of SiO_2) [33]. Thus for a fibre of diameter 125μm placed in a hydrogen chamber at a temperature of 21°C, the time taken for the hydrogen concentration to reach 95% of this equilibrium solubility value is ~13 days. Typically, the hydrogenation process increases the photosensitivity of the fibre by a factor of two, relative to non-hydrogenated fibre. Standard telecommunications fibre has typically 3mol.% of germanium in the core, giving a refractive index change of $\sim 3\times10^{-5}$ and the hydrogen-loading of such a fibre results in an increase in a refractive index to $\sim 6\times10^{-3}$. In order to obtain a change larger than this, fibre with a higher germanium content is required.

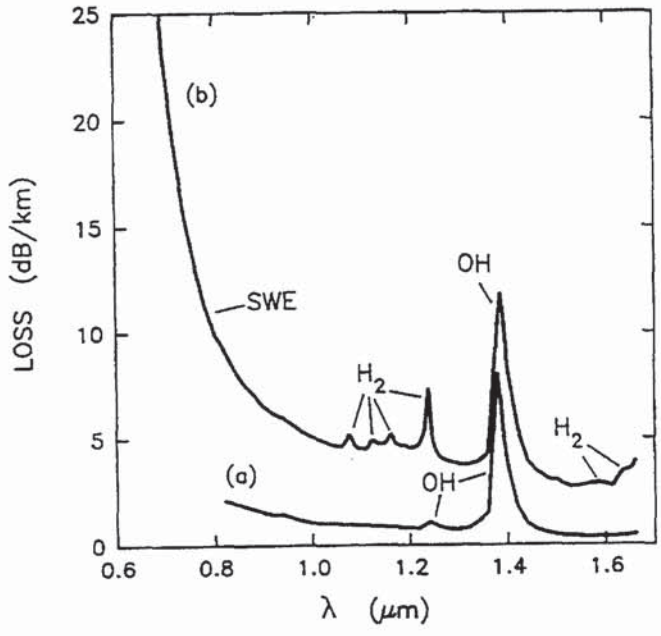

Figure 2.8: Loss spectra for a GeO_2 doped single mode fibre: (a) before hydrogenation; (b) after hydrogenation at 1 atm. and 150°C for 3 days. SWE is the short wavelength absorption edge related to the hydrogen reaction at Ge defects [32]

It can be seen in Figure 2.8 that using the technique of hydrogen loading to increase the photosensitivity of the fibre produces an increase in the OH overtone loss peaks.

The hydroxyl ion, which is bonded to silicon sites, gives rise to an overtone centred at 1.385μm, while OH associated with germanium sites will have an absorption peak centred at 1.4μm, thus limiting the use of such gratings at these wavelengths. To avoid this there have been reports of using deuterium, rather than hydrogen, as the loading gas [34,35].

Unlike 'flame-brushing' [28] where the material is exposed to the flame of an oxygen-hydrogen burner, hydrogen loading is only a temporary measure. Therefore, the induced hydrogen losses will slowly diminish as the gas diffuses out of the fibre once it is removed from the hydrogenation chamber. This means that UV exposure must be carried out on the fibre soon afterwards [36]. The diffusion of hydrogen in optical fibre can be calculated to be ~7.5μm²/hour, from experimental results concerning bulk silica glasses [37] and classical diffusion solutions for cylindrical geometry [38].

The UV-induced refractive index change is permanent and any unreacted hydrogen left will diffuse back out of the fibre. This diffusion process can be speeded up by gently heating the gratings in an oven for a period of several hours.

2.6 Thermal Annealing

As previously discussed, the formation of Bragg gratings in photosensitive fibre involves the creation of UV-induced defects which modify the absorption bands in the UV spectrum, producing an associated change in the refractive index of the fibre.

It has been shown that once the grating has been written in the fibre, there will be some decay of these UV-induced defects, which lead to a decay in the properties of the grating. This decay occurs regardless of whether the fibre has been hydrogen loaded or not, and results in a reduction of the reflectivity and a shift in the Bragg wavelength of the grating. Both of these changes are undesirable since most grating applications require a high degree of stability in the optical properties of the grating over its lifetime, which is generally accepted to be in excess of 25 years.

Erdogan *et al* [39] proposed a model to explain the thermal degradation characteristics of gratings written in germanium doped silica fibre. The initial degradation was found to be rapid, followed by a decreasing rate of change and could be characterised by a power law function in time. Since then many groups have studied the thermal decay of fibre gratings in various types of fibre [40,41,42] and general opinion is that the thermal decay does follow Erdogan's power law fit for unhydrogenated fibres, with each type of fibre having a different function coefficient. There is some disagreement for hydrogenated fibres, with Patrick *et al* [40] reporting that such gratings are less stable than their unhydrogenated counterparts, while Egan *et al* [43] reported results to the contrary.

Chishoke *et al* [44] reported that there are actually two mechanisms responsible for the shift in Bragg wavelength of gratings written in boron germanium co-doped fibre. The first was that detailed by Erdogan, involving the decay of the induced refractive index modulation, which decreases the average refractive index and produces a negative shift in the Bragg wavelength. The second mechanism was connected with the material decay of the fibre itself [45].

All the reports reached the same conclusion, which was that in order to thermally stabilise the grating prior to implementation in a system, then the grating should be annealed in order to remove the UV-induced defects which would rapidly decay, and leave only those which are stable over long time periods. The final Bragg wavelength which the grating settles at is determined by the annealing conditions.

2.7 Fibre Types

Silica-based fibres are widely used in Bragg grating fabrication, due to the large refractive index changes achievable, especially when used in conjunction with the hydrogen-loading technique. A number of different dopants have been used to increase the photosensitivity of optical fibre. Boron co-doped germania fibre [46] is the fibre most commonly used in the research detailed in the following chapters of this thesis. A number of other dopants are available and for completeness these are discussed in this section. Also included in this section are different types of fibre which have been manufactured in order to overcome some of the problems encountered when using standard fibre.

If gratings are to be successfully integrated into a commercial environment they will need to cope with a wide range of environmental conditions and therefore the information included here is of vital importance in order to determine the most suitable type of fibre for each individual application.

2.7.1 Co-doping

Co-doping has enhanced the photosensitivity of fibre, allowing refractive index changes of up to 10^{-2}. As stated previously, boron is one of the most common dopants of germania fibre. Other dopants examined include Ce^{+3} [47], tantalum [48], tin [49], nitrogen [50] and lead. The aim of these dopants is to increase the refractive index in the core of the fibre. Fluorine has been used in the cladding of the fibre to decrease the refractive index of the silica. For high NA fibre, i.e. having a high germania content, the increase in the germania content in the core of the fibre obviously increases the achievable refractive index change but produces a reduced mode spot

size and additional losses when the fibre is spliced onto standard telecommunications fibre.

2.7.2 Polarisation Maintaining Fibre

In single mode fibre, two orthogonally polarised modes can usually propagate equally well down the fibre. In circularly symmetric fibre these two modes have identical propagation velocities. However, most real fibres are not perfectly symmetrical therefore the two modes will inevitably have slightly different velocities.

If light is launched into the two orthogonal polarised modes of a single mode fibre they will change their phase relationship, as is illustrated in Figure 2.9.

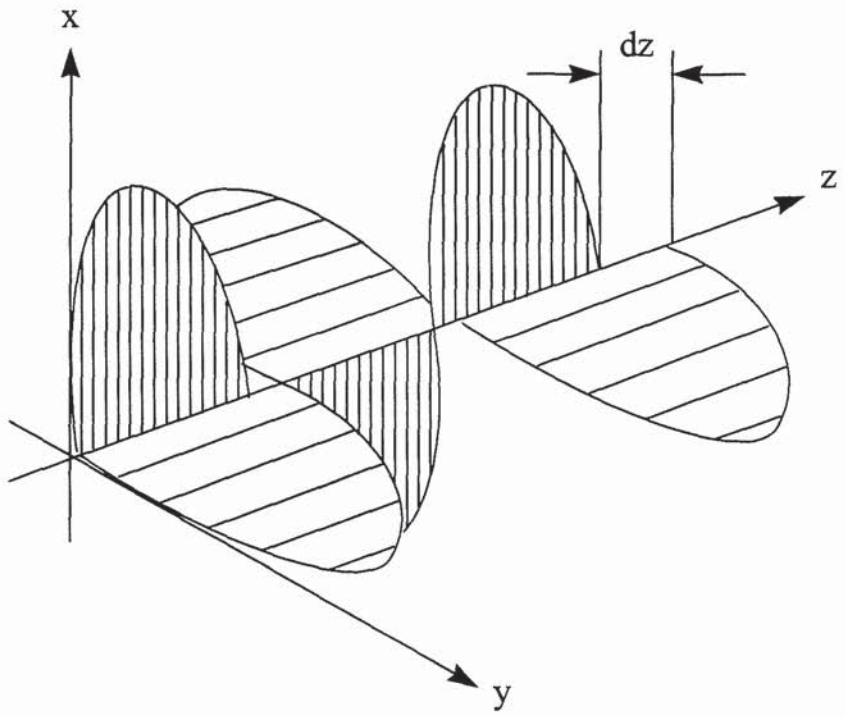

Figure 2.9: Phase shift, caused by fibre birefringence, between the mode polarised in the x-direction (vertically shaded) and that polarised in the y-direction travelling down a single-mode fibre(horizontally shaded) [51]

After a certain length, called the beat length L_p, the phase difference reaches 2π and the original polarisation states are re-established. Typical circular-core single mode fibres have beat lengths in the range 100 mm< L_p < 5 m.

Modes which have similar propagation constants can be coupled together by fibre perturbations which have relatively long periodicities. So if one polarisation state is launched into one end of the fibre, mode coupling will ensure that some of this energy is coupled into the orthogonal mode. However, if the fibre has a large birefringence, the two polarisation modes can only be coupled by short period

perturbations, which are less likely to be present. These fibres are known as 'Hi-Bi' (high birefringence) fibres and can maintain their initial polarisation state over large distances.

Most polarisation maintaining fibres are intrinsically birefringent [52] and there are several manufacturing techniques available [53,54]. All the techniques rely on producing a fibre cross section which is asymmetric about the two axes. In 'form birefringent' fibre, the core is elliptical, with a beat length of about 1m. For 'stress birefringent' fibre the birefringence is induced by incorporating a localised stress region in the fibre.

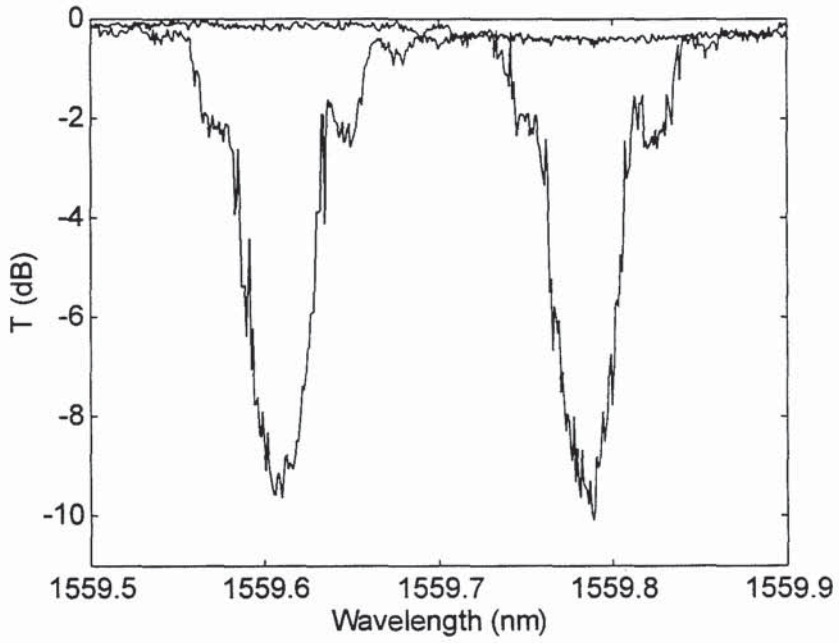

Figure 2.10: A fibre grating fabricated in polarisation maintaining fibre. The grating is displayed in the two orthogonal modes

Figure 2.10 shows a single uniform period grating written in polarisation maintaining hydrogen loaded fibre. A polarisation controller was integrated into the grating characterisation arrangement making it possible to change the polarisation state of the light entering the grating. Using this, the transmission profile of the grating in both its orthogonal states was obtained, as shown in Figure 2.10.

2.7.3 Depressed Cladding Fibre

A feature of a highly reflecting Bragg grating, with a large induced refractive index modulation, is the sharp spectral resonances which can be seen on the short wavelength side of the grating transmission spectra, as illustrated in Figure 2.11.

These resonances, which were first noted in UV-exposed gratings by Archambault *et al* [55], are not present when the grating is viewed in reflection and therefore must be due to light leaving from the side of the fibre. They have been attributed to light being coupled into cladding and radiation modes [56], instead of the guided core mode [57]. Radiation mode coupling is a smooth function of wavelength [58] so the peaks which modulate this coupling are a result of the cylindrical cladding-air interface, where the cladding acts as a cylindrical Fabry-Perot, imposing its resonant structure on the radiation mode spectrum.

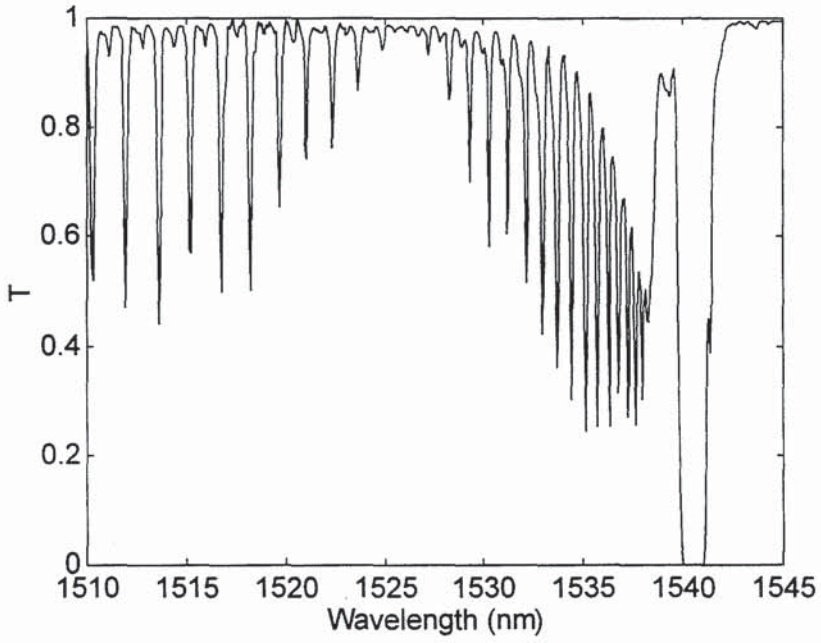

Figure 2.11: The experimental transmission spectrum of a strong Bragg grating exhibiting a large amount of short wavelength loss

This short wavelength loss can be very significant in strong gratings and restricts the use of these gratings in wavelength division multiplexed (WDM) systems. A number of methods have been proposed to counter this effect, including the use of fibre with photosensitive cladding [59] and high NA fibre [60]. The leading method to suppress short wavelength loss seems to be the use of a fibre having a depressed cladding in between the photosensitive core and normal cladding [61,62]. Such a depressed cladding reduces the cladding mode field strength over the core region of the optical fibre and therefore reduces the coupling strength between the guided mode to the cladding modes. Figure 2.12 shows an example of a grating fabricated in depressed cladding fibre, which was supplied by Southampton University, UK.

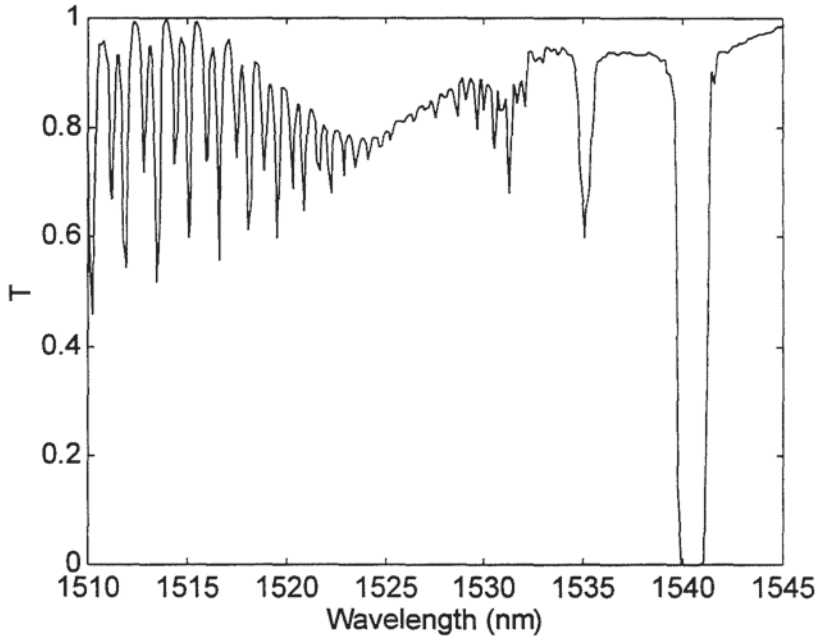

Figure 2.12: The experimental transmission spectrum of a grating made in depressed cladding fibre

An additional, sharp transmission peak occurs in depressed cladding fibre to the left of the main peak. It has been reported [63] that this peak is a result of a small asymmetry in the transverse profile of the grating, arising from either an angular misalignment of the UV fringe pattern in the fibre, or from a radial taper in the UV fluence due to a large colour-centre absorption [64].

2.8 Fabrication Techniques

There are many techniques used to fabricate in-fibre Bragg gratings and the most widely used methods will be detailed in the following section. The majority of the grating fabrication work incorporated in this thesis was performed using the phase mask technique, thus a greater emphasis is placed on the issues surrounding the phase mask fabrication method.

2.8.1 Holographic Fabrication Technique

In 1978, Hill *et al* [65,66] demonstrated, for the first time, the formation of permanent gratings in optical fibre. Intense Argon-ion laser radiation was launched into a germania-doped fibre and it was observed that after several minutes an increase in the reflected light intensity occurred and this grew until almost all the light was reflected from the fibre. Spectral measurements confirmed that a narrowband Bragg grating filter had been formed over the whole of the 1-m length of fibre. These *Hill Gratings* are thought to be produced by a standing-wave pattern set up by

counterpropagating light from a small far-end reflection, causing the fibre to change its transmission characteristics. This results in a periodic refractive index change within the fibre, reflecting light at the same wavelength as that of the writing source. This restriction in the wavelength of the resultant grating severely limits the flexibility of this fabrication technique.

Very little interest was generated in this field of research until 1989, when Meltz *et al* demonstrated a far more flexible method of grating fabrication [67]. The method of inscription used was based on a holographic interferometric technique, where the fibre was illuminated with UV-radiation through the side of the cladding (See Figure 2.13).

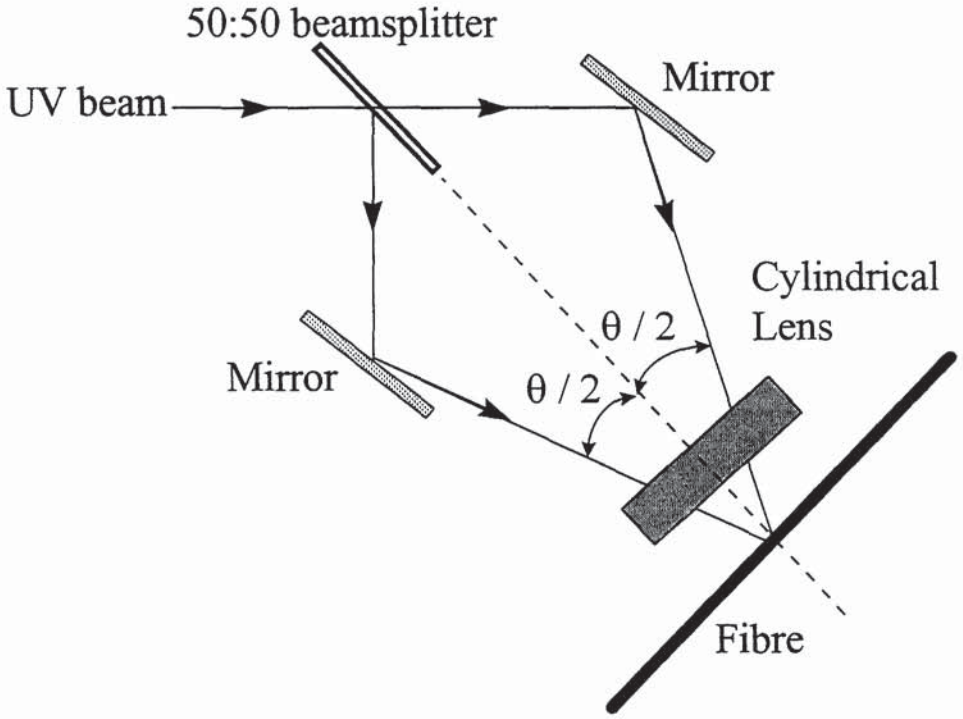

Figure 2.13: Schematic diagram of the two beam holographic interferometric fabrication technique

A beamsplitter produces two UV-beams, which intersect, at some angle θ, directly in front of the fibre. The period of the interference is set by the angle between the interfering beams and also by the wavelength of the UV-radiation, rather than solely by the wavelength of the visible radiation launched into the fibre, as in Hill's initial technique [65]. These relationships can be described by the equation

$$\Lambda = \frac{\lambda_{UV}}{2\sin(\theta/2)}$$

Equation 2-17

where Λ is the period of the resulting grating, λ_{UV} is the irradiation wavelength of the UV beam and $\theta/2$ is half the angle between the interfering beams.

Gratings fabricated in this manner were found to be much more efficient and were not limited by saturation effects [8]. An inherent problem of this dual-beam holographic technique is that it requires the UV-source to have good spatial and temporal coherence to allow for the longer writing lengths and times which are often required.

In 1990, Kashyap *et al* [68] experimentally confirmed that using this method of grating inscription is was possible to write Bragg reflectors at a wavelength of 1500nm. This wavelength region corresponds to that used for the majority of telecommunications work, hence this research vastly expanded the possible applications of Bragg gratings.

There have been various other holographic arrangements reported, as alternatives to the interferometric set-up, including a number of prism based methods, which are far more stable but less flexible than the holographic interferometric technique [69,70,71,72].

A disadvantage of the holographic technique is that the total length of each grating fabricated is limited by the size of the two interfering beams. Also, inherent with this system is the 'self-chirping' of the gratings which occurs due to the beam profile producing a non-uniform exposure over the length of the grating.

2.8.2 Phase Mask Fabrication Technique

Although the holographic technique is particularly flexible, in 1993 Hill *et al* [73] reported on an alternative technique based on the exposure of the fibre through a phase mask, placed in near-contact to the fibre. This has now proved itself to be the preferred method of grating fabrication due to the simplicity and reproducibility of the technique. The phase mask is made from a flat plate of silica which is transparent to UV-light. A one dimensional periodic surface relief structure is etched onto the surface of the plate, using photolithographic techniques. The periodic corrugations diffract UV-light incident on the mask into a number of different orders, as can be seen in Figure 2.14.

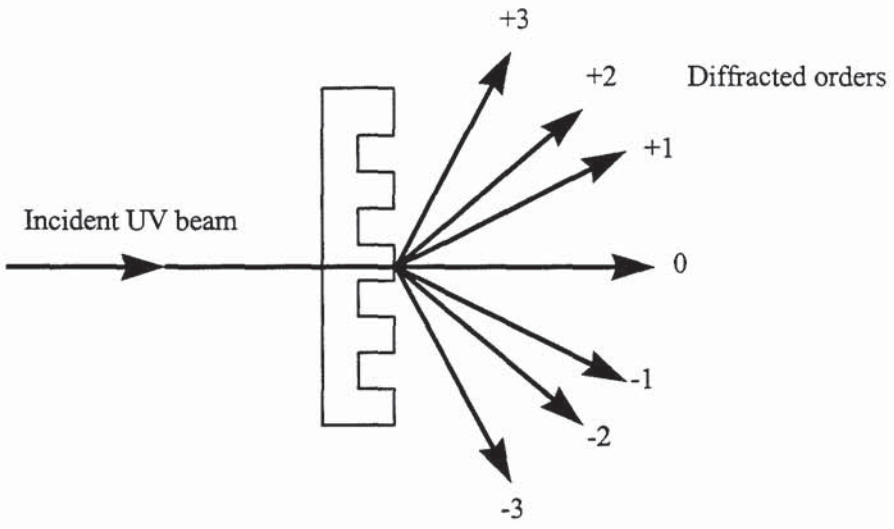

Figure 2.14: Some of the diffraction orders generated when UV light is incident on a phase mask

By controlling the depth of the corrugations, the phase mask can be designed so that most of the light is diffracted into the +1 and -1 orders and the 0 order is suppressed as much as possible. This allows the ± 1 orders to interfere and this interference produces a periodic pattern which is then photoimprinted into the core of the fibre (Figure 2.15).

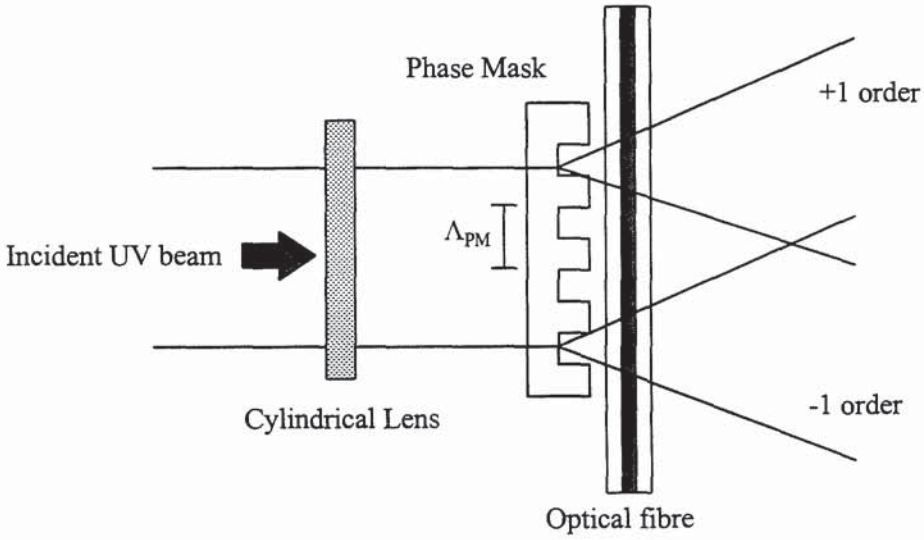

Figure 2.15: Schematic diagram of the phase mask fabrication technique

The gratings are written with a period, $\Lambda = \Lambda_{PM}/2$, where Λ_{PM} is the period of the phase mask. Commercially available phase masks achieve 80% of the total light intensity equally divided between the ± 1 orders and less than 5% of the total light intensity in the zero order.

The phase mask technique offers a number of advantages over the holographic interferometric technique. The fabrication process allows for highly reproducible gratings and the spatial and temporal coherence of the UV-source is less crucial. There is also the possibility of fabricating several gratings at the same time. To write a long grating originally required a large beam magnification. Martin *et al* [74] first reported on the translation of the UV-beam in order to write a 'long' 1.5cm grating. The UV-beam was kept stationary, whilst the phase mask and fibre arrangement were scanned along the length of the phase mask. As long as the phase mask and fibre do not move relative to each other then the fringes created in the core of the fibre are determined by the mask. An alternative method translated the beam across the phase mask and fibre, producing a 5cm-long grating [75]. Using a translation technique means that the length of a grating is determined by the length of phase mask being used. This technique has been extended by the use of a number of 'step-chirped' phase masks to increase the overall length and thus the bandwidth of the grating [76].

Since the wavelength of the grating is defined by the periodicity of the mask then, for each mask, gratings can only be written at one wavelength. This is obviously a disadvantage of the phase mask technique, although there are a number of ways to adjust the Bragg wavelength of the grating. One method reports the use of a magnifying lens, placed before the mask, which allows a wavelength variation of almost 2nm, relative to the unmagnified case [77]. It has also been shown that stretching the fibre prior to exposure enables the Bragg wavelength to be shifted [78,79]. If the fibre is pre-stretched, then the grating is written at the wavelength defined by the phase mask. After exposure, when the fibre is relaxed, the fringe spacing compresses, shifting the grating to a shorter Bragg wavelength. Using this method it has been possible to adjust the wavelength of the grating by up to 10nm, although the maximum shift depends on the fibre type.

A novel variation on the exposure of a phase mask by UV irradiation has been reported by Starodubov *et al* [80] and other research groups [81]. In this case, a Bragg grating is fabricated in optical fibre through its polymer jacket, using near UV light. Dianov *et al* first demonstrated this with the partial erasure of long period gratings, using near UV light, indicating a refractive index change of $\sim 10^{-5}$ in germanosilicate fibre [82]. This technique was then extended to the fabrication of Bragg gratings at a wavelength of around 1550nm [83]. Boron co-doped germanosilicate fibres were shown to be sensitive enough to write gratings with 334nm light. Since the outer polymer jacket is transparent in this spectral region, then the fibre does not require any stripping or re-coating. This has the obvious benefits that the fabrication process is greatly simplified and the fibre suffers less mechanical degradation than for the case where the jacket is removed [84].

2.8.2.1 *Phase Mask Fabrication*

A popular method of phase mask fabrication is to use electron beam lithography (EBL) and dry-etching to fabricate the square-wave gratings in quartz substrates which acts as a phase mask [85,86]. Figure 2.16 shows a schematic diagram of phase mask fabrication using a 'resist' method.

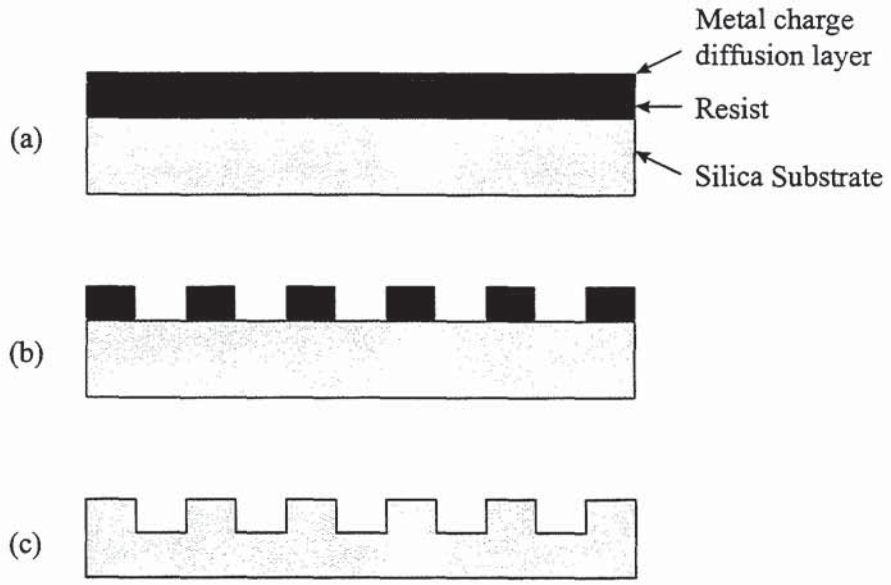

Figure 2.16: Schematic diagram of phase mask production using a simple positive resist method: (a) The unpatterned mask; (b) After e-beam patterning and development; (c) After reactive ion etching (RIE) and resist removal

In simple terms, this involves projecting a pattern onto a substrate coated with a light sensitive material, the resist, in the same way that a negative is printed onto photographic paper. Chemicals can then be used to reveal the pattern on the substrate. This can be either by using a 'positive resist' to dissolve the regions of resist which were exposed to the light (as shown in Figure 2.16), or by using a 'negative resist', where the regions which were not exposed to the light are dissolved. Finally, the pattern is permanently imprinted on the quartz substrate by etching away the areas which are not protected by the resist. Electron beam lithography is a very flexible method of photo imprinting, since it allows multiple patches to be written on the same quartz plate. Other advantages include the possibility of increasing the pitch of the pattern, which will lead to the final device being chirped, or introducing a phase shift into the periodic structure of the pattern which will open up a transmission band within the fibre grating profile. In order to optimise the output power in the diffracted orders, it is necessary to have tight control over the phase mask parameters, such as the ridge duty cycle, groove depth and ridge shape. The ridge

duty cycle is defined as L/Λ, where L is the length of each ridge and Λ is the periodicity of the pattern. These parameters are related to the electron beam dose and resolution, electron beam spot size, resist type and the resist combinations used. The dry-etch (RIE) conditions, such as the gases and pressure used, are equally as important.

One problem associated with phase mask fabricated gratings is that of stitch errors [87]. Present phase mask requirements are for masks on a millimetre or centimetre scale. Since the typical e-beam field writing size is around 500μm then this leads to the inevitable need to stitch together a number of fields to achieve these longer length masks. A small error is introduced at the point where two fields are joined together and the size of this 'stitch error' depends on the precision of the e-beam writing machine. The effect which these stitch errors have on the resulting Bragg gratings is illustrated in Figure 2.17.

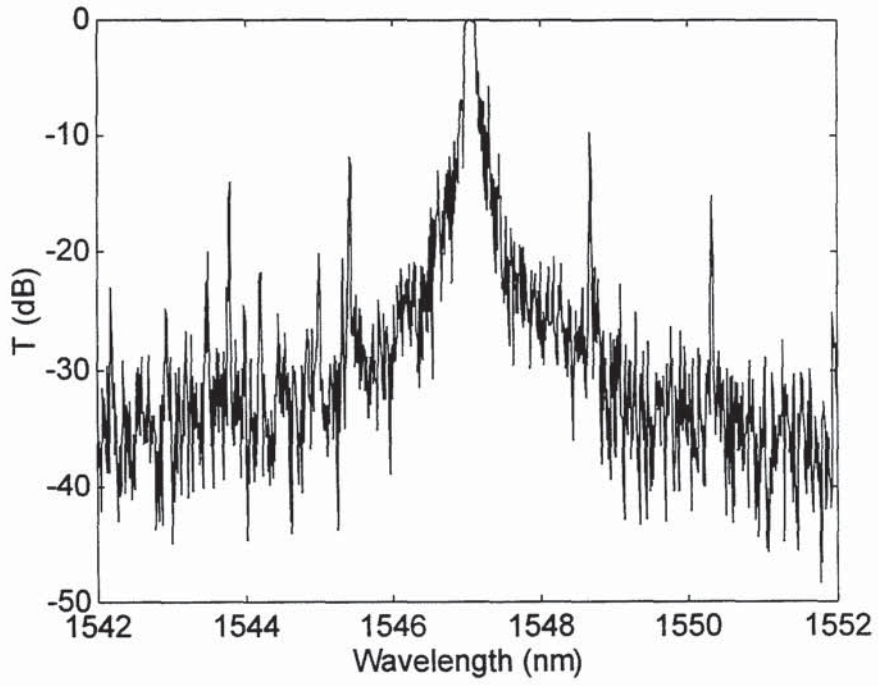

Figure 2.17: Reflection spectrum of a typical Bragg grating, fabricated using a 5cm phase mask containing numerous stitch errors

Here we can see that either side of the main grating reflection peak there are a number of symmetric peaks. These occur at a wavelength spacing which depends on the field size used, i.e. the periodicity of the stitches. Such stitch errors obviously have a degrading effect on the overall grating spectra, either by inducing these additional peaks or by increasing the overall noise level of the grating [88,89].

The majority of phase masks used for the work contained within this thesis were obtained through a collaboration with Glasgow University, who engineered the phase

masks. These could then be characterised at Aston University and feedback given as to their quality. In this manner the phase mask parameters could be optimised to give the best mask performance, ensuring a high standard of Bragg gratings.

The electron beam writing was carried out using a Leica EBPG 5HR Beamwriter, which stitched together 400 × 400μm fields to produce long phase masks. A field size of 400μm was found to be the optimum. A larger field size increases the 'edge distortion' which occurs at the edge of each writing field. A larger field size also produces larger stitch errors at each stitch point, whereas if the field size is made any smaller then a larger number of fields are needed to be joined together to produce the entire mask, which introduces more stitch errors into the resulting pattern.

Figure 2.18 shows a high resolution scanning electron microscope (SEM) picture of a typical stitch error introduced at the point where two writing fields are joined together. As indicated earlier, these stitch errors are a major concern for phase mask fabricated gratings.

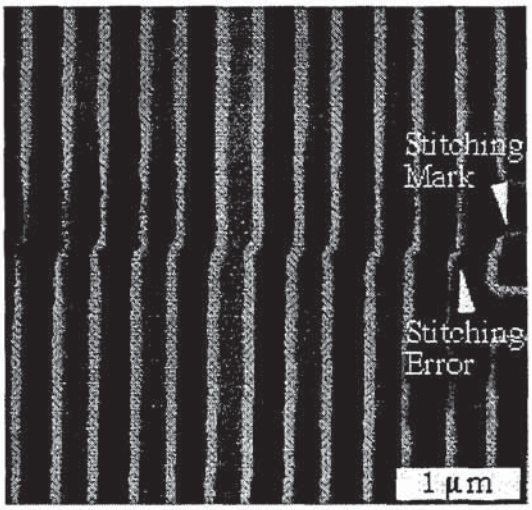

Figure 2.18: Picture produced using a Scanning Electron Microscope, illustrating stitch errors on an e-beam fabricated phase mask

Random stitch errors produced by the Glasgow University e-beam writer were given by the manufacturers as being less than 80nm for a field size of 800 × 800μm. Methods of stitch error reduction include the use of a smaller writing field size, as explained above, and the stabilising of the thermal drift which occurs when a new sample in placed into the machine. The resolution for the electron beam writing process was chosen to be $1/20^{th}$ of the grating period and the spot size was approximately twice the specified resolution. One of the most important parameters in EBL is the e-beam dose. The optimised range was found to be from 200 to 500 $\mu C/cm^2$ for a typical positive resist, such as polymethyl methacrylate (PMMA) and from 10 to 20 $\mu C/cm^2$ for negative resists, such as Shipley AZPN114. All the writing

was carried out using a 50keV electron beam and dry etching was carried out using an Oxford Plasma Technology RIE80 and BP80 machine.

Although a number of distinct processing approaches have been examined [90], the one used most often is a simple resist-mask method. For this, a PMMA e-beam resist layer (or number of layers) was applied on the top of the quartz substrate for both electron beam patterning and dry etch masking, with CHF_3 at a flow rate of 20 sccm. A schematic diagram of this process was illustrated in Figure 2.16. The choice of charge diffusion metal, deposited on top of the resist, is important in the prevention of large edge and groove bottom deformation [91]. A number of resists and metal profiles were tested and it was found that the combination of an Au metal charge diffusion layer and a PMMA resist produced the cleanest phase mask grooves and gave the highest first-order UV-beam diffraction.

The advantages of this process include simplicity, ease of control of the ridge duty cycle and the highly vertical side walls produced, which resulted in rectangular ridge-shaped etchings in the quartz substrate. The quality of a phase mask is assessed on a number of points, including the degree of suppression of the zero-order diffraction component and the optimisation of power in the ± 1 diffraction orders. This is achieved by obtaining a ridge duty-cycle as close to a value 0.5 as possible, having good ridge shape, vertical side walls and the grooves being of depth 240nm. To monitor all of these parameters a trial sample is fabricated and is then examined with a scanning electron microscope. Using this, the total groove depth can be estimated to within 10nm allowing the final writing parameters to be modified to produce the desired mask.

As was stated at the beginning of this section, electron beam lithography is only one method used to fabricate phase masks and recently an interferometric fabrication technique has been applied to the fabrication of commercial masks. This technique uses the interference between two large coherent laser beams to create a periodic pattern on the quartz substrate. The holographic fabrication technique generates phase mask patterns which are free from stitch errors [92] and should therefore produce gratings with lower sidelobes. At present this technique is limited to writing shorter length masks, but as the fabrication technology develops then the holographic fabrication technique has the potential to succeed e-beam lithography as the choice method of phase mask fabrication.

2.8.3 Point-by-Point Technique

A non-interferometric fabrication technique for the production of gratings is the point-by-point approach developed by Hill *et al* [11]. Figure 2.19 shows a schematic diagram of this technique, which involves exposing a small section of fibre to a UV-

beam passing through a narrow slit. The UV-exposure changes the refractive index in the core of the fibre, in the exposed region only. The beam can then be translated a distance, corresponding to the pitch of the grating, and a second section of fibre exposed.

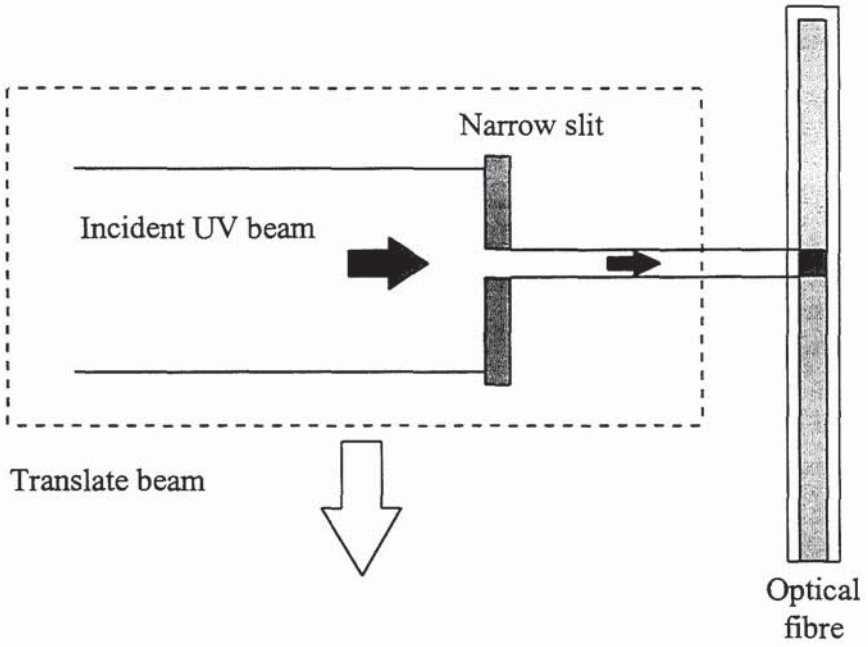

Figure 2.19: Schematic diagram of the point-by-point grating fabrication technique

This technique was first used to fabricate in-fibre mode converter gratings at a wavelength of 360μm [93]. Since these gratings are written in small sections, this technique was not very efficient for writing very long gratings, which required a large number of index perturbations. The technique was then extended to fabricate micro-Bragg gratings at 1500nm [94] having a period of around 1μm. Again, due to the number of points needing to be written, the maximum grating length was less than 0.5mm.

The point-by-point technique is most useful for fabricating long period gratings, with pitches of the order 100μm. Recently there has been a great deal of interest in long period gratings and their many applications [95,96,97]. It is this method of grating inscription which has been used to fabricate long period gratings for the work contained within this thesis and full details of the technique and the resultant gratings can be found in Chapter 6.

2.8.4 Amplitude Mask

Another non-interferometric technique for grating fabrication is that using an amplitude mask [98,99]. The amplitude mask is generally a chrome-on-silica photolithographic mask [100], which has a periodic pattern inscribed onto it. The

periodic refractive index modulation is then produced by the irradiation of this mask, which is placed directly in front of the fibre, in place of the phase mask. Although Bragg gratings of period around 1μm have been written using an amplitude mask [101], this technique is more suitable for gratings written with periods of hundreds of microns, long period gratings. As with phase masks, the periodicity of the subsequent grating is determined by the periodicity of the amplitude mask used in fabrication.

2.9 Grating Types

This section contains details on some of the different types of gratings which have been fabricated. For completeness Type I, Type II and Type IIa are all described in the following section, although it should be noted that the work contained within subsequent chapters of this thesis relates to Type I gratings only.

2.9.1 Type I, Type II, Type IIA

As stated previously, the first photorefractive gratings were written by Hill using a visible argon-ion laser launched directly into the fibre core, to produce a standing wave pattern [65]. Subsequent gratings used a UV laser to write gratings through the fibre cladding [67]. During the fabrication process, it was observed that the centre wavelength of the grating increased during the writing process, indicating that a positive refractive index change was being induced. These gratings are known as 'Type I' gratings. Such gratings are the most commonly fabricated, both holographically and using the phase mask technique, but are the least stable at high temperatures.

After the saturation of Type I gratings (having refractive index around 10^{-4}) then the growth of a 'Type IIa' grating commences, basically formed by the overexposure of a conventional grating. Such a grating grows in reflectivity, with a positive index change (Type I) until saturation, when the grating decreases in reflectivity, to almost zero and a further increase in reflectivity is then observed. During the final stages of the growth process, the centre wavelength of the grating decreases, indicating a negative induced refractive index change. The growth eventually saturates, producing what is known as a 'Type IIa' grating [102]. Using an excimer laser allows Type IIa gratings to be fabricated within a matter of minutes, in comparison to a laser operating at 240nm, an Argon-ion for example, which can take an exposure time of up to one hour to fabricate an identical grating. Type IIa gratings show greater temperature stability than Type I gratings, at higher temperatures [103]. Dong *et al* [104] used a three-level model to explain the observed experimental behaviour, where excitation from the ground state to the second level produces a Type I grating, and subsequent excitation to the third level leads to the formation of a Type IIa grating.

The final grating type, Type II, are formed by exposing fibre to high intensity UV light from a pulsed laser [105]. In this situation an interferometric set-up is usually used, since the high fluence levels used in Type II grating fabrication are likely to damage a phase mask. The grating is formed via a damage mechanism which takes place at the core/cladding interface. These gratings appear to be the most temperature resistant, surviving up to approximately 800°C.

2.9.2 Chirped Gratings

All of the fabrication techniques detailed in section 2.8 are concerned with the fabrication of uniform period gratings only but can be extended to fabricate chirped gratings, where the grating period changes incrementally. Figure 2.20 illustrates a linearly chirped grating, showing different wavelengths are reflected at different points along the grating.

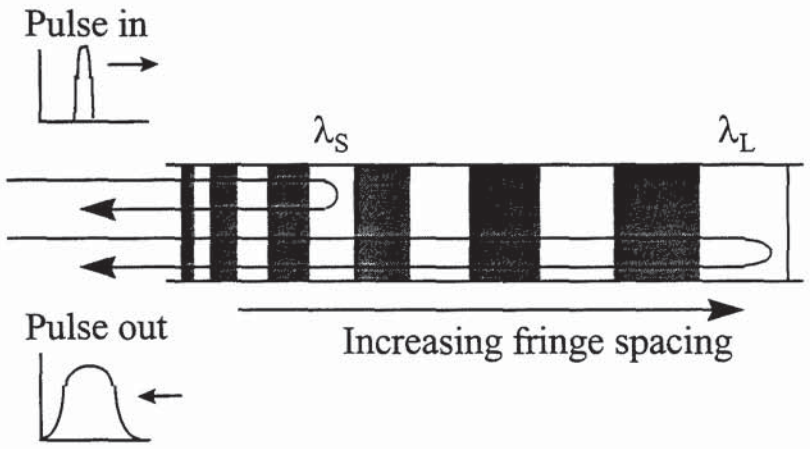

Figure 2.20: Chirped in-fibre Bragg grating, where longer wavelengths travel further in the grating than shorter ones

With the grating in the orientation shown in Figure 2.20, shorter wavelengths λ_s are reflected first, at the near end of the grating, whilst longer wavelengths, λ_L get reflected at the far end of the grating. Since the longer wavelengths travel further within the grating they encounter a delay relative to the shorter wavelengths and hence the reflected profile is broadened, as illustrated in Figure 2.21.

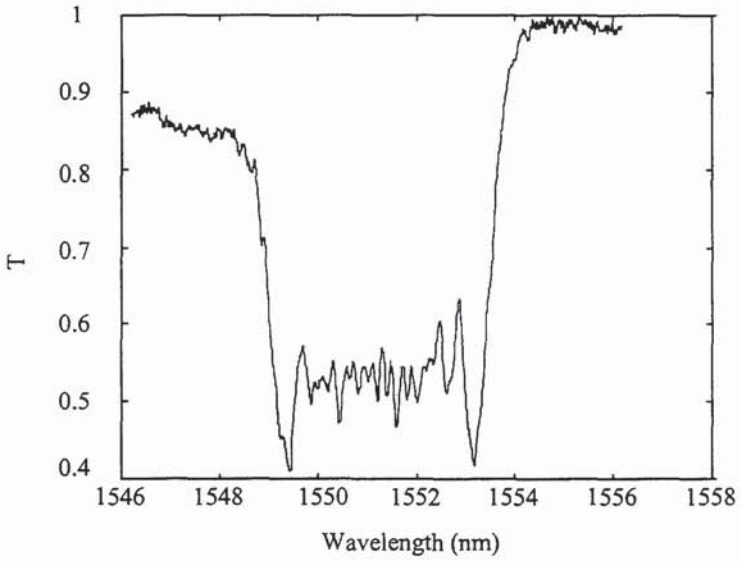

Figure 2.21: The transmission spectrum of a typical unapodised chirped Bragg grating, of bandwidth 5nm

The rationale behind the fabrication of broader bandwidth gratings is that uniform period gratings can be too narrow for some applications, since the longer the grating, the narrower the bandwidth. Writing a very strong uniform period grating increases the bandwidth but also increases the associated short wavelength loss. Using the Bragg condition $2n_{eff}(z)\Lambda(z) \equiv \lambda_B(z)$ (Equation 2-2) it can be seen that by varying either the period or the refractive index results in a broader bandwidth grating.

The concept of chirping was related to slab waveguide structures [106] long before it was applied to fibre gratings. The first chirped gratings were fabricated in 1992 by Farries *et al* [107], at the same time as the development of highly photosensitive fibre. These chirped gratings were side-etched into the cladding of the fibre. Since that time there has been extensive work carried out on a variety of methods for producing chirped structures [101,108,109,110]. Using the basic two-beam holographic fabrication technique [67] chirped structures have been fabricated by the use of an optical fibre taper [111], where the chirp is achieved by a linear variation in the effective refractive index of the fibre. Other techniques incorporating the holographic technique include the deformation of the fibre during exposure [112], where the fibre is bent and the resultant chirp is dependent on the angle between the fibre and the exposing fringe pattern. One of the most well used chirping techniques uses a modified two beam holographic interferometric set-up. The introduction of cylindrical lenses into the arms of the interferometer creates two beams having dissimilar wavefront curvatures [113]. This has proved itself to be a very flexible method of producing a wide range of chirps.

The scanning phase mask technique may also be extended to fabricate chirped fibre gratings. Using a system employing a uniform period phase mask it is possible to fabricate chirped gratings. Kashyap *et al* [76] used a number of uniform period phase masks and stitched together a series of short, uniform period gratings written at consecutive wavelengths to produced a chirped device. Byron *et al* [114] demonstrated a stretch and write technique where the fibre was first placed under strain and a short grating was written. The fibre strain was then either increased or decreased and another short grating was written in the position exactly adjacent to the first. Other methods to induce a chirp in gratings include the tilting of the fibre relative to the phase mask [115] and the use of a piezoelectric stack [116]. The use of a piezoelectric stack produces a temporary chirp only. Here the stack is bonded to the grating and is able to produce a strain at 21 different locations along the length of the grating. On the application of a voltage, the segments expand in the axial direction and this strain is transferred to the fibre Bragg grating producing a chirped structure.

Another technique reported by Hill *et al* [117] uses the dual exposure of the fibre to chirp the gratings. In the first exposure, the beam irradiates a section of fibre screened by the mask, the mask being translated along the length of the fibre at a constant velocity. This translation continuously increases the length of fibre exposed to the beam, producing a linear variation in the effective refractive index. In the second exposure a grating is fabricated by scanning the beam along the phase mask. Although this produces a uniform period grating in the fibre, the linear variation in refractive index due to the first exposure produces a chirped device.

In addition to these techniques, chirped phase masks are now widely available [76,118], where the linear variation in period is etched into the mask itself. This ensures that very reproducible chirped period fibre Bragg gratings can be fabricated, but again the chirp rate is pre-defined by the mask and therefore each pattern produces gratings of only one bandwidth.

2.10 Dispersion

The possible capacity for information in telecommunication systems is large, mainly due to the high carrier frequency of light (~ 10^{14} Hz). A fundamental bandwidth limitation in optical waveguides is dispersion, which causes each pulse to spread out in time as it is transmitted down an optical fibre. The temporal spreading of these pulses gives the maximum data rate for a communication link since, above this maximum data rate, the pulses would eventually overlap and would become indistinguishable at the receiver input.

In a single mode fibre, there are two dominant sources of dispersion: waveguide dispersion and material dispersion. Pulse broadening due to material dispersion occurs due to the wavelength dependence of the refractive index. This means that the various spectral components within the pulse will travel at differing velocities down the fibre length. It has been observed that, in a silica based fibre, the material dispersion tends to zero in the wavelength region around 1.3μm [119]. This provided an incentive for telecommunications systems to operate at this wavelength.

Waveguide dispersion arises because the mode velocity depends on wavelength, through the propagation constant, β. This would be true even if the refractive index were independent of wavelength. Provided that the guide dimensions are such that the mode is independent of wavelength, waveguide dispersion is usually much smaller than the material dispersion.

From Figure 2.20, which shows a pulse reflected from a linearly chirped grating, the following expression can be approximated for the group delay dispersion, D:

$$D = \frac{2n_{eff}L}{c\Delta\lambda}$$

Equation 2-18

where n_{eff} is the effective refractive index, L is the length of the grating, c is the velocity of light in free space and $\Delta\lambda$ is the difference in wavelengths reflected from the two ends of the grating. From Equation 2-18 it is possible to design chirped gratings which will compensate for the ~ 17ps/nm/km chromatic dispersion which occurs in standard telecommunications fibre. Such dispersion compensation allows the existing non-dispersion shifted fibre network to be upgraded for high data rate operation (10Gbit/s and beyond), within the 1550nm low-loss window. For example, to compensate for a 100km length of standard fibre (having a dispersion of 17 ps/nm/km) at 1550nm, over a bandwidth of 0.5nm then, from Equation 2-18, a chirped grating of length ~8.5cm is required. From this it is obvious that the larger the required bandwidth, i.e. to cover semiconductor laser diode wavelength tolerances of around 5nm, then a longer grating is needed, in the order of meters in length. The fabrication of such a long device is currently the focus of much research activity within the Bragg grating field [120].

2.11 Chapter Conclusions

The aim of this chapter was to provide an overview of the most fundamental concepts which concern those involved with the design and fabrication of in-fibre Bragg gratings. In the subsequent chapters of this thesis issues introduced here will be

utilised in the fabrication of a wide range of gratings, optimised for various applications. A number of modelling techniques were detailed and these will be used to support the experimental work.

---

1 H. Kogelnik, 'Coupled Wave Theory for Thick Hologram Gratings', *Bell Syst. Tech. J.*, **48**, (9), 1969, pp. 2909-2947

2 A. Yariv, 'Coupled-mode theory for guided-wave optics', *IEEE J. Quantum Electron.*, **QE-9**, (9), 1973, pp.919-933

3 K.O. Hill, 'Aperiodic distributed-parameter waveguides for integrated optics', *Appl. Opt.*, **13**, 1974, pp. 1853-1856

4 H. Kogelnik, 'Filter Response of nonuniform almost-periodic structures', *Bell Syst. Tech. J.*, **55**, (1), 1976, pp. 109-125

5 B.-G. Kim, E. Garmire, 'Comparison between the matrix method and the coupled-wave method in the analysis of Bragg reflector structures', *J. Opt. Soc. Am. A*, **9**, 1992, pp. 132-136

6 M. Yamada, K. Sakuda, 'Analysis of almost-periodic distributed feedback slab waveguides via a fundamental matrix approach, *Appl. Opt.*, **26**, 1987, pp.3474-3478

7 S. Radic, N. George, G.P. Agrawal, 'Analysis of nonuniform distributed feedback structures: Generalized Transfer matrix method', *IEEE J. Quantum Electron.*, **31**, (7), 1995, pp.1326-1336

8 D.K.W. Lam, B.K. Garside, 'Characterization of single-mode optical fiber filters', *Appl. Opt.*, **20**, (3), 1981, pp.440-445

9 G.V. Agrawal, *Nonlinear Fibre Optics*, 2nd Edn. (Academic Press, San Diego, 1995), pp.451

10 A. Yariv, P. Yeh, *Optical Waves in Crystals*, (John Wiley & sons, New York, 1984)

11 K.O. Hill, B. Malo, K.A. Vineberg, F. Bilodeau, D.C. Johnson, I. Skinner, 'Efficient mode conversion in telecommunication fibre using externally written gratings', *Electron. Lett.*, **26**, (16), 1990, pp.1270-1271

12 T. Erdogan, 'Fibre grating spectra', *J. Lightwave Technol.*, **15**, (8), 1997, pp.1277-1294

13 W.X. Xie, P. Niay, P. Bernage, M. Douay, J.F. Bayon, T. Georges, M. Monerie, B. Poumellec, 'Experimental evidence of two types of photorefractive effects occurring during photoinscriptions of Bragg gratings within germanosilicate fibres', *Opt. Commun.*, **104**, (1,2,3), 1993, pp.185-195

14 R.M. Atkins, V. Mizrahi, T. Erdogan, '248nm Induced vacuum UV spectral changes in optical fibre preform cores: support for a colour centre model of photosensitivity', *Electron. Lett.*, **29**, (4), 1993, pp.385-387

15 T-E. Tsai, G.M. Williams, E.J. Friebele, 'Index structure of fibre Bragg gratings in Ge-SiO_2 fibres', *Opt. Lett.*, **22**, (4), 1997, pp.224-226

16 L. Dong, J.L Archambault, L. Reekie, P.St.J. Russell, D.N. Payne, 'Photoinduced absorption change in germanosilicate preforms: evidence for the colour -center model of photosensitivity', *Appl. Opt.*, **34**, (18), 1995, pp.3436-3440

17 M.G. Sceats, G.R. Atkins, S.B. Poole, 'Photolytic index changes in optical fibers', *Annu. Rev. Mater. Sci.*, **23**, 1993, pp.381-410

18 J.P. Bernardin, N.M. Lawandy, 'Dynamics of the formation of Bragg gratings in germanosilicate optical fibres', *Opt. Commun.*, **79**, (3,4), 1990, pp.194-199

19 B. Poumellec, P. Guenot, I. Riant, P. Sansonetti, P. Niay, 'UV induced densification during Bragg grating inscription in Ge:SiO^2 preforms', *Opt. Mat.*, **4**, 1995, pp.441-449

20 H.G. Limberger, P.Y. Fonjallaz, R.P. Salathe, F. Cochet, 'Compaction and photoelastic induced index changed in fibre Bragg gratings', *Appl. Phys. Lett.*, **68**, (22), 1996, pp.3069-3071

21 P.Y. Fonjallaz, H.G. Limberger, R.P. Salathe, F. Cochet, B. Leuenberger, 'Tension increase correlated to refractive-index change in fibres containing UV-written Bragg gratings', *Opt. Lett.*, **20**, (11), 1995, pp. 1346-1348

22 D.P. Hand, P.St.J. Russell, 'Photoinduced refractive-index changes in germanosilicate fibres', *Opt. Lett.*, **15**, (2), 1990, pp.102-104

23 P.N. Butcher, D. Cotter, *Elements of Nonlinear Optics*, (Cambridge University Press, Cambridge, UK, 1990)

24 H.G. Limberger, P.Y. Fonjallaz, R.P. Salathe, 'Spectral characterisation of photoinduced high efficient Bragg Gratings in standard Telecommunications fibres', *Electron. Lett.*, **29**, (1), 1993, pp.47-49

25 M. Douay, W.X. Xie, T. Taunay, P. Bernage, P .Niay, P. Cordier, B. Poumellec, L. Dong, J.F .Bayon, H. Poignant, E. Delevaque, 'Densification involved in the UV- based photosensitivity of silica glasses and optical fibres', *J. Lightwave Technol.*, **15**, (8), 1997, pp.1329-1342

26 P. Cordier, J.C. Doukhan, E. Fertein, P. Bernage, P. Niay, J.F. Bayon, T. Georges, 'TEM characterisation of structural changes in glass associated to Bragg grating inscription in germanosilicate optical fibre preform', *Opt. Commun.*, **111**, 1994, pp.269-275

27 B. Poumellec, P. Niay, M. Douay, J.B. Bayon, 'The UV induced refractive index grating in Ge:SiO_2 performs: additional CW experiments and the macroscopic origin of the change in index', *J. Phys. D: Appl. Phys,* **29**, 1996, pp.1842-1856

28 F. Bilodeau, B. Malo, J. Albert, D.C. Johnson, K.O. Hill, 'Photosensitization of optical fiber and silica-on-silicon waveguides', *Opt. Lett.*, **18**, (12), 1993, pp.953-955

29 K.O. Hill, Y. Fujii D.C. Johnson, B.S. Kawasaki, 'Photosensitivity in optical fibre waveguides: Application to reflection filter fabrication', *Appl. Phys. Lett.* **32**, 1978, pp.647

30 P.J. Lemaire, A.M. Vengsarkar, W.A. Reed, 'Thermal enhancement of UV photosensitivity in H_2- loaded optical fibres', *Conf. Optic. Fibre Commun. (OFC'95) Tech. Digest*, WN1, 1995, pp.158-159

31 P.J. Lemaire, R.M. Atkins, V. Mizrahi, W.A. Reed, 'High pressure H_2 loading as a technique for achieving ultra-high UV photosensitivity and thermal sensitivity in GeO_2 doped optical fibres', *Electron. Lett.*, **29**, (13), 1993, pp.1191-1193

32 P.J. Lemaire, 'Reliability of optical fibres exposed to hydrogen: prediction of long-term loss increases', *Opt. Eng.*, **30**, (6), 1991, pp.780-789

33 J.F. Shackelford, P.L. Studt, R.M. Fulrath, 'Solubility of gases in glass. II. He, Ne and H_2 in fused silica', *J. Appl. Phys.*, **43**, (4), 1972, pp.1619-1626

34 K. Tsujikawa, M Ohashi, 'Reduction of OH absorption loss by deuterium in new glass materials for ultralow-loss fibre', *Conf. Optic. Fibre Commun. (OFC '97) Tech. Digest*, TuB2, 1997, pp.2

35 V. Mizrahi, P.J. Lemaire, T. Erdogan, W.A. Reed, D.J. DiGiovanni, R.M. Atkins, 'Ultraviolet laser fabrication of ultrastrong optical fibre gratings and of germania-doped channel waveguides', *Appl. Phys. Lett.*, **63**, (13), 1993, pp.1727-1729

36 B. Malo, J. Albert, K.O. Hill, F. Bilodeau, D.C. Johnson, 'Effective index drift from molecular hydrogen diffusion in hydrogen-loaded optical fibres and its effect on Bragg grating fabrication', *Electron. Lett.*, **30**, (5), 1994, pp.442-444

37 J.E. Shelby, 'Molecular diffusion and solubility of hydrogen isotopes in vitreous silica', *J. Appl. Phys.*, **48**, (8), 1977, pp.3387-3394

38 J. Crank, *The mathematics of diffusion*, Oxford University Press, London, 1975, pp.49-53, 71-74

39 T. Erdogan, V. Mizrahi, P.J. Lemaire, D. Monroe, 'Decay of ultraviolet induced fibre Bragg gratings', *J. Appl. Phys.*, **76**, (1), 1994, pp.73-80

40 H. Patrick, S.L. Gilbert, A. Lidgard, M.D. Gallagher, 'Annealing of Bragg gratings in hydrogen loaded optical fiber', *J.Appl. Phys*, **78**, (5), 1995, pp.2940-2945

41 S. Kannan, K.Z.Y. Guo, P.J. Lemaire, 'Thermal stability analysis of UV-induced fibre Bragg gratings', *J. Lightwave Technol.*, **15**, (8), 1997, pp.1478-1483

42 S.R. Baker, H.N. Rourke, V. Baker, D. Goodchild, 'Thermal decay of fibre Bragg gratings written in boron germanium codoped silica fibre', *J. Lightwave Technol.*, **15**, (8), 1997, pp.1470-1477

43 R.J. Egan, H.G. Inglis, P. Hill, P.A. Krug, F. Ouellette, 'Effects of hydrogen loading and grating strength on the thermal stability of fibre Bragg gratings', *Conf. Optic. Fibre Commun. (OFC '96), Tech. Digest*, Tu03, 1996, pp.83-84

44 K.E. Chisholm, K. Sugden, I. Bennion, 'Effects of thermal annealing on Bragg fiber gratings in boron/germania co-doped fibre', *J. Phys. D: Appl. Phys.*, **31**, 1998, pp.61-64

45 I. Camlibel, D.A. Pinnow, F.W. Dabby, 'Optical aging characteristics of borosilicate clad fused silica core fiber optical waveguides', *Appl. Phys.Lett.*, **25**, (4), 1975, pp.185-187

46 D.L. Williams, B.J. Ainslie, J.R. Armitage, R. Kashyap, R. Campbell, 'Enhanced UV photosensitivity in boron codoped germanosilicate fibres', *Electron. Lett.*, **29**, (1), 1993, pp.45-47

47 L. Dong, J.-L. Archambault, L. Reekie, P.St.J. Russell, D.N. Payne, 'Bragg gratings written in Ce^{+3} -doped fibres by a single excimer pulse', *Opt. Lett.*, **18**, (11), 1993, pp.861-863

48 L. Dong, J.-L. Archambault, E. Taylor, M.P. Roe, L. Reekie, P.St.J. Russell, 'Photosensitivity in tantalum-doped silica optical fibers', *J. Opt. Soc. Am. B*, **12**, (9) 1995, pp.1747-1750

49 L. Dong, J.L. Cruz, L. Reekie, M.G. Xu, D.N. Payne, 'Enhanced photosensitivity in tin co-doped germanosilicate optical fibres', *IEEE Photon. Technol. Lett.*, **7**, 1995, pp.1048-1050

50 E.M. Dianov, K.M. Golant, V.M. Mashinsky, O.I. Medvedkov, I.V. Nikolin, O.D. Sazhin, S.A. Vasiliev, 'Highly photosensitive nitrogen doped germanosilicate fibre for index grating writing', *Electron. Lett.*, **33**, (15), 1997, pp.1334-1335

51 J. Wilson, J.F.B. Hawkes, *Optoelectronics: An Introduction, 2nd Edn.*, (Prentice Hall, UK, 1989)

52 D.N. Payne, A.J. Barlow, J.J.R Hansen, 'Development of low-and-high-birefringence optical fibres', *IEEE J. Quantum. Electron.*, **QE-18**, (4), 1982, pp.477-488

53 R.D. Birch, D.N. Payne, M.P. Varnham, 'Fabrication of polarisation maintaining fibres using gas-phase etching, *Electron. Lett.*, **18**, 1982, pp.1036-1038

54 R.H. Stolen, W. Pleibel, J.R. Simpson, 'High-birefringence optical fibres by preform deformation', *J. Lightwave Technol.*, **LT-2**, 1985, pp.639-641

55 J.-L. Archambault, L. Reekie, P.St.J. Russell, '100% reflectivity Bragg resonators produced in optical fibres by single excimer laser pulses', *Electron. Lett.*, **29**, 1993, pp.453-455

56 T. Erdogan, J.E. Sipe, 'Radiation mode coupling loss in tilted fibre phase gratings', *Opt. Lett.*, **20**, (18), 1995, pp.838-1840

57 V. Mizrahi, J.E. Sipe, 'Optical properties of photosensitive fiber phase gratings', *J. Lightwave Technol.*, **11**, (10), 1993, pp.1513-1517

58 C.J. Rowe, I. Bennion, D.C.J. Reid, 'High-reflectivity surface relief gratings in single-mode optical fibres', *J. Optoelectronics.*, **134**, (3) 1987, pp.197-202

59 E. Delevaque, S. Boj, J.F. Bayon, H. Poignant, J Le Mellot, M. Monerie, 'Optical fibre design for strong gratings photoimprinted with radiation mode suppression', *Conf. Optic. Fibre Commun. (OFC '95)*, San Diego, California, Post-deadline paper PD5, 1995

60 T. Komukai, M. Nakazawa, 'Efficient fibre gratings formed on high NA dispersion-shifted fibres', *European Conf. Optic. Commun. (ECOC '95) Tech. Digest,* MoA3.3, 1995, pp.31-34

61 W.W. Morey, G. Meltz, J.D. Love, S.J. Hewlett, 'Mode-coupling characteristics of UV-written Bragg gratings on depressed-cladding fibre', *Electron. Lett.*, **30**, (9), 1994, pp.730-733

62 L. Dong, L. Reekie, J.L. Cruz, J.E. Caplen, J.P. de Sandro, D.N. Payne, 'Optical fibres with depressed claddings for suppression of coupling into cladding modes in fibre Bragg gratings', *IEEE Photon. Technol. Lett.*, **9**, (1), 1997, pp.64-66

63 T. Poulsen, M.O. Berendt, A. Bjarklev, L. Gruner-Nielsen, C.E. Soccolich, 'Bragg grating induced cladding mode coupling caused by Ultra-violet light absorption', *Electron. Lett.*, **24**, (10), 1998, pp.1007-1009

64 S.J. Hewlett, J.D. Love, G. Meltz, T.J. Bailey, W.W. Morey, 'Cladding-mode coupling characteristics of Bragg gratings in depressed-cladding fibre', *Electron. Lett.*, **31**, (10), 1995, pp.820-822

65 K.O. Hill, Y. Fujii, D.C. Johnson, B.S. Kawasaki, 'Photosensitivity in optical fibre waveguides: Application to reflection filter fabrication', *Appl. Phys. Lett.*, **32**, 1978, pp.647-649

66 B.S. Kawasaki, K.O. Hill, D.C. Johnson, Y, Fujii ,'Narrowband Bragg reflectors in optical fibres, *Opt. Lett.*, **3**, 1978, pp. 66-68

67 G. Meltz, W.M. Morey, W.H. Glenn, 'Formation of Bragg gratings in optical fibers by a transverse holographic method', *Opt. Lett.*, **14**, (15), 1989, pp.823-825

68 R. Kashyap, J.J Armitage, R. Wyatt, S.T. Davey, D.L. Williams, 'All-fibre narrowband reflection gratings at 1550nm', *Electron. Lett.*, **26**, 1990, pp.730-731

69 R. Kashyap, J.R. Armitage, R.J. Campbell, D.L. Williams, G.D. Maxwell, B.J. Ainslie, C.A. Millar, 'Light-sensitive optical fibres and planar waveguides', *BT Technol. J.*, **11**, (2), 1994, pp.150-158

70 H. Patrick, S.L. Gilbert, 'Growth of Bragg gratings produced by continuous-wave ultraviolet light in optical fibre', *Opt. Lett.*, **18**, (18), 1993, pp. 1484-1486

71 B.J. Eggleton, P.A. Krug, L. Poladian, 'Experimental demonstration of compression of dispersed optical pulses by reflection from self-chirped optical fibre Bragg gratings', *Opt. Lett.*, **19**, (12), 1994, pp.877-879

72 Q. Zhang, D.A. Brown, L. Reinhart, T.F. Morse, 'Simple prism-based scheme for fabricating Bragg gratings in optical fibres', *Opt. Lett.* **19**, (23), 1994, pp.2030-2032

73 K.O. Hill, F. Bilodeau, B. Malo, D.C. Johnson, J. Albert, 'Bragg gratings fabricated in monomode photosensitive optical fibre by UV exposure through a phase mask', *Appl. Phys. Lett.*, **62**, (10), 1993, pp.1035-1037

74 J. Martin, F. Ouellette, 'Novel writing technique of long and highly reflective in-fibre gratings', *Electron. Lett.*, **30**, (10), 1994, pp.811-812

75 H.N. Rourke, S.R. Baker, K.C. Byron, R.S Baulcomb, S.M. Ojha, S. Clements, 'Fabrication and characterisation of long, narrowband fibre gratings by phase mask scanning', *Electron. Lett.*, **30**, (16), 1994, pp.1341-1342

76 R. Kashyap, P.F. McKee, R.J. Campbell, D.L. Williams, 'Novel method of producing all fibre photoinduced chirped gratings', *Electron. Lett.*, **30**, (12), 1994, pp.996-998

77 J.D. Prohaska, E. Snitzer, S. Rishton, V. Boegli, 'Magnification of mask fabricated fibre Bragg gratings', *Electron. Lett.*, **29**, (18), 1993, pp.1614-1615

78 R.J. Campbell, R. Kashyap, 'Spectral Profile and multiplexing of Bragg gratings in photosensitive fiber', *Opt. Lett.*, **16**, (12), 1991, pp.898-900

79 Q. Zhang, D.A. Brown, L. Reinhart, T.F. Morse, J.Q. Wang, G. Xiao, 'Tuning Bragg wavelength by writing gratings on pre-strained fibres', *IEEE Photon. Technol. Lett.*, **6**, 1994, pp.839-841

80 D.S. Starodubov, V. Grubsky, J. Feinberg, 'Efficient Bragg grating fabrication in a fibre through its polymer jacket using near UV- light', *Electron. Lett.*, **33**, (15), 1997, pp.1331-1333

81 R.P. Espindola, R.M. Atkins, D.A. Simoff, K.T. Nelson, M.A. Paczkowski, 'Fibre Bragg gratings written through a fibre coating', *Conf. Optic. Fibre Commun. (OFC '97)*, PD4, 1997

82 E.M. Dianov, D.S. Starodubov, A.A. Frolov, 'UV argon laser induced luminescence changes in germanosilicate fibre preforms', *Electron. Lett.*, **32**, (3), 1996, pp.246-247

83 D.S. Starodubov, V. Grubsky, J. Feinberg, B. Kobrin, S. Juma, 'Bragg grating fabrication in germanosilicate fibres by use of near-UV light: a new pathway for refractive-index changes', *Opt. Lett.*, **22**, (14), 1997, pp.1086-1088

84 D. Varelas, H.G. Limberger, R.P. Salathe, 'Enhanced mechanical performance of singlemode optical fibres irradiated by a CW UV laser', *Electron. Lett.*, **33**, (8), 1997, pp.704-705

85 L. Harriott, A. Liddle, Electron Beam lithography', *Physics World,* **Apr. 97**, 1997, pp.41-45

86 D.M. Tennant, T.L. Koch, P.P. Mulgrew, R.P. Gnall, 'Characterization of near-field holographic grating masks for optoelectronics fabricated by electron beam lithography', *J. Vac. Sci. Technol. B*, **10**, (6), 1992, pp.2530-2535

87 J. Albert, S. Theriault, F. Bilodeau, 'Minimization of phase errors in long fiber Bragg gratings made using E-beam lithography', *IEEE Photon. Technol. Lett.*, **8**, (10), 1996, pp.1334-1336

88 X. Liu, R.M. De La Rue, P.V.S. Marques, S. Thoms, J.S. Aitchison, L.A. Everall, J.A.R. Williams, I. Bennion, 'The influence of phase mask stitch errors on the performance of UV-written Bragg gratings', *Conf. On Bragg Gratings, Photosensitivity, and Poling in Glass Fibres and Waveguides, Williamsburg (BGPP '97) Tech. Digest,* **17**, BMG9,1997, pp.210-212

89 T. Kjellberg, R. Schatz, 'The effect of stitching errors on the spectral characteristics of DFB Lasers fabricated using Electron Beam lithography', *J. Lightwave Technol.,* **10**, (9), 1992, pp.1256-1266

90 X. Liu, J.S. Aitchison, R.M. De La Rue, S. Thoms, L. Zhang, J.A.R. Williams, I. Bennion, 'Electron Beam lithography of phase mask gratings for near field holographic production of optical fibre gratings', *Microelectron. Eng.*, **35**, 1997, pp.345-348

91 X. Liu, S. Thoms, J. S. Aitchison, R. M. De La Rue, L A Everall, J.A. R. Williams, I. Bennion, 'Defect reduction and diffraction efficiency optimisation for E-beam written

phase masks', *MNE'97- International Conference on Micro- and Nano-Engineering*, Athens, Greece, 1997

92 S.J. Mihailov, F. Bilodeau, K.O. Hill, D.C. Johnson, J. Albert, D. Stryckman, C. Shu, 'Comparison of fibre Bragg grating dispersion-compensation made with holographic and e-beam written phase masks', *European Conf. Optic. Commun. (ECOC '98) Tech. Digest*, (1998), pp.283-284

93 F. Bilodeau, K.O. Hill, B. Malo, D.C. Johnson, I.M. Skinner, 'Efficient narrowband LP01 - LP02 mode convertors fabricated in photosensitive fibre: Spectral response', *Electron. Lett.*, **27**, 1991, pp.682-683

94 B. Malo, K.O. Hill, F. Bilodeau, D.C. Johnson, J. Albert, 'Point by point fabrication of micro Bragg gratings in photosensitive fibre using single excimer pulse refractive index modification techniques', *Electron. Lett.*, **29**, (18), 1993, pp.1668-1669

95 A.M. Vengsarkar, J.R. Pedrazzani, J.B. Judkins, P.J. Lemaire, N.S. Bergano, C.R. Davidson, 'Long period fibre grating based gain equalizers', *Opt. Lett.*, **21**, (5), 1996, pp.336-338

96 B. Ortega, L. Dong, W.F. Liu, J.P. de Sandro, L. Reekie, S.I. Tsypina, V.N. Bagratashvili, R.I. Laming, 'High-performance Optical Fibre Polarizers Based on Long-Period Gratings in Birefringent Optical Fibres', *IEEE Photon. Technol. Lett.*, **9**, (10), 1997, pp.1370-1372

97 V. Bhatia, A.M. Vengsarkar, 'Optical fibre long-period grating sensors', *Opt. Lett.*, **22**, (9), 1996, pp.692-694

98 S.J. Mihailov, M.C. Gower, 'Recording of efficient high-order Bragg reflectors in optical fibres by mask image projection and single pulse exposure with an excimer laser', *Electron. Lett.*, **30**, 1994, pp.179-182

99 H.J. Patrick, C.G. Askins, R.W. McElhanon, E.J. Friebele, 'Amplitude mask patterned on an excimer laser mirror for high intensity writing of long period fibre gratings', *Electron. Lett.*, **33**, (13), 1997, pp.1167-1168

100 A.M. Vengsarkar, P.J. Lemaire, J.B. Judkins, V. Bhatia, T. Erdogan, J.E. Sipe, 'Long-period Fibre Gratings as Band Rejection Filters', *J. Lightwave Technol.*, **14**, (1), 1996, pp.58-65

101 M.C. Farries, K. Sugden, D.C.J. Reid, I. Bennion, A. Molony, M.J. Goodwin, 'Very broad reflection bandwidth (44nm) chirped fibre gratings and narrow bandpass filters produced by the use of an amplitude mask', *Electron. Lett.*, **30**, (11), 1994, pp.891-892

102 P. Niay, P. Bernage, S. Legoubin, M. Douay, W.X. Xie, J.F. Bayon, T. Georges, M. Monerie, B. Poumellec, 'Behaviour of spectral transmissions of Bragg gratings written

in germania doped fibres: writing and erasing experiments using pulsed or CW UV exposure', *Opt. Commun.*, **113**, 1994, pp.176-192

103 I. Riant, S. Borne, P. Sansonetti, 'Dependence of fibre Bragg grating thermal stability on the grating fabrication process', *Conf. Optic. Fibre Commun. (OFC '96)*, San Jose, California, TuO5, 1996, pp.86-87

104 L. Dong, W.F. Liu, L. Reekie, 'Experimental and theoretical study of stable negative index gratings formed at 193nm', *SPIE Conference Proc. On Photosensitive Optical Material and Devices*, 1997

105 J.L Archambault, L. Reekie, P.St.J Russell, '100% reflectivity Bragg reflectors in optical fibres by single pulse excimer laser', *Electron. Lett.*, **29**, 1993, pp.453-455

106 H. Kogelnik, 'Filter response of non-uniform almost-periodic structures', *Bell Syst. Technol. J.*, **55**, 1976, pp.109-127

107 M. Farries, C.M. Ragdale, D.C.J. Reid, 'Broadband chirped fibre Bragg filters for pump rejection and recycling in erbium doped fibre amplifiers', *Electron. Lett.*, **28**, 1992, pp.487-489

108 K.O. Hill, F. Bilodeau, B. Malo, T. Kitagawa, S. Theriault, D.C. Johnson, J. Albert, 'Aperiodic In fibre Bragg gratings for optical fibre dispersion compensation', *Conf. Optic. Fibre Commun. (OFC '94)*, San Diego, California, PD2, 1994, pp.335

109 J.L. Cruz, A. Diez, M.V. Andres, A. Segura, B. Ortega, L. Dong, 'Fibre Bragg gratings tuned and chirped using magnetic fields', *Electron. Lett.*, **33**, (3), 1997, pp.235-236

110 D. Garthe, R.E. Epworth, W.S. Lee, A. Hadjifotiou, C.P. Chew, Y. Bricheno, A. Fielding, H.N. Rourke, S.R. Baker, K.C. Byron, R.S. Baulcomb, S.M. Ohja, S. Clements, 'Adjustable dispersion equaliser for 10 and 20Gbit/s over distances up to160km', *Electron. Lett.*, **30**, (25), 1994, pp.2159-2160

111 K.C. Byron, K. Sugden, T. Bricheno, I. Bennion, 'Fabrication of chirped gratings written holographically in optical fibre tapers', *Electron. Lett.*, **29**, 1993, pp.1659-1660

112 K. Sugden, I Bennion, A. Molony, N.J. Copner, 'Chirped gratings produced in photosensitive optical fibre by fibre deformation during exposure', *Electron. Lett.*, **30**, (5), 1994, pp.440-441

113 K. Sugden, L. Zhang, J.A.R. Williams, I. Bennion, 'Dissimilar wavefront technique for linear and quadratic chirps', *Topical meeting on Photosensitivity and Quadratic nonlinearity in Glass waveguides: Fundamentals and Applications' Technical Digest*, Portland, Oregon, 1995, pp136-139

114 K.C. Byron, H.N. Rourke, 'Fabrication of chirped fibre gratings by novel stretch and write technique', *Electron. Lett.*, **31**, (1), 1995, pp.60-61

115 Y. Painchaud, A. Chandonnet, J. Lauzon, 'Chirped fibre gratings produced by tilting the fibre', *Electron. Lett.*, **31**, (3), 1995, pp.171-172

116 M.M. Ohn, A.T. Alavie, R. Maaskant, M.G. Xu, F. Bilodeau, 'Tunable fibre grating dispersion using a piezoelectric stack', *Conf. Optic. Fibre Commun. (OFC'97),* 1997, *Technical Digest*, pp.155

117 K.O. Hill, F. Bilodeau, B. Malo, T. Kitagawa, S. Theriault, D.C. Johnson, J. Albert, K. Takiguchi, 'Chirped in-fibre Bragg gratings for compensation of optical-fibre dispersion, *Opt. Lett.*, **19**, (17), 1994, pp.1314-1316

118 X. Liu, R.M. De La Rue, P. Silva Marques, S. Thoms, S.E. Hicks, J.S. Aitchison, J.A.R. Williams, L.A. Everall, L. Zhang, I. Bennion, 'Realisation of specific filter responses in photosensitive fibre gratings produced by UV exposure through holographic phase masks', *Conf. Lasers and Electro Opt. (CLEO '97)*, Baltimore, CThL57, 1997

119 D.N. Payne, W.A. Gambling, 'Zero material dispersion in optical fibres', *Electron. Lett.*, **11**, (8), 1975, pp.176-178

120 M. Durkin, M. Ibsen, M.J. Cole, R.I. Laming, '1m long continuously-written fibre Bragg gratings for combined second and third order dispersion compensation', *Electron. Lett.*, **33**, (22), 1997, pp.1891-1893

3. GRATING CHARACTERISATION

3.1 Chapter Overview

The following chapters contain numerous different in-fibre devices that have all been designed for specific applications. All of these devices will have been characterised to assess how near to the design criteria they are. The aim of this chapter is therefore to detail the techniques and parameters used in the control of the design and characterisation of in-fibre Bragg gratings.

There are a number of different parameters which 'characterise' a grating. The type of fibre into which the grating is written obviously has a major effect on the resulting grating. The maximum achievable strength of a grating depends partially on the photosensitivity of the fibre, which can be enhanced in several ways. In early work, the photosensitivity of GeO_2 doped silica was found to depend on Ge defects resulting from the high temperature processing used in the production of the optical fibre [1]. It was later shown that the concentration of these Ge defects could be increased by treating the material in high-pressure low temperature hydrogen [2], as was detailed in Chapter 2.

In this chapter, the maximum possible UV-induced refractive index change is evaluated for both hydrogenated and unhydrogenated fibres and the results are compared. An investigation into the change in photosensitivity for gratings written at elevated temperatures is also included. This provides information on the maximum grating reflectivity which can be obtained in a particular fibre under certain fabrication conditions.

When using the phase mask fabrication technique to write gratings, the quality of the mask also changes the characteristics of the resulting filter. Hence phase mask characterisation work is included in this chapter, with details of zero-order diffraction measurements and atomic force microscopy results which show the periodic structure of a phase mask. Two of the most important measurements which must be made in order to fully characterise a Bragg grating are those concerning the reflection and transmission profiles. Within this chapter a simple experimental arrangement is described which allows high resolution measurements of these parameters to be obtained, providing information on the strength, bandwidth and overall shape of the filter. This measurement technique is able to resolve spectral features on a picometer scale, making it possible to closely examine the grating profile for sidelobe suppression etc.

Sidelobes are an unwanted characteristic of Bragg gratings and so this chapter details work on the suppression of these sidelobes through a process called apodisation. Apodisation is essentially a technique whereby the amplitude of the grating fringe pattern is varied, resulting in a spectrally shaped transmission and reflection profile.

3.2 Photosensitivity Study

When germanium doped glass is exposed to UV light a permanent increase in the refractive index of that glass is observed. This observation led to the fabrication of in-fibre Bragg gratings, where a UV interference pattern, generated either holographically or with a phase mask, resulted in a permanent periodic refractive index change within optical fibre. From observations of the growth of such Bragg gratings, where initially the grating growth is very quick but is seen to slow down after a period of time, then it is obvious that the change in the refractive index in the core of the fibre has a saturation characteristic.

This section details work carried out to examine this non-linear refractive index growth in optical fibre samples. Examined is the maximum achievable UV induced refractive index change in each sample and a comparison is made between hydrogenated and unhydrogenated fibre. The latter part of this section gives the results of an investigation into the effect which increasing the temperature of the fibre during the writing process has on the maximum achievable grating strength.

3.2.1 UV-Induced Refractive Index Change Measurements

3.2.1.1 Background

As mentioned previously, the fabrication of Bragg gratings relies on the UV photosensitivity of optical fibre in order to produce an increase in the refractive index of the fibre. The increase in refractive index change, with increasing UV exposure, is a non-linear one and this fact needs to be taken into account when filters of a specific strength are required.

To measure the photoinduced refractive index change in an optical fibre a simple interferometric technique was used. A Mach-Zehnder interferometer was set-up by splicing two fused couplers together, as is illustrated in Figure 3.1. Generally, a Mach-Zehnder comprises two Y-junctions, which give an equal division of input optical power. The input optical power is split in the two arms at the first junction and arrives at the second in phase, giving an intensity maximum at the output port. If the path length of one of the arms is altered then this results in a difference in the phase

of the two signals received at the second junction, producing an output intensity proportional to the change in phase.

3.2.1.2 Experimental Procedure

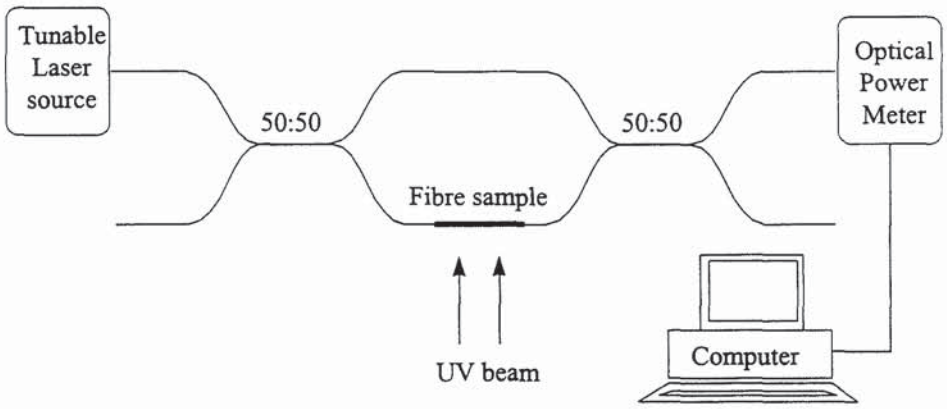

Figure 3.1: Simple set-up for measuring refractive index changes in UV exposed fibre

This principle is easily adapted in order to measure the refractive index change in different samples of fibre. A fibre sample is spliced into one arm of the Mach-Zehnder interferometer, as shown in Figure 3.1. This sample is then exposed to UV light, which induces a change in refractive index, thus changing the effective path length of that arm, relative to the unexposed arm of the interferometer. If the UV induced change in refractive index is large then the path difference changes by a multiple of 2π and it is possible to measure the fringes directly, using an optical power meter. The measured change in phase can then be directly turned into change in refractive index.

The phase ϕ, measured at the output of the Mach-Zehnder, can be defined by $\frac{2\pi}{\lambda} \times (\textit{optical path difference})$, so initially the phase is $\phi = \frac{2\pi}{\lambda} nL$. After a change in phase, $\Delta\phi$, this becomes $(\phi + \Delta\phi) = \frac{2\pi}{\lambda}(n + \Delta n)L$. Thus, the induced change in phase, $\Delta\phi$ is

$$\Delta\phi = \frac{2\pi}{\lambda}\Delta nL$$

Equation 3-1

where $\Delta\phi$ is the measured phase change, λ is the wavelength, Δn is resulting change in refractive index and L is the length of fibre exposed to the UV beam.

This set-up is very sensitive to environmental changes, such as thermal fluctuations or apparatus vibration, so the length of the interferometer arms must be kept to a minimum and the set-up is housed in a stable thermal environment.

For small changes in the refractive index, where the phase does not change by a multiple of 2π, then it is not possible to measure the fringes directly and so a different approach needs to be employed. In this case the unexposed arm of the Mach-Zehnder is wrapped around a piezoelectric cylinder, as illustrated in Figure 3.2.

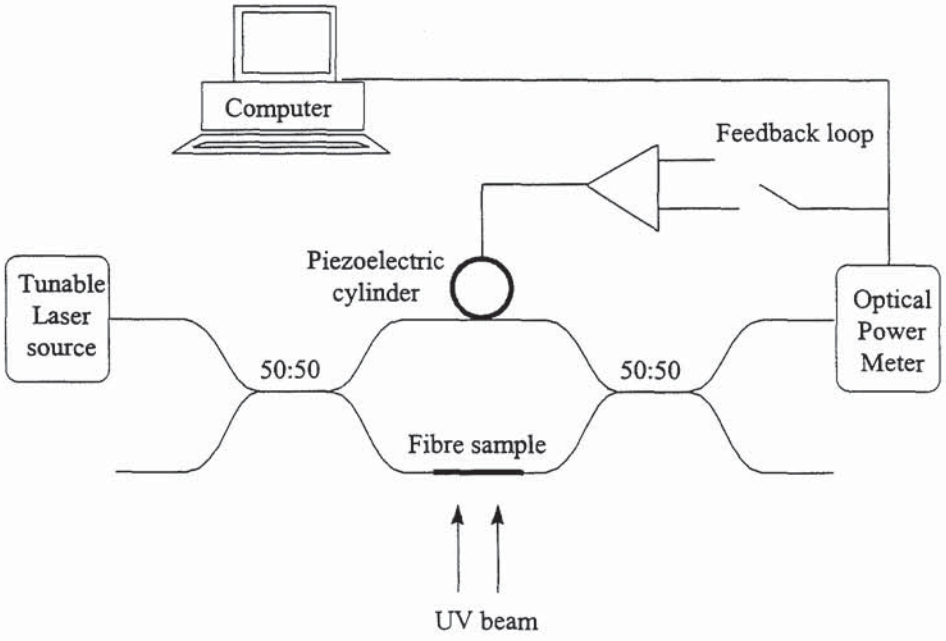

Figure 3.2: Schematic diagram of the experimental set-up to measure small changes in the refractive index in a sample of fibre

When a voltage is applied to the piezoelectric cylinder it expands in a radial direction, stretching the fibre and inducing a phase change in the unexposed arm of the interferometer. Thus, the Mach-Zehnder can be kept in balance during the UV exposure, using a feedback loop to identify the voltage required to keep the Mach-Zehnder balanced. The signal used to maintain this balance is proportional to the change in phase and this can be used to calculate the change in refractive index. The maximum phase change measured using this technique is limited by the maximum change possible from the piezoelectric cylinder.

Throughout these experiments, the geometry and focusing of the UV beam was kept constant. Typically, the UV laser power was 100mW and the beam, prior to focusing, had a height of 12mm and a full width of 2.5mm. A cylindrical lens focused the beam onto the fibre, with a beam waist of the order 120μm, which gave an energy density of typically 7 W/cm^2. This is only an estimated value, since the actual beam waist at the

fibre depends on the position of the fibre relative to the focal position of the beam and therefore could not be measured accurately.

3.2.1.3 Results

Refractive index measurements were made for a sample of boron-germanium co-doped fibre, containing an unknown level of these dopants, in both hydrogenated and unhydrogenated exposure conditions. As expected, the results demonstrated that the refractive index of the fibre experiences its maximum rate of change at the beginning of the exposure and can be seen to saturate after a substantial exposure time.

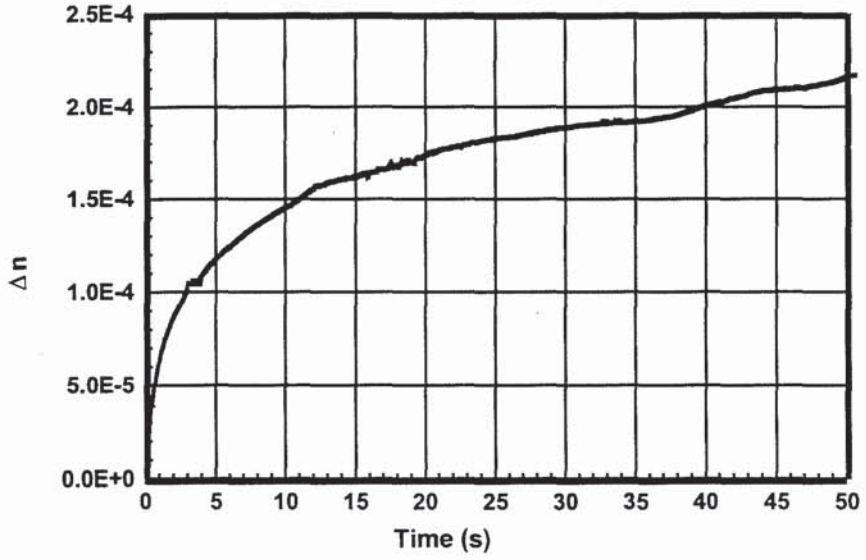

Figure 3.3: A graph showing the rate of change of refractive index for one sample of unhydrogenated B-Ge co-doped fibre

Figure 3.3 shows a set of typical results for such a co-doped fibre. The maximum refractive index change for the unhydrogenated fibre sample was found to be ~2.2 × 10^{-4} for an exposing power of 100mW. At a UV exposure time of 50 seconds the sample appeared to be saturated and the increase in Δn after this time was minimal.

A function suitable to be fitted to such exponentially decaying data is one of the form:

$$\Delta n = \Delta n_0 \left(1 - \exp\left[\frac{-t}{\tau_0} \right] \right)$$

Equation 3-2

where Δn_0 gives the maximum refractive index change. Such a model corresponds to the decreasing number of defect centres available to be altered by UV exposure, as would be expected. Fitting this model to the experimental data shown in Figure 3.3, at

a UV exposing power of 100mW, gives a maximum refractive index change, Δn_0 of 2.0 $\times 10^{-4}$ and τ_0= 6.5 seconds.

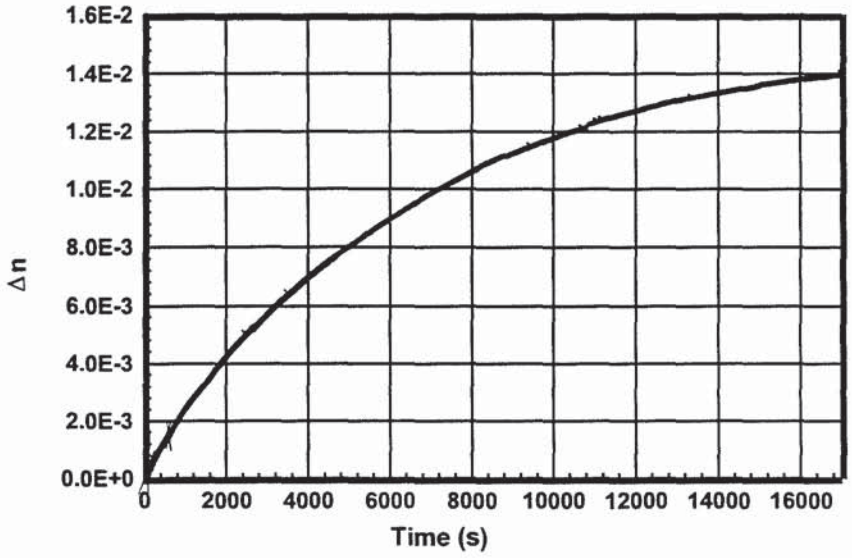

Figure 3.4: A graph showing the rate of change of refractive index for hydrogenated fibre

Figure 3.4 shows the results for the hydrogenated fibre sample. Prior to UV exposure, the fibre sample was placed in a hydrogenation chamber, which was held at room temperature, at a pressure of 120 bar (where 1bar pressure = 0.9869 atmospheres) for longer than 10 days. Assuming that these fibre samples had the standard diameter of 125μm, then under the previously described hydrogenation conditions, this results in a hydrogen concentration of ~1.37 $\times 10^4$ ppm (~1.4 mol% hydrogen) in the fibre core [3]. The hydrogenated fibre results given in Figure 3.4 were found to have two parts to them. Initially, the change in refractive index exhibited a very fast response, inducing a change of the order 5 $\times 10^{-5}$ within the first few seconds of UV exposure. After this, then a much larger, slower refractive index response occurred, producing a final UV induced change in refractive index of 1.4 $\times 10^{-2}$ after a time period of ~17000 seconds had elapsed. Equation 3-2 was again used as the function to describe the experimental data, but in this case two exponential fits, for the two different responses, were obtained. The maximum refractive index change for the initial response was found to be 8.5 $\times$ 10^{-5} and a value of 1.5 $\times$ 10^{-2} was obtained for the larger, slower refractive index response.

This work confirmed that the hydrogenation of fibre increases the maximum UV induced refractive index change. For this particular fibre, the unhydrogenated sample achieved a maximum refractive index change of 2.2 $\times 10^{-4}$, whereas for a sample having

~1.4% H_2 concentration in the fibre core, the induced refractive index change increased to 1.4×10^{-2}.

3.2.2 Grating Fabrication at Elevated Temperatures

3.2.2.1 Introduction

There have been several methods of increasing the photosensitivity of doped optical fibre, as detailed at the beginning of this chapter. It seems reasonable to assume that increasing the fibre UV absorption would increase its photosensitivity. This can be done by moving to shorter exposure wavelengths where the UV losses are higher, for example, by using 193nm ArF radiation [4]. Alternatively, the UV absorption edge can be shifted to longer wavelengths by increasing the temperature of the glass, thus increasing the attenuation at a given wavelength, as illustrated in Figure 3.5.

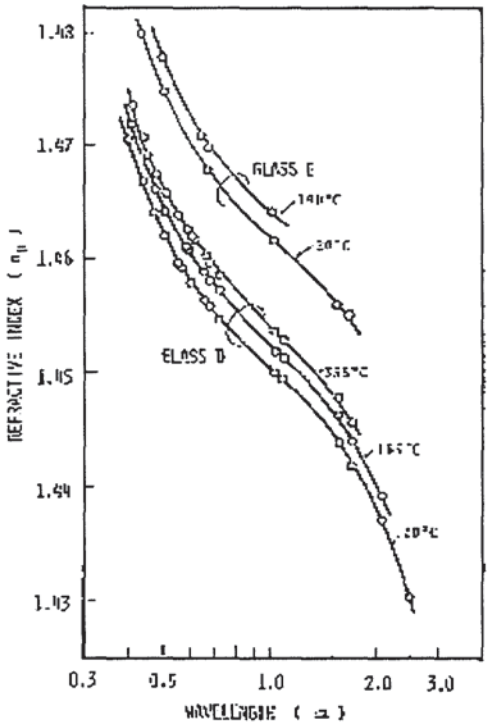

Figure 3.5: A graph showing the temperature dependence of the refractive index for high-silica glasses [5]

This latter approach was used by several groups to examine how an increase in temperature can influence the 248nm photosensitivity of hydrogen-loaded germanosilicate fibres [6,7]. In one case, a fibre sample loaded with 1mol% hydrogen was exposed to a CW CO_2 laser beam which produced temperatures of >600 °C. After exposure, the UV spectrum was clearly altered, with the growth of a germanium

oxygen deficiency centre (GODC) band near 240nm (Figure 3.6). The attenuation can be seen to rise from ~20 dB/mm before exposure to ~380 dB/mm after exposure.

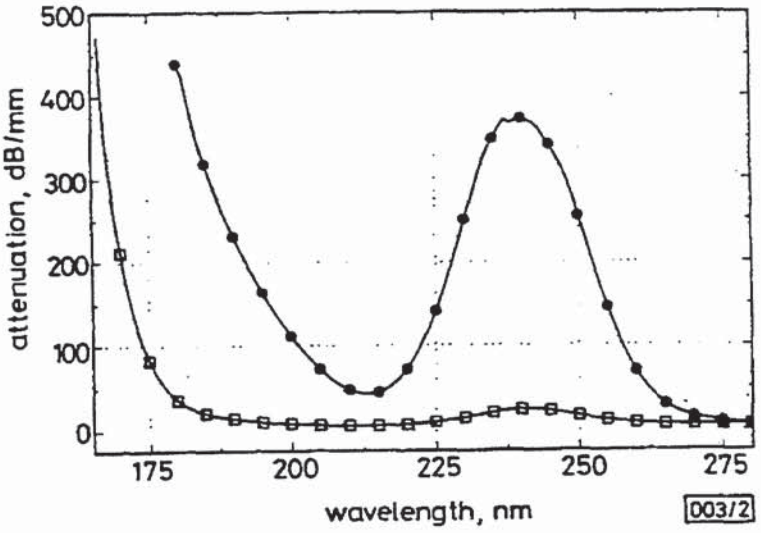

Figure 3.6: UV absorption spectrum of hydrogen loaded germanosilicate glass before and after exposure from a CO_2 laser operating at 10.6 μm [7] (□ represents the spectrum before exposure; • represents the spectrum after 10s exposure)

The increased UV induced absorption in the short wavelength UV spectrum for hydrogen loaded samples was presumed to occur via a combination of thermal and photolytic mechanisms. It was postulated that there is a thermally driven reaction resulting in the formation of (Si)OH and GODCs followed by UV bleaching of the GODCs and hence a change in refractive index. Also postulated was that a photolytically driven reaction between hydrogen and germania forms (Si)OH and associated Ge defect sites.

Following this line of research, an experimental investigation was undertaken to determine whether elevated temperatures could increase the fibre photosensitivity during grating fabrication, producing stronger gratings. Results were obtained for hydrogenated and non-hydrogenated fibre gratings written at both room temperature and at elevated temperatures. A comparison between room and temperature-elevated gratings provides evidence as to whether an increase in writing temperature has any effect on the overall achievable refractive index change. A comparison between hydrogenated and non-hydrogenated gratings is designed to identify whether the addition of hydrogen into the fibre exaggerates this effect.

Any variation in the temperature applied to a fibre grating induces a shift in the Bragg wavelength, due to a change in the grating period caused by the thermal expansion of the fibre and also a change in the core refractive index due to the thermo-optic effect.

The change in Bragg wavelength, $\Delta\lambda_B$ due to a change in temperature of ΔT can be described by [8]

$$\frac{\Delta\lambda_B}{\lambda_B} = (a + \xi)\Delta T$$

Equation 3-3

where a is the thermal expansion coefficient for the fibre, given as 0.55×10^{-6} for fused silica [5], and ξ is the thermo-optic coefficient, of value 8.3×10^{-6} for a germania-doped silica fibre core. The change in refractive index due to the thermo-optic effect is the dominant cause of the Bragg wavelength shift.

3.2.2.2 *Experiment*

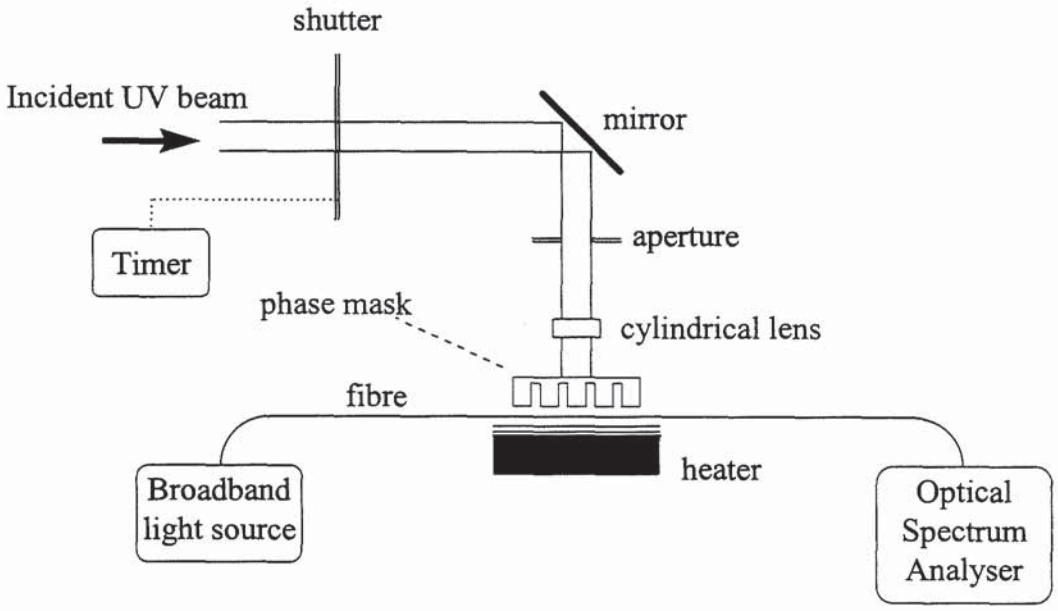

Figure 3.7: Experimental set-up for fabricating Bragg gratings at elevated temperatures

The experimental set-up was a very simple one, as can be seen in Figure 3.7. The expanded beam from a frequency doubled Argon-ion laser was reflected by a set of fixed-position mirrors and focused by a cylindrical lens, through the phase mask, onto the fibre. An aperture placed before the cylindrical lens truncated the beamwidth and its size therefore defined the maximum length of the grating. Initially, a weak grating was written into the fibre under investigation. The phase mask was then removed and the grating exposed to the UV beam for a succession of set time periods. A shutter, connected to an electronic timer, controlled the UV exposure in order to monitor the time for which the shutter was open and thus the total UV exposure. Throughout the experiment, the grating transmission and reflection spectra could be

monitored via an optical spectrum analyser and at the end of each exposure the changes in grating strength and wavelength could be measured. This procedure was repeated until the grating was completely erased. For experiments carried out at elevated temperatures, a heater was placed in close proximity to the fibre prior to exposure and the temperature was allowed to stabilise before any experiments were undertaken. The experimental procedure was then identical to that described above. All the gratings were written in boron-germanium co-doped fibre.

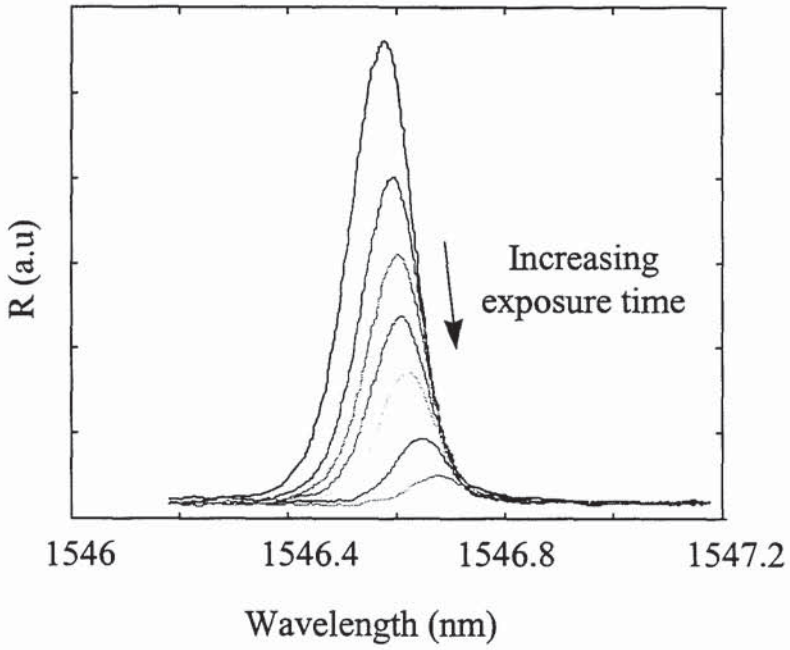

Figure 3.8: A selection of reflection spectra for one grating, illustrating the change in grating profile with increasing UV exposure

For the unhydrogenated fibre, the weak initial grating was written at room temperature by exposing the phase mask/fibre arrangement to the UV beam for 3.68 seconds, at a laser power level of 30mW. The laser was kept at this power level for the entire investigation. Once the phase mask was removed, the grating was then exposed for another 115.47 seconds, until it could no longer be distinguished on the optical spectrum analyser. Figure 3.8 shows a selection of the grating reflection profiles, taken at increasing exposure times. This shows that as the exposure increases, the grating reflectivity decreases and the Bragg wavelength shifts to longer values. From these spectral profiles it is possible to evaluate the refractive index change induced in the fibre, using the Bragg condition, $\lambda_B = 2n_{eff}\,\Lambda$. The effective refractive index of the fibre was taken to be 1.47.

Some of the subsequent results were taken at elevated temperatures; hence the fibre had thermally expanded, increasing the periodicity of the grating. Since all the profiles

were attained at a constant temperature - either room or high temperature - then it has been assumed that the grating period does not change during the course of each individual experiment and hence the Bragg condition can be used to evaluate the refractive index change in both cases. The change in wavelength due to the UV exposure is then taken to be proportional to the change in refractive index and by measuring the Bragg wavelength shift the change in refractive index can be evaluated.

3.2.2.3 Results

3.2.2.3.1 Unhydrogenated Fibre

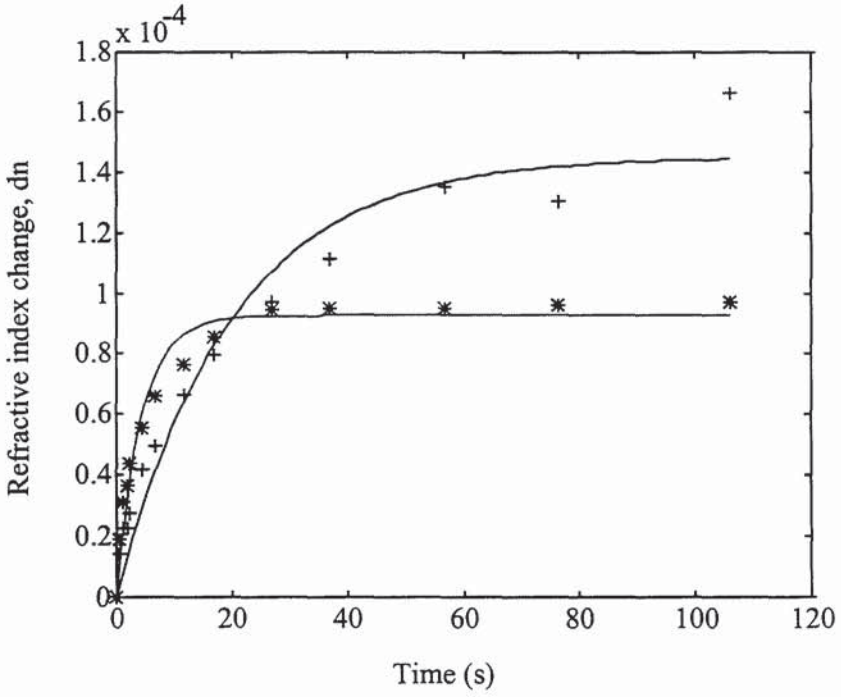

Figure 3.9: A graph showing the rate of change of refractive index for unhydrogenated Boron-Germanium co-doped fibre, at room temperature. Refractive index calculations based on peak wavelength measurements (+) or central wavelength measurements (*). (Solid line indicates theoretical fit to data)

Figure 3.9 shows the rate of refractive index change for the grating detailed previously. The wavelength shift of the grating profile due to UV exposure was evaluated in two ways- either by taking the difference in peak wavelengths or by taking the difference in centre wavelengths, the centre of the grating being defined by its centre of mass. Figure 3.9 clearly shows that the method by which the wavelength is determined produces a vast difference in the calculated refractive index change. A theoretical function was fitted to the experimental data and this is given by the solid

line in Figure 3.9. The function chosen to fit the data was an exponentially decaying function, defined by

$$fit = a(1)\left[1 - \exp\left(\frac{-t}{a(2)}\right)\right]$$

Equation 3-4

where *a(1)* is the maximum wavelength of the grating, either peak or central, *a(2)* is half the total exposure time of the grating and *t* is set of linearly spaced points, taken between the minimum and maximum exposure time.

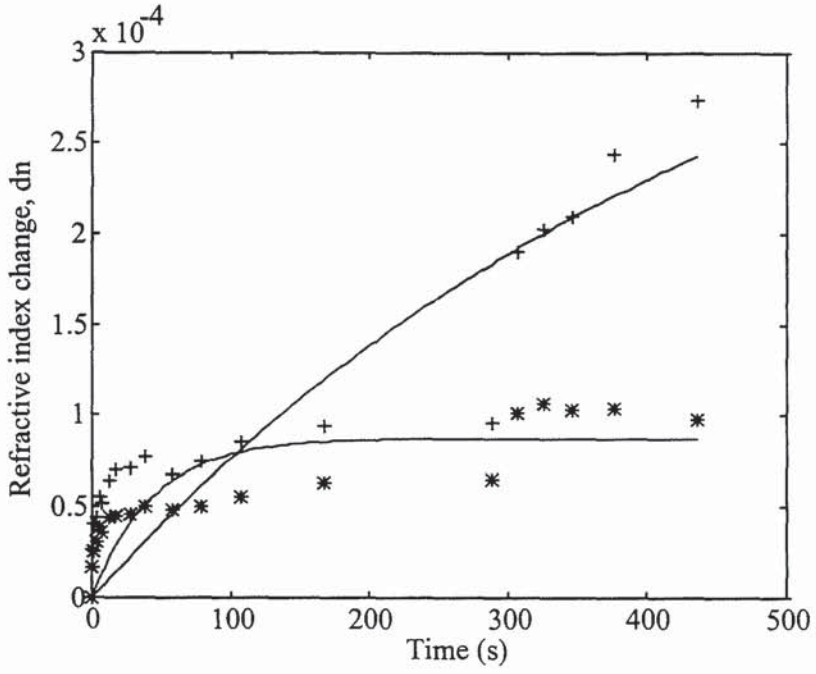

Figure 3.10: A graph showing the rate of change of refractive index for unhydrogenated fibre, held at an elevated temperature. Refractive index calculations based on peak wavelength measurements (+) or central wavelength measurements (*). (Solid line indicates theoretical fit to data)

Figure 3.10 shows the results for a grating written and post-exposed at an elevated temperature. The elevated temperature conditions during the writing process produced a grating at a wavelength 0.62nm higher than for one written at room temperature, due to the increase in grating period described previously.

A comparison of the calculated refractive index changes obtained using the 'central wavelength' and 'peak wavelength' approaches show that although the grating written and post-exposed at a higher temperature did exhibit a larger overall refractive index change for the wavelength changes defined by the peak value, this was not the case

for those calculated using the 'central wavelength' approach. The difference between the peak and central wavelength values is greatest after long exposure times. This is caused by the change in shape of the grating profile, where the grating peak broadens as the reflectivity of the grating decreases, making it more difficult to define a single 'peak' wavelength. So, in this case, the central wavelength approach appears to be more reliable.

From Equation 3-3 it is possible to calculate the temperature which will cause a wavelength shift of this magnitude. Using the values previously given for the thermal expansion coefficient and the thermo-optic coefficient, then a wavelength shift of 0.62nm at a Bragg wavelength of 1550nm gives a change in temperature of +45°C. This temperature increase seems relatively small since the heater had a temperature range of up to 400°C. One proposed reason for this small temperature increase was that the fibre did not absorb the wavelength of the radiation which the heater supplied. This would mean that, despite the heater producing a temperature of up to 400°C, the fibre only reached a temperature equal to that of the air which surrounded it and therefore did not get hot enough to observe any significant increase in refractive index change.

3.2.2.3.2 Hydrogenated Fibre

The results for the grating written in hydrogen loaded fibre, at room temperature can be seen in Figure 3.11. The initial grating was written by UV exposing the phase mask and fibre for 0.81 seconds. Once the phase mask had been removed, the grating was exposed for another 1867.6 seconds. It can be seen that the maximum refractive index change has increased relative to the non-hydrogenated case (c.f. Figure 3.9), but this is to be expected. The function fitted to the experimental data was identical to that used for the unhydrogenated results. In this case it has a far better fit to this set of experimental data points. It can also be seen that the method by which the Bragg wavelength is chosen has less effect on the calculated change in refracted index of the fibre.

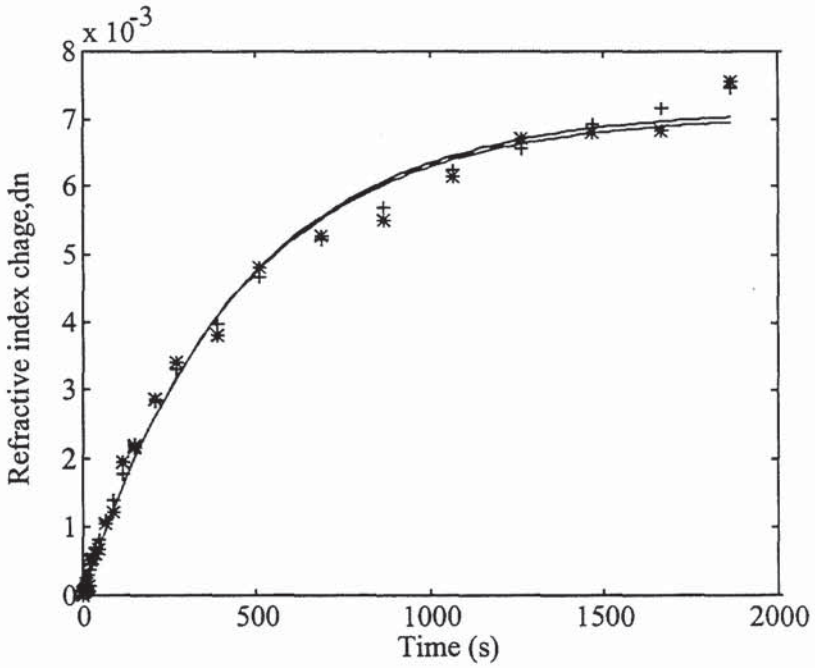

Figure 3.11: A graph showing the rate of change of refractive index for hydrogenated fibre, at room temperature. Refractive index calculations based on peak wavelength measurements (+) or central wavelength measurements (*). (Solid line indicates theoretical fit to data)

Finally, a grating was made in hydrogenated fibre at an elevated temperature. The initial grating was written with a UV exposure time of 1.1 second and the total secondary exposure was for 1174.1 seconds. The combination of elevated temperature and hydrogenation meant that the initial grating was written at a wavelength 0.72nm higher for non-hydrogenated fibre at room temperature. A graph showing the rate of change in refractive index for a sample of hydrogenated boron-germanium co-doped fibre, at an elevated temperature can be seen in Figure 3.12. The results show that the central wavelength approach gives slightly larger values of the change in refractive index, although the difference between the two methods is minimal. Again, the theoretical fit can be seen to closely follow the experimental data.

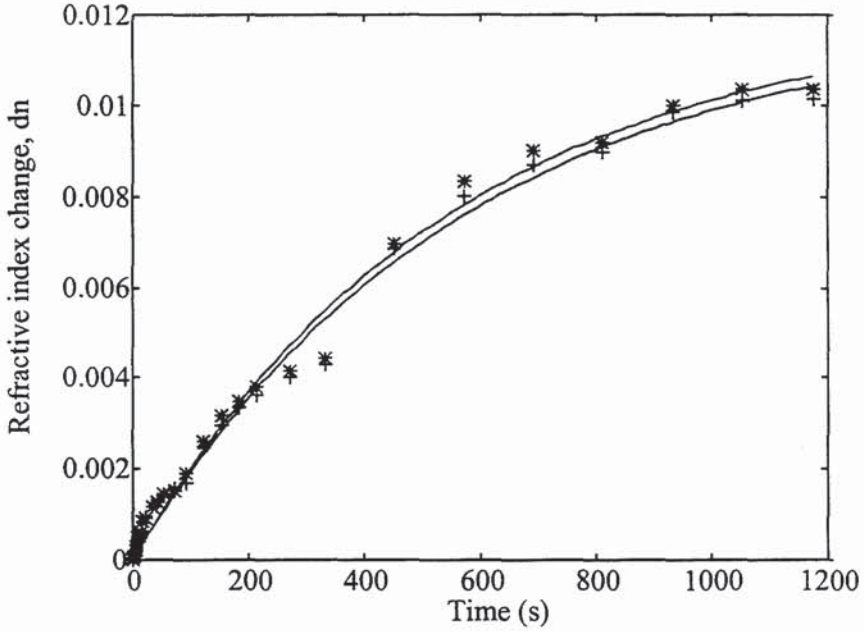

Figure 3.12: A graph showing the rate of change of refractive index for hydrogenated fibre, at an elevated temperature. Refractive index calculations based on peak wavelength measurements (+) or central wavelength measurements (*). (Solid line indicates theoretical fit to data)

It is interesting to note that at elevated temperatures both the results for the non-hydrogenated fibre and those for the hydrogenated fibre exhibit a small discontinuity in the results, in the form of a small jump in refractive index change. In the non-hydrogenated case (Figure 3.10) this occurs at a time of approximately 290 seconds and in the hydrogenated case (Figure 3.12) the discontinuity is at approximately 330 seconds. This has been attributed to a change in fibre alignment caused by the heating effect on the fibre. Throughout the elevated temperature experiments, the alignment of the fibre was periodically checked to ensure that UV exposure was focused onto the core of the fibre. This discontinuity could be due to temperature fluctuations resulting from one such fibre re-alignment.

From these results, it is difficult to determine whether fabricating gratings at elevated temperatures does indeed increase their maximum achievable reflectivity, although this may partially be due to the size of the achieved increase in fibre temperature. In the case of the non-hydrogenated fibre, the elevated temperatures do appear to increase the maximum refractive index change, but only when the results are calculated using the peak wavelength of the grating as the Bragg wavelength. The results using the central wavelength approach both have the same maximum change in refractive index. For the case using hydrogenated fibre, at either room temperature or elevated temperature, the results taken using both the peak and central wavelength

approach for determining the Bragg wavelength give a similar overall refractive index change. There appears to be a small difference in maximum achievable refractive index between the results taken at room temperature and at elevated temperature, of value $\sim 2\times10^{-3}$. Due to the re-alignment problem at elevated temperatures, the reliability of these results comes into doubt and the increase in refractive index is not great enough to warrant this technique being employed as a standard technique for increasing the photosensitivity of fibre.

3.3 Phase Mask Characterisation

To a large extent, the quality of the Bragg gratings produced using the phase mask fabrication technique depends on the quality of the phase mask used. As detailed in Chapter 2, there are a number of parameters that determine the overall characteristics of the phase mask including the groove depth, ridge duty cycle and side wall flatness.

In this section, several techniques have been used to evaluate these phase mask parameters in order to assess their overall quality prior to the fabrication of any Bragg gratings.

3.3.1 Atomic Force Microscopy (AFM)

There are many techniques available for magnifying the detailed features of a surface, such as the periodic etching which makes up a phase mask. It has already been demonstrated, in Chapter 2, that a scanning electron microscope (SEM) can be used after the production of a phase mask to examine its surface features such as groove depth and flatness. The SEM operates in a vacuum and can resolve nanometer features if there is a high atomic number contrast. There are several disadvantages to using this technique, since there is the possibility of destructive effects on the surface of the sample and in order to properly inspect the features of the mask it is usually cleaved in half and neither of these effects are desirable.

This section deals with a different technique of phase mask interrogation- that using a scanning probe microscope (SPM). This method relies on a mechanical probe for the generation of magnified images. An SPM can operate in air, liquid or vacuum to resolve features down to the angstrom level. It is comprised of a sensing probe, piezoelectric ceramic, feedback electronic circuit and computer for generating and presenting images. There are two types of sensors available - tunnelling and force sensors and this section is concerned with the later.

The force sensor, illustrated in Figure 3.13, measures the deflection of a cantilever. A tip is mounted on the cantilever such that, when the cantilever moves, the light beam

from a small laser moves across the face of a four-section photo detector. The amount of motion of the cantilever can be calculated from the difference in light intensity on the sectors. The control of the force sensor over extremely small distances is made possible by the use of a piezoelectric ceramic. A feedback electronic circuit is combined with the probe and piezoelectric ceramic to provide a positioning mechanism that can maintain the sensor at a fixed distance from the surface of the sample. When the sensor moves towards the sample surface, the output of the electronics increases. The differential amplifier compares the increased value from the sensor electronics to the reference value (Vs) and outputs a correction voltage. This then excites the piezoelectric ceramic such that the sensor is pulled away from the sample.

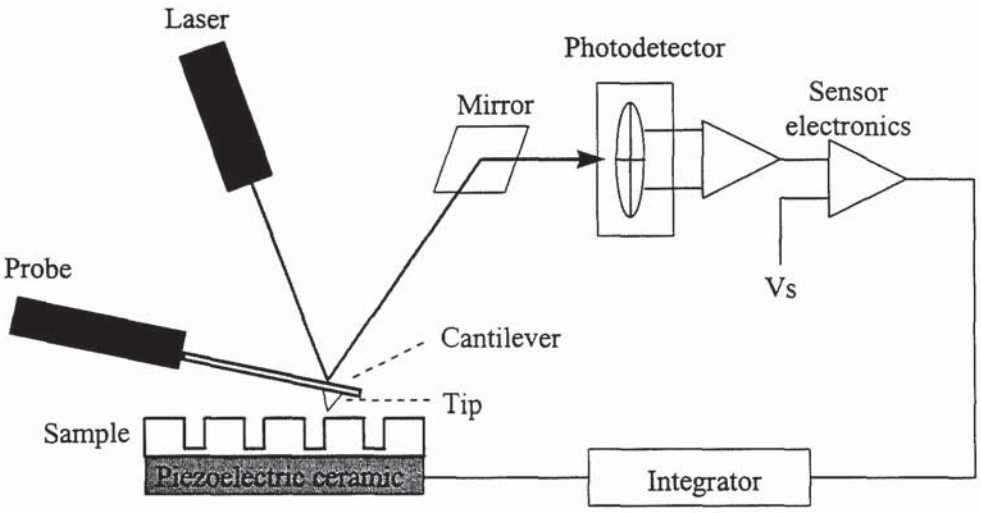

Figure 3.13: The Atomic Force Microscope (AFM) system

Figure 3.14 shows one such image obtained from the atomic force microscope. The uniform periodicity of the phase mask is clearly illustrated in this figure. Several attempts were made to interrogate a phase mask containing multiple phase shifts within its structure. Unfortunately, due to the impurities on the surface of the phase mask and the difficult experienced in aligning the relevant part of the mask in the AFM set-up, the phase shifts remained undetectable using this technique.

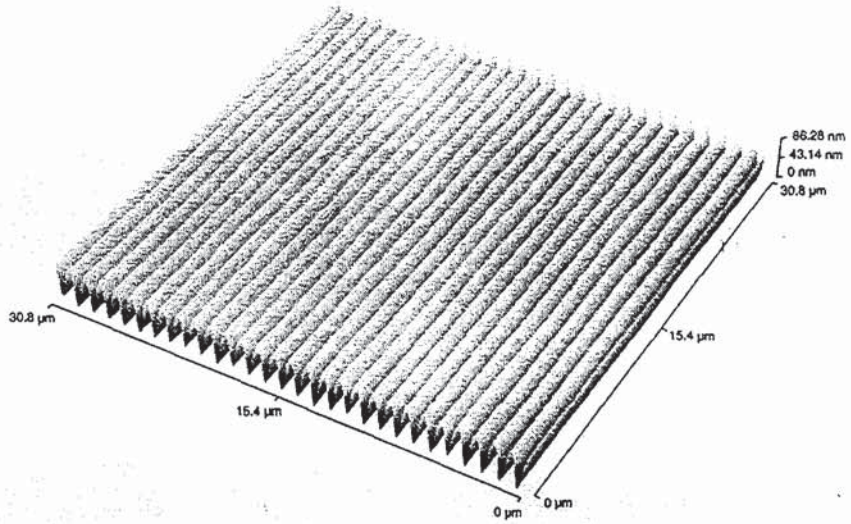

Figure 3.14: AFM image of a uniform period phase mask

3.3.2 Measurement of the Zero Diffraction Order

The diffraction efficiency of a phase mask is important in the fabrication of good quality Bragg gratings. The diffraction efficiency depends on the phase mask surface relief parameters such as the groove depth, ridge duty cycle, groove bottom and side wall flatness. During the phase mask fabrication process measures are taken to maximise the optical output in the first two diffracted orders, since these usually interfere to produce a Bragg grating. The maximum suppression of the zero order diffracted output is achieved by good control of the dry etch depth. However, the suppression of the higher diffracted orders and minimisation of scattering is achieved by concentrating on the reduction of the groove bottom and side wall roughness, as well as controlling the ridge profile and duty cycle during the electron beam patterning.

Once the mask has been produced, it is useful to test its quality prior to grating fabrication. One 'quality' parameter that can readily be measured is that of the zero order suppression. The experimental arrangement to measure the power in the zero diffraction order of the phase mask is illustrated in Figure 3.15. The phase mask is fixed in a holder on the translation stage, in place of the cylindrical lens. A UV optical power meter is placed a short distance behind the phase mask. It is positioned such that it detects the UV light that is not diffracted by the phase mask and has therefore passed though the mask without deviation from its initial direction of travel. The phase mask can then be translated in a direction perpendicular to the UV beam and whilst the beam is on the phase mask pattern (i.e. the etched part of the silica plate)

then the amount of light detected by the power meter gives an indication of the zero order diffraction of that mask.

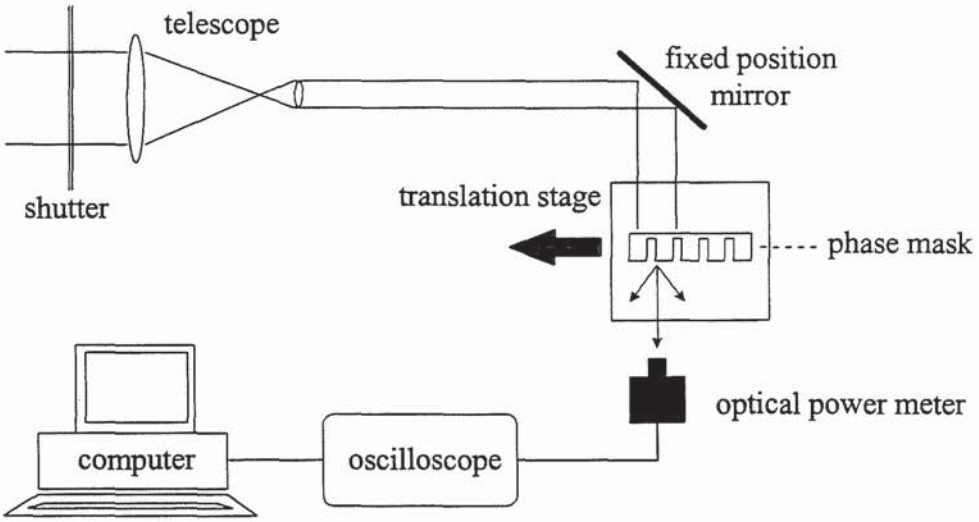

Figure 3.15: Experimental set-up to measure the zero order diffracted UV power from a phase mask

3.3.2.1 Results

Figure 3.16 shows the results of one such zero order measurement. The phase mask being evaluated in this case was one fabricated at Glasgow University and designed to be 3cm in length, having no chirp and therefore producing uniform period gratings at a wavelength of around 1560nm.

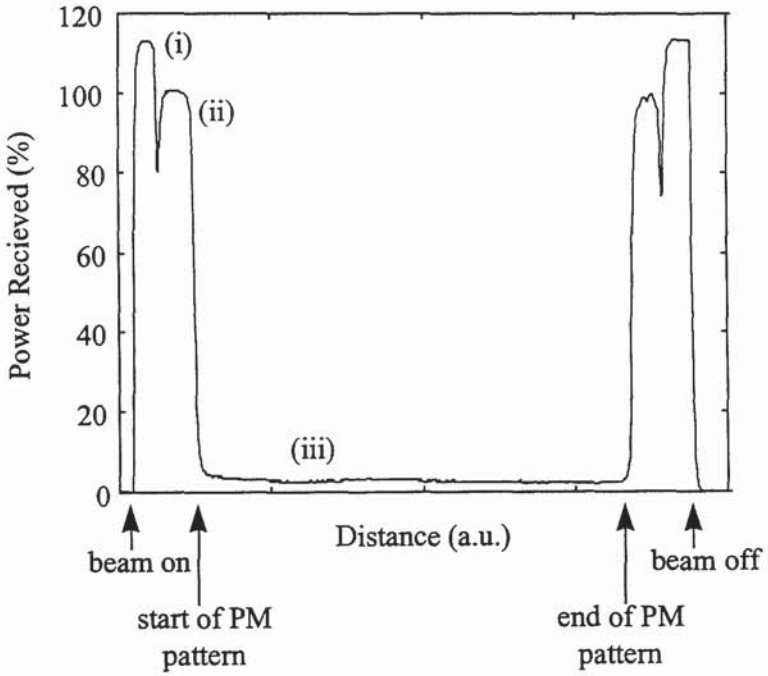

Figure 3.16: Typical zero order result from a uniform period phase mask

After numerous experimental trials, the electron beam writing field size was set at 400μm as standard. The metal charge diffusion layer was chosen to be gold (Au) with a standard polymethyl methacrylate (PMMA) layer for the resist. The dry etch was with CHF_3 for a time of 9 minutes.

A number of conclusions can be drawn from an examination of the zero order measurement shown in Figure 3.16. Figure 3.16(i) indicates the position at which the shutter was opened and thus the UV light could be detected by the power meter. (ii) indicates a drop in received optical power. This is the position at which the silica plate reaches the UV beam and some of the light is either absorbed or scattered by the plate, reducing the amount detected at the power meter. This received power was taken to be the 100% level, since it is the amount of light which is detected by the power meter prior to the etched phase mask pattern reaching the beam and subsequently diffracting some of the light. Position (iii) clearly shows the point at which the phase mask pattern reached the UV beam and the received 'zero order' power drops significantly. The average zero order diffracted power along the 3cm length of the phase mask was calculated to be 2.7%. That is, of the light passing directly through the silica plate, only 2.7% continues undeviated once the beam comes into contact with the phase mask pattern. Commercially available masks aim to achieve a zero diffraction order of less than 5%, so the results from this mask are excellent.

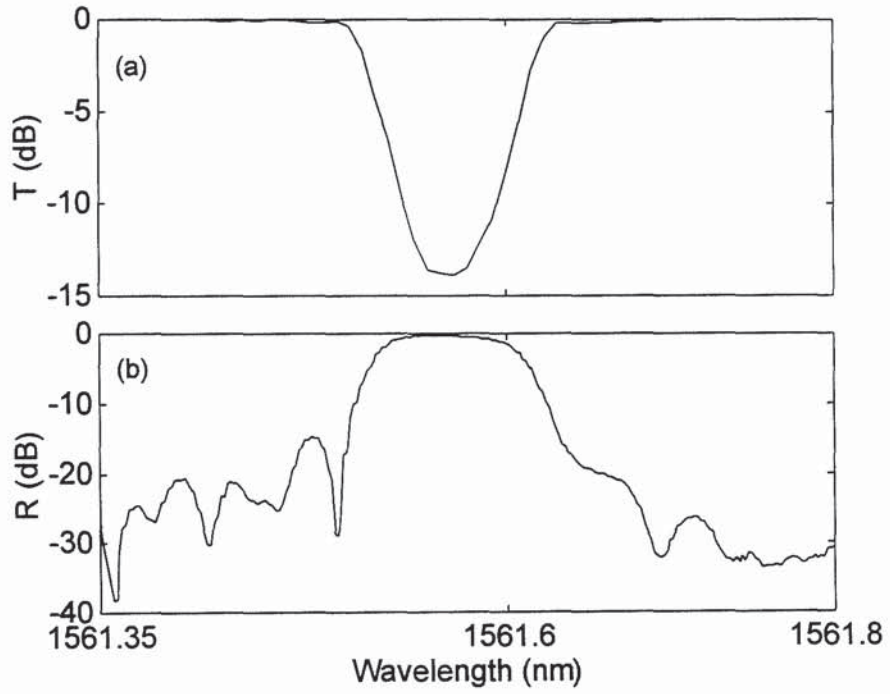

Figure 3.17: A grating produced using a uniform period phase mask, whose zero order measurement is shown in Figure 3.16; (a) Transmission data; (b) Reflection data

Figure 3.17 gives the corresponding spectral measurement for a Bragg grating produced using this phase mask. The Bragg wavelength is 1561.58nm, although this value depends not only on the period of the phase mask, but also on the type of fibre used. The effects of stitch errors anticipated from an EBL-fabricated phase mask are not apparent in the grating reflection spectrum shown in Figure 3.17, nor in a broader scan which was subsequently taken. This simply means that the magnitude of the spectral defects caused by the stitch errors is less than the magnitude of the grating sidelobes. If the spectral sidelobes were suppressed to a greater extent, by apodisation, then the effect of the stitch errors might become apparent in the reflection profile. The process of apodisation suppresses the sidelobes and a detailed explanation can be found later in this chapter. Briefly, apodisation is a means of tailoring the amplitude profile of the grating to optimise the spectral profiles of the filter. This can be done during the UV exposure in one of a number of ways, including the post-processing of a grating to induce a linear change in the refractive index along the length of the grating, the dithering of the fibre or phase mask to alter the visibility of the interference fringes along the length of the grating, or by the use of an apodised phase mask.

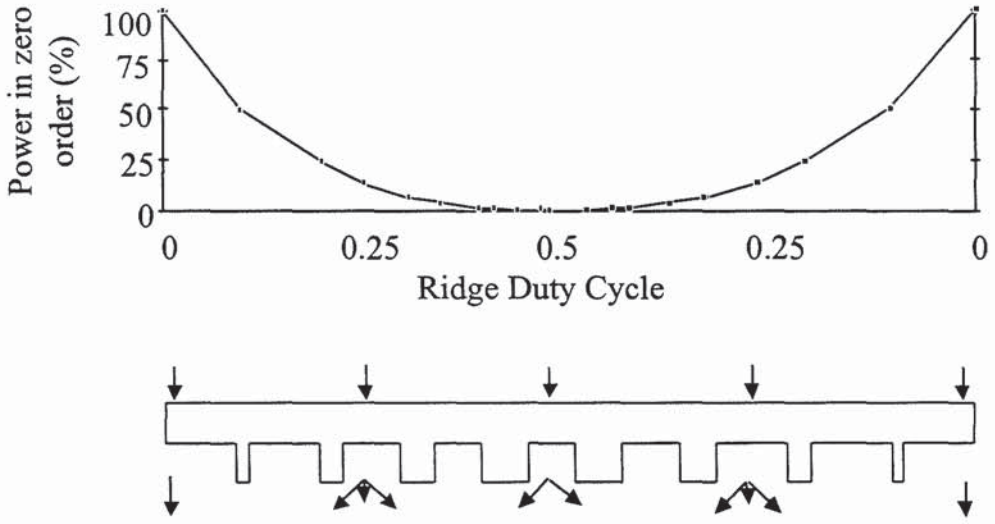

Figure 3.18: The variation in the power received from the zero order of a phase mask with change in ridge duty cycle (top) and the 'apodised' phase mask structure corresponding to this variation (bottom) [9]

Using an apodised phase mask to produce apodised fibre gratings requires a change in the ridge duty cycle of the mask, as illustrated in Figure 3.18. The ridge duty cycle is defined as the ratio of the length to the depth of a periodic ridge. Usually, in the fabrication of a uniform period phase mask, the ideal ridge duty cycle has a value of 0.5. The change in ridge duty cycle produces a change in the corresponding zero order transmission, such that the maximum zero order occurs at the edges of the

mask and the minimum zero order diffraction occurs at the centre of the mask. In this way, an apodised grating can be fabricated via the phase mask alone.

Figure 3.19 gives an example of the zero order result from an apodised phase mask. The phase mask had a length of 2cm and a period of 1.08μm. Again, the mask had no chirp but had an apodisation parameter of 1.5. The apodisation parameter is defined as the maximum value of the ratio between the apodised to unapodised groove.

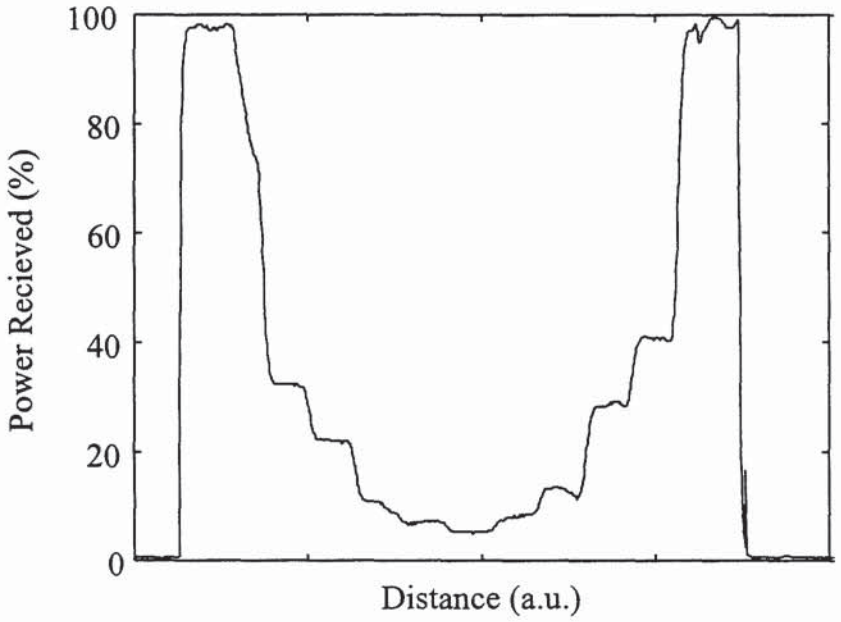

Figure 3.19: The zero order diffraction result from a 'step-apodised' phase mask

Although the design of the phase mask was to produce a near continuous change in ridge duty, an SEM inspection of the mask carried out at Glasgow University indicated that this was not the case and that there was a 'step' change in the ridge duty cycle. In an ideal situation, the change in ridge duty cycle would be continuous, as indicated in Figure 3.18, but obviously the fundamental limitation to this is the resolution of the electron-beam writing process being used during the mask inscription process, which was $1/20^{th}$ of the grating period for masks fabricated at Glasgow University. For this mask, a resolution of 50nm and a beam spot-size of 112nm was used which meant that the change in ridge duty was implemented in discrete steps. This step change is apparent in the zero order measurement shown Figure 3.19. Further analysis determined the stepsize to be around 1mm, which is far bigger than the steps caused by the size and resolution of the beam. The steps apparent in Figure 3.19 were therefore attributed to some fault in the phase mask design program.

The zero order measurement of another apodised phase mask is given in Figure 3.20. This mask was 2.5cm in length, with an apodisation parameter of 1.0 and had a chirp designed to produce an apodised grating of bandwidth 15nm.

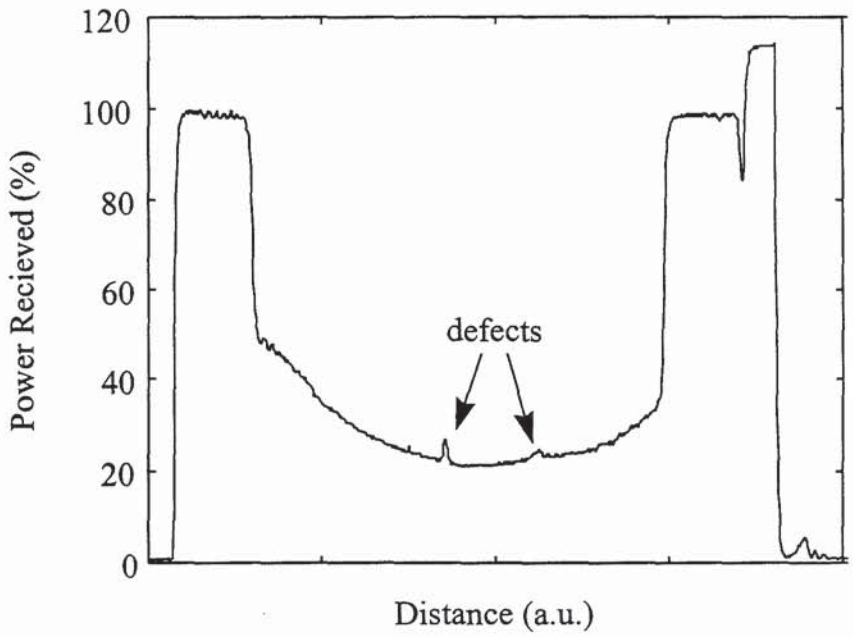

Figure 3.20: The zero diffraction order measurement for a 2.5cm long apodised phase mask

The zero order can be seen to change far more uniformly than for the previous phase mask pattern, indicating that the change in ridge duty cycle is more continuous. The design function for the apodisation was cosinusoidal. Figure 3.20 clearly shows that the zero order measurement is greatest at either end of the phase mask, reducing the first order diffraction components and decreasing the amplitude of the interference fringes at the corresponding places in the grating. The best zero order suppression is achieved at the centre of the phase mask, so producing interference fringes of largest amplitude. This design produces an apodised grating having a variation in the amplitude of the fringes, but with the overall average refractive index remaining constant. Near the centre of the zero order measurement the detected power can be seen to increase briefly. This measurement was repeated a number of times and this strange irregularity was found to be a real but unwanted feature of the mask. The reflection spectrum of a grating produced using this phase mask can be seen in Figure 3.21. This apparently small defect within the phase mask can be seen to have a significant effect on the resulting grating spectrum. It should also be noted that the zero order suppression achieved by this mask is only down to 20% and it is not an ideal mask for grating fabrication.

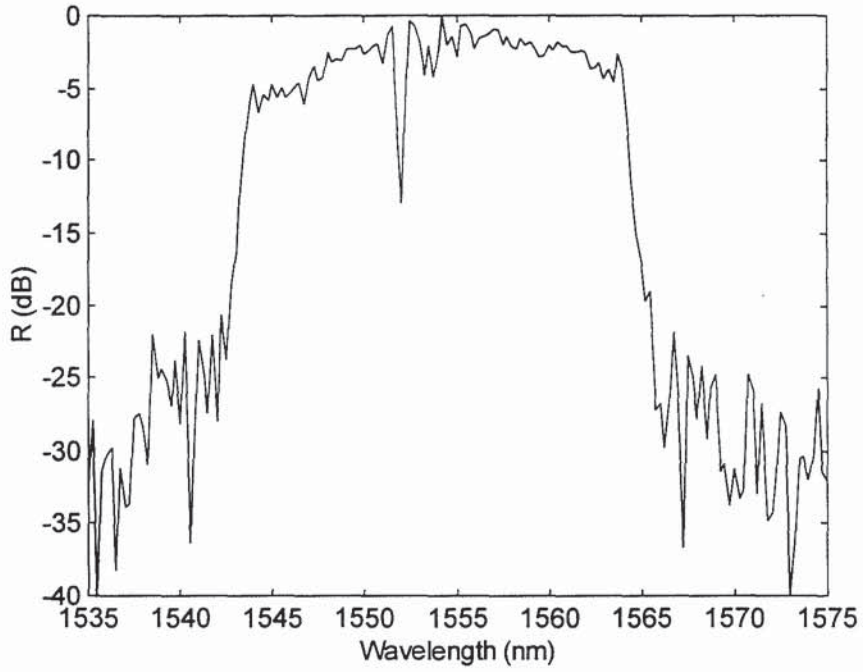

Figure 3.21: The reflection profile from a Bragg grating produced with a chirped, apodised phase mask (Zero order diffraction results for this mask are given in Figure 3.20)

3.4 Grating Characterisation

One of the most important requirements when fabricating gratings is the ability to monitor their growth during UV exposure and to characterise the final reflection and transmission profiles resulting from this exposure. In this work, this has been achieved using the set-up illustrated in Figure 3.22. The tunable wavelength source is a Photonetics TUNICS 1550, with a tuning range between 1480 and 1580nm (at a power of -3dBm) and a linewidth of less than 0.001nm. Light from this source is coupled into the grating via a three-port circulator. The circulator allows the light reflected by the grating to be monitored at the third port. An optical spectrum analyser (OSA) is used to obtain the grating reflectivity and transmissivity data over the desired wavelength range. The light source, which is controlled by a computer, is set to tune over the relevant wavelength range with a nominated stepsize. The peak output from the laser can then be monitored at each wavelength. The optical spectrum analyser is programmed to follow the peak output from the tunable laser and so is able to detect any intensity changes in the received peak power due to the interaction of the laser with the grating. Use of this method of grating characterisation requires that the reflection and transmission be obtained separately. The maximum resolution of the wavelength information is determined by the minimum stepsize of the tunable laser, which is 0.001nm in this case.

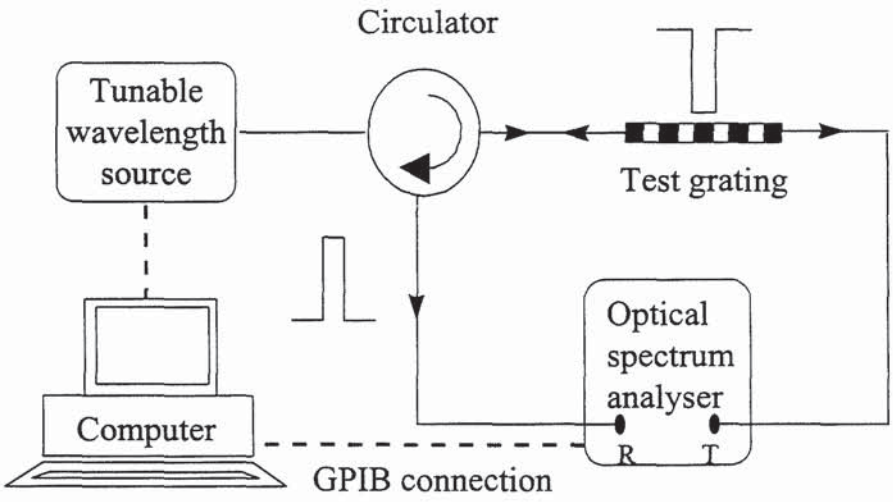

Figure 3.22: Schematic diagram of the experimental arrangement for grating characterisation

Figure 3.23 shows the typical transmission profile of a grating obtained using the characterisation technique described above. The profile was measured between the wavelengths of 1553 and 1557nm, with a stepsize of 0.01nm.

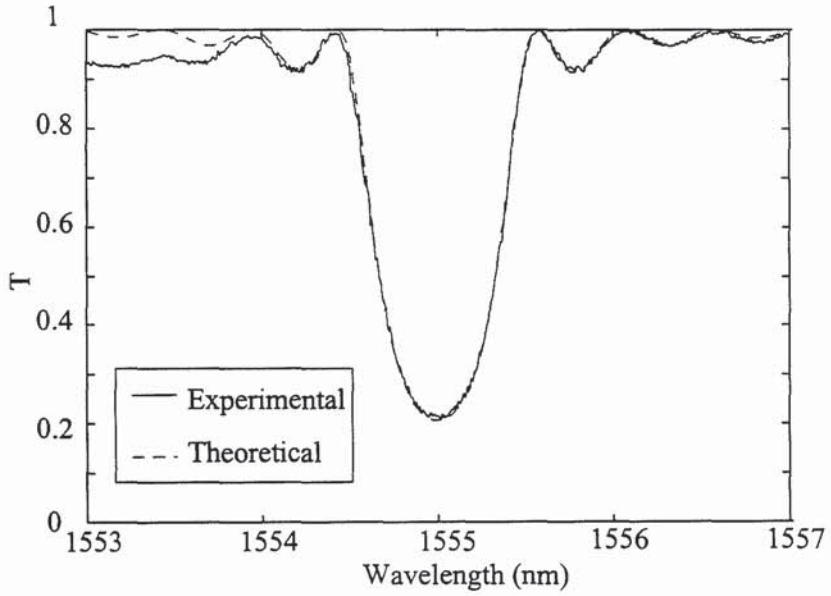

Figure 3.23: Comparison of experimental and theoretical transmission profile of a short Bragg grating: Solid line indicates experimental results; dashed line indicates theoretical results

The grating had an unapodised uniform periodic structure and was of length 1.6mm. The FWHM bandwidth of the device was found to be 0.75nm, with a peak reflectivity of 79%. The modelled transmission profile for this grating is also included in Figure

3.23 and can be seen to be in excellent agreement with the experimental data. There is a small discrepancy between the two sets of results at the short wavelength side of the grating, where the experimental grating experiences short wavelength loss due to modal outcoupling, as was discussed in section 2.7.3. Using the theoretical results enabled the UV induced refractive index change to be evaluated, at 0.93×10^{-3}.

3.5 Grating Apodisation

It is well known that in addition to the central reflection peak, standard fibre Bragg gratings exhibit a series of sidelobes either side of the main peak. These sidelobes are inherent in Bragg gratings and are highly undesirable for most grating applications. In wavelength division multiplexing (WDM) systems these sidelobes induce crosstalk between adjacent channels and in dispersion compensating systems they induce ripples in the dispersion characteristic of a chirped Bragg grating, degrading the system performance [10]. If the envelope of the induced refractive index modulation is given some additional profile, then it is possible to suppress these sidelobes and give the resulting filter a more acceptable shape. The profiling of such a grating is called apodisation.

Over the past few years apodisation has generated vast research interest. A large effort has been in the theoretical design of apodised filters [11,12,13,14] in an attempt to find the ideal filter profile for a grating, although the outcome of this research deduced that the profile chosen to be the optimum ultimately depends on the specific application of the grating. Many techniques have also reported on the actual experimental fabrication of apodised gratings [15,16,17,18]. This work has highlighted the importance of apodisation for the majority of applications employing Bragg gratings, but has concentrated on an overall optimum profile for a grating of unrestricted length. For many applications there is a maximum grating length which is allowed, therefore requiring different filter design parameters. Such applications include the use of Bragg gratings as point sensors and applications where filters are housed in pre-determined packages.

The following sections contain new work examining various apodisation profiles and techniques for applications where there are defined filter length constraints.

3.5.1 Apodisation Techniques for Fibre Bragg Gratings

As previously stated, there have been many methods suggested for the apodisation of phase mask fabricated Bragg gratings. One of the simplest techniques, reported by Hill *et al* [17], involves varying the rate of exposure along the length of the grating, which produces a corresponding variation in the average refractive index, thereby

apodising the grating profile. Unfortunately this technique generates an unwanted chirp along the length of the grating [19]. This is because, in order to impose an apodisation function onto a uniform period grating, the refractive index profiling technique relies on the fact that a variation in the scan speed of the UV beam produces a variation in the average refractive index along the length of the grating. This effectively produces a variation in the coupling coefficient along the length of the grating, producing a corresponding variation in grating reflectivity, and enabling a profiled grating to be fabricated. However, this variation in average refractive index induces a slight chirp onto the uniform period profile due to the Fabry-Perot effect which is generated by multiple reflections from the ends of the grating. Consequently, this apodisation technique will not be detailed here, but is included in Chapter 4, which is concerned with the fabrication of apodised chromatic dispersion compensators.

Alternative techniques for apodisation include the repeated longitudinal stretching of the fibre during grating fabrication [18] which reduces the fringe visibility at either end of the grating, whilst maintaining the visibility at the centre, or a technique which involves moving the fibre as the mask is scanned [20,21]. Storøy *et al* [22] reported on a position weighting technique of apodisation whereby a number of subgratings are made to overlap, thus controlling the local grating strength. Using this method, a 10cm-long grating was fabricated with a truncated sinc apodisation profile.

A different approach is to use an apodised phase mask [15,23] and this has become a popular method of apodisation due to the inherent reproducibility of the resulting gratings. Apodisation is achieved by varying the diffraction efficiency of the mask, which is usually achieved by varying the ridge duty cycle of the mask. J.J. Pan *et al* [24] reported on the use of a commercially fabricated phase mask which had a constant ridge duty cycle of ~50%, but which had a change in phase shift, from π in the middle to zero at both ends of the mask.

3.5.1.1 Phase Mask Dither Technique

The apodisation technique used for this work is based on the dithering of the phase mask during exposure. It provides all the advantages of the techniques described in the previous section, but has increased flexibility that enables a device of any desired profile to be fabricated.

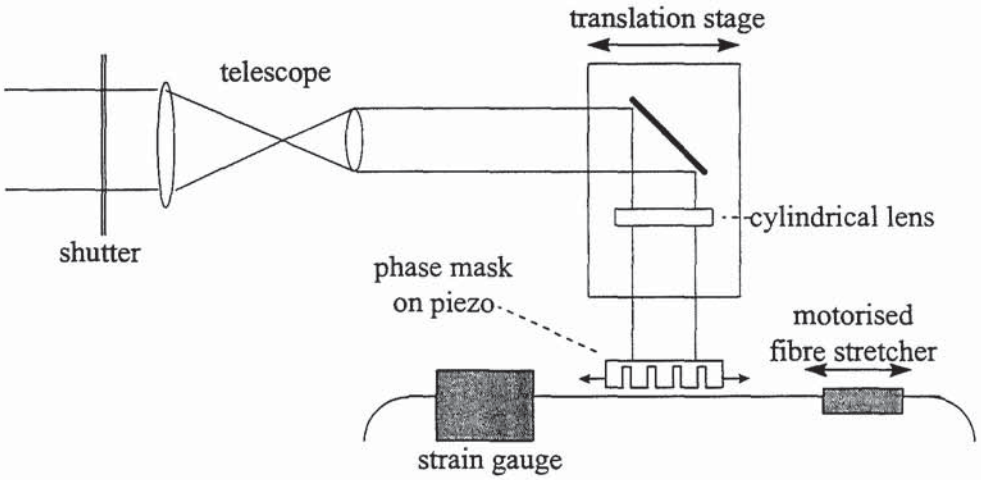

Figure 3.24: A schematic diagram of the experimental arrangement for the fabrication of apodised gratings using a phase mask dither technique

The apodised gratings included in this section were fabricated using a frequency doubled Argon-ion laser, of average power 100mW. Figure 3.24 shows a schematic diagram of the experimental set-up used for the fabrication of apodised gratings. The UV beam diameter was reduced to ~0.5mm in the direction parallel to the fibre and was focused in the perpendicular direction on the fibre by a cylindrical lens. The mirror and cylindrical lens were mounted on a translation stage, which allowed the beam to be scanned along the length of the phase mask/fibre arrangement. The phase mask itself was mounted onto a single piezo, driven to dither the phase mask by using a triangular waveform from a function generator. The desired apodisation profile could then be generated and controlled directly by computer. The magnitude of the dither was varied as the beam scanned the length of the phase mask: maximum dither occurred when the beam was at either end of the mask, and minimum dither at the centre of the mask, for a symmetric profile. The only constraint for a fully apodised grating was that the phase mask had to be moved by exactly half a period at both edges of the grating in order for the fringe visibility to be minimised and no grating to be written. The periodicity is defined by that of the phase mask being used. A uniform period phase mask, written using electron beam lithography and reactive ion etching, was used to fabricate all the gratings for the apodisation. The same patch of mask was used throughout the investigation to ensure that any grating features due to the phase mask, such as stitch errors, were consistent. All gratings were written in boron-germania co-doped fibre, which had been hydrogen-loaded at room temperature at a pressure of 140 bar for several weeks.

3.5.2 Apodisation Functions

There have been many functions suggested for the apodisation of Bragg gratings, including tanh, hamming, blackmann and sinc [13]. Here gaussian, truncated cosine and raised cosine functions are examined for their ability to suppress sidelobes and minimise the grating bandwidth over the allowed filter length.

The aim of the investigation was to examine the various apodisation functions, under specific length constraints, and therefore a selection of 5mm gratings were fabricated with the above mentioned profiles.

3.5.2.1 Gaussian Apodisation Function

The first apodisation profile examined was a gaussian, defined by the equation

$$y = \exp\left(-\left[x\left(2\sqrt{\log 2}\right)\right]^2\right)$$

Equation 3-5

where x is the normalised distance along the grating. This equation gives a profile of unity height and unity width centred at the origin, as shown in Figure 3.25.

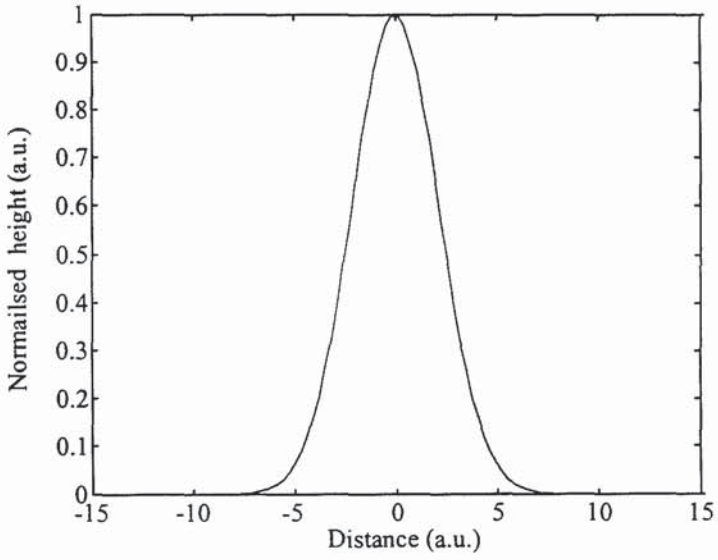

Figure 3.25: Gaussian apodisation profile given by Equation 3-5

Since a gaussian function has infinite length then it is necessary to truncate the profile to some degree. The degree of truncation will obviously have an effect on the final grating profile since, as detailed earlier, the ideal grating profile has a large flat top with moderately steep edges to maximise the length of the grating whilst suppressing the sidelobes. Figure 3.26 shows a set of curves described by Equation 3-

5. The functions are plotted over a length of 5mm, but since the function is of infinite length then it is the function FWHM which is varied to demonstrate the effect it has on the apodisation profile.

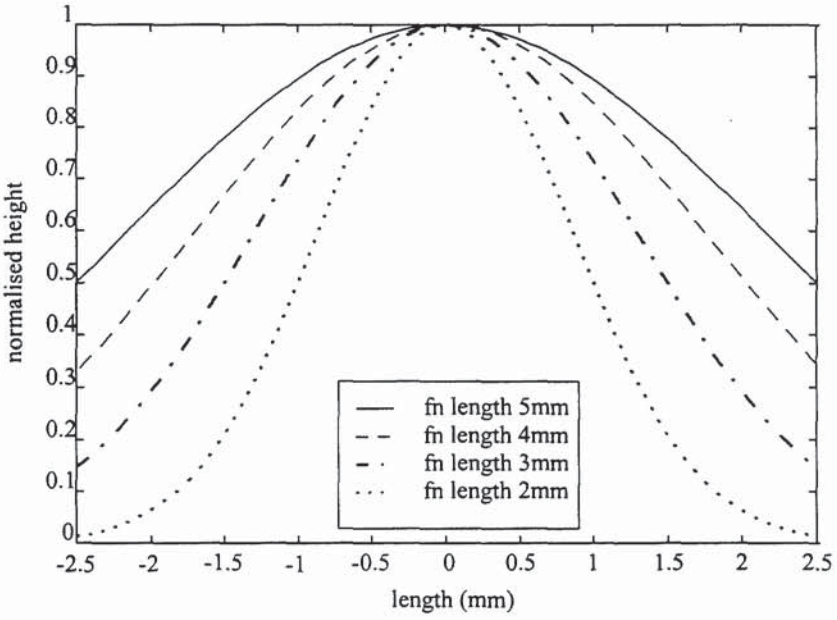

Figure 3.26: Normalised gaussian apodisation function of FWHM varying from 2mm to 5mm

It can clearly be seen from Figure 3.26 that as the FWHM of the gaussian function increases, the truncation of the profile increases substantially. This produces a sharp cut-off at both edges of the profile but provides a flatter top. So, as the function width is increased it is expected that the sidelobes will also increase, although due to the larger flat-top of the profile, the overall bandwidth should decrease.

To confirm this hypothesis it was necessary to fabricate a number of short gratings each apodised with a gaussian profile of different function length. A grating length of 5mm was chosen, in accordance with the lengths required for each grating in the concatenated array filters which are detailed in Chapter 5. For the same UV exposure, a variation in the function width results in a change in reflectivity, due to the change in the effective length of the grating, as was previously described. It is inappropriate to compare grating parameters, such as sidelobe suppression, for gratings of differing reflectivity since the strength of the grating obviously affects the strength of the resulting sidelobes. Therefore, in order to obtain a realistic comparison, the UV dose was adjusted accordingly enabling a set of identical strength gratings to be produced. The reflectivity aimed for was around 95% (13.70 ± 0.55 dB) thus ensuring that the gratings were not saturated but were strong enough to exhibit measurable sidelobes.

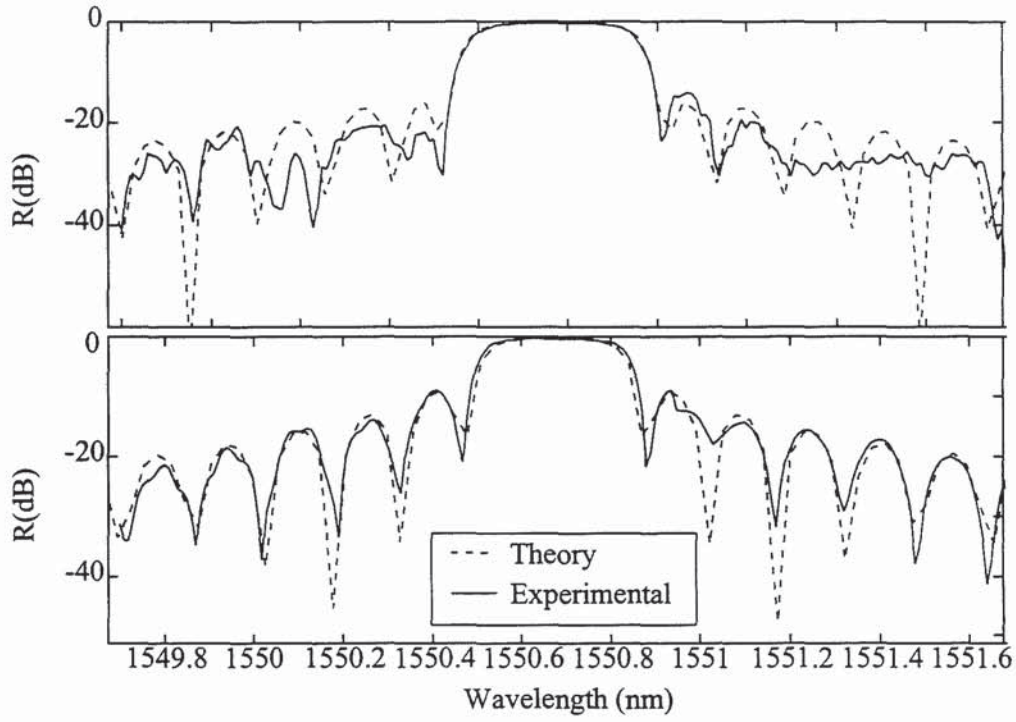

Figure 3.27: Comparison of experimental and theoretical gratings, of length 5mm and apodised with a truncated gaussian profile: (top) Function FWHM 4.2mm; (bottom) Function FWHM 8.3mm

Figure 3.27 gives the results of two gaussian apodised gratings, having function widths of 4.2mm and 8.3mm respectively. The solid line shows the high resolution characterisation of the experimental results, obtained using the tunable laser set-up. The dashed line shows the corresponding numerically calculated profile which was obtained by the integration of the Riccati equation [25]. The experimental results are in good agreement with those numerically calculated. The top profile, of function width 4.2mm, had a measured reflectivity of 14.81dB and a 3dB bandwidth of 47.4GHz (The bandwidth figure is given in units of frequency since this is the most useful format for WDM applications). The sidelobe suppression was calculated as the difference in reflectivity between the central peak and the next biggest sidelobe. Usually it is the first sidelobe which would be taken into consideration, but this is not always valid, as in some cases the first sidelobe is not always the largest. For this grating, the sidelobe suppression was calculated to be 14.01dB. For the bottom profile, having a function width of 8.3mm, the reflectivity was measured to be 14.6dB, with a 3dB bandwidth of 41.1GHz. The sidelobe suppression was only 8.73dB.

From Figure 3.27 it can be seen that the experimental results follow the hypotheses made earlier. Although the top grating profile has the best sidelobe suppression it is clear that the bandwidth of this grating is greater than for the bottom profile and this

may cause problems where gratings are to be employed in applications with limited available bandwidth.

Function FWHM (mm)	Grating reflectivity (dB)	3dB bandwidth (GHz)	1dB bandwidth (GHz)	Bandwidth drop-off (1dB-3dB) (GHz)	Sidelobe suppressi-on (dB)
2.5	12.1	51.1	38.6	12.5	15.4
3.3	14.3	49.9	39.9	10.0	18.8
4.2	14.8	47.4	37.5	10.1	14.0
5.0	13.1	42.3	34.3	8.0	13.2
6.7	14.7	42.3	34.9	7.6	9.5
7.5	10.8	36.2	27.4	8.7	10.2
8.3	14.6	41.1	34.9	6.2	8.7
10.0	15.2	39.9	34.9	5.0	7.8

Table 3-1: Measured values for grating parameters of various gaussian profiled filters

Table 3-1 gives a summary of the experimental results for the set of gratings fabricated to investigate the gaussian apodisation profile. The bandwidth drop-off parameter is the difference between the measured 1dB bandwidth and the 3dB bandwidth. This parameter gives some indication of the steepness of the grating edges, since it is a measure of how quickly the bandwidth drops off between the two defined points.

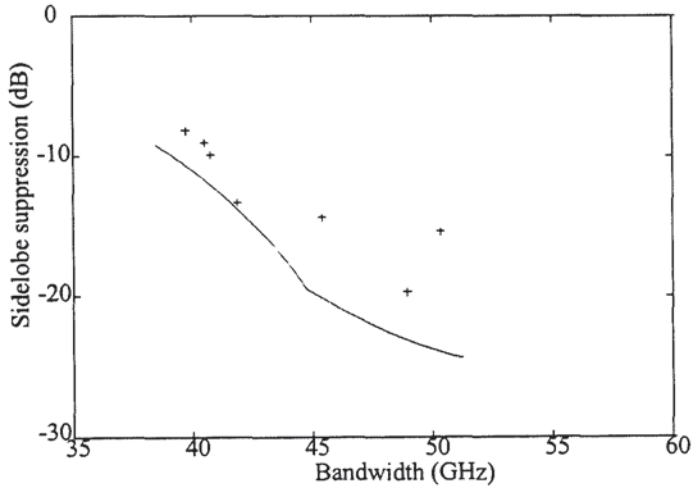

Figure 3.28: A graph showing the change in sidelobe suppression with bandwidth for gaussian apodised gratings, length 5mm: experimental results (+);theoretical results (-)

Figure 3.28 gives the results for the sidelobe suppression with varying bandwidth of the grating. The experimental and theoretical results are compared and show fair agreement. It should be noted that the theoretical results are based on the average experimental reflectivity value. The graph clearly shows the bandwidth compromise which has to be made for increased sidelobe suppression. Essentially, to achieve a high level of suppression in short devices requires a large grating bandwidth and as pointed out earlier, this is not always physically possible.

3.5.2.2 Truncated Cosine Apodisation Function

The cosine function was also examined, in both its truncated and raised forms. The standard truncated cosine used in this experiment can be described by the equation

$$y = \cos(\pi x)$$

Equation 3-6

where x is the normalised grating length. This function can be described by its absolute length, since it is finite, and therefore this is the parameter which is varied in Figure 3.29 to give a set of curves showing the effect that truncation has on the cosine apodisation profile. The function lengths chosen are 5mm, 7.5mm and 10mm and these are plotted over a grating length of 5mm. Again, it is clear that the greater the function length, the flatter the top of the profile is but the sharper the edges of the grating are.

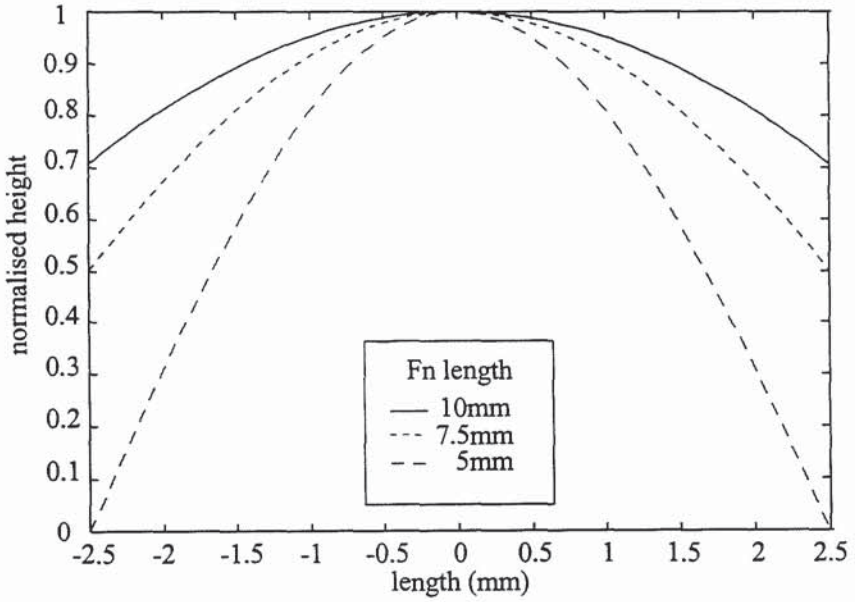

Figure 3.29: Normalised truncated cosine apodisation function of length varying from 5mm to 10mm

Figure 3.30 illustrates two 5mm long gratings apodised with the truncated cosine function given by Equation 3-6. The top figure shows a grating apodised with a cosine of function length of 5mm and the bottom grating of function length 10mm. Again, it can be clearly seen that a shorter function length gives a higher level of sidelobe suppression, but compromises the bandwidth of the grating. The top figure, with a 5mm function length, produces a grating of 3dB bandwidth of 49.9GHz, compared to that of the bottom figure, which has a 3dB bandwidth of only 38.7GHz. The sidelobe suppression for the 5mm function is 17.6dB, whereas for the 10mm function length, the resulting grating has a sidelobe suppression of only 9.7dB. In this case, both of gratings had a reflectivity of ~12dB.

The theoretical and experimental results show good agreement, especially for the function length of 10mm, where the sidelobes are not well supressed.

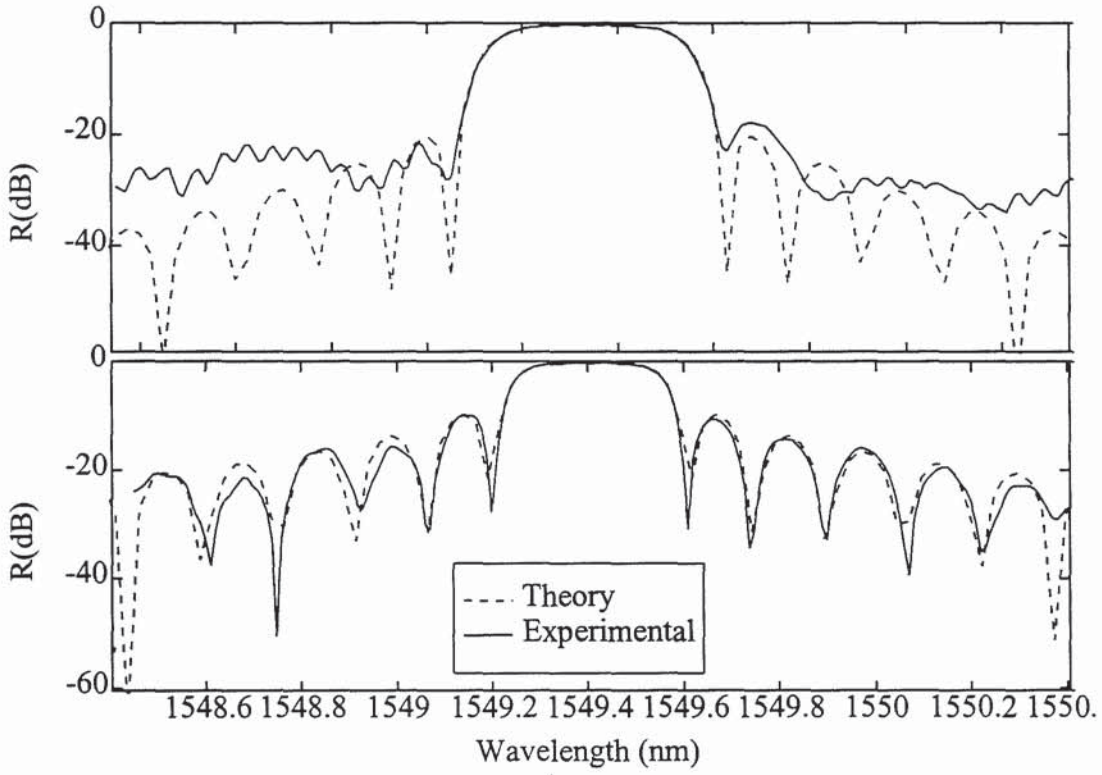

Figure 3.30: Comparison of experimental and theoretical gratings, of length 5mm and apodised with a truncated cosine profile: (top) function width 5mm; (bottom) function width 10mm

A set of 5mm long gratings were fabricated with different function lengths and the resulting grating parameters are summarised in Table 3-2.

Function length (mm)	Grating reflectivity (dB)	3dB bandwidth (GHz)	1dB bandwidth (GHz)	Bandwidth drop-off (1dB-3dB bw) (GHz)	Sidelobe suppression (dB)
5.0	12.1	49.9	39.9	10.0	17.6
5.6	14.5	52.4	42.4	10.0	17.7
6.1	14.2	47.4	37.4	10.0	16.0
7.2	15.6	46.2	38.7	7.5	11.4
7.8	15.4	46.2	38.7	7.5	10.6
8.9	13.7	39.9	34.9	5.0	10.6
10.0	12.4	38.7	31.2	7.5	9.7

Table 3-2: Truncated cosine apodised grating parameters

The sidelobe suppression and bandwidth were then plotted, as shown in Figure 3.31, to examine the effectiveness of the apodisation in suppressing the sidelobes whilst keeping the bandwidth of the grating to a minimum. Again, the theoretical results are calculated using an average reflectivity value and with the bandwidth is defined at the 3dB point. The theoretical and experimental results show good agreement and follow a similar trend to that displayed by the gaussian apodisation function in Figure 3.28.

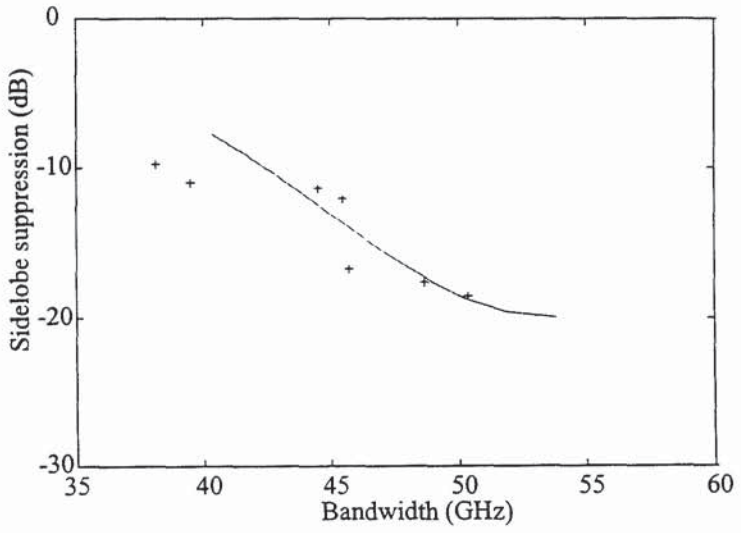

Figure 3.31: A graph showing the change in sidelobe suppression with bandwidth for truncated cosine apodised gratings of actual length 5mm: Experimental results (+); Theoretical results (—)

3.5.2.3 *Raised Cosine Apodisation Function*

The final apodisation profile investigated was that of raised cosine. The equation used to describe this function is given by

$$y = \frac{1}{2} - \frac{1}{2}\sin\left(\frac{1}{2}\frac{\pi\left(\left|x(2+2\alpha-1)\right|\right)}{\alpha}\right)$$

Equation 3-7

where x is the normalised length along the grating and α is the roll-off factor, which can take any value from 0 to 1. In this case the final grating is defined by two parameters - the length of the apodisation function and the roll-off factor. Figure 3.32 shows the effect which changing the apodisation function length has on the apodisation profile. Here the roll-off parameter, α is kept constant at a value of 1 and the length of the function is varied from 5mm to 10mm. The functions are plotted over a length of 5mm to coincide with the total grating length of the structures being fabricated.

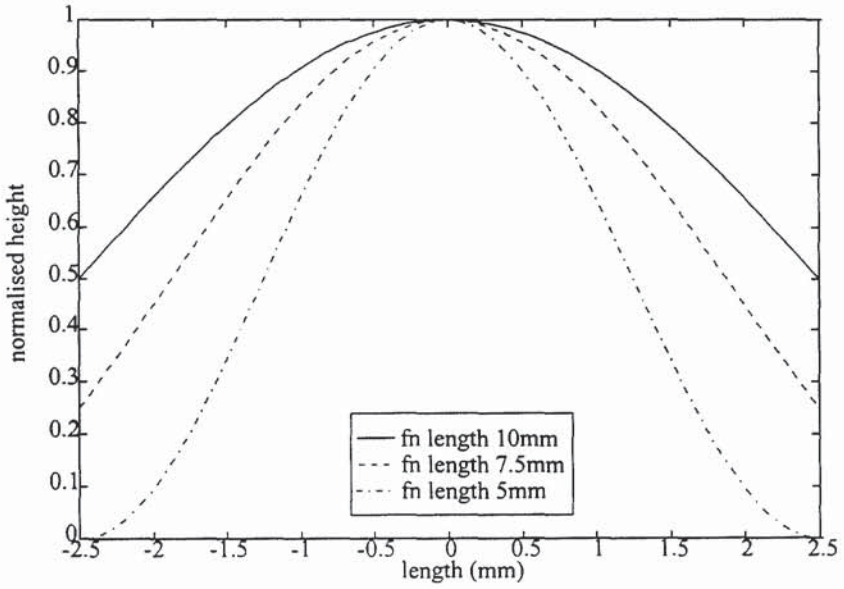

Figure 3.32: Normalised raised cosine apodisation function all of α=1, but varying in function length from 5mm to 10mm

The effect of varying the roll-off parameter alone was also investigated. Figure 3.33 shows various normalised raised cosine profiles, all having a function length of 5mm but with a roll-off parameter varying from α=0 to α=1. The first case, of α=0, clearly represents a top hat function, effectively producing an unapodised grating. Although this profile has a wide, flat top the sides are far too steep to suppress the grating sidelobes.

The last case, of $\alpha=1$, represents a fully raised cosine apodisation function which would result in a broad but well apodised grating.

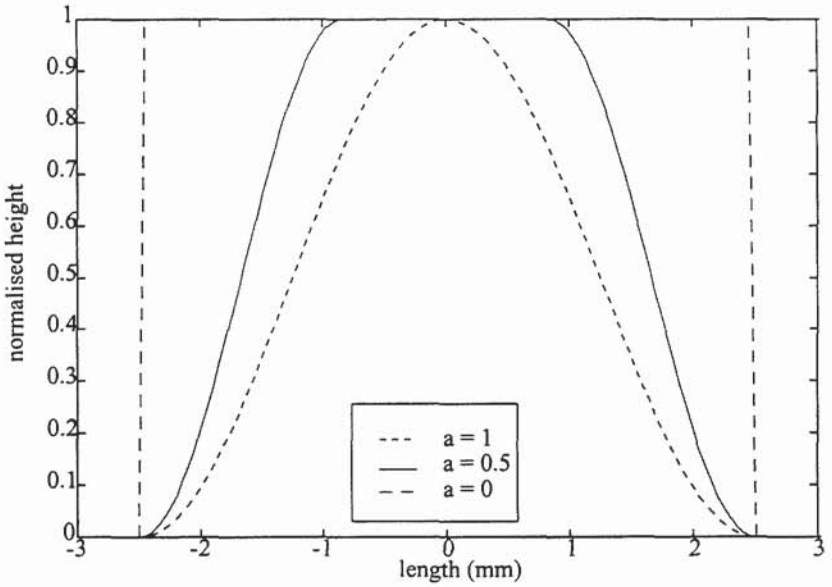

Figure 3.33: Normalised raised cosine apodisation of function length 5mm, but with varying alpha parameter from 0 to 1 ($\alpha=0$ is a top hat function; $\alpha=1$ is a fully raised cosine)

In order to see the resulting structure which is produced from such apodisation, a series of 5mm long gratings were fabricated. All had a function length of 5mm, but the roll-off parameter was varied, as in Figure 3.33. The two extremes of raised cosine apodisation, that for a roll-off value of 0 and 1, are shown in Figure 3.34. As expected, the grating fabricated with a fully raised cosine profile has the best sidelobe suppression, with a value of 20.61dB. This suppression is accompanied by an increase in grating bandwidth from 43.6GHz for $\alpha=0$, to 62.3GHz for $\alpha=1$. The grating apodised with a top hat function ($\alpha=0$) only manages to suppress the sidelobes down to a level of 6.59dB below the main grating peak.

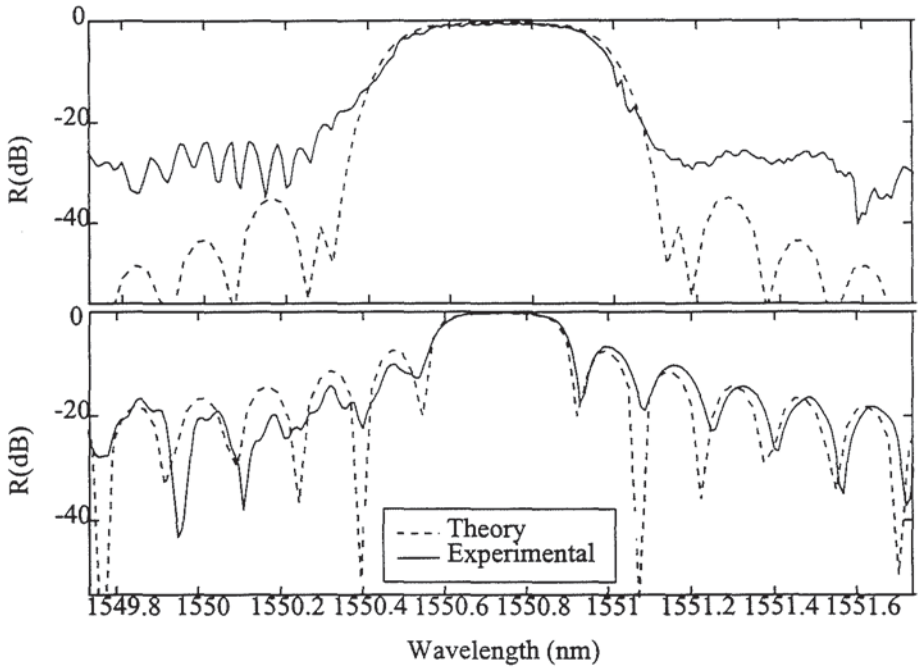

Figure 3.34: Comparison of experimental and theoretical gratings, of length 5mm and apodised with a raised cosine profile: (top) function with roll-off of α=1; (bottom) α=0

The comparison between the theoretical and experimental data shows excellent agreement in the case for α=0. For the case α=1 then there appears to be a limit to the spectral rejection which can be achieved. This limit appears to be around 20dB and below this level a discrepancy is apparent between the experimental and theoretical data. This limitation is attributed to the quality of phase mask used. Any defects in the periodic modulation of the mask, such as stitch errors or dust particles, which accumulate on the surface of the mask, will result in an increase in the overall noise floor of the grating, rendering it impossible to see features below this 'noise' level.

This is confirmed in the results of Figure 3.35, where experimental and theoretical values of the sidelobe suppression are plotted for various roll-off factors. As the value of the roll-off, α, increases, there becomes a clear discrepancy between the expected results and those experimentally achieved. The two final experimental points, of α=0.8 and α=1, converge to a sidelobe suppression value of -20dB, which appears to set a maximum experimental sidelobe suppression level when using this particular phase mask.

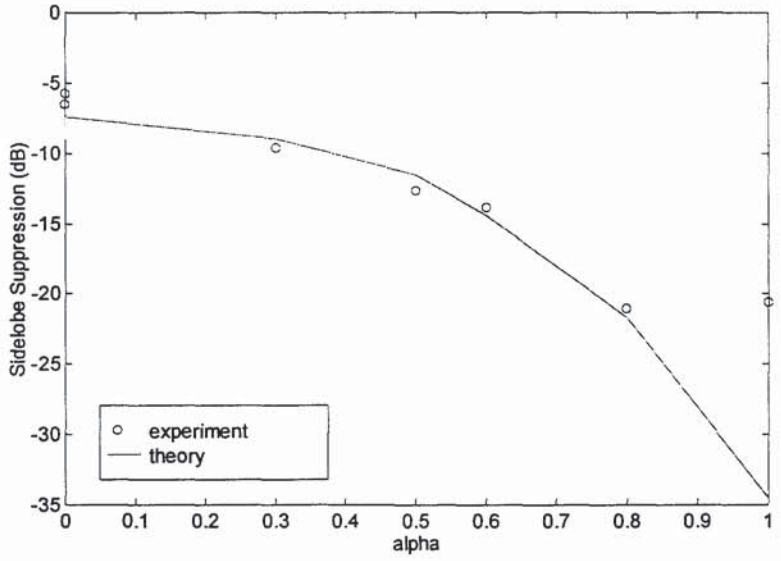

Figure 3.35: The variation in sidelobe suppression with change in roll-off factor, α for raised cosine apodised devices.

A summary of the experimental results obtained for gratings apodised with a raised cosine profile is contained in Table 3-3.

Roll-off (α)	**Grating reflectivity (dB)**	**3dB bandwidth (GHz)**	**1dB bandwidth (GHz)**	**Bandwidth drop-off (1dB-3dB bw) (GHz)**	**Sidelobe suppressi-on (dB)**
0.0	12.3	43.6	37.4	6.6	6.5
0.3	12.8	56.1	43.6	12.5	9.6
0.5	13.9	62.3	43.6	18.7	12.7
0.6	12.4	56.1	46.8	9.3	13.9
0.8	12.0	62.3	49.8	12.5	21.0
1.0	12.2	56.1	38.6	17.5	20.6

Table 3-3: Raised cosine apodised grating parameters

The results for the sidelobe suppression of the raised cosine profiles, with the resulting variation in 3dB bandwidth, are graphically illustrated in Figure 3.36. Both the experimental and theoretical results are shown, where the theoretical results are based on an average reflectivity value. Again the trend is identical for both the experimental and theoretical results although the bandwidth for the experimental results is less than that predicted.

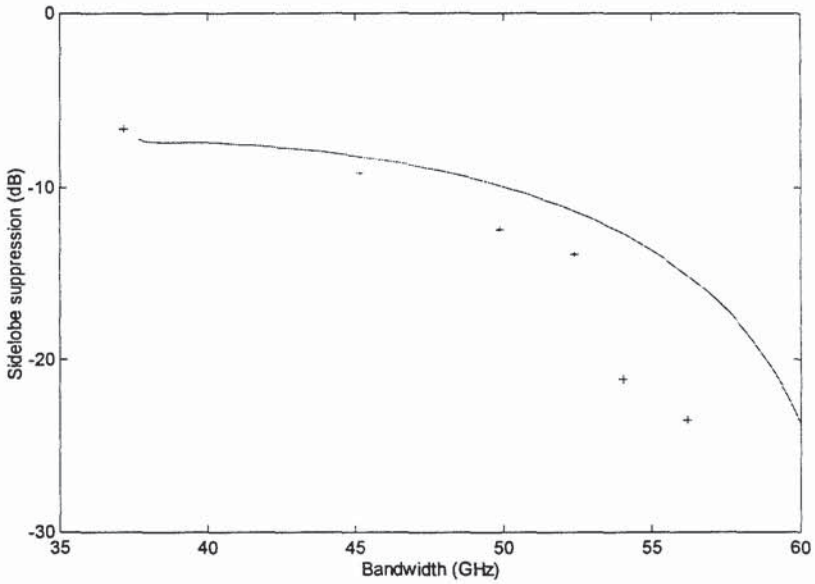

Figure 3.36: A graph showing the change in sidelobe suppression with bandwidth for raised cosine apodised gratings of actual length 5mm: Experimental results (+); Theoretical results (—)

3.5.3 Comparison of Various Apodisation Profiles

In order to determine whether there is an optimum apodisation profile for length constrained gratings it is necessary to compare the sidelobe suppression and bandwidth results for the various profiles. For complete accuracy this is most easily achieved by comparing the theoretical results, as shown in Figure 3.37.

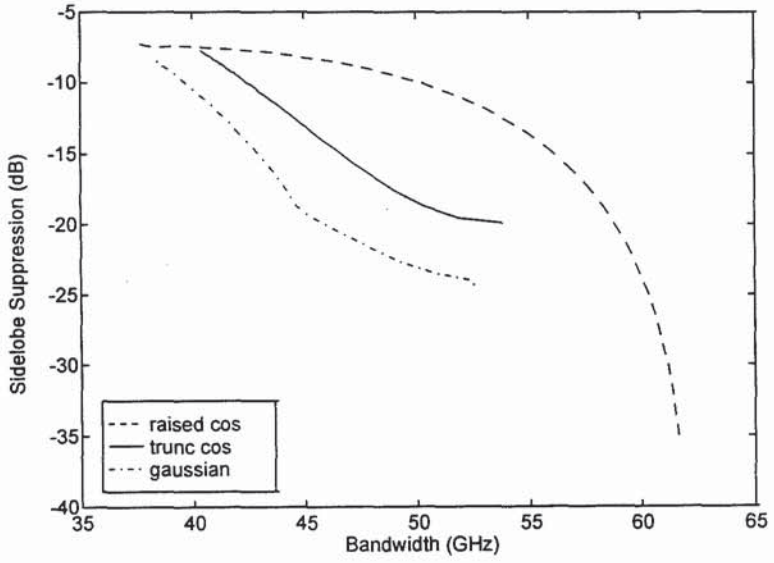

Figure 3.37: Comparison of the theoretical results showing the change in sidelobe suppression with bandwidth for different apodisation profiles

Figure 3.37 clearly shows that for length constrained gratings the optimum apodisation function depends upon the design criteria for the specified device. For a given sidelobe suppression, the 3dB bandwidth of the device varies greatly depending on the apodisation profile chosen. It should be noted that the optimum profile is not necessarily the one that decreases slowly to zero at the grating edges, as was initially anticipated.

The trend of each function is towards a point of convergence, as the bandwidth and sidelobe suppression decrease. This is to be expected, since the function width is increasing, thus increasing the fraction of the exposure length contributing to the grating, but severely truncating the apodisation function used.

For a specific grating length and required sidelobe suppression, the bandwidth of a device apodised with a raised cosine profile is always the greatest. The reasoning behind this is that a raised cosine apodisation profile decreases more slowly to zero at the edges than for the other profiles, reducing the effective grating length and thus increasing the bandwidth. For the case where bandwidth is not an issue then the raised cosine will give the best sidelobe suppression.

3.5.4 Fast Tunable Filter Prototype incorporating a Short, Apodised Bragg Grating

One application where short apodised gratings are essential is as tunable filters, where the grating is required to have a high spectral rejection in addition to being as short as possible, in order in maximise the tuning speed of the device.

This section contains detailed work carried out on the use of a short, apodised Bragg grating as a tunable filter. The results of the research previously described, on the optimisation of a short apodised Bragg grating enabled the design of apodised devices optimised to the tunable filter specification. The result of this work was a tunable filter which has achieved the largest tuning range to date [26].

The tunable filter work contained within this section was carried out by Alessandro Iocco and co-workers, at the Institute of Applied Optics (Swiss Federal Institute of Technology).

3.5.4.1 Background

The majority of fibre Bragg grating applications require devices which are environmentally stable, such that the central Bragg wavelength does not alter under changing strain or temperature conditions. Despite this fact there is an increasing need for gratings whose wavelength can be controllable tuned. Grating tuning is generally achieved using strain and temperature variations.

Straining a Bragg grating changes the Bragg wavelength via the expansion or contraction of the grating periodicity and through the strain-optic coefficient. Changing the temperature at which a grating is held alters its Bragg wavelength through the thermal expansion and contraction of the grating periodicity and through the thermo-optic effect. The Bragg wavelength shift in a single-mode, low-birefringence fibre is given by [27]

$$\frac{\Delta\lambda_B}{\lambda_B} = (1 - p_e)\varepsilon$$

Equation 3-8

where ε is the longitudinal strain and p_e is an effective photoelastic constant. This photoelastic constant can be defined as

$$p_e = \frac{n_{core}^2}{2}\left[p_{12} - \nu(p_{11} + p_{12})\right]$$

Equation 3-9

where p_{11} and p_{12} are photoelastic constants of the strain optic tensor and ν is Poisson's ratio, equal to 0.17 for silica. The photoelastic constant p_e can be approximated to 0.22.

The low temperature sensitivity to thermal variations which optical fibres have, at ~10pm/°C, severely limits the thermal tuning range of a grating, therefore it is better to apply a mechanical stress to the fibre. This can be done in one of two ways, either by tension or compression. Due to the better resistance properties of silica under compression, where it is 23 times stronger than under tension [28], then tunable filters are preferentially designed to undergo compressive rather than tensile strain. Using a technique where the gratings are confined in ceramic ferrules and compressed using a stepper motor, tuning ranges of up to 32nm have been reported [29] although the tuning speed was limited to a few seconds. In a more recent report an unapodised 3mm-long grating was placed in metallic ferrules and compressed using a piezoelectric actuator [30]. This resulted in a quicker setting time, in the order of milliseconds, but only had a tuning range of 15nm. The combination of a short apodised grating and compression tuning using a piezoelectric actuator has recently resulted in a fast tunable filter, working over a linear tuning range of up to 48nm with a maximum tuning speed of 21nm/ms [26]. This is the first report on a fast optical tunable filter prototype working over the EDFA range with a tuning time in the range of milliseconds.

A short apodised grating is required since the response of a tunable filter is monitored by the shift in the reflection peak of the grating and the out-of-band

rejection is required to be as great as possible, ideally greater than 25dB. In order to achieve this, as well as having a grating reflectivity of around 90%, then an apodised grating is required. The maximum length of the device is defined by the housing into which the grating is placed. This restricts the grating length to no more than 2.5mm. A shorter grating is desirable to maximise the tuning speed of the device, although this naturally produces a broader bandwidth grating which makes it harder to track a single wavelength, as is also required from the device. Thus, there are a number of trade-offs that need to be prioritised before the optimum grating can be fabricated.

3.5.4.2 Tunable Filter Description

For this tunable filter device, the grating specification was for a length less than or equal to 2.5mm, with a 3dB bandwidth of 0.7nm and a spectral rejection of 20dB or higher. The reflectivity was required to be around 90%. The apodisation work detailed earlier in this chapter identified a truncated cosine apodisation profile as the optimum for this device specification. Therefore, an apodised 2.5mm grating was fabricated with a truncated cosine profile, using the technique described in Section 3.5.1.1. The function length was defined to be 2.5mm. The grating was written into hydrogenated boron-germanium co-doped fibre, using a small section of a 5cm-long uniform period phase mask. The high-resolution reflection measurement of the resulting grating can be seen in Figure 3.38.

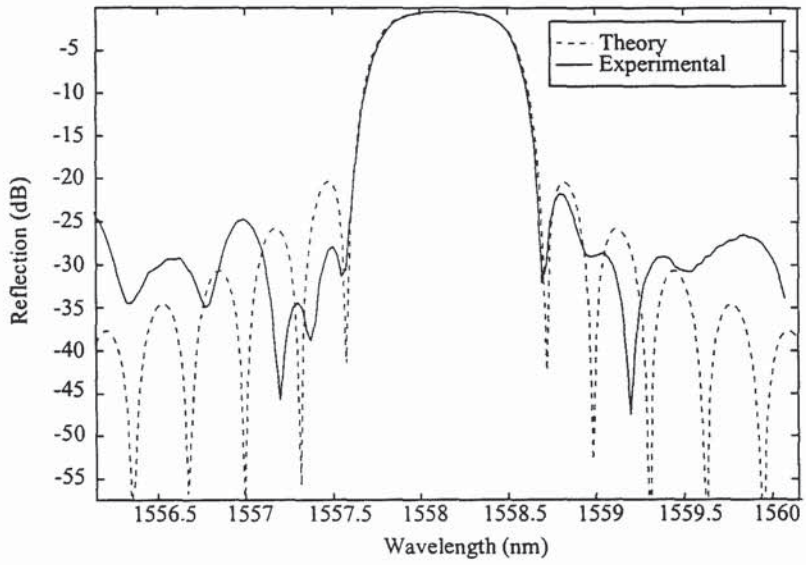

Figure 3.38: Modelled and experimental reflection spectra of a typical grating to be used as a tunable filter

The grating was centred at a wavelength of 1558.1nm and had a reflectivity of 11dB, which corresponds to ~92%. The 3dB bandwidth was measured to be 0.7nm and the spectral isolation was 22dB. The level of isolation achieved can be limited by the noise

generated by the phase mask, from things such as stitch errors and dust on the mask. A comparison of the experimental and modelled results, as shown in Figure 3.38, indicates that in this case the spectral isolation of the device is not expected to be any better than that obtained and so the phase mask is not a limiting factor.

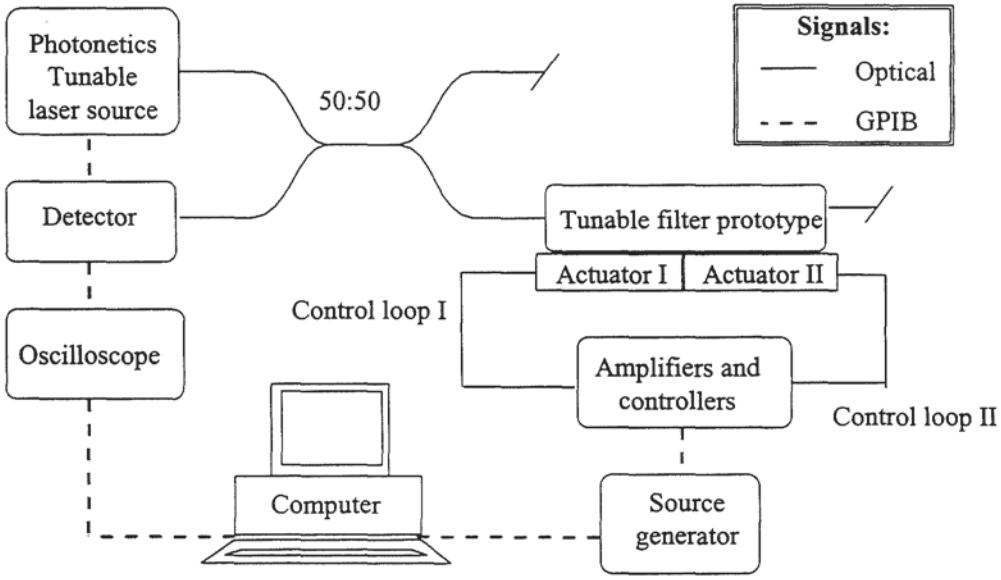

Figure 3.39: Schematic diagram of the tunable filter system (system shown in reflection configuration)

This grating was then employed in the system illustrated in Figure 3.39. The set-up is shown in the reflection configuration. For transmission measurements, the laser and detector can be connected directly to the ends of the fibre under stress. Metallic ferrules hold and guide the fibre once it is placed into the system. In order to strain the grating, piezoelectric stack actuators are used. These each have a maximum displacement of 120μm with a resonant frequency of 5kHz. A mechanical system transmits the piezoelectric actuator displacement to the fibre, via the metallic ferrules, and this strain shifts the Bragg wavelength of the grating. A control loop incorporating a strain gauge allows the position of each actuator to be adjusted individually. High resolution measurements of the change in the peak wavelength of the grating when under strain were obtained using a tunable laser, with a tuning range of between 1460-1580nm and resolution of 1pm. The complete system is controlled by computer.

Only a short length of fibre can be housed within the tunable filter packaging and so it is necessary to know the exact positioning of the grating within the length of fibre to ensure that it is placed in the region that is homogeneously compressed. To achieve this an optical low coherence reflectometry (OLCR) technique was used [31]. The OLCR set-up consists of a Michelson interferometer illuminated with a broadband light source, such as an LED. The grating under interrogation is placed in one arm of

the interferometer and the second arm contains a reference mirror which is set on a stepper translation stage allowing a movement of up to 200mm in order to vary the time delay in the reflected light. Interference fringes are observed if the optical path lengths in the two arms are matched to within the coherence length of the illuminating light source.

3.5.4.3 Results

The 2.5mm-long grating shown in Figure 3.38 was compressed using the previously described technique. The grating was compressed to the maximum displacement for both the piezoelectric actuators, a total distance of 240μm, which resulted in a total peak wavelength shift of -44.7nm, as can be seen in Figure 3.40. The change in 3dB bandwidth as the grating was compressed was measured to be less than ±0.01nm. The spectral rejection of the device remains constant, at a value of ~20dB for the majority of the shift, although the rejection reduces to 16.6dB when under maximum compression. The spectral shape of the grating was found to remain the same during the compression.

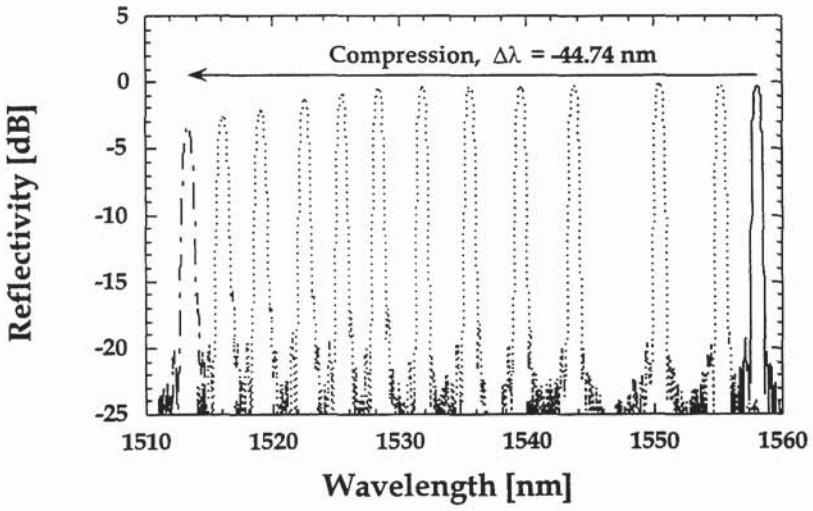

Figure 3.40: Reflection spectra of a 2.5mm-long apodised grating under compression, with a total actuator displacement of 240μm

The change in reflectivity with increasing grating compression was examined more closely, and the measured reflectivity variations with wavelength shift are shown in Figure 3.41. The reflectivity variation was measured to be less that 0.4dB for a wavelength shift of up to 30nm. At this point it can be seen that the grating reflectivity decreases, with a variation of 3.4dB at maximum actuator displacement. This loss is a result of bends occurring in the fibre when it is placed under large

strain. Despite careful alignment of the grating in the ferrules, a reduction in grating reflectivity indicates possible problems in the guiding system of the fibre or from the glue, which can relax and allow bending to occur when under strain.

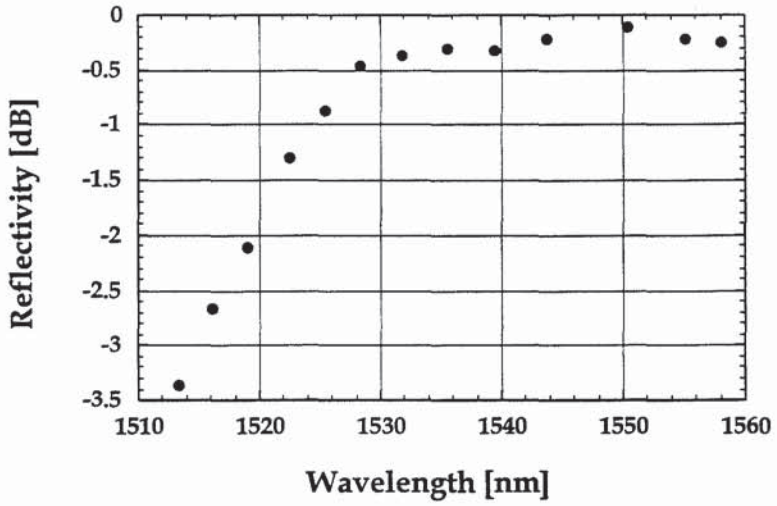

Figure 3.41: The variation in the reflectivity of the central Bragg resonance peak of the grating with increasing applied strain

The relationship between the measured wavelength shift and the piezoelectric actuator displacement can be seen in Figure 3.42. It was found to be a near linear relationship, as would be expected, with a gradient of 0.18nm/μm.

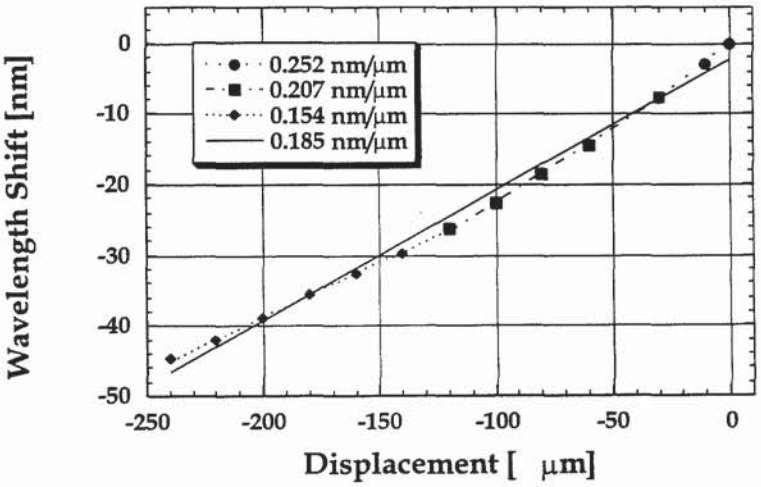

Figure 3.42: The wavelength shift induced by a change in the piezoelectric actuator displacement

The deviation from exact linearity of the gradient was attributed to the fact that the compressed fibre has different buckling minimal energy configurations during the compression process [26]. The fibre was relaxed and re-compressed and this deviation was again observed. From Equation 3-8, the resulting longitudinal strain ε_z, experienced by the fibre was calculated to be 3.7%.

Measurements on the setting time of the tunable filter were also carried out. To do this it is necessary to measure the delay between the external square-wave trigger signal that drives the piezoelectric actuator and the signal from the tunable laser, which is back reflected by the compressed Bragg grating. A square-wave signal is used to reduce the rise times and delays between the driving signal and the piezoelectric actuator response. The delay measurement was found to be accurate to 16ps.

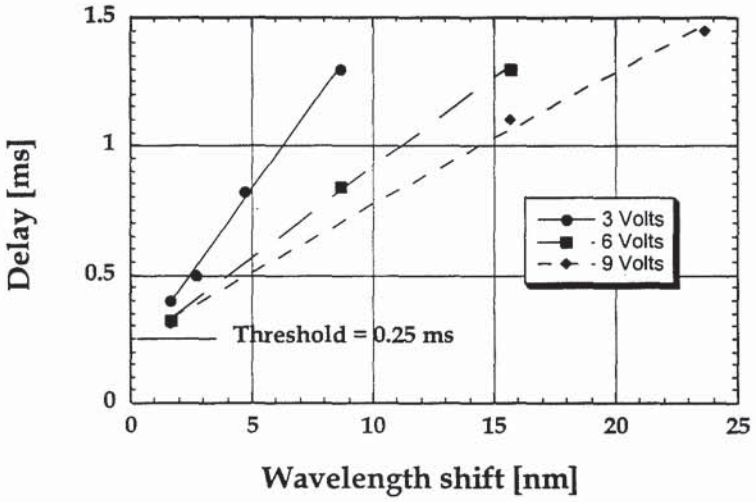

Figure 3.43: Measured setting times for the tunable filter to reach given a wavelength shift

Figure 3.43 shows the measured setting times for various wavelength shifts. The setting time was found to be less than 1.5nm within the total displacement range of one actuator. A threshold value of 0.25 was noted, as can be seen in Figure 3.43. This was thought to be caused by number of things, including the resonant frequency of the piezoelectric actuator which limits its maximum speed to 0.2ms.

3.6 Chapter Summary

This chapter has given details on numerous parameters which can characterise an in-fibre Bragg grating. Section 3.2 included work examining the photosensitivity of the fibre into which a Bragg grating is written. This included measuring the total UV

induced refractive index change in both hydrogenated ($\Delta n = 1.5 \times 10^{-2}$) and non-hydrogenated fibre ($\Delta n = 2.2 \times 10^{-4}$). Other research was concerned with the effect which holding the fibre at an elevated temperature during writing had on the overall fibre photosensitivity. From a comparison of the induced refractive index changes for gratings written at room and elevated temperatures it is unclear as to whether the increase in temperature increases the maximum induced refractive index change. The temperature increase of the fibre, calculated by the shift in Bragg wavelength, was estimated to be ~45°C and this was probably not large enough to obtain conclusive results about the effect of writing-temperature on gratings.

For gratings that are fabricated using the phase mask technique, the mask itself gives the resultant Bragg grating the majority of its characteristics, including Bragg wavelength, chirp and bandwidth and it can also be responsible for noise in the resulting reflection spectrum. Several techniques to examine the quality of a phase mask are detailed in this section. These include the use of Atomic Force Microscopy to get an overview of the periodicity of the mask and zero-order diffraction measurements to check the accuracy of the specified e-beam etching.

Measurement of the reflection and transmission profiles of the resultant phase mask fabricated grating are essential if gratings are to be fully characterised prior to their use. A simple experimental arrangement has been used to obtain high resolution measurements of the grating reflection and transmission profiles. Such a technique is able to resolve spectral features down to a wavelength resolution of 1pm, thus making it possible to examine the level of sidelobe suppression for standard, uniform period gratings. A thorough investigation was then carried out to examine the effect that refractive index profiling had on the final grating structure. Several techniques for apodisation were examined and the most flexible was found to be that employing the dithering of a phase mask to alter the fringe visibility along the length of the grating. This technique was used to apodise gratings with various functions, in order to identify if there was an optimum apodisation profile for length-constrained Bragg gratings.

Following on from this work, an optimised apodised short-length Bragg grating was fabricated to be used as a tunable filter. The prototype achieved results of a tuning range of 44.7nm, with a setting time of 1.5ms. This is the largest tuning range of such a device reported on to date.

---

1 G. Meltz, W.M. Morey, W.H. Glenn, 'Formation of Bragg gratings in optical fibers by a transverse holographic method', *Opt. Lett.*,**14,** (15), 1989, pp.823-825

2 P.J. Lemaire, R.M. Atkins, V. Mizrahi, W.A. Reed, 'High pressure H_2 loading as a technique for achieving ultrahigh UV photosensitivity and thermal sensitivity in GeO_2 doped optical fibres', *Electron. Lett.*, **29**, (13), 1993, pp.1191-1193

3 P.J. Lemaire, 'Reliability of optical fibres exposed to hydrogen: prediction of long-term loss increases', *Opt. Eng.*, **30**, (6), 1991, pp.780-789

4 J. Albert, B. Malo, F. Bilodeau, D.C. Johnson, K.O. Hill, Y. Hibino, M. Kawachi, 'Photosensitivity in Ge-doped silica optical waveguides and fibres with 193-nm light from an ArF excimer laser', *Opt. Lett.*, **19**, (6), 1994, pp.387-389

5 S. Takahashi, S. Shibata, 'Thermal variations of attenuation for optical fibres', *J. Non-Crys. Solids*, **30**, 1979, pp.359-370

6 R.M. Atkins, P.J. Lemaire, 'Effects of elevated temperature hydrogen exposure on short-wavelength optical losses and defect concentrations in germanosilicate optical fibres', *J. Appl. Phys.*, **72**, (2), 1992, pp.344-348

7 R.M. Atkins, P.J. Lemarie, T. Erdogan, V. Mizrahi, 'Mechanisms of enhanced UV photosensitivity via hydrogen loading in germanosilicate glasses, *Electron. Lett.*, **29**, (14), 1993, pp.1234-1235

8 W.W. Morey, G. Meltz, W.H. Glenn, 'Fibre optic Bragg sensors', *SPIE Fibre Optic and Laser Sensors VII*, **1169**, 1989, pp.98-107

9 X. Liu, J.S. Aitchison, R.M. De La Rue, J.A.R. Williams, L.A. Everall, I. Bennion, 'Realization of geometrically apodised phase masks for the production of apodised fibre gratings by UV exposure', *Conf. Lasers and Electro-Optics (CLEO '98)*, **6**, (CFE3), 1998 OSA Tech. Digest, pp.514-515

10 W.H. Loh, R.I. Laming, A.D. Ellis, D. Atkinson, '10Gbit/s transmission over 700km of standard single-mode fibre with a 10-cm chirped fibre grating compensator and doubinary transmitter', *IEEE Photon. Technol. Lett.*, **8**, (9), 1996, pp.1258-1260

11 M. Matsuhara, K.O. Hill, 'Optical-Waveguide filters: design', *Appl. Opt.*, **13**, (12), 1974, pp.2886-2888

12 B.E. Little, C. Wu, 'Window functions for ideal response in distributed feedback reflection filters', *IEEE Photon. Technol. Lett.*, **9**, (1), 1997, pp.76-78

13 D. Pastor, J. Capmany, D. Ortega, V. Tatay, J. Marti, 'Design of apodized linearly chirped fibre gratings for dispersion compensation', *J. Lightwave Technol*, **14**, (11), 1996, pp.2581-2588

14 M. Ibsen, M.K. Durkin, M.J. Cole, R.I. Laming, 'Optimised square passband fibre Bragg grating filter with in-band flat group delay response', *Electron. Lett.*, **34**, (8), 1998, pp.800-802

15 J. Albert, K.O. Hill, B. Malo, S. Theriault, F. Bilodeau, D.C. Johnson, L.E. Erickson, 'Apodisation of the spectral response of fibre Bragg gratings using a phase mask with variable diffraction efficiency', *Electron. Lett.*, **31**, 1995, pp.222-223

16 P.-Y. Cortes, F. Ouellette, S. LaRochelle, 'Intrinsic apodisation of Bragg gratings written using UV-pulse interferometry', *Electron. Lett.*, **34**, 1998, pp.396-397

17 K.O. Hill, S. Theriault, B. Malo, F. Bilodeau, T. Kittigawa, D.C. Johnson, J. Albert, K. Takiguchi, K. Hagimoto, 'Chirped in-fibre Bragg grating dispersion compensators: Linearisation of dispersion characteristics and demonstration of dispersion compensation in 100km 10Gbit/s optical fibre link', *Electron. Lett.*, **30**, 1994, pp.1755-1756

18 R. Kashyap, A. Swanton, D.J. Armes, 'Simple technique for apodising chirped and unchirped fibre Bragg gratings', *Electron. Lett.*, **32**, 1996, pp.1226-1228

19 K.O. Hill, B. Malo, F. Bilodeau, D.C. Johnson, J. Albert, 'Bragg gratings fabricated in monomode photosensitive optical fibre by UV exposure through a phase mask' , *Appl. Phys. Lett.*, **62**, 1993, pp.1035-1037.

20 M.I. Cole, 'Moving fibre/phase mask-scanning beam technique for enhanced flexibility in producing fibre gratings with a uniform phase mask', *Electron. Lett.*, **31**, 1995, pp.92

21 W.H. Loh, M.J. Cole, M.N. Zervas, R.I. Laming, 'Compensation of imperfect phase mask with moving fibre-scanning beam technique for production of fibre gratings', *Electron. Lett.*, **31**, (17), 1995, pp.1483-1485

22 H. Storøy, H.E. Engan, B. Sahlgren, R. Stubbe, 'Position weighting of fibre gratings for bandpass filtering', *Opt. Lett.*, **22**, (11), 1997, pp.784-786

23 J. Albert, K.O. Hill, D.C. Johnson, F. Bilodeau, M.J. Rooks, 'Moiré phase masks for automatic pure apodisation of fibre Bragg gratings', *Electron. Lett.*, **32**, (24), 1996, pp.2260-2261

24 J.J. Pan, Y. Shi, 'Steep skirt fibre Bragg grating fabrication using a new apodised phase mask', *Electron. Lett.*, **33**, (22), 1997, pp.1895-1896

25 H.Kogelnik, 'Filter response of nonuniform almost-periodic structures', *Bell Sys. Tech. J.*, **55**, (1), 1976, pp.109-125

26 A. Iocco, H.G. Limberger, R.P. Salathé, L.A. Everall, I. Bennion, 'Bragg grating fast tunable filter prototype', *submitted to J. Lightwave Technol.*, 1998

27 S.M. Melle, A.T. Alavie, S. Karr, T. Coroy, K. Liu, R.M. Measures, 'A Bragg grating-tuned fibre laser strain sensor system', *IEEE Photon. Technol. Lett.*, **5**, (2), 1993, pp.263-266

28 G.A. Ball, W.W. Morey, 'Tunable Bragg grating fibre filters and their applications', *Conf. Electro-Optcs and Lasers, CLEO '97, Baltimore, USA, Tech. Digest,* (CTuN5), 1997, pp.108-109

29 G.A. Ball, W.W. Morey, 'Compression-tuned single-frequency Bragg grating fibre laser', *Opt. Lett.*, **19**, (23), 1994, pp.1979-1981

30 A. Iocco, H.G. Limberger, R.P. Salathe, 'Bragg grating fast tunable filter', *Electron. Lett.*, **33**, (25), 1997, pp.2147-2148

31 P. Lambelet, P.Y. Fonjallaz, H.C. Limberger, R.P. Salathe, C.H. Zimmer, H.H. Gilgen, 'Bragg grating characterisation by optical low-coherence reflectometry', *IEEE Photon. Technol. Lett.*, **5**, (5), 1993, pp.565-567

4. DISPERSION COMPENSATION

4.1 Introduction

As detailed in Chapter 2, uniform period gratings can have a bandwidth too narrow for some applications and increasing the reflectivity to increase the bandwidth brings with it the additional problem of increased short wavelength loss. A simple solution to this problem is to use a chirped Bragg grating, as illustrated in Figure 4.1. A chirped grating is one where the period changes incrementally along its length and such a linear variation in grating period with increasing device length provides a wider reflection bandwidth, in accordance with the Bragg condition, $\lambda_B(z) = 2n_{eff}\Lambda(z)$ (Equation 2-2). From this it can be seen that for a chirped Bragg grating, where the Bragg wavelength varies linearly with distance, different wavelengths are reflected at different positions along the grating, thus giving the device dispersive properties over its bandwidth. The fabrication of chirped in-fibre gratings was reported on in 1992 by Farries *et al* [1]. In this case, the fibre was polished to remove the cladding and the grating was formed in a layer of photoresist which had been spun onto the fibre. After this the grating can be etched into the silica fibre by ion milling. The method of fabrication used was that of the holographic interference of two beams having dissimilar wavefronts [2], whereby the difference in the wavefronts induces a chirp in the grating period with length. The introduction of an aperiodic structure greatly expanded the potential applications of in-fibre Bragg gratings.

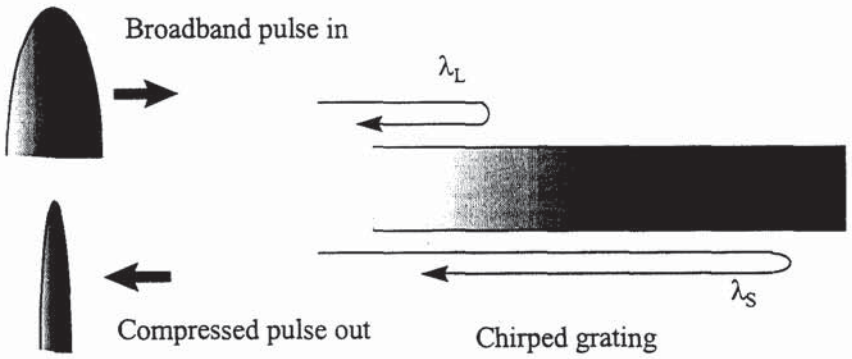

Figure 4.1: A chirped Bragg grating, which reflects short wavelengths at the near end of the grating and longer wavelengths at the far end of the grating

Ouellette [3] proposed that such gratings could be used to compensate for dispersion in high bit-rate transmission systems and this is the most notable application for chirped Bragg gratings at the present time. Much research went into the design and fabrication of chirped fibre gratings for dispersion compensation [4,5,6,7] and thus

gratings have become a serious competitor to using fibre in dispersion compensated transmission systems. This has been proved by the numerous experiments incorporating such devices [8,9,10]. The advantages which fibre gratings have over dispersion compensating fibre (DCF) is their small size, in comparison to the lengths of dispersion compensating fibre which are required to compensate for the same propagation distance, and the potential for gratings to have lower overall loss than their fibre counterparts. Chirped fibre Bragg gratings have not yet achieved propagation distances equivalent to those using DCF, but have shown the potential to compete with DCF and with the recent advances in grating technology, gratings could become the method of choice for dispersion compensation. The delay required in order to compensate for a several kilometres of standard fibre, having a dispersion of 17ps/nm/km, is large and this leads to the requirement for long Bragg gratings. This is an issue which has recently been addressed, with the extension of existing fabrication technologies to produce gratings of ultra-long length [11,12,13].

The group delay dispersion of a chirped grating is given, in Chapter 2, by the approximation

$$D = \frac{2n_{eff}L}{c\,\Delta\lambda}$$

Equation 2-16

where n_{eff} is the effective refractive index, L is the grating length, c is the free-space velocity and $\Delta\lambda$ is the difference in wavelengths reflected by the two ends of the grating. This provides a simple relationship between the required dispersion compensation and the length of grating which will provide this, and is a key equation in dispersion compensating work.

This chapter contains work carried out to design and fabricate chirped fibre Bragg gratings for chromatic dispersion compensation. Detailed in Section 4.2 is a high resolution technique used to characterise dispersion compensating gratings and this is the technique used to measure all subsequent gratings in this chapter.

Also detailed are a number of fabrication techniques utilising different phase masks. A uniform period mask is employed in a novel technique which involves refractive index profiling the grating using a dual scan and results in an apodised, chirped structure. Following the recent advances in phase mask fabrication, a second technique involving a pre-chirped phase mask is described. Although this technique is not as flexible as that previously described, the inclusion of a chirped phase mask has the advantage that the fabrication of chirped gratings becomes highly reproducible.

As transmission systems move to higher bit rates then the compensation of higher orders of dispersion becomes an issue. This chapter includes the first work done on designing and fabricating chirped gratings for quadratic dispersion compensation.

Section 4.5 details an experiment assessing the performance of a chirped grating in a standard fibre transmission system. It highlights potential problems in real systems which incorporate dispersion compensating gratings. Section 4.6 goes on to address such problems, looking at the ways of minimising polarisation mode dispersion in gratings by making changes to the fabrication process.

4.2 Characterisation of Chirped Gratings

There have been numerous reports on techniques to measure the dispersion characteristics of a chirped fibre grating [14,15]. The experimental arrangement used to obtain high resolution spectral measurements is illustrated in Figure 4.2.

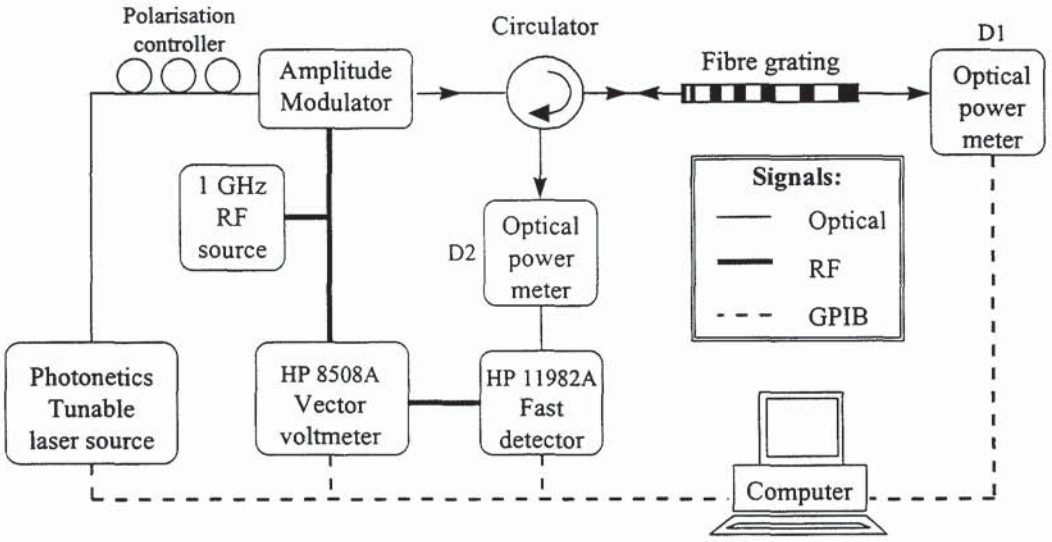

Figure 4.2: Schematic diagram of the experimental arrangement to measure the transmission, reflection and dispersion characteristics of in-fibre Bragg gratings

The light source used is a Photonetics Tunics 1550 tunable laser, with a tuning range of between 1480-1580nm (at a power of -3dBm). The laser can be tuned in wavelength steps of 0.001nm and this value sets the minimum tuning wavelength value for subsequent reflection and transmission measurements. The maximum resolution for the tuning wavelength when using the 1GHz modulator at a wavelength of around 1550nm is governed by its bandwidth, thus the maximum resolution has a value of 0.008nm. The light from the tunable laser is coupled to the grating under investigation via a three-port optical circulator. At this point the light transmitted through the grating can be detected by an optical power meter (D1), to give the

transmission profile of the grating. Likewise, the reflected signal can be obtained via a second optical power meter (D2), placed at the output of the third port of the circulator. Figure 4.3 shows a typical high resolution reflection and transmission measurements obtained using this set-up. The grating characterised in Figure 4.3 is a 1cm-long uniform period grating, having a reflectivity of 97% and a FWHM bandwidth of 0.17nm. Both the reflection and transmission measurements were made with a wavelength stepsize of 0.001nm, over a range spanning from 1550nm to 1550.7nm.

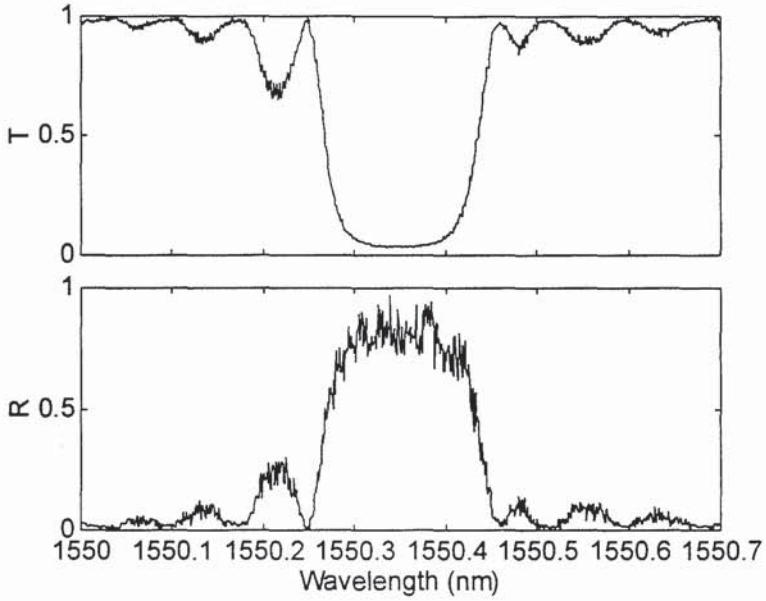

Figure 4.3: Typical high resolution reflection and transmission measurements of a 1cm-long Bragg grating

To obtain the grating dispersion characteristics, a more complex experimental arrangement is required. The output from the tunable laser is amplitude modulated by a 1GHz fixed frequency source. This signal is reflected by the grating and detected by a fast photodetector, which converts the optical signal into an electrical one. The vector voltmeter then compares phase of this electrical signal to the reference phase from the 1GHz modulator. By measuring the change in phase of the signal as the tunable laser is scanned across a range of wavelengths, then the time delay due to grating dispersion can be calculated using

$$\Delta t = \frac{\delta\phi}{2\pi f}$$

Equation 4-10

where $\delta\phi$ is the change in phase and f is the frequency of modulation - 1GHz in this case. The dispersion is then obtained by calculating $\frac{d(\Delta t)}{d\lambda}$ i.e. calculating the gradient of the graph of delay against wavelength, over the wavelength range concerning the grating.

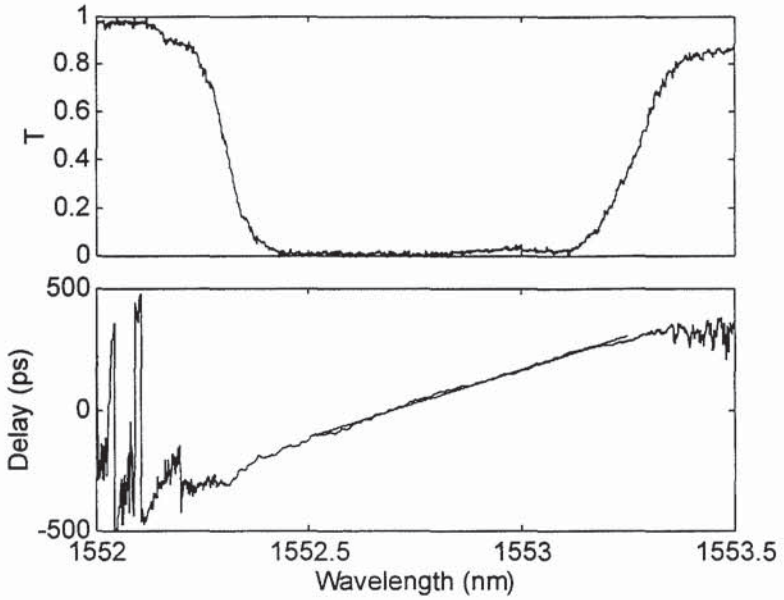

Figure 4.4:Typical high resolution transmission and dispersion measurement of a chirped Bragg grating

Figure 4.4 shows the high resolution transmission and dispersion measurements of a typical chirped Bragg grating. In this case, the grating is 5cm-long, with a FWHM bandwidth of 0.98nm. As was detailed above, the group velocity dispersion of the grating can be calculated from the gradient of the delay graph. A linear fit was superimposed onto the delay against wavelength graph, over the wavelength range concerning the grating and thus the dispersion was calculated to be 552ps/nm.

4.3 Methods of Fabricating Chirping Gratings

4.3.1 Refractive Index Profiling using the Dual Scan Technique

There have been reports of a number of methods of fabricating chirped in-fibre Bragg gratings, including fibre deformation [16], tilting of the fibre [17], and a stretch and write technique [18]. The technique employed in this section of the thesis is based on the double exposure of the fibre, described by Hill *et al* [19] in 1994. This technique

involves the scanning of a uniform period phase mask to fabricate a long in-fibre Bragg grating, as illustrated in Figure 4.5.

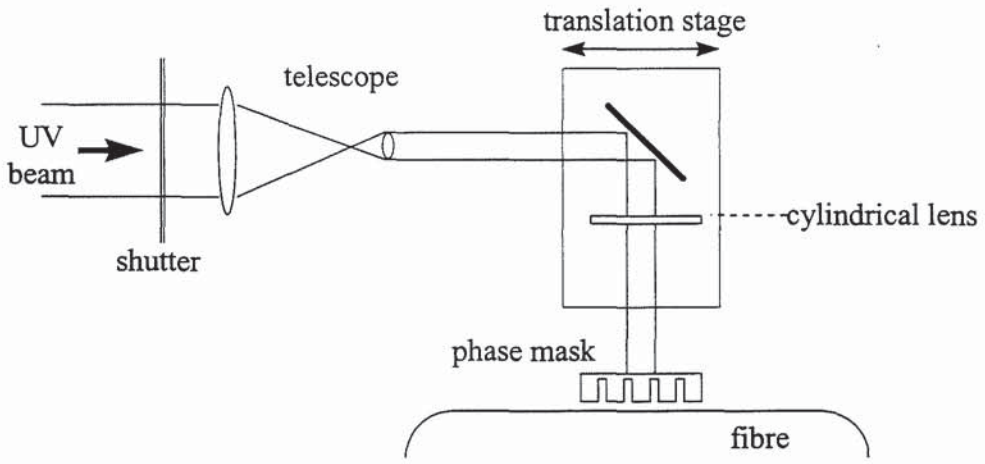

Figure 4.5: Schematic diagram of the 'dual-scan' experimental arrangement to fabricate chirped Bragg gratings

The UV beam from a frequency doubled Argon ion laser, operating at 244nm, is reduced eight-fold by a telescope, to a diameter of ~0.5mm. The beam is then reflected by a mirror, mounted onto a translation stage, and focused through the phase mask and onto the fibre core using a cylindrical lens. The beam can be translated in the direction parallel to the length of fibre, thus allowing long gratings to be written. The UV exposure of the fibre core is controlled by either varying the UV beam intensity or by varying the velocity at which the beam is scanned. For the work contained in this section, the UV exposure was varied by altering the velocity of the beam, typically in a range between 20-20000 μm/s.

As explained previously, the technique for fabricating chirped fibre Bragg gratings involves the dual scan of the fibre. For the initial scan, a uniform period phase mask is placed in close proximity to the fibre and the UV beam is scanned along its length to produce a grating in the fibre core. For the second scan, the phase mask is removed and the UV exposure simply changes the average refractive index along the length of the grating, thus allowing control of the grating chirp. If the velocity of the UV beam is linearly varied along the length of the grating then this will provide a linear variation in the average induced refractive index thus producing a chirped structure. The programmable translation stage uses an optical linear encoder to give feedback control of the motion with a 0.1μm resolution and a velocity control accurate to 1%. The velocity profiles used to control the second scan typically consist of 500-1000 velocity changes, which are triggered at points along the length of travel of the translation stage. These features provide the high level of flexibility and accuracy required when fabricating filters with specific novel chirps.

This method of fabricating chirped gratings requires highly photosensitive fibre, due to the large change in induced refractive index required by the second 'chirping' exposure. Thus chirped gratings made using this technique were generally fabricated in hydrogenated, boron-germanium co-doped fibre. As was discussed in Chapter 3, prior to hydrogenation, the maximum attainable refractive index change is 2×10^{-4}, which corresponds to a maximum induced wavelength shift of ~0.2nm at 1550nm. After hydrogenation, at 150 bar pressure and at room temperature for longer than 10 days, then the maximum induced refractive index change is increased to a value of 1.4×10^{-2}, which corresponds to a maximum induced shift in wavelength of ~15nm at 1500nm.

As detailed in Chapter 3, the UV induced change in refractive index follows a decay curve having a saturation characteristic. This fact becomes particularly important when a large refractive index change is induced in the fibre and the magnitude of this change needs to be known exactly. The induced refractive index change for the initial UV exposure is small enough to be accommodated in the initial, near-linear region of the saturation curve, since the first scan is done at a low UV power, typically between 10-30 mW when using hydrogenated fibre. This exposure is less critical and thus any slight non-linearity in the photosensitivity response of the fibre can be neglected. For the second scan, the photosensitivity response of the fibre is more critical, since the refractive index change is induced in the non-linear region of the curve. If specific filters are to be realised then this non-linearity in photosensitive response must be taken into account. To do this a set of calibration curves were produced from experimental data, giving the induced refractive index change as a function of the scanning velocity, for different UV exposure levels and initial exposure conditions. Figure 4.6 shows one such calibration curve, for an initial grating exposure of power 30mW followed by a second UV exposure of power 50mW.

The solid line shown in Figure 4.6 corresponds to a function fitted to the experimental data, of the form

$$\Delta\lambda = a(1)\left[1 - \exp\left(\frac{-1}{a(2)v}\right)\right]$$

Equation 4-11

where $\Delta\lambda$ is the wavelength shift in nm and v is the exposure velocity in μm/s. $a(1)$ and $a(2)$ are coefficients of the equation; $a(1)$ being the maximum induced wavelength shift. For this specific case $a(1) = 6.25$ and $a(2) = 0.02$.

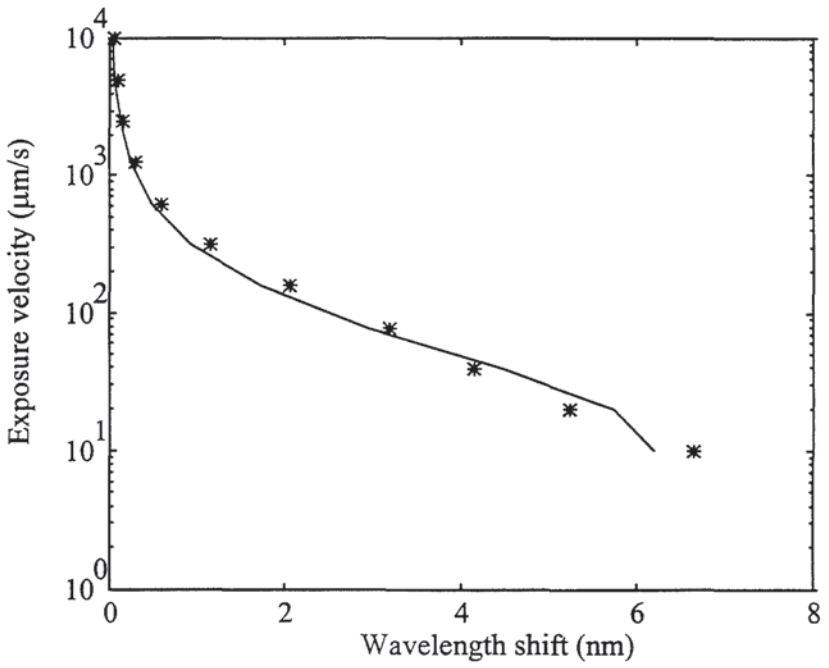

*Figure 4.6: Calibration curve showing the UV induced wavelength shift resulting from various scanning velocities, for a 50mW beam. The initial exposure was 30mW at a velocity of 1000μm (* represents the experimental data points; solid line represents fit to data)*

Using Equation 2-16 and Equation 4-11, it is possible to calculate the exposure velocity required, under the specified exposure conditions, to give a specified grating dispersion. It must be noted that the translation stage has a maximum acceleration and deceleration which, in practice, limits the maximum velocity of the stage and thus sets a limitation on the minimum wavelength shift which can be achieved by the second scan.

Figure 4.7 shows the high resolution reflection and dispersion characteristics of an unapodised, chirped Bragg grating, fabricated in hydrogenated fibre using the dual scan technique. The technique used for grating characterisation was described in section 4.2. The phase mask used in the fabrication process was a 5cm-long uniform period mask, which fabricated gratings at a Bragg wavelength of ~1547nm. The initial UV exposure was at a power of 10mW and a scan speed of 1000μm/s. The second exposure was at a UV power of 50mW and at a maximum translation stage velocity of 2000μm/s. The desired dispersion was set to a value of 1000ps/nm which, from Equation 2-16, should be achieved with a 5cm device of full-width-half-maximum (FWHM) bandwidth 0.48nm. The final chirped device shown in Figure 4.7 has a bandwidth of 0.71nm and a dispersion of 623ps/nm, which was lower than expected and is due to the bandwidth of the device being broader than anticipated. The grating exhibits the typical characteristics of an unapodised, chirped device. From coupled

mode theory, it can be shown that the spectral profile of an unapodised broadband grating displays large sidelobes either side of the main reflection peak, an uneven reflection profile and large oscillations in the group delay characteristic caused by the sharp edges of the profile [20].

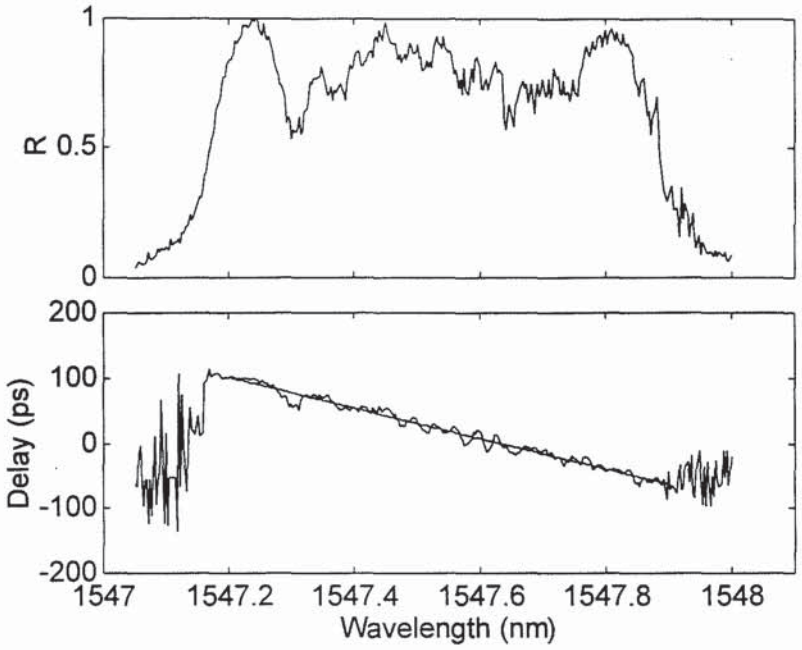

Figure 4.7: Typical reflection and dispersion characteristics for a chirped grating fabricated using the dual scan technique

In order to address these issues, it is necessary to apodise the grating during fabrication, tailoring the refractive index profile. This is done very simply by imposing some function onto the grating as it is being written. By carefully varying the velocity of the initial scan it is possible to profile the induced refractive index change to reduce the sharp edges of the grating and improve the spectral characteristics of the final filter.

Figure 4.8 gives a comparison between modelled results for an unapodised (Figure 4.8 a) and apodised (Figure 4.8 b) grating. Both gratings were modelled with the same basic grating parameters, having a length of 1cm and an induced refractive index change of 3×10^{-4}. (a) exhibits all the aforementioned spectral features, such as ripples in reflectivity profile and the group delay oscillations, whilst (b) has the desired smooth reflection and group delay profile. (b) was apodised with a raised cosine function, given by the equation:

$$\frac{1}{2}\left(\cos\left[\frac{2\pi\left(x-\frac{L}{2}\right)}{L}\right]+1\right)$$

Equation 4-12

where x is the distance along the grating and L is the total length of the device. It can be seen that the apodisation of a chirped grating results in the end device having a narrower bandwidth. This is due to the effective grating length being shortened in order to shape the profile. Since it is the phase mask which gives the grating its chirp, then a grating shorter than the total length of the mask will have a bandwidth which is narrower than that defined by the whole mask.

The modelled results of Figure 4.8 clearly show the importance of apodisation in the grating fabrication process.

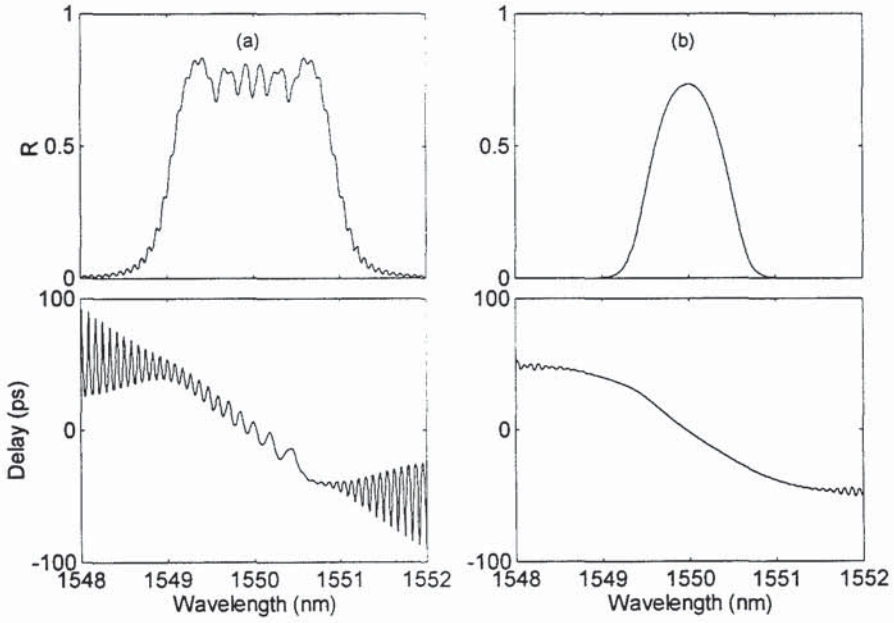

Figure 4.8: Modelled reflection and group delay characteristics for two chirped Bragg gratings, using a 1cm-long phase mask, having a chirp of 2nm: (a) unapodised grating; (b) grating apodised with raised cosine function

For the experimental results presented here, the apodisation was of the function

$$K(z)=\frac{K_0}{2}\left\{\tanh\left[S\left(\frac{1}{2}+\frac{z}{L}\right)\right]\tanh\left[S\left(\frac{1}{2}-\frac{z}{L}\right)\right]\right\}$$

Equation 4-13

where K_o is the maximum coupling coefficient at the centre of the grating, S is a measure of the steepness of the grating edges (S=1 being very shallow and S=12 being sharp) and L is the length of the grating.

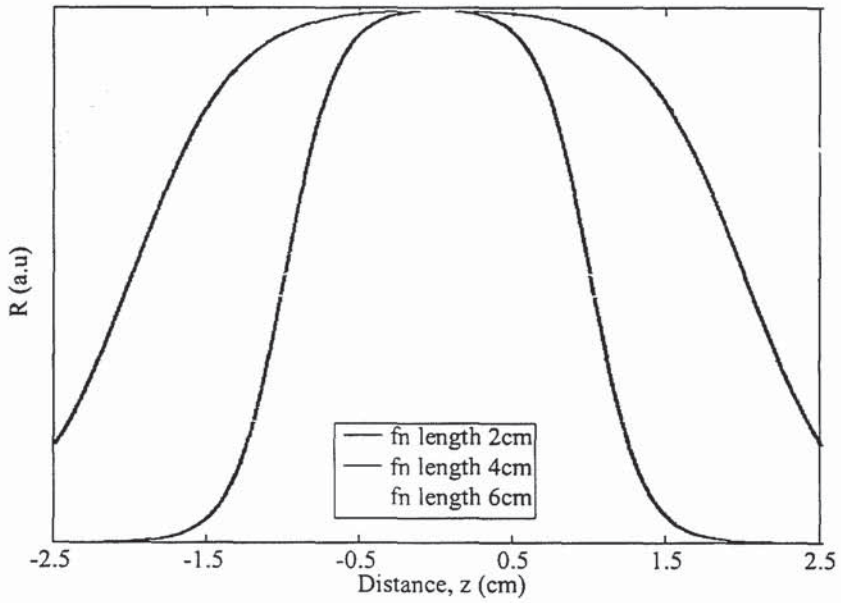

Figure 4.9: Modelled results illustrating the tanh apodisation function, given by Equation 4-13: maximum coupling coefficient K_0 =100, Overall length of device = 5cm, steepness parameter S = 6

Figure 4.9 shows the modelled results for the tanh apodisation function. The function modelled is for a grating of length 5cm, having a maximum coupling coefficient of 100 and with an average steepness value of S=6. The FWHM length of the function has been varied between L=2 and L=6 cm, thus illustrating the amount of care which must be taken in choosing a FWHM function length. For L=2, it can be seen that the apodisation function is only marginally truncated, which should result in a well apodised grating. Unfortunately this means that the effective length of the grating is shorter, resulting in a device that has a narrower bandwidth, as was illustrated in Figure 4.8. For L=6, although maximum use is made of the total grating length available, the function is clearly truncated resulting in a non-ideal grating profile.

This clearly shows that there is a trade off between the length of the final grating and the amount by which the function is truncated. Maximising the length of the apodisation function provides the broadest bandwidth possible but results in an apodisation which is truncated and therefore does not provide the degree of apodisation required to minimise group delay oscillations.

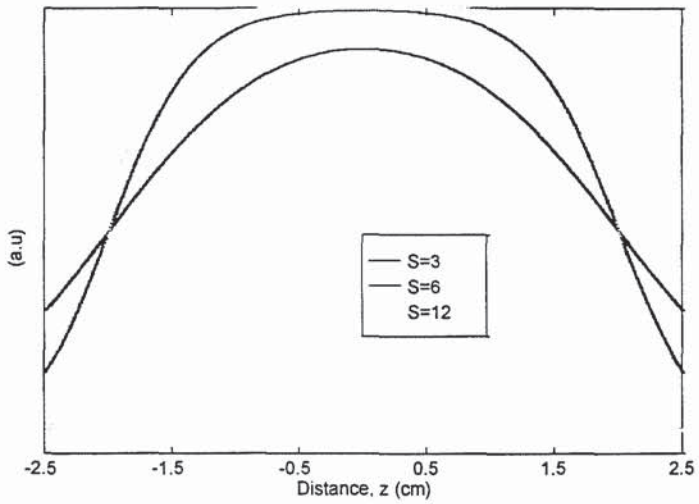

Figure 4.10: Modelled results for the tanh apodisation function, given by Equation 4-13: maximum coupling coefficient K_0 =100, FWHM function length = 4cm, Length of device 5cm, steepness parameter = (3,6,12)

The effect which varying the steepness parameter S has on the resulting apodisation function is illustrated in Figure 4.10. As explained previously, it is important to choose a value for S such that the reflectivity of the grating has a large flat plateau (requiring a large S) but whose edges are shallow enough to minimise out-of-band oscillations (requiring a small S). A steepness value of S=6 was generally chosen since it represents the best compromise between these two design constraints.

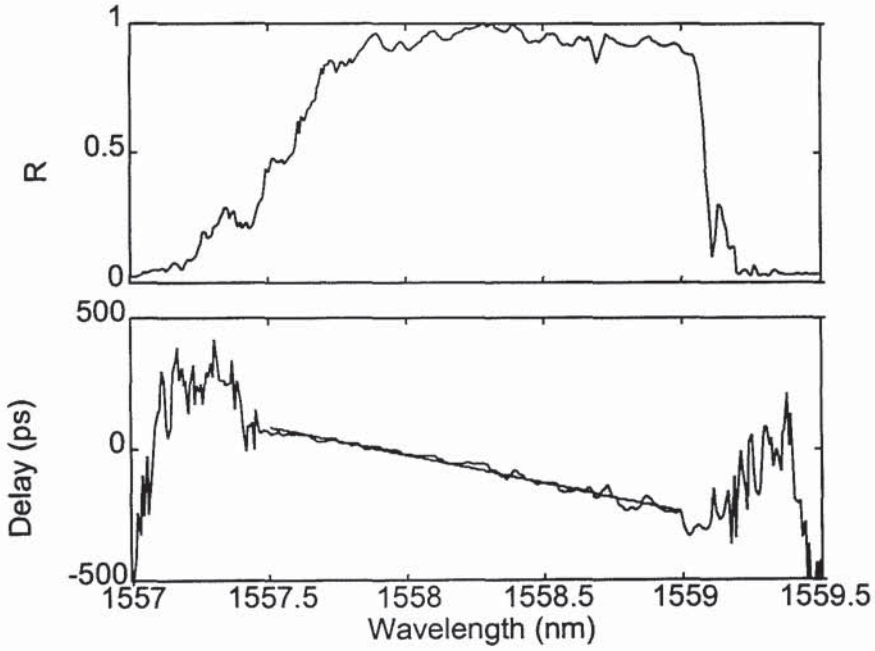

Figure 4.11: High resolution reflection and dispersion measurements of a 5cm long apodised, chirped Bragg grating fabricated using the dual scan technique

Figure 4.11 shows a 5cm-long apodised, chirped Bragg grating fabricated using the dual scan technique. For this case, a value of S=6 was used in the equation for the apodisation function, to ensure that the grating edges were sharp enough to provide a large flat plateau across most of the grating but not so steep as to generate additional oscillations in the profile. A full width half-maximum length, L, of 4cm was chosen to ensure that the apodisation function was not significantly truncated inside the 5cm grating scan length. The initial scan was at a velocity of 1000μm/s and a UV exposure of 10mW. The chirping scan was made at a UV exposure of 50mW, with a maximum scanning velocity of 2000μm/s. The desired dispersion for this device was set to 500ps/nm. The final device, shown in Figure 4.11, has a Bragg wavelength of 1558.4nm and a FWHM bandwidth of 1.47nm (the desired bandwidth of the device was actually 0.97nm). This led to a grating having a dispersion value of 241ps/nm, which was again less than the required value.

4.3.2 Chirped Phase Masks

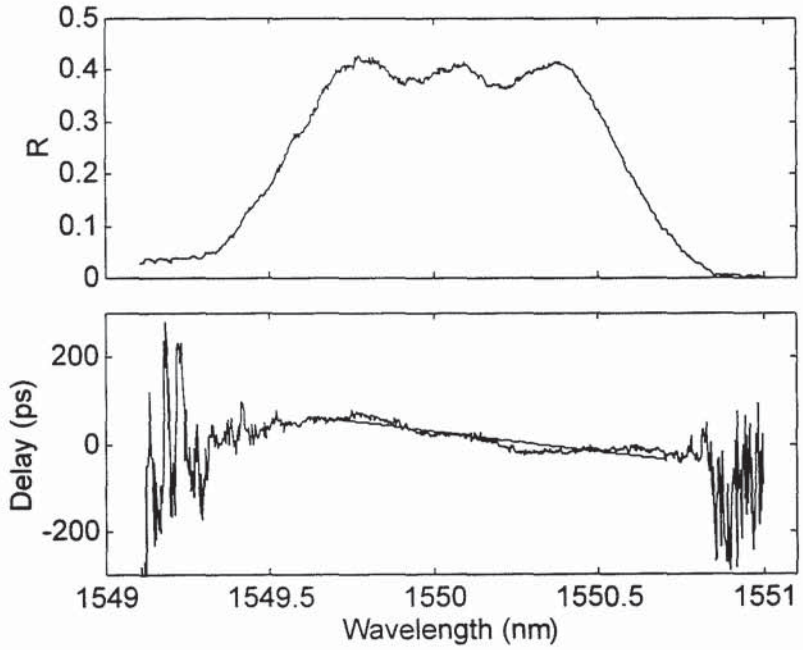

Figure 4.12: Typical transmission and dispersion profiles from 1cm long, unapodised chirped phase mask

A second technique used to fabricate gratings suitable for dispersion compensation was that incorporating a chirped phase mask. Obviously, the final dispersion of the device is then dictated by the design of the particular phase mask being used. Although this means that each phase mask can only fabricate gratings of one value of dispersion, the use of a chirped phase mask greatly simplifies the grating fabrication process, since only one scan is required to produce a chirped device. Again, as for the

dual scan technique, the device can be apodised by varying the velocity of the scan, such as to give the induced refractive index a certain profile.

Figure 4.12 shows a 1cm-long unapodised chirped grating, written with a chirped phase mask. The mask was designed to produce gratings of bandwidth 1nm, thus giving a dispersion value of ~97 ps/nm. The device shown in Figure 4.12 has a FWHM of 1.1nm and a dispersion of ~90ps/nm Again, the absence of apodisation produces additional features in the reflection and dispersion profiles, not generated by the phase mask itself. The mask used in this case had an unusually high zero order, of around 30%, which will cause a reduction in fringe visibility which results in noise on the group delay response and a reduction in the rejection of the unwanted wavelengths [21].

4.4 Quadratic Dispersion Compensation

As was demonstrated in the previous section, linearly chirped gratings when used in reflection, can be used as chromatic dispersion compensating devices in transmission systems. Such devices have so far shown 40 Gbit/s error-free transmission at 1.55μm over 109km of non-dispersion shifted fibre [22]. As the bit rates of such systems increase, the management of this and other higher orders of dispersion is important if the systems are not to be limited by pulse deterioration over long distances. Although the dispersion slope is small in optical fibre (~0.08ps/nm²/km), it has been shown that it can be a limiting factor in high-speed, long distance data transmission systems [23,24]. This problem has been addressed with the proposed fabrication of dispersion slope compensating fibre [25] and fabrication of gratings designed for higher-order dispersion compensation [26]. Williams *et al* initially reported on the theoretical design of gratings to compensate for these higher orders of dispersion [27] where it was given that, if using a chirped grating in reflection and assuming that each wavelength λ is reflected from a single point along the length of the grating, then the variation in resonant wavelength $\Delta\lambda(z)$ with distance z can be described by

$$\Delta\lambda(z) = \frac{-\left(D_2 \pm \sqrt{D_2^2 + 4D_3 n_{av} z - 2D_3 D_1}\right)}{D_3}$$

Equation 4-14

where D_1 is the delay (in ps), D_2 is the dispersion (in ps/nm), D_3 is the dispersion slope (in ps/nm²) and n_{av} is the average refractive index along the length of the grating.

From this, the resulting design parameters can be used to fabricate a wide range of chirped structures to compensate for higher-order dispersion [26,28,29], the results of which are contained in this section.

The technique used for writing gratings suitable for dispersion slope compensation, is that of a dual scan of the fibre, using a uniform period phase mask, as was described in the section 4.3.1. The initial scan with the phase mask in place writes a uniform period grating into the core of the fibre. Again it is possible to apodise the grating during this first UV exposure, by varying the scanning velocity and thus profiling the induced refractive index of the grating. Previously, for the second scan, the phase mask was removed and a linear change in refractive index was induced along the length of the grating. In order to compensate for higher orders of dispersion, a quadratic change in refractive index was imposed on top of the linear one, thus achieving a quadratic change in the delay of the grating. The calibration curves produced for the work on linear dispersion compensation can also be used in this work, to calculate the exposure velocity required to generate the necessary wavelength shift.

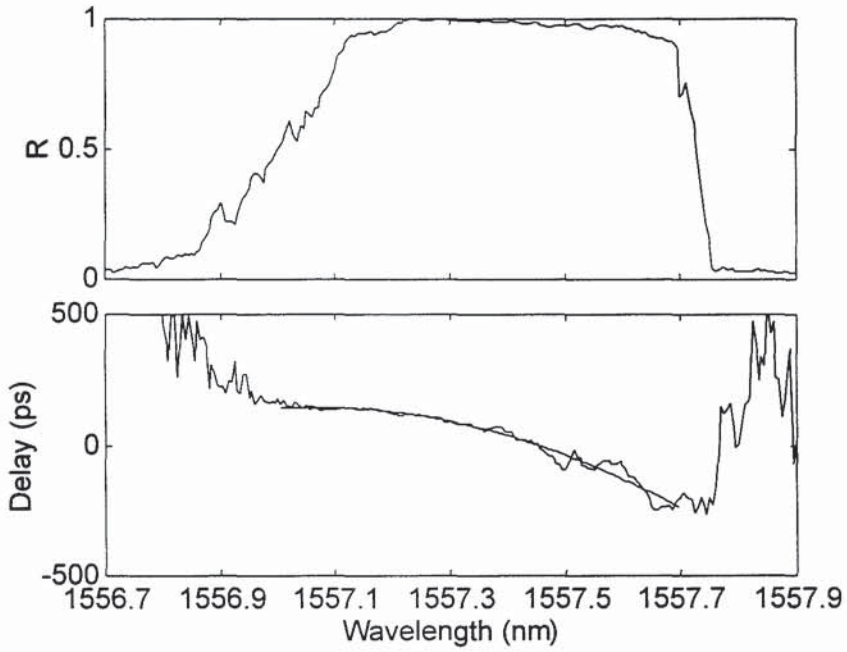

Figure 4.13: Reflection and group-delay characteristics of a chirped Bragg grating, designed to compensate for a large dispersion slope; dispersion -377ps/nm and dispersion slope -1800ps/nm²

Figure 4.13 gives the typical reflection and group-delay characteristics of a 5cm-long chirped Bragg grating, designed to have a large dispersion slope. Also shown is a least-squares fit to the experimental group-delay data. The initial uniform period grating was written in hydrogenated boron-germanium co-doped fibre, with a UV exposure power of 30mW and a scanning velocity of 1000μm/s. The grating was again apodised with the tanh function described in the previous section. The second scan was at a power of 50mW, with a maximum velocity of 4000μm/s.

Using the high resolution grating measurement set-up, the grating was found to have a bandwidth of 0.7nm and a central wavelength of 1557.4nm. The measured dispersion of the grating was -377ps/nm and the dispersion slope, measured at the central wavelength, was -1800ps/nm^2. This is sufficient to compensate for >22000km of optical fibre.

Figure 4.14 gives the spectral profile of a grating fabricated under the same conditions as that shown in Figure 4.13, but designed to give the final device a smaller dispersion slope. This device was measured to have a broader bandwidth, of 1.8nm, which resulted in a dispersion of -240ps/nm and a dispersion slope of -256ps/nm^2. The central Bragg wavelength of the grating was 1558.4nm.

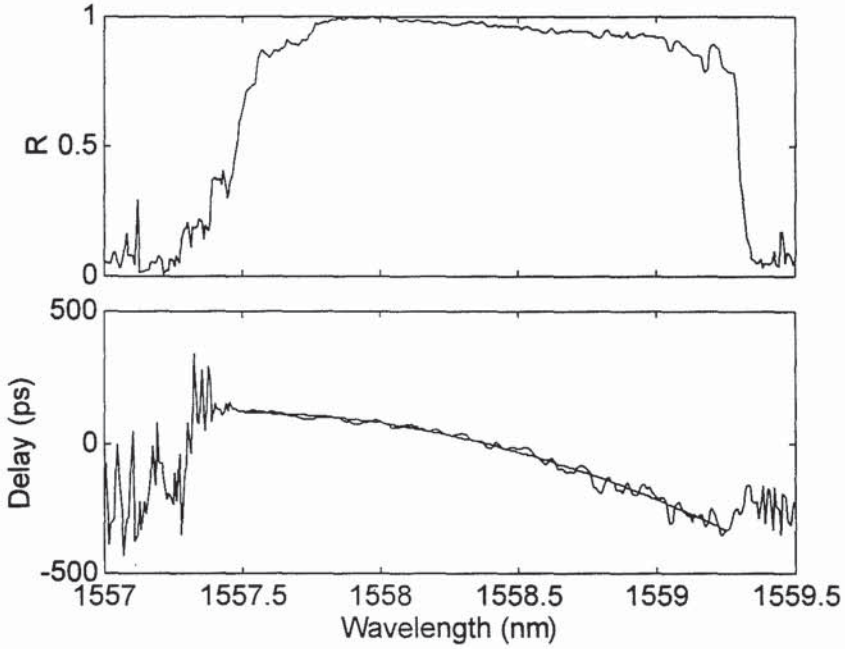

Figure 4.14: Spectral profile of a chirped grating designed for a moderate dispersion slope compensation; dispersion -240ps/nm and dispersion slope -256ps/nm^2

Both of these devices can be seen to have high reflectivity values and relatively flat reflection profiles. The group-delay characteristics follow the general trend of the fitted curves, although there are some small deviations from the ideal curve. The majority of these deviations occur at the long wavelength end of the spectrum, where larger oscillations are apparent. These oscillations are most prominent in Figure 4.13, for the device which has the largest value of dispersion slope. They are thought to be caused by an accumulation of small errors along the length of the grating. For long exposures, there is always the possibility of fluctuations in the UV laser power and variations in the translation stage velocity compared to the required values programmed into the stage and these will accumulate as the scanned length of fibre increases.

4.5 Dispersion Compensation Experiment using a Chirped Bragg Grating

The dual scan technique, incorporating a 5cm-long uniform period phase mask, was used to fabricate the chirped Bragg grating shown in Figure 4.15. The device was apodised, using the tanh function described by Equation 4-13, where the grating edge-steepness parameter S, was set to a value of 6 and the FWHM of the apodisation profile was set to a length of 4cm to ensure that the function was not significantly truncated by the total length of the phase mask. The initial UV exposure was at a power of 10mW and a velocity of 1000μm/s. The second chirping scan had a maximum velocity of 2000μm/s, at a UV exposure of 50mW. Using these exposure conditions, the calibration coefficients, *a(1)* and *a(2)*, from Equation 4-11 were calculated to be 3.7078 and 0.0034 respectively (*a(1)* being the maximum wavelength shift achievable with the exposure conditions given above). The group-delay dispersion required was 500ps/nm, which can be achieved with a chirped Bragg grating of bandwidth 0.78nm.

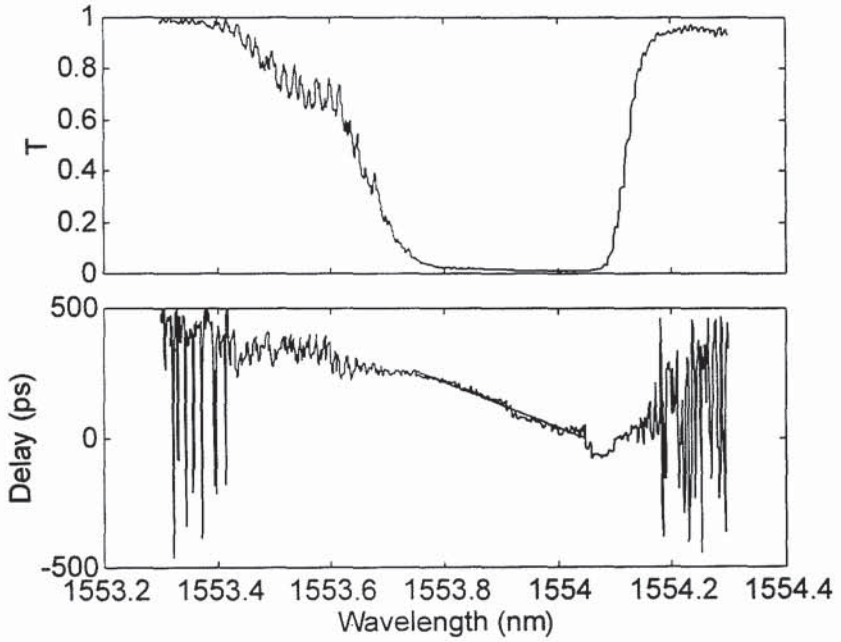

Figure 4.15: Transmission and group-delay characteristics of a 5cm-long linearly chirped Bragg grating used in a test transmission system; bandwidth 0.48nm; dispersion 870ps/nm

High resolution measurements evaluated the bandwidth of this device to be 0.48nm, with a peak reflectivity of 99% centred at a wavelength of 1553.9nm. The dispersion of the device was ~870ps/nm, although this value was dependent on the wavelength range over which the dispersion was evaluated since the group-delay characteristics

were not ideally linear. The grating could therefore compensate for ~52km of standard fibre, assuming that standard fibre has a dispersion of +16.5ps/nm/km.

This grating was then incorporated in a pulse propagation experiment to monitor its success as a dispersion compensating element. The experiment involves setting up a re-circulating loop in which 10 Gbit/s pulses are allowed to propagate and the quality of these pulses can be evaluated each time they pass round the loop. The set-up used for this experiment is shown in Figure 4.16.

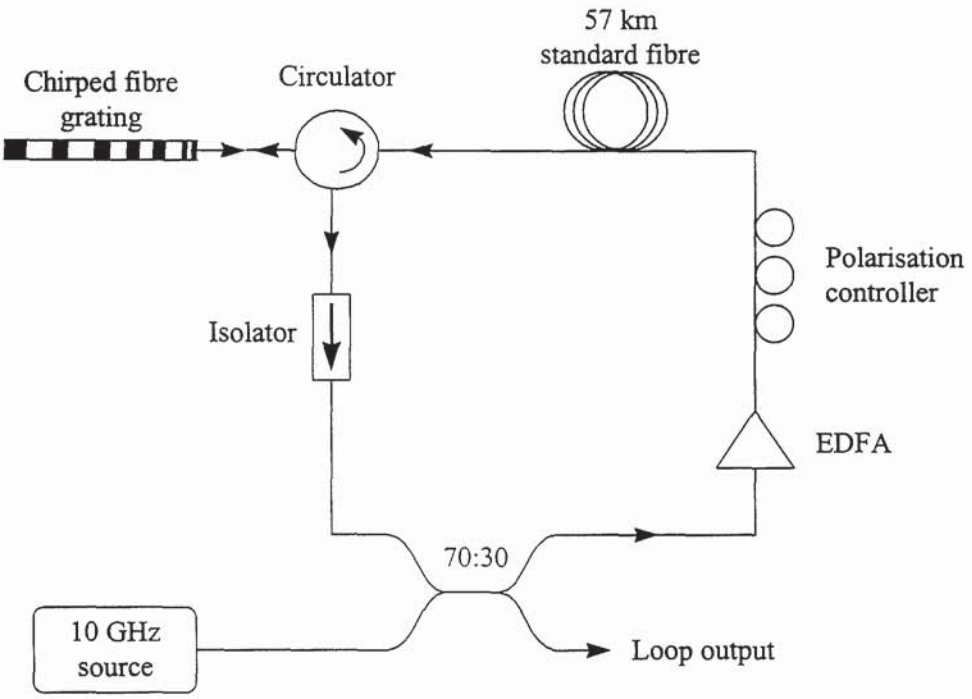

Figure 4.16: Schematic diagram of the experimental arrangement used to test the dispersion compensating properties of a chirped fibre grating

The source used was a 10GHz pseudo random bit generator which had been tuned to the peak wavelength of the grating, at about 1554nm. A 57km length of standard fibre was incorporated in the set-up to give a net anomalous dispersion in the loop. A three-port circulator enabled the light from the loop to be coupled into the fibre grating, from port 1 to port 2. The signal was subsequently compressed by the chirped grating and reflected back into the loop, via port 3. It is important to ensure that this circulator has a high isolation to avoid light being reflected back into the loop. An isolator was also included in the loop to minimise back reflected light.

The dispersion of the fibre, circulator and grating was measured and the delay was found to be ~6ps, giving an average dispersion of 0.22ps/nm/km for the loop. Whilst the experiment was being performed, the two available outputs could be used to monitor the average power level and the power in the 10GHz component of the

electrical spectrum of the propagating signal. The average power was found to be stable with time, although the electrical spectrum seemed unstable, rapidly decreasing with increasing propagation distance. The performance of the system seemed poorer than had been initially anticipated, therefore results were examined for the signal after only a single pass of the grating. A comparison of the input data stream to the output data stream, monitored on a sampling oscilloscope, showed that there was a large increase in the timing and amplitude jitter after a single pass, as illustrated in Figure 4.17. This jitter was far larger than expected for the short propagation distance involved.

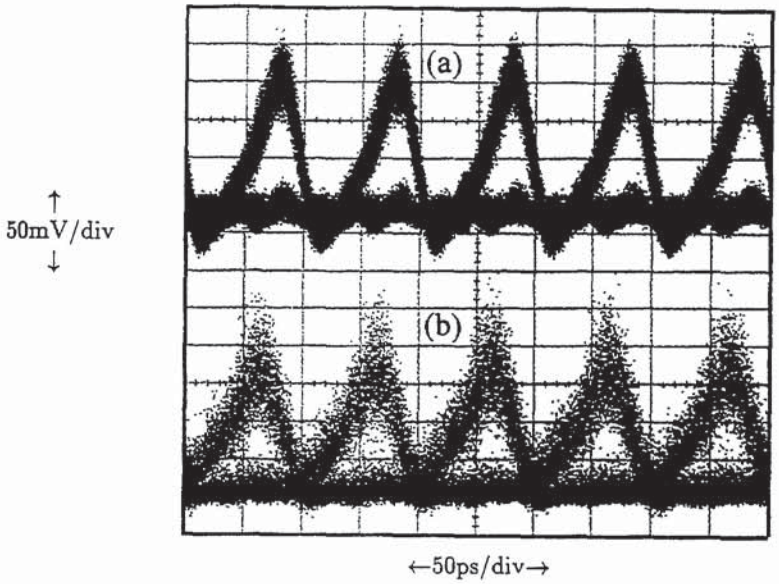

Figure 4.17: Eye diagrams taken on a sampling oscilloscope after a single pass of the chirped Bragg grating: (a) the input data stream; (b) the output data stream

In order to simplify the experiment, the source was exchanged for a laser output pulse stream at 2.5GHz. For this source the stability of the experiment increased compared to the 10GHz experiment. It was noted that when the polarisation of the input pulses was altered, using the polarisation controller, the sampling oscilloscope displayed a variation in the position of the output pulse, as shown in Figure 4.18. The variation in output pulse position with varying input polarisation was attributed to a high value of polarisation mode dispersion (PMD) in the system, where one state of polarisation propagates through the loop at a different velocity to the other state of polarisation. From Figure 4.18, it was estimated that the value of the observed PMD was ~10ps. The individual components of the system were tested and the polarisation dependent effects were found to originate from the fibre grating and it was thus removed from the loop to undergo further testing.

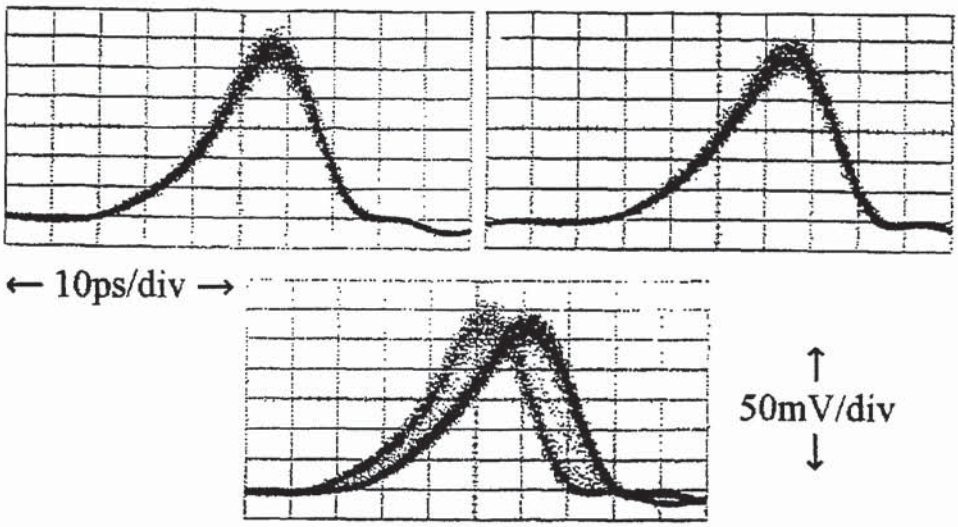

Figure 4.18: Sampling oscilloscope traces showing two output pulses with orthogonal input polarisations

In order to accurately determine the value of the PMD for this grating it was incorporated into the standard dispersion measurement set-up, illustrated in Figure 4.2. The signal from the tunable laser was tuned to the central wavelength of the grating, at a value of around 1554nm. The 1GHz modulator was again used to modulate the tunable laser output. The phase difference generated by the chirped Bragg grating at this single wavelength was calculated by comparing the signal reflected from the grating to a reference signal received directly from the modulated source. A polarisation controller was introduced before the circulator in order to change the polarisation state of the input signal. The change in phase caused by the grating was monitored as a function of change in the input polarisation and hence the value of the PMD for the grating could be calculated, using Equation 4-10. The PMD was evaluated to be 13.8ps, which was in good agreement with the value estimated from the sampling oscilloscope traces (Figure 4.18).

The poor performance of the system was attributed to the high value of PMD for the grating. There has been a report of an experiment where a pulse propagation distance of over 1000km was achieved, despite the dispersion compensating gratings having ~8ps PMD [30]. Despite this, it is acknowledged that if chirped fibre gratings are to be accepted as realistic alternatives to dispersion compensating fibre, then the problem of PMD must be addressed.

4.6 Polarisation Mode Dispersion in Fibre Gratings

As discussed in Chapter 2, optical fibre is inherently birefringent due to the material it consists of. The techniques by which it is pulled also make it difficult to produce a perfectly symmetric core, which subsequently induces birefringence. The addition of dopants, such as boron, into the fibre core have a softening effect making it harder to draw the fibre with a perfectly circular core and thus increasing the overall birefringence in that fibre. In addition to this it has been observed that the fabrication of a device in the fibre core, either by the holographic or phase mask technique, increases the value of the birefringence. This is presumed to be caused by the UV-induced refractive index change in the core of the fibre being anisotropic with respect to the polarisation of the light propagating in the fibre [31]. Section 4.5 showed that this birefringence caused the degradation of pulses which are made to pass such a device. Another example where birefringence causes a problem is in a fibre grating laser, where the two orthogonal polarisation states can experience different cavity Q-values as a result of the grating birefringence, forcing the laser to operate in a single polarisation state [32].

Erdogan *et al* [33] concluded that there are two tangible causes of the birefringence in the UV-induced refractive index. The first is attributed to the asymmetric geometry of the device, UV exposed from one side of the fibre, thus causing a non-uniform UV absorption across the fibre core. The second cause of the birefringence is possibly from the state of polarisation of the UV-light used in the fabrication of these devices. The dominant cause of the birefringence in the UV-induced index was found to be from the state of polarisation of the UV light and this idea was investigated as a method of reducing the polarisation mode dispersion of dispersion compensating gratings.

Poirier *et al* conducted an experiment on the UV-induced bleaching of the 400nm luminescence associated with the 240nm absorption band in germania doped optical fibre [34]. Proposed was a model in which the absorbing GeE' defects have oriented dipoles and preferentially absorb light in the polarisation aligned with their dipole moment. Therefore, it was concluded that bleaching should also occur preferentially for defects aligned with the polarisation of the incident light. The experimental results obtained confirmed this hypothesis, but although absorption bleaching was thought to be responsible for the anisotropy of the total index change, it was recognised the defects resulting from this bleaching become more important [35].

Standard convention, when writing fibre gratings, is to use a UV beam which is polarised perpendicular to the plane of incidence defined by the fibre axis and the incident beam. This polarisation is usually denoted by *s*. This is the state of polarisation used to fabricate all of the chirped devices described previously within

this chapter. The orthogonal polarisation state is that parallel to the plane of incidence and is denoted by *p*. From the conclusions drawn by Erdogan and Poirier it appeared that the birefringence could be reduced if the UV beam was polarised parallel to the plane of incidence, in the so-called *p* state polarisation. An investigation was undertaken to examine the extent to which the polarisation of the UV beam influences the behaviour of a dispersion compensating grating.

A half-wave plate was introduced at the output of the Argon ion laser, which allowed the polarisation state of the UV beam to be changed prior to grating fabrication and enabled gratings to be written in both the *s* and *p* state of polarisation. The method of fabrication to produce the grating used in the pulse propagation experiment, whose transmission and group-delay characteristics are shown in Figure 4.15, was that of the dual scan technique. It has already been shown that this method of fabricating chirped Bragg gratings is not an efficient one and requires a large UV-induced change in refractive index to achieve larger bandwidths. Since the birefringence is proportional to the total index change for a given fibre and exposure geometry, then it is obvious that this fabrication technique is not ideal for the minimisation of PMD in fibre gratings. A chirped phase mask requires a smaller change in refractive index to produce a grating having an identical bandwidth and therefore this method of chirped grating fabrication was used as a first step to minimising the PMD in dispersion compensating gratings.

Figure 4.19 show a comparison of two chirped gratings, both written under the same exposure conditions, but with different polarisation states for the UV-beam. Both gratings were written in boron-germanium co-doped fibre which had been hydrogenated at 130 bar pressure and room temperature for longer than 10 days. Unapodised, chirped Bragg gratings were fabricated by the single scan of a 5cm-long chirped phase mask, designed to fabricate gratings of bandwidth 1nm. The UV exposure was at a power of 20mW with a scan velocity of 2000μm/s. Figure 4.19(a) gives the high resolution transmission and group-delay measurements for a grating fabricated with the UV-beam being vertically polarised, in the *s*-state. This results in a grating, centred at a wavelength of 1550.3nm, with bandwidth 1nm and reflectivity 29.5 dB. Since the grating was not apodised, large oscillations in the group delay were apparent and the measured dispersion was approximated to be 500ps/nm. The PMD, measured at the centre wavelength of the grating, was ~5ps. As stated, the second grating, that of Figure 4.19(b), was fabricated under identical exposure conditions, but with the UV-beam being horizontally polarised with respect to the fibre axis. This resulted in a grating, again having a bandwidth of 1nm, but with a reflectivity of only 22dB. The dispersion of the grating was measured to be 495ps/nm, indicating that altering the polarisation state of the writing beam had no clear influence on the value of the group-delay dispersion. However, the PMD was measured, at the peak

wavelength of the grating, to be <1ps. This is the smallest dispersion value measurable using this particular experimental characterisation arrangement.

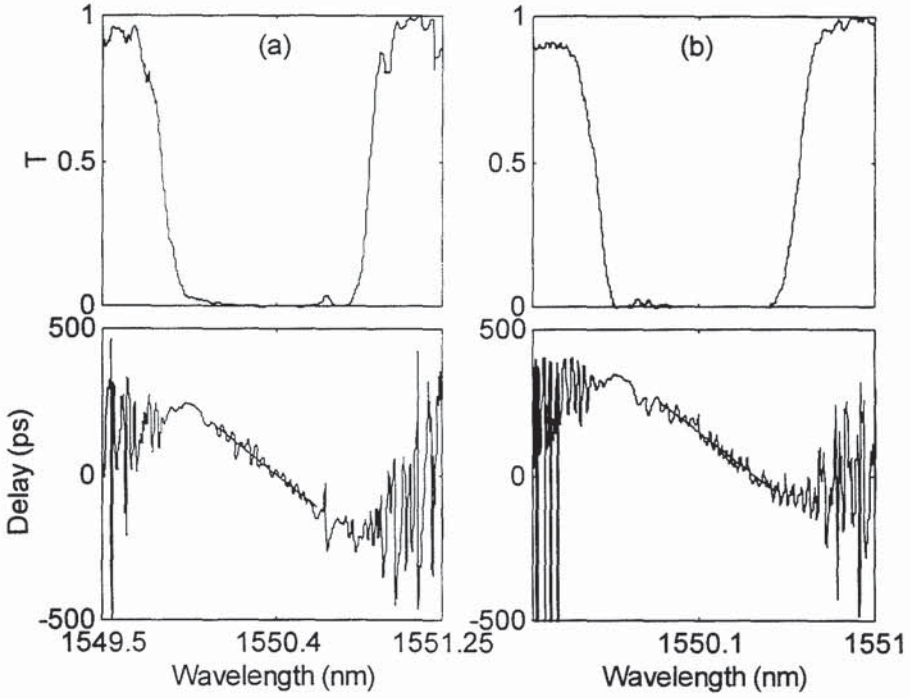

Figure 4.19: A comparison of chirped fibre gratings written under identical exposure conditions but having different UV-beam polarisation states: (a) polarisation of the UV-beam perpendicular to the fibre axis, s-state; (b) polarisation of the UV-beam parallel to the fibre axis, p-state

A comparison of these two gratings clearly shows the difference in efficiency between the two inscription techniques. With the exception of the UV polarisation state, the UV exposure was identical for both gratings and so it can be seen that writing a grating using an *s* polarised beam is more efficient. It is not feasible to compare the PMD measurements for these two gratings since for a fair comparison to be made the gratings should have identical reflectivity values. Several pairs of gratings were made, having the same reflectivity but being fabricated using different states of polarisation. Further investigation concluded that gratings written with a *p-state* polarised beam did indeed exhibit a smaller value of PMD than for their *s-state* counterparts.

From these findings a final device was produced to be incorporated into the re-circulating loop of a standard fibre transmission system. A 5cm-long phase mask having a total chirp of 1nm was used in conjunction with a UV beam polarised in the *p-state*, parallel to the direction of the fibre axis. The exposure conditions were set at a velocity of 2000μm/s and a power of 20mW. The resulting device is shown in Figure 4.20. The FWHM bandwidth was measured to be 0.99nm with a peak reflectivity of 98% at the centre wavelength of 1550.3nm. The group delay dispersion was calculated

to be 508ps/nm, which was the dispersion value required for the system (500ps/nm). The PMD was measured at the centre wavelength of the grating and was found to be ~3ps, which is far smaller than that for the device used previously. The reflection and group delay characteristics also appear to be far smoother and this should reduce the jitter in the output pulses of the transmission system. Unfortunately, at the time of writing, transmission system results are not available for this device.

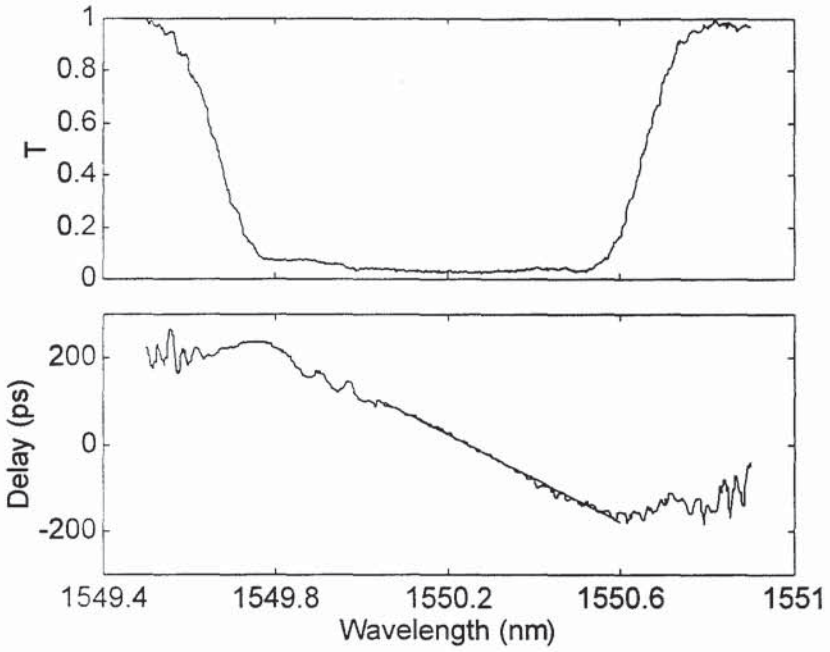

Figure 4.20: Transmission and group-delay characteristics of a 5cm-long chirped grating fabricated with a chirped phase mask, for dispersion compensation

4.7 Chapter Conclusions

Chirped fibre Bragg gratings have many applications where the bandwidth of a standard uniform period Bragg grating is too narrow, although their main application is as dispersion compensating elements for long distance fibre transmission systems. As the data rates for such systems increase it will become more important to compensate for higher orders of dispersion, in addition to the group-delay dispersion, which is most commonly compensated for at present.

There are many issues to be addressed when fabricating chirped gratings. As with standard gratings, the reflection profile is expected to have a flat top, with suppressed side-lobes to minimise out-of-band reflections. But for a chirped grating the group-delay characteristic is required to follow a smooth function, with minimal ripples across its operating wavelength. In order to follow these constraints it is essential to apodise the device, using one of the methods described in Chapter 3.

There are many methods of fabricating chirped in-fibre Bragg gratings, including the use of a uniform period phase mask in the dual scan of the fibre and the use of a pre-chirped phase mask. In this chapter, it has been shown that the later method should be used preferentially, since it is a more reproducible technique and does not rely so heavily on a large photosensitive response of the fibre. The combination of a chirped phase mask and the apodisation of the grating produces the most ideal grating profile.

The inclusion of such a dispersion compensating element within a pulse transmission system highlighted another design constraint which needs to be taken into consideration, that of polarisation mode dispersion. This is due to the birefringence in the fibre and causes the wavelength of the pulses to be polarisation dependent, thus systems incorporating devices with large PMD values show poor performances. It has been found that the grating polarisation mode dispersion can be minimised by ensuring that the UV exposing beam is in a state of polarisation parallel to the direction of the fibre axis during the fabrication process. Since the magnitude of the UV-induced refractive index change is proportional to the amount of induced birefringence in the device, then the chirped phase mask fabrication technique gives a smaller value of PMD, since it requires a smaller change in refractive index compared to that for the dual scan technique.

---

1 M. Farries, C.M. Ragdale, D.C.J. Reid, 'Broadband chirped fibre Bragg filters for pump rejection and recycling in erbium doped fibre amplifiers', *Electron. Lett.*, **28**, 1992, pp.487-489

2 M.C. Farries, K. Sugden, D.C.J. Reid, I. Bennion, A. Molony, M.J. Goodwin, 'Very Broad reflection bandwidth (44nm) chirped fibre gratings and narrow bandpass filters produced by the use of an amplitude mask', *Electron. Lett.*, 30, (11), 1994, pp.891-892

3 F. Ouellette, 'Dispersion cancellation using linearly chirped Bragg grating filters in optical waveguides', *Opt. Lett.*, **12**, (10), 1987, pp.847-849

4 U. Eriksson, P. Blixt, J.A. Tellefsen Jr., 'Design of fibre gratings for total dispersion compensation', *Opt. Lett.*, 19, (14), 1994, pp.1028-1030

5 F. Ouellette, J-F. Cliché, S. Gagnon, 'All-Fiber devices for chromatic dispersion compensation based on chirped distributed resonant coupling dispersion compensation', *J. Lightwave Technol.*, 12, (10), 1994, pp.1728-1737

6 K. Ennser, M.N. Zervas, R.I. Laming, 'Optimization of linearly chirped grating dispersion compensation systems', *Opt. Fibre Technol.*, **3**, 1997, pp.120-122

7 G. Lenz, B.J. Eggleton, N. Litchnitser, 'Pulse compression using fibre gratings as highly dispersive nonlinear elements', *J. Opt. Soc. Am. B*, **15**, (2), 1998, pp.715-721

8 M.J. Cole, H. Geiger, R.I. Laming, S.Y. Set, M.N. Zervas, W.H. Loh, V. Gusmeroli, 'Broadband dispersion-compensating chirped Bragg gratings in a 10Gbit/s NRZ 110km non-dispersion-shifted fibre link operating at 1.55um', *Electron. Lett.*, **33**, (1), 1997, pp.70-71

9 W.H. Loh, R.I. Laming, N. Robinson, A. Cavaciuti, F. Vaninetti, C.J. Anderson, M.N. Zervas, M.J. Cole, 'Dispersion compensation in excess of 500 km for 10 Gbit/s systems using chirped fibre gratings' *IEEE Photon. Technol. Lett.*, **8**, (7), 1996, pp.944-946

10 T. Stephens, P.A. Krug, Z. Brodzeli, G. Dhosi, F. Ouellette, L. Poladian, '257km transmission at 10gbit/s in non-dispersion-shifted fiber using an unchirped fiber Bragg grating dispersion compensator', *Electron. Lett.*, **32**, (17), 1996, pp.1599-1601

11 R. Kashyap, H.G. Froehlich, A. Swanton, D. Armes, '1.3m long super-step chirped fibre Bragg grating with a continuous delay of 13.5ns and bandwidth 10nm for broadband dispersion compensation', *Electron. Lett.*, **32**, (19), 1996, pp.1807-1809

12 M.J. Cole, S. Aina, M. Durkin, M. Ibsen, F. Vaninetti, L. Arcangeli, V. Gusmeroli, R.I. Laming, 'Design and application of long, continuously chirped fibre gratings', *IEE Colloquium on Optical Fibre Gratings, Savoy Place, London*, 1997, pp.16/1-16/4

13 A. Asseh, H. Storoy, B.E. Sahlgren, S. Sandgren, R.A.H. Stubbe, 'A writing technique for long fibre Bragg gratings with complex reflectivity profiles', *J. Lightwave Technol.*, **15**, (8), 1997, pp.1419-1423

14 S. Barcelos, M.N. Zervas, R.I. Laming, D.N. Payne, L. Reekie, J.A. Tucknott, R. Kashyap, P.F. McKee, F. Sladen, B. Wojciechowicz, 'High accuracy dispersion measurements of chirped fibre gratings', *Electron. Lett.*, **31**, (15), 1995, pp.1280-1282

15 F. Ouellette, D.Y. Stepanov, 'A new technique for measuring the group delay of chirped fibre Bragg gratings', *Conf. Optical Fibre Commun. '97 (OFC'97) Tech. Digest*, (WJ1), 1997, pp.153-154

16 K. Sugden, I. Bennion, A. Molony, N.J. Copner, 'Chirped gratings produced in photosensitive optical fibre by fibre deformation during exposure', *Electron. Lett.*, **30**, (5), 1994, pp.440-441

17 Y. Painchaud, A. Chandonnet, J. Lauzon, 'Chirped fibre gratings produced by tilting the fibre', *Electron. Lett.*, **31**, (3), 1995, p.171-172

18 K.C. Byron, H.N. Rourke, 'Fabrication of chirped fibre gratings by novel stretch and write technique', *Electron. Lett.*, **31**, (1), 1995, pp.60-61

19 K.O. Hill, F. Bilodeau, B. Malo, T. Kitagawa, S. Theriault, D.C. Johnson, J. Albert, K. Takiguchi, 'Chirped in-fibre Bragg gratings for compensation of optical-fibre dispersion', *Opt. Lett.*, **19**, (17), 1994, pp.1314-1316

20 K.O. Hill, S. Theriault, B. Malo, F. Bilodeau, T. Kitagawa, D.C. Johnson, J. Albert, K. Takiguchi, T. Kataoka, K. Hagimoto, 'Chirped in-fibre Bragg grating dispersion compensators: Linearization of dispersion characteristics and demonstration of dispersion compensation in 100km, 10Gbit/s optical fibre link', *Electron. Lett.*, **30**, 21, 1994, pp.1755-1756

21 F. Ouellette, 'The effect of profile noise on the spectral response of fibre gratings', *Bragg Gratings, Photosensitivity and Poling in Glass Fibres and Waveguides (BGPP '97), Tech. Digest,* **17**, (BMG13), 1997, pp.222-224

22 L. Dong, M.J. Cole, A.D. Ellis, M. Durkin, M. Ibsen, V. Gusmeroli, R.I. Laming, '40 GBit/s 1.55μm transmission over 109km of non-dispersion shifted fibre with long continuously chirped fibre gratings', *Conf. Optical Fibre Commun. '97 (OFC'97) Tech. Digest- post deadlines,* PD6, 1997

23 E. Desurvire, J.-P. Hamaide, E. Brun, 'Solitons in long-haul communications systems', *Conf. Optical Fibre Commun.'96 (OFC '96) Tech. Digest,* **2**, (WC2), 1996, pp.103-104

24 S. Saito, 'Long-distance optical transmission: comparison between NRZ and solitons', *Conf. Optic. Commun. (OFC '96) Tech. Digest,* **2**, (WC3), 1996, pp.104-106

25 M. Onishi, T. Kashiwada, Y. Koyano, Y. Ishiguro, M. Nishimura, H. Kanamori, 'Third-order dispersion compensating fibres for non-zero dispersion shifted fibre links', *Electron. Lett.*, **32**, (25), 1996, pp.2344-2345

26 J.A.R. Williams, L.A. Everall, I. Bennion, N.J Doran, 'Fiber Bragg grating fabrication for dispersion slope compensation', *IEEE Photon. Technol. Lett.*, **8**, (9), 1996, pp.1187-1189

27 J.A.R. Williams, I. Bennion, N.J. Doran, 'The design of in-fibre Bragg grating systems for cubic and quadratic dispersion compensation', *Opt. Commun.*, **116**, 1995, pp.62-66

28 M. Durkin, M. Ibsen, M.J. Cole, R.I. Laming, '1m long continuously-written fibre Bragg gratings for combined second and third order dispersion compensation', *Electron. Lett.*, **33**, (22), 1997, pp.1891-1893

29 T. Komukai, M. Nakazawa, 'Fabrication of nonlinearly chirped fibre Bragg gratings for higher order dispersion compensation', *Conf. Optical Fibre Commun. '98 (OFC '98) Tech. Digest*, (TuM2), 1998, pp.71-72

30 R.I. Laming, M.N. Zervas, 'Fibre Bragg gratings and their applications', *European Conf. In Optical Commun. (ECOC '97) Technical Digest*, **4**, 1997, pp.81-83

31 G. Meltz, W.W. Morey, 'Bragg grating formation and germanosilicate fibre photosensitivity', *International Workshop on Photoinduced Self-Organisation Effects in Optical fibre*, Proc. Soc. Photo-Opt. Instrum. Eng., **1516**, 1991, pp.185-199

32 V. Mizrahi, D.J.D. DiGiovanni, R.M. Atkins, S.G. Grubb, Y.K. Park, J.M.P. Delavaux, 'Stable single-mode erbium fibre-grating laser for digital communications', *J. Lightwave Technol.*, **11**, 1993, pp.2021-2025

33 T. Erdogan, V. Mizrahi, 'Characterisation of UV-induced birefringence in photosensitive Ge-doped silica optical fibres', *J. Opt. Soc. Am. B*, **11**, (10), 1994, pp.2100-2105

34 M. Poirier, S. Thibault, J. Lauzon, F. Ouellette, 'Dynamic and orientational behaviour of UV-induced luminescence bleaching in Ge-doped silica optical fibre', *Opt. Lett.*, **18**, (11), 1993, pp.870-870

35 D.L. Williams, S.T. Davey, R. Kashyap, J.R. Armitage, 'Direct observation of UV induced bleaching of 240-nm absorption-band in photosensitive germanosilicate glass-fibers', *Electron. Lett.*, **28**, (4), 1992, pp.369-

5. BANDPASS FILTERS

5.1 Chapter Overview

Currently, there is a high level of interest in the fabrication of filters for providing wavelength selectivity and noise filtering in WDM systems [1,2] and quasi-distributed point sensing systems [3]. In-fibre filters, using properly designed Bragg gratings, have the potential to provide wide stopbands, narrow passbands and high rejection levels and have the further advantages of fibre-compatibility and potentially low-cost. The use of single-beam phase mask exposure has brought greater ease and reproducibility to the Bragg grating inscription process [4]. Such advances have allowed more complex gratings, such as bandpass filters, to be readily fabricated. Bandpass filters have been achieved by introducing a phase shift during the scanning of a uniform period mask [5] and also by using a specially designed uniform period phase mask containing a phase shift [6]. Other techniques involve the fabrication of a Moiré grating - either holographically [7] or by the use of a phase mask [8]- which contains numerous passbands within its stopband.

This chapter gives details of a number of novel techniques which have been applied to fabricate bandpass filters, including phase-shifted phase masks, Moiré and concatenation approaches. The work on multiple grating arrays was carried out within the PHOTOS project (PHOtosensitive Technology for Optical Systems), funded by the European Union under the ACTS programme. The grating arrays designed for this project were temperature stabilised by a specially designed device package and subsequently incorporated into an optical network to examine their performance. Both the device packaging and testing were carried out collaboratively with other partners within the PHOTOS project.

5.2 Moiré Gratings

A grating resonator consists of two closely spaced sections of grating separated by a phase shift. The introduction of this phase shift results in the formation of one or more narrow passbands in the grating reflection spectrum. The Moiré technique is one of a number used to fabricate Bragg grating resonators. The fabrication of narrowband transmission filters using this technique was originally described by Reid *et al* [9], where a modified holographic technique was used to form two surface relief gratings, each having a slightly different period, in the fibre core. This 'double exposure' formed an interference pattern in the fibre, introducing phase shifts at various points along the length of the fibre, as illustrated in Figure 5.1.

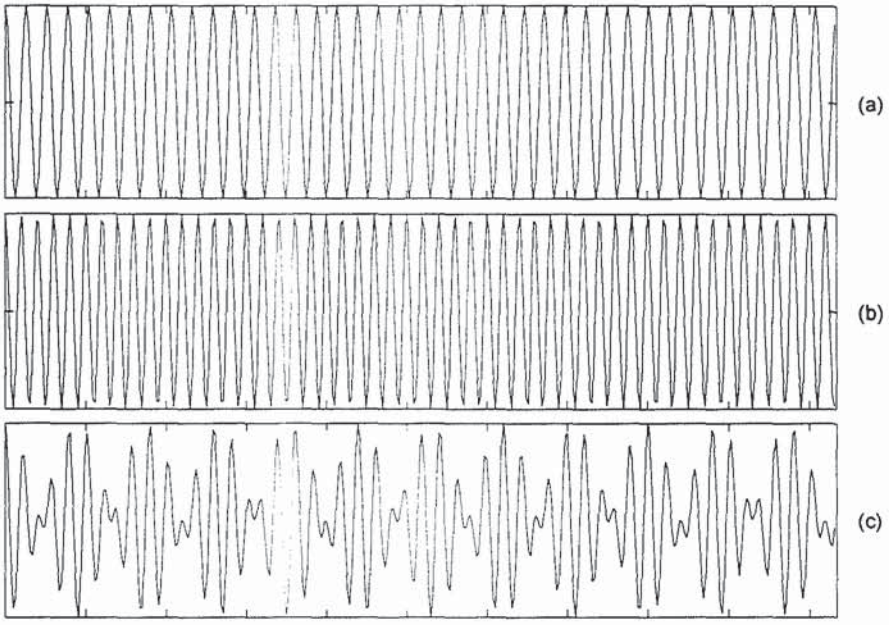

Figure 5.1: Superposition of two unchirped gratings - (a) and (b): fringe patterns with differing periods; (c) superposition of two gratings resulting in a number of passbands within the grating structure

Legoubin *et al* [10] later applied the same technique in the direct inscription of uniform period gratings by UV exposure of highly photosensitive germanosilicate fibre. It should be noted that the overall bandwidth of these filters was still too narrow for many applications such as wavelength division multiplexing (WDM) and amplified stimulated emission (ASE) noise suppression. The first report of the extension of the technique to accommodate chirped grating exposures, thus increasing the stopband width, was by Zhang *et al* [7]. Chirped gratings were used to fabricate high finesse transmission filters and these filters were then concatenated to other standard broadband reflection gratings to obtain a narrow passband within a very wide stopband, achieving finesse values of up to 48. All of these reports relate to the free-space holographic exposure technique using two interfering beams.

Section 5.2.3 describes the first published work on the design and fabrication of multipassband Moiré filters using chirped phase masks. The phase mask technique allows highly reproducible gratings to be fabricated and the use of a chirped mask produces broader filters.

5.2.1 Moiré Theory

As described in the introduction, a Moiré filter consists of two Bragg gratings separated by a phase shift, which results in the modulation of the refractive index within the fibre core. This superposition of gratings produces an effective 'beating',

where the slowly varying grating envelope contains a rapidly varying component. Each null in the grating envelope gives rise to a passband in the resulting grating response.

A comparison can be drawn between this and the amplitude modulation which arises in telecommunications [11,12]. In the case of amplitude modulation, the amplitude of a radio-frequency carrier wave is varied by a modulating voltage. If the modulating signal amplitude is greater than the unmodulated carrier amplitude then 'overmodulation' occurs. This results in the distortion of the carrier envelope and a phase reversal of the carrier (similar to the phase shift in the Moiré situation).

The refractive index modulation, $\Delta n(z)$, can be expressed as :

$$\Delta n(z) = \Delta n\left(2 + 2\cos\frac{2\pi z}{\Lambda_c}\cos\frac{2\pi z}{\Lambda_s}\right),$$

Equation 5-1

where Δn is the amplitude of the refractive index modulation of the Bragg grating, z is the position along the axis of the fibre, Λ_c is the period of the slowly varying envelope and Λ_s is the period of the rapidly varying component. For a chirped structure, the period of the rapidly varying component Λ_c is a function of position, z. The cosine variation in refractive index produces a crossover point where the phase of the grating changes by π. This corresponds to an optical phase change of $\pi/2$, producing a passband in the grating response profile. Stretching the fibre in between exposures changes the length (and the period) of the initial grating with respect to the second. This has the effect of shifting the wavelength of the second grating, thus producing a Moiré resonator. The interference pattern corresponding to this chirped case can be seen in Figure 5.2.

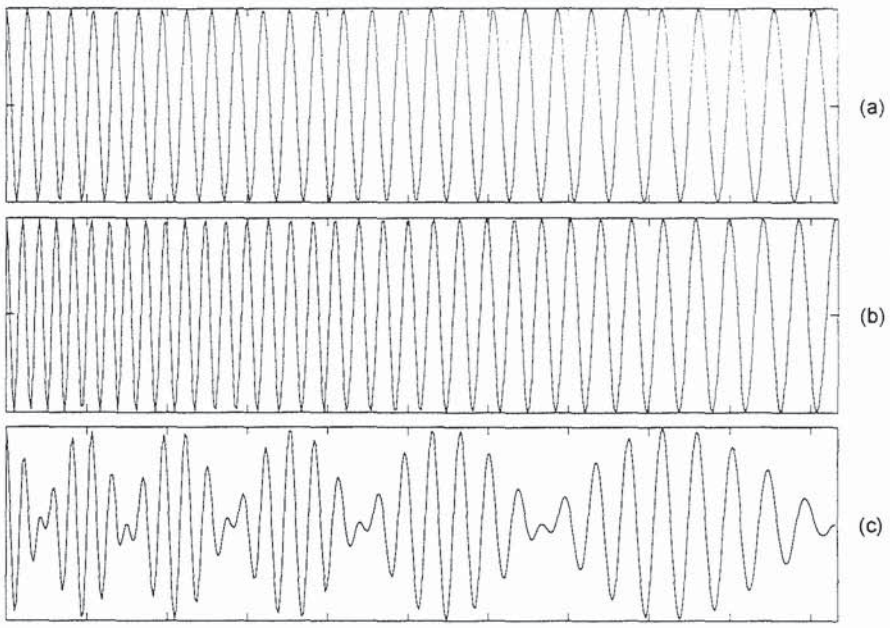

Figure 5.2: The superposition of two chirped fringe patterns of different periodicities - (a) and (b) -resulting in an overall modulated interference pattern in the core of the fibre (c)

The change in wavelength is proportional to the change in fibre length or refractive index and can be expressed as:

$$\frac{\Delta\lambda}{\lambda} = \frac{\Delta\Lambda}{\Lambda} + \frac{\Delta n}{n},$$

Equation 5-2

where $\Delta\lambda$ is the change in wavelength λ, $\Delta\Lambda$ is the change in period Λ and Δn is the change in refractive index n. This means that a precise wavelength shift can be induced between exposures, hence controlling the number of passbands obtained allowing specific filters to be designed.

5.2.2 Moiré Modelling

The effect of superimposing two chirped gratings can be modelled using a transfer matrix technique [13,14]. For the transfer matrix technique, the grating structure is divided up into a large number of thin segments, in which the grating is assumed to be constant, and these can be represented by a corresponding transfer matrix, M. For each segment, the electric field can be split into forward and backward propagating components $E^{+}(z)$ and $E^{-}(z)$, as illustrated in Figure 5.3. Solving for the boundary conditions and phase changes across each segment gives a transfer matrix of the electric field between two adjacent segments. The characteristics across the whole of

the grating structure can be obtained by multiplying all these matrices, although the accuracy will depend on the number of segments into which the structure is divided.

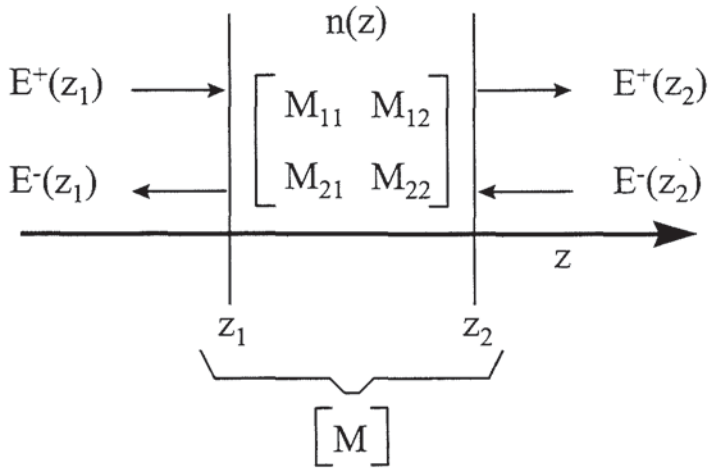

Figure 5.3: Transfer matrix analysis of one thin segment of a grating structure

Using this technique several different structures were modelled to examine the effect which changing the various grating parameters has on the final device. A representative selection of modelled devices are shown in Figure 5.4.

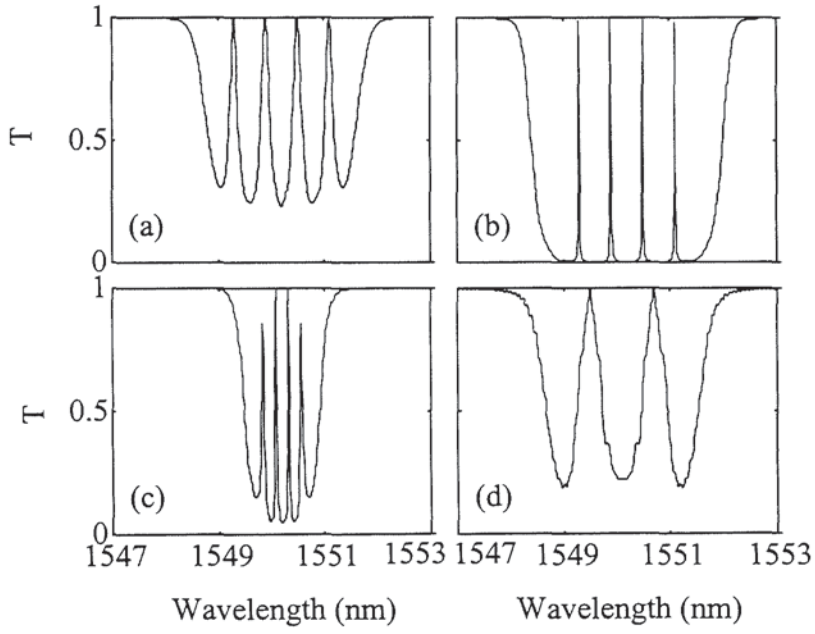

Figure 5.4: Modelled responses of Moiré gratings. (a) superposition of two 1cm gratings at wavelengths 1550nm and 1550.4nm, bandwidth of each grating ~3nm, amplitude of refractive index 2×10^{-4}; (b) increase in the refractive index change to 5×10^{-4}; (c) decrease in the bandwidth of each grating to 1.5nm; (d) wavelength of second grating reduced to 1550.2nm

Figure 5.4(a) shows the modelled response of two 1cm long gratings, each of bandwidth 3nm, which have been superimposed. They have centre wavelengths at 1550nm and 1550.4nm respectively and the amplitude of the refractive index modulation, Δn, is 2×10^{-4}. Figure 5.4(b) shows the effect of increasing the amplitude of this refractive index modulation to 5×10^{-4}, with all the other initial parameters remaining the same: the strength of the filter increases and the size of each passband decreases. Figure 5.4(c) shows the effect of decreasing the amount of chirp on the gratings, reducing their bandwidth down to 1.5nm: in this case the number of passbands remains constant but the free spectral range is reduced. Figure 5.4(d) shows the effect of decreasing the stretch in between exposures. The wavelength of the second grating has been reduced to 1550.2nm and it may be seen that the number of passbands reduces accordingly.

5.2.3 Fabrication Methods

A number of novel techniques for the fabrication of chirped Moiré gratings were investigated and evaluated for their ease of use and flexibility. These techniques are detailed in the following section.

5.2.3.1 *Dual Scan of a Uniform Period Phase Mask*

The first technique employed to fabricate Moiré filters was a slight modification of the dual scan technique, which was detailed in Chapter 2. Here, a single uniform period grating is written into the core of the fibre and the translation of the UV beam along the length of a uniform period phase mask allows a long grating to be fabricated. The fibre is then stretched and a second grating is written on top of the first using the same phase mask. The amount of stretch applied at this point determines the number of passbands which the resulting Moiré structure will contain. A schematic diagram for the fabrication technique can be seen in Figure 5.5.

As explained in section 5.2.1, the superposition of fringe patterns gives rise to a narrowband, uniform period Moiré filter. In order to chirp the structure, the phase mask is removed and a refractive index profile is UV-written on top of the filter. The variation in the effective refractive index with length is achieved either by increasing the velocity of the UV beam as it scans along the length of the phase mask or by varying the intensity of the beam.

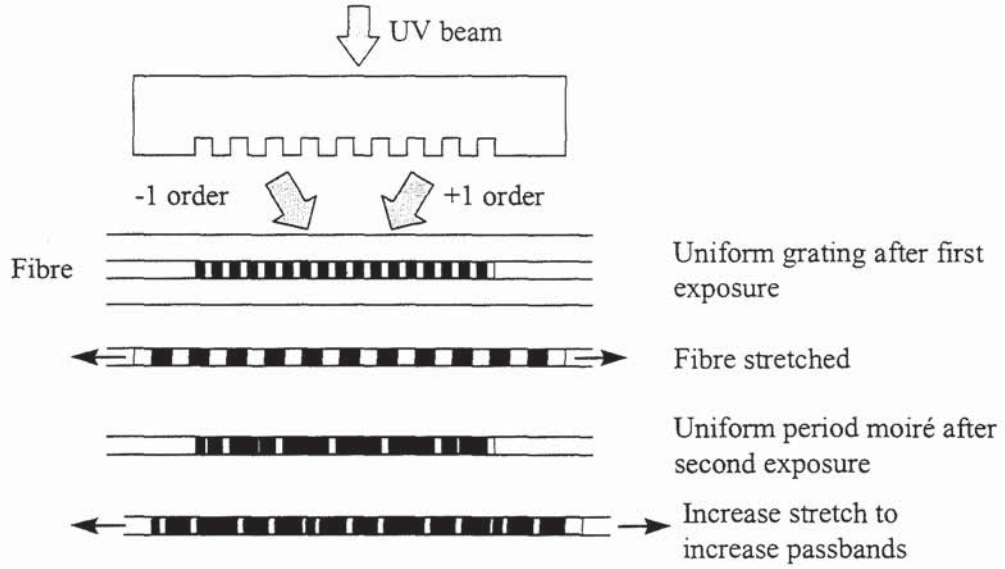

Figure 5.5: Dual scan fabrication technique with stretch in between scans to produce a Moiré structure

The experimental set-up consists of a CW argon-ion laser, intracavity frequency doubled to 244nm, with an average power of 150mW. The beam is focused down eight-fold onto the fibre by a cylindrical lens, which is mounted onto a motorised translation stage, as shown in Figure 5.6. This stage enables the beam to be scanned across the length of the phase mask. Direct-write electron beam lithography and reactive ion etching were used to fabricate rectangular ridge-shape gratings on a fused silica substrate which was used as a phase mask in the near-field fabrication of gratings.

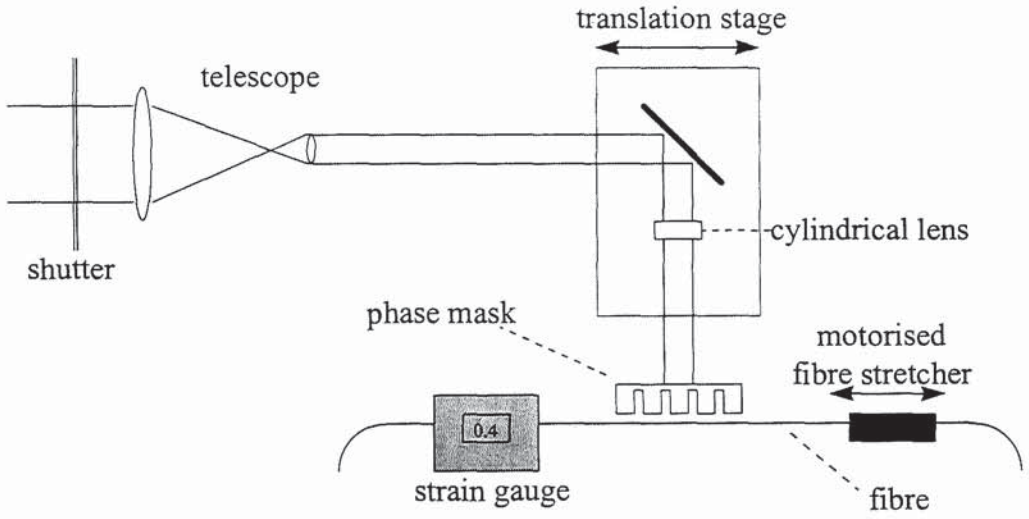

Figure 5.6: Schematic diagram of the experimental set-up to write Moiré gratings

To achieve high reflectivity levels, gratings are generally fabricated in hydrogenated, boron-germania co-doped fibre. The measured transmission spectrum of a typical

filter produced using this method of fabrication is shown in Figure 5.7. The high resolution characterisation of this grating was obtained by a tunable laser source, which was scanned in wavelength steps of 0.001nm. The grating was connected to one port of an optical circulator and the power reflected and transmitted could then be measured using an optical spectrum analyser.

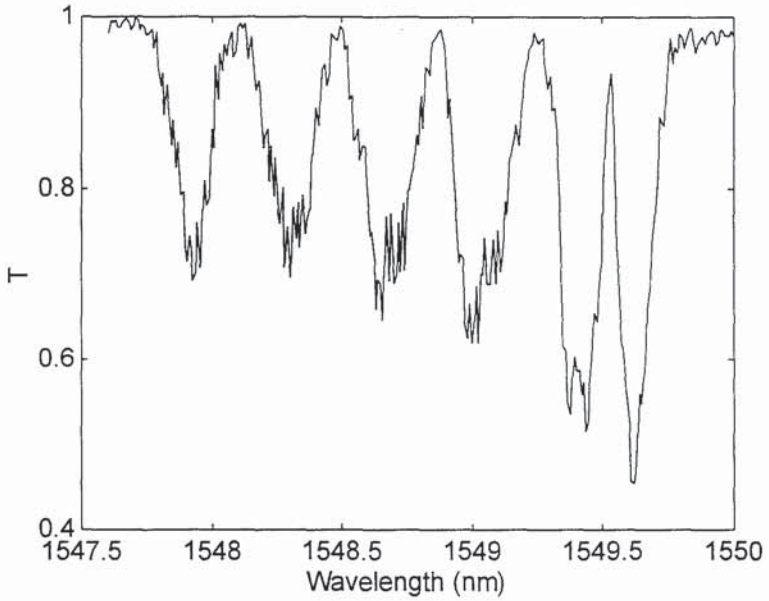

Figure 5.7: The measured transmission spectrum of a chirped Moiré grating fabricated using the dual scan fabrication technique

The filter shown in Figure 5.7 was produced using a uniform period phase mask, of length 5cm. The fibre was clamped in between two posts, 12cm apart and the intermediate stretch was produced by the 8.3μm movement of one of these posts, using a motorised micrometer translation stage. The fibre strain was measured using a strain gauge. The applied strain produced a 0.1nm wavelength shift between the two gratings. Once the phase mask was removed, the computer was set to control the chirp at a rate of 500ps/nm and the resulting structure had six passbands over a bandwidth of 1.9nm. As may be seen in Figure 5.7, the passbands get closer together as the wavelength increases along the length of the filter. This has been attributed to the saturation of the achievable refractive index change within the fibre [15]. The chirping of the grating using refractive index profiling requires a large difference between the final effective refractive index at the ends of the grating and this proves to be a major limitation of this chirping technique. Although hydrogenated, boron-germania co-doped fibre was used in the grating fabrication, it appears that a more highly photosensitive fibre is required to increase either the strength or the bandwidth of the filter. This is likely to limit the use of the dual scan Moiré technique if chirped devices are required.

5.2.3.2 Chirped Phase Mask Technique for Moiré Grating Fabrication

A simpler method of Moiré grating fabrication involves the dual scan of a chirped phase mask. In this case the chirp is provided by the phase mask and so the bandwidth of the filter can be broadened without the refractive index limitation imposed by the previous technique. Using a chirped phase mask, all of the available refractive index change can be used to increase the strength of the gratings, resulting in sharper passbands within the filter stopband.

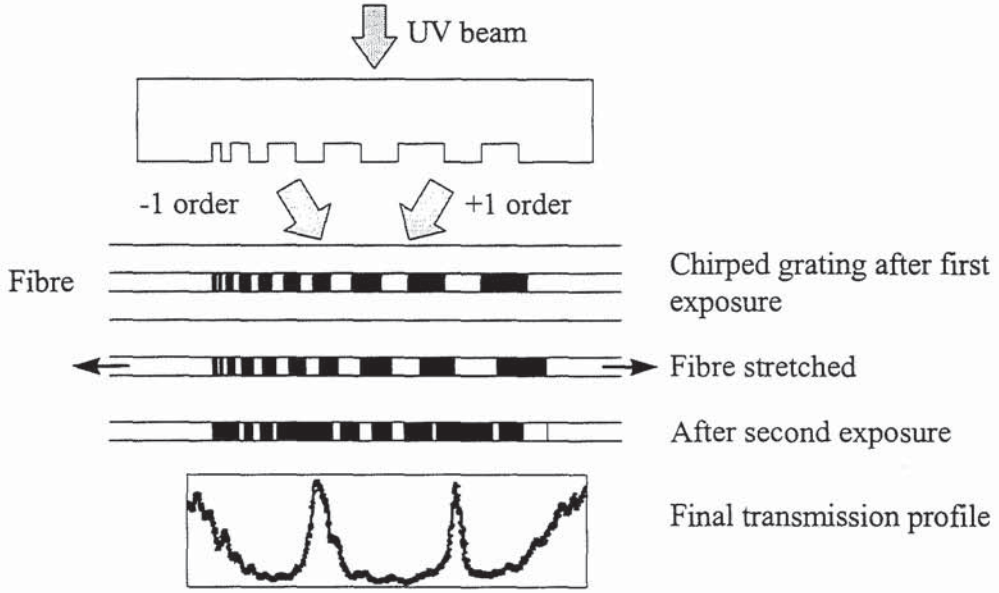

Figure 5.8: Chirped phase mask technique for the fabrication of chirped Moiré structures

The experimental arrangement is identical to that of the dual scan technique, shown in Figure 5.6, apart from the use of a chirped phase mask. The first chirped grating is written into the fibre by scanning the beam along the length of the phase mask. Calibration data gives the exact relationship between the amount of stretch and the corresponding wavelength shift of the grating, allowing the grating to be shifted by an exact amount. After the fibre is stretched by a small amount, a second grating is written on top of the first, producing the chirped Moiré filter. A schematic diagram of the fabrication technique is given in Figure 5.8. The bandwidth is determined by the chirp on the phase mask, allowing a wide range of filters to be fabricated.

Figure 5.9 shows the transmission spectra of two experimentally obtained filters designed to have different numbers of passbands. The phase mask used was 1cm in length and designed to have a total chirp of 1.383nm, producing a grating of bandwidth 2nm. Experimental characterisation of the phase mask showed the average

zero to first order power across the length of the mask was 50%, with 12% of the total transmitted power in the higher diffracted orders, highlighting the fact that this was not an ideally designed phase mask. The power in the zero order produces an increased overall 'dc' level in the refractive index profile of the grating thereby decreasing the fringe visibility of the grating. Again, the fibre used was boron-germania co-doped that had been hydrogen loaded at a pressure of 140 atmospheres, at room temperature for several weeks.

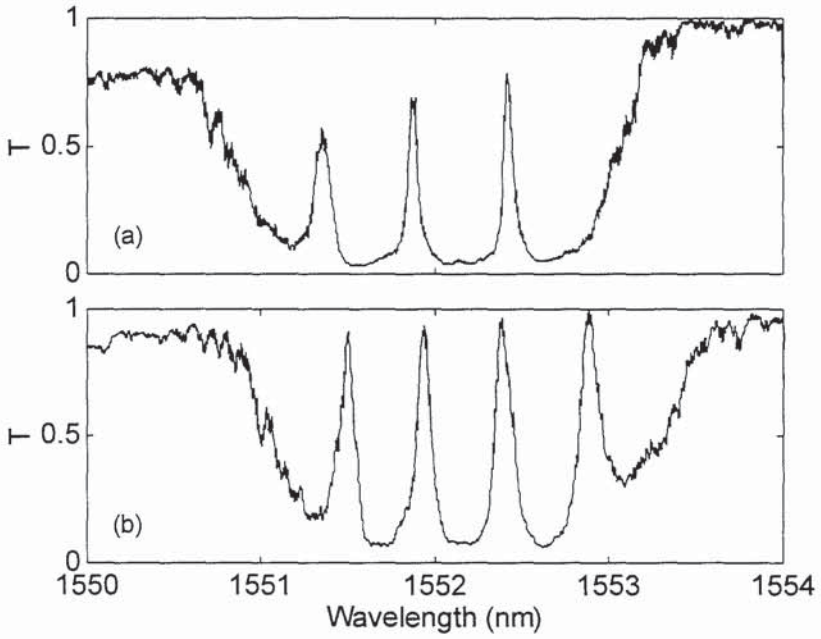

Figure 5.9: Chirped Moiré filters having varying numbers of passbands within the overall stopband: (a) three-passband device; (b) four passband structure

Figure 5.9(a) shows a filter designed with a 0.24nm wavelength shift, corresponding to a change in grating length of 0.016%. The resulting three-passband filter exhibits a finesse of 7 and a stopband which rejected >90% of the incident light. Results for a four-passband structure are illustrated in Figure 5.9(b). This device was fabricated with the same exposure as the previous filter, but had an increased stretch equivalent to a change in grating length of 0.018%. This produced a 0.28nm wavelength shift leading to an increase in the number of passbands and a filter finesse of 4.

Using the experimental set-up shown in Figure 5.6, the translation stage movement, s (in μm), required to produce a grating with a particular number of passbands is given by

$$s = \frac{48n\Lambda_{PM}L_f}{\left(2n\Lambda_{PM} + L_g\right)}$$

Equation 5-3

where n is the number of passbands required, L_f is the length of fibre held between the motorised fibre translation stage and the strain gauge, L_g is the length of the grating and Λ_{PM} is the periodicity of the phase mask.

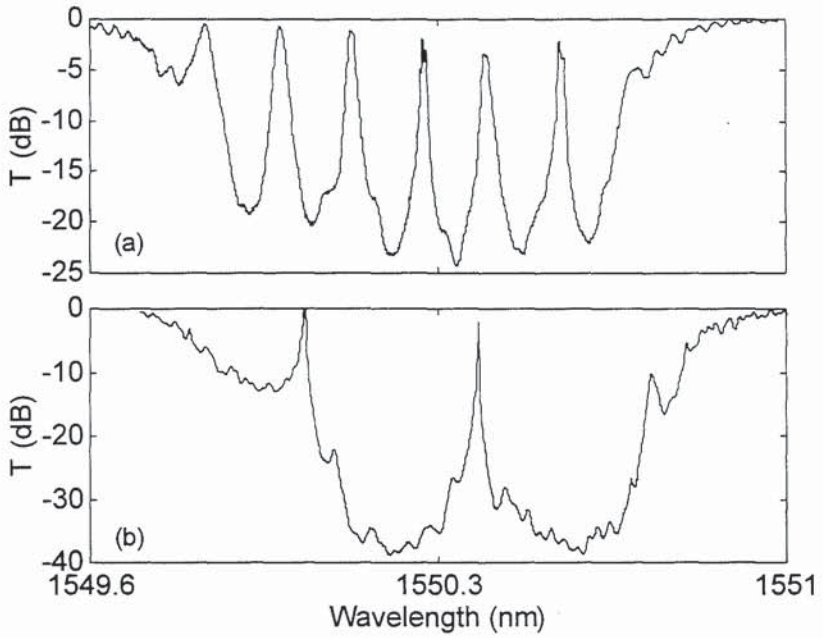

Figure 5.10: Transmission spectra of chirped Moiré gratings: (a) five-passband device; (b) very narrow single passband (≤0.001nm) device

Figure 5.10 shows the spectral profiles of two chirped Moiré structures. Both devices were made with a 5cm phase mask, designed to have a total chirp of 0.692nm, producing a grating of bandwidth 1nm. Figure 5.10(a) shows a five-passband device, written in hydrogenated boron-germania co-doped fibre. The inter-scan stretch was 17μm, which was equivalent to a 0.01% change in grating length. Figure 5.10(b) shows a stronger device, having an inter-scan stretch of 8μm, which corresponds to a 0.005% change in grating length. The resulting filter has a single passband within a stopband which rejects 35dB. The bandwidth of the passband was measured using a tunable laser and found to be 0.001nm, which corresponds to the smallest wavelength step achievable by the tunable laser. The features of the grating do not appear to be fully resolved and the bandwidth of the passband is likely to be narrower than it appears in Figure 5.10(b).

The experimental results of Figure 5.9 and Figure 5.10 follow the trends predicted using the transfer matrix technique, as per section 5.2.2. These filters are difficult to model exactly due to the number of parameters which have to be estimated, including the core and cladding diameter, the induced refractive index change and the periodicity of the two gratings. Also, the model does not take into account factors like

the quality of the phase mask or variations which occur during the fabrication process.

The experimental results confirmed that an increase in stretch between UV exposures increases the wavelength of the second grating with respect to the first, and results in a greater number of passbands. The limit on the number of passbands is determined by the total amount of stretch which fibre is given. The limit on the finesse of the filter is determined by the maximum refractive index change achievable in the fibre.

5.2.4 Ripple Effect on Moiré Filter Profiles

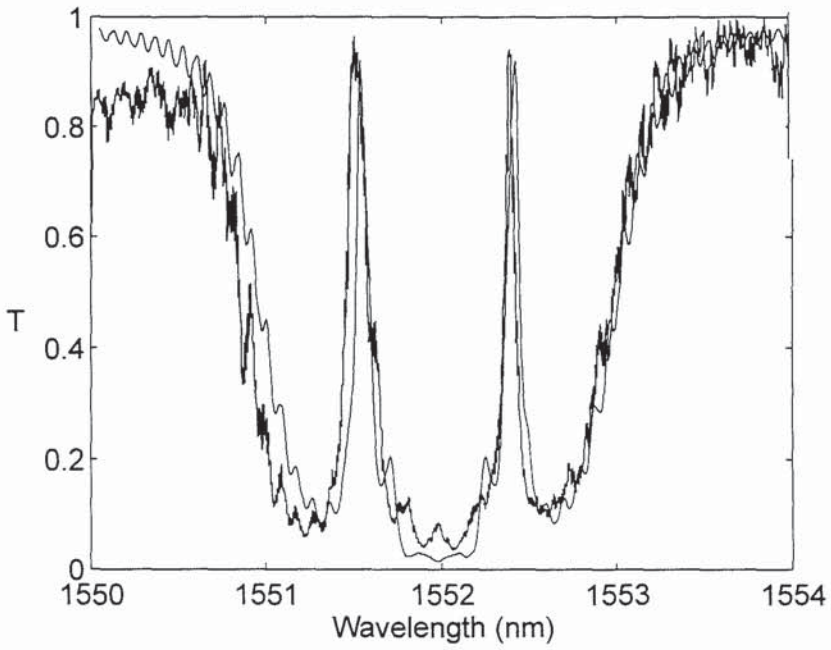

Figure 5.11: Comparison between a modelled (thin line) and experimentally obtained (thick line) Moiré resonator having two passbands.

Figure 5.11 illustrates a two-passband chirped Moiré structure. For the fabrication of this filter, the wavelength shift induced in between the two uniform velocity exposures was 0.16nm. This shift corresponded to a change in grating length of 0.01%. The device has two clear passbands within a stopband which reject 90-95% of the incident light and has a finesse of 9. Figure 5.11 shows that the resulting Moiré filter closely follows that modelled using the transfer matrix technique. The modelled filter consisted of two identical gratings each having a refractive index modulation of 2.5×10^{-4} with centre wavelengths separated by 0.165nm.

It is interesting to note that both the experimental and modelled filter profiles exhibit a 'ripple' effect. Further investigation was undertaken into this effect and the ripple

was found to be due to the non-optimisation of the intermediate strain between the two UV exposures, the cause of which is discussed below.

Figure 5.12 shows a selection of 1cm Moiré filters modelled using the transfer matrix technique. The wavelength shift induced between the two uniform velocity scans is incrementally increased in order to examine the effect which a small change in wavelength (or strain in the experimental case) has on the overall filter profile. It may be seen that a wavelength separation of 0.25nm gives the smoothest spectral profile whereas, for the other separations, a number of ripples are apparent.

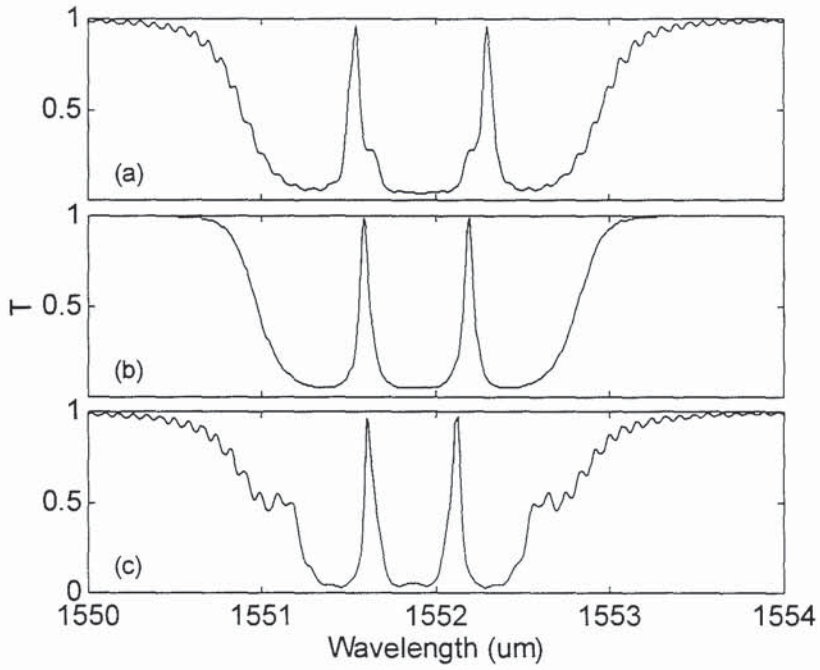

Figure 5.12: Modelled Moiré filters showing the effect of incrementally increasing the wavelength shift in between the two gratings: (a) wavelength separation 0.165nm; (b) wavelength separation 0.25nm; (c) separation 0.29nm

Provided that the optimised strain is applied to the fibre, this Moiré technique has the advantage that it can be used to fabricate apodised gratings, since the two Bragg gratings are out of phase at the boundaries of the structure. If a non-optimised stretch is applied to the fibre then the apodisation is truncated and the final grating profile exhibits ripples. Previously, apodisation has been carried out by varying the UV exposure along the length of the grating [16], which varies the refractive index modulation and the average photoinduced refractive index. This leads to an additional undesirable chirp of the Bragg wavelength. The dual scan method of grating fabrication reported here produces a constant average photoinduced refractive index whilst having a modulated fringe pattern. This results in the pure apodisation of the gratings produced.

5.3 Phase Shift Gratings

In addition to the Moiré technique, there are a number of other methods of fabricating multi-passband devices. These include the introduction of a phase shift into the grating structure. Alferness *et al* [17] originally demonstrated that the introduction of a quarter-wave shift at the centre of a waveguide opens up a transmission peak within its stopband. There have been many reports on different techniques to introduce phase shifts into a grating, including post-processing [18] and phase shifted masks [19]. These provide a very narrow passband having a high rejection ratio. However, for high data rate optical communications systems the requirement is for broader transmission and rejection bands. Several research groups have proposed the inclusion of multiple quarter-wave phase shifts in the grating in order to tailor the transmission profile of the filter [20,21].

Agrawal *et al* [20] demonstrated the principle of phase-shifted structures, where it was proposed that phase shifts could be introduced into the master phase mask by shifting the pattern by a fraction of a period. This type of grating structure is used for distributed feedback (DFB) lasers [22]. Bakhti *et al* [23] realised structures which contained two phase shifts within an optical fibre, placed at one quarter and three quarters of the way along the length of the grating, respectively. This had the effect of widening the passband compared to a single phase shifted structure but still did not provide a wide enough stopband. Another theoretical report [21] considered the insertion of phase shifts into InP/InGaAsP-based Bragg grating filters in order to shape the profile. This was found to lead to a 0.3dB ripple on the top of the transmission peak. More recently was the theoretical and experimental report on bandpass filters having up to eight quarter-wave phase shifts introduced along their length [24].

The following section presents details of a theoretical and experimental investigation into the insertion of single and multiple phase shifts at various locations along the length of a grating. Not only do these phase shifts give an insight into the shaping of transmission filters, but they also help to understand the effect that various sized stitch errors have on phase mask fabricated gratings [25].

5.3.1 Methods of Introducing a Phase Step into a Grating

There have been numerous reports on the various methods of introducing phase shifts into fibre gratings. A number of these have been concerned with the post-processing or trimming of a uniform period grating in order to generate a more complex spectral transmission profile [18,26]. Using this technique, a particular region along the length of a Bragg grating is exposed to UV light, thus increasing the refractive index change at that particular point, as is demonstrated in Figure 5.13.

Alternatively, the grating can be exposed to short bursts of localised heat which erases a small region of the grating. This post-processing produces two gratings which are out phase with each other and so produces a wavelength selective Fabry-Perot resonator [27] allowing light at the resonance wavelength to be transmitted through the grating.

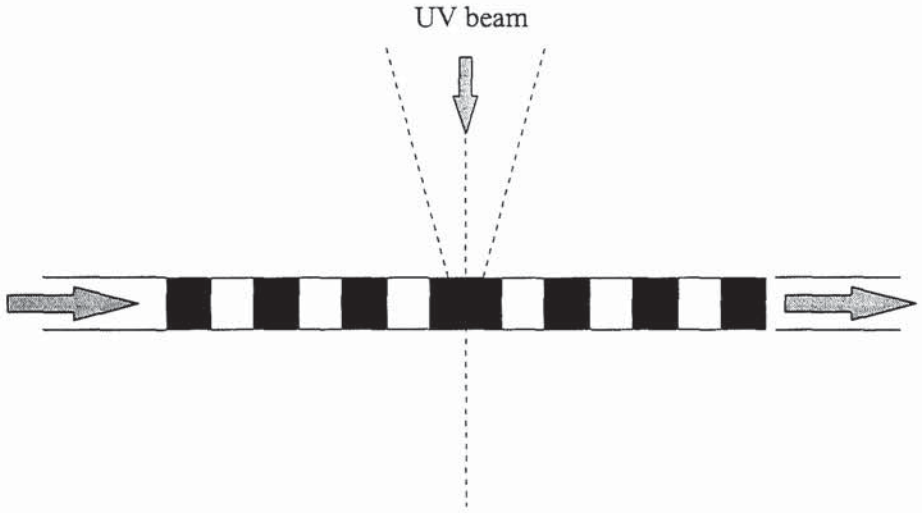

Figure 5.13: The introduction of a phase shift in a fibre grating by post-exposure

Janos *et al* [28] also reported on the production of both permanent and transient resonances by thermal post-processing. Again the grating was subjected to heat treatment and it was found that for temperatures less than 570K no permanent changes in the grating spectrum were observed. This meant that, below 570K, the temperature could be varied, allowing the resonance of the phase shifted grating to be wavelength tuned to give the desired spectral response.

Another preferred method of introducing a phase shift into a grating is with the use of a specially designed phase mask. Kashyap *et al* [19] reported the replication of quarter-wave shifted gratings written using a phase mask which had a single $\pi/4$ phase shift in the middle. The phase step is easily introduced during the etching process, as illustrated in Figure 5.14, and this means that gratings fabricated using this method are far more reproducible than by the post-processing technique. It is this method of fabrication which has been used for the work described in the following section of the thesis.

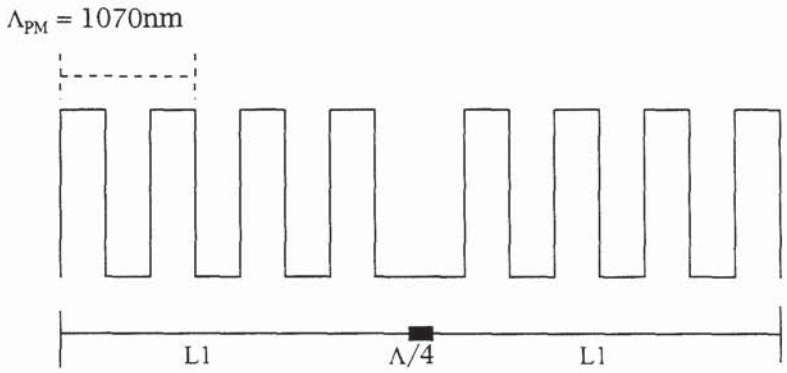

Figure 5.14: Schematic diagram of a phase shift introduced into a uniform period phase mask

5.3.2 Phase Steps in E-Beam Written Phase Masks

Phase mask-written phase-shifted Bragg gratings are fabricated in exactly the same way as standard phase mask gratings, as described in Chapter 2. The fibre is placed directly behind the phase mask and a UV beam is scanned along the length of the mask. This produces a grating from the interference pattern produced by the ± 1 diffracted orders. The distance from the phase mask to the fibre core is typically about half the total fibre diameter, 65μm. Since this distance is much larger than the typical phase mask period of 1.07μm, then a simple far-field diffraction model is appropriate to determine the pattern produced in the fibre core.

Production of phase masks by electron beam lithography (EBL) and dry etching provides the control of grating period, ridge duty cycle and depth required to meet the specifications for telecommunications, sensor and laser systems [29,30]. With e-beam writing fields being typically around 500μm, then there is the inevitable requirement to stitch a number of these fields together in order to produce a phase mask pattern on a millimetre or centimetre length scale. This introduces random errors at the stitch points, whose size depends on the precision of the e-beam machine. These random errors can sometimes be systematically and stochastically predicted for a particular machine [31] but cannot be eliminated completely. In addition to these 'random' phase steps, other intentional steps may be introduced as a means of tailoring the transmission profile of the grating, as was previously discussed.

When a phase step is introduced into a phase mask, it does not generate a discrete phase step in the subsequent fibre Bragg grating, as one might assume. Far from the ordinate of the phase step, at either side, the same interference fringe pattern as before is induced, but obviously the two sides have a phase shift in between them. In

the region close to the phase step, however, the two patterns overlap and a more complex interference pattern emerges. Effectively, the phase steps in the mask correspond to structures with a scale much larger than the distance to the image plane, and therefore near-field components cannot be ignored. The resulting interference pattern which is imprinted in the fibre core depends on a number of things, including the distance from the phase mask to the fibre core. This distance is determined by the size of the fibre and the way the fibre has been mounted in the fabrication set-up. Other important parameters include the angular separation of the two first diffraction orders and the contribution from the zero diffraction order generated by the phase mask. The angular separation is determined by the wavelength of the UV light used in the exposure and the period of the phase-mask. The additional zero order contribution arises from an imperfect mask and also from the phase-shift region due to the change in the ridge duty-cycle at that point where the phase shift has been introduced.

5.3.3 Far Field Diffraction Simulations

There are a number of different approaches to diffraction theory. The Huygens-Fresnel diffraction theory deals with the distribution of monochromatic point sources, which make up the wavefront. These are treated as sources of spherical secondary wavelets and thus the resultant optical disturbance at a point, P, can be evaluated as the superposition of all the individual wavelets.

Kirchhoff's scalar diffraction theory uses a different approach since it is concerned with the scalar optical disturbance and its derivatives over an arbitrary closed surface surrounding point *P*. Taking the monochromic optical disturbance to be

$$E = \xi \ \exp\left[-ikct\right]$$

Equation 5-4

where ξ represents the complex-space part of the disturbance, then the optical disturbance existing at a point *P* can be written as [Appendix 8.2]

$$\xi_p = -\frac{\varepsilon_0 i}{\lambda} \iint_s \frac{\exp\left[ik(\rho + r)\right]}{\rho r} K(\theta)\, dS$$

Equation 5-5

where ε_0 is defined as the source strength and $K(\theta)$ is the obliquity factor, given by $\frac{\cos\theta + 1}{2}$.

For this case, where a phase step has been introduced into the phase mask, the resulting Bragg grating was evaluated using the numerical integration of the Kirchhoff diffraction equation using the scalar approximation, as detailed above.

Such a simulation was carried out to examine the effect of introducing a ¼ Λ_{pm} shift into the centre of a phase mask. For this simulation the phase mask was assumed to be infinite in the direction perpendicular to the fibre and of period 1μm. The length of the phase mask in the direction parallel to the fibre was taken to be 8mm. The fibre was situated 65μm from the mask and the wavelength of the UV exposure was 250nm. Figure 5.15 shows the central region of the phase mask at the position where the phase shift has been introduced. This rectangular phase mask pattern was approximated using 8 discrete points per period.

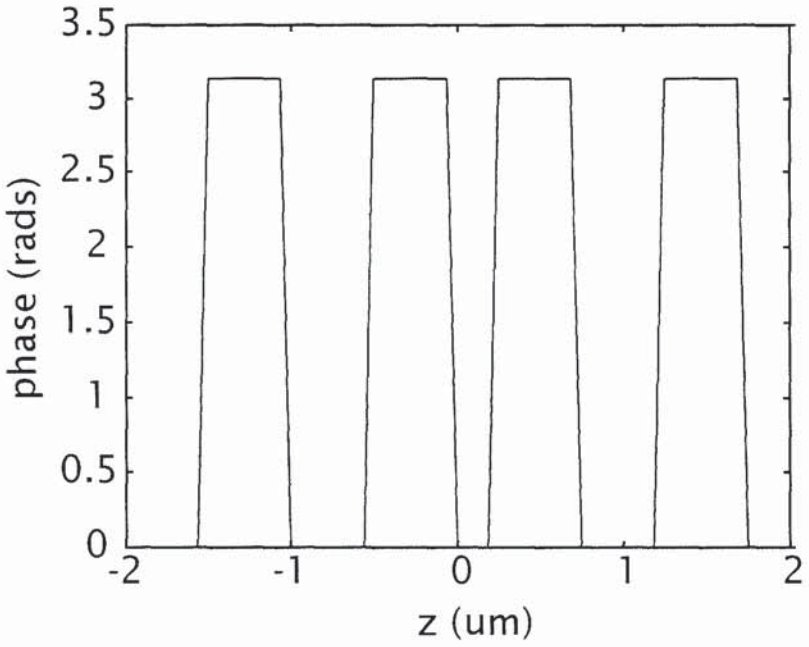

Figure 5.15: Simulated results of phase mask corrugations having a ¼ Λ_{PM} phase shift in the central region

Figure 5.16 shows the calculated interference pattern incident on the fibre core in the central region where the ¼ Λ_{pm} phase shift has been introduced. It can clearly be seen that the interference pattern in this central region has been altered due to this shift, as would be expected.

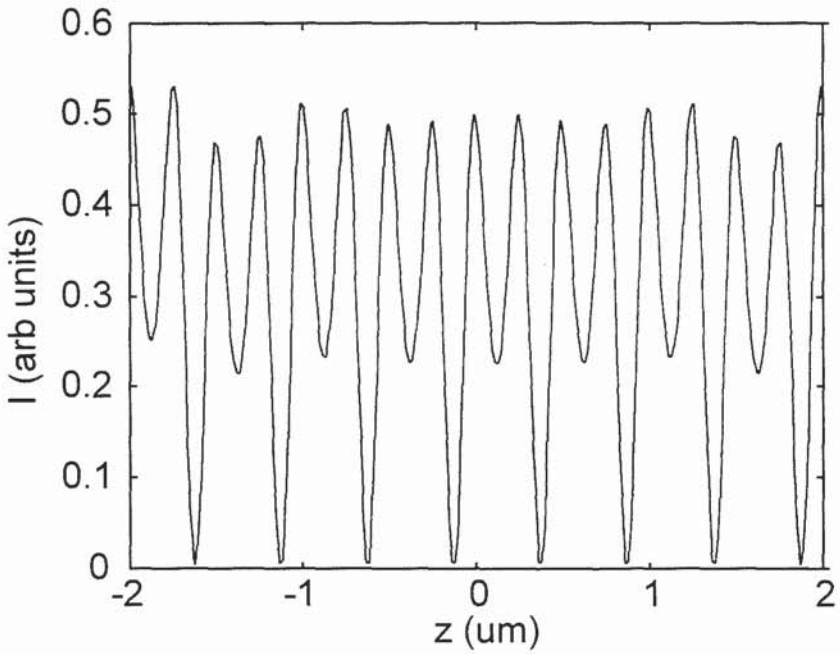

Figure 5.16: Calculation of the effect which a ¼Λ_{PM} phase shift has on the interference fringes in the central region of the fibre core

As mentioned in the previous section, the insertion of a phase shift into the structure of a phase mask alters the interference pattern over an region larger than that containing the shift. To determine the extent to which the phase shift has an influence on the interference pattern, the running maximum, minimum and average of the interference pattern over several periods was calculated, as illustrated in Figure 5.17. From this we see clearly that the discrete localised phase step in the phase mask has given rise to features in the interference pattern extending out to over ±75μm. It is interesting to note that, with the fibre placed at a distance of 65μm from the phase mask, the ±1 diffraction orders only fan out to ±15μm, so it is important to consider the near-field components as well those in the far-field. This result would not be predicted from far-field considerations alone.

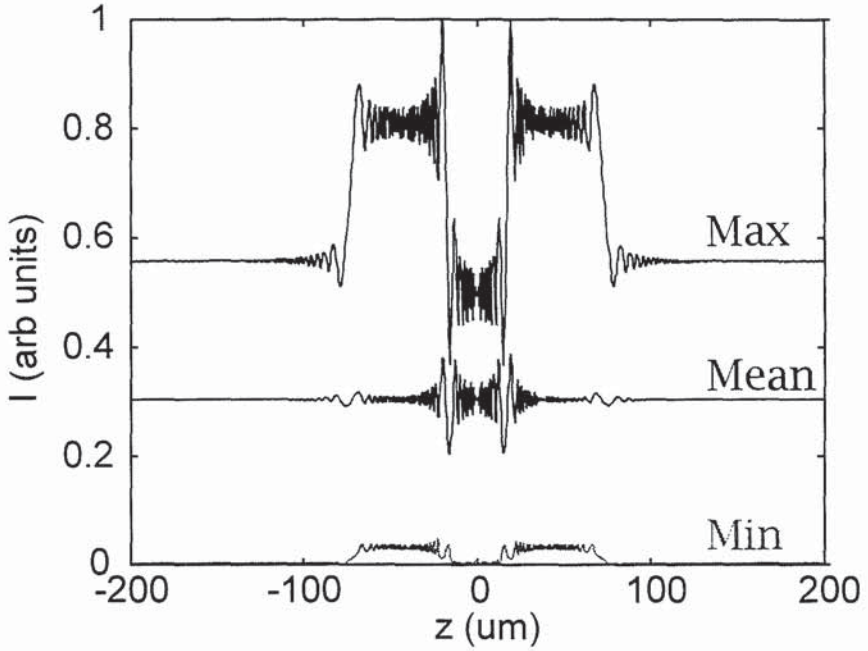

Figure 5.17: Theoretical calculation of the maximum, average and minimum effect which a ¼ Λ_{PM} phase shift has on the subsequent interference pattern

5.3.4 Numerical Calculations for a Mask Containing a Single Phase Shift

Using the results from Figure 5.16 and Figure 5.17, of the interference pattern generated in the fibre core, it is possible to use a Fresnel based transfer matrix approach to calculate the spectrum of the Bragg gratings resulting from the use of this mask. In this analysis we assume that the photo-induced refractive index change is proportional to the incident intensity of the UV light in the interference pattern. Again, the fibre was assumed to be placed at a distance of 65μm from the phase mask and the wavelength of the incident UV light was 250nm. The length of the grating was taken to be 0.625mm and the effective average index in the fibre n_{eff} was assumed be 1.5. The amplitude of the refractive index Δn at the limits of the grating was taken to be 10^{-3}. The numerical results of Figure 5.18 show the calculated Bragg grating spectra from a mask containing a single phase shift of varying size within its structure.

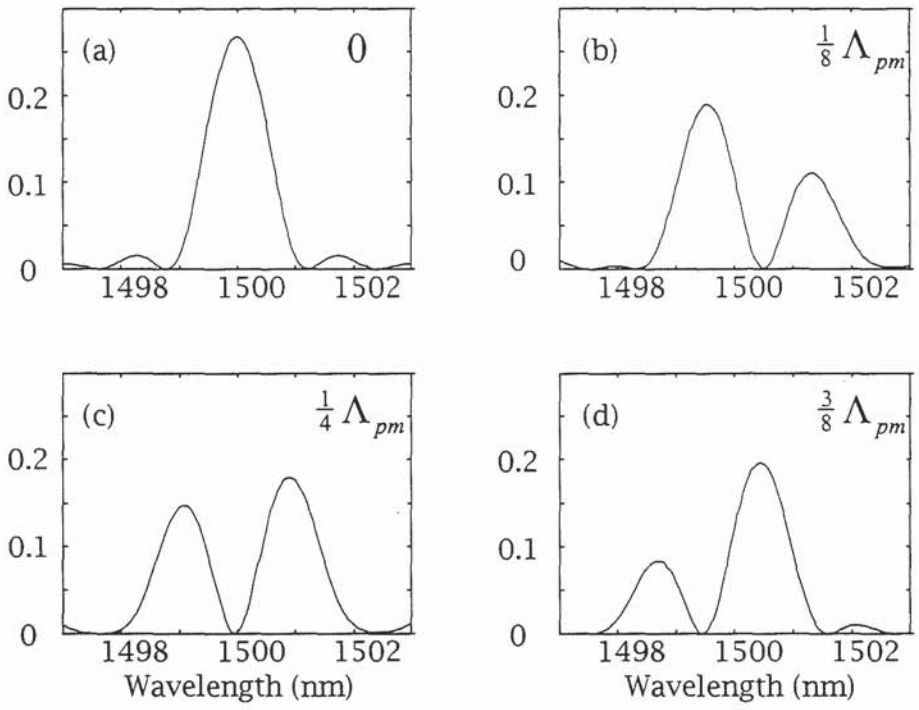

Figure 5.18: Calculated Bragg grating spectra from a phase mask containing a single phase shift of size: (a) 0; (b) 1/8 Λ_{PM}; (c) ¼ Λ_{PM}; (d) 3/8 Λ_{PM}

These results show that, as expected, the introduction of a single phase shift opens up a passband in the grating profile, in comparison with the non-phase shifted case (Figure 5.18(a)). The spectra in Figure 5.18(b),(c),(d) exhibit an asymmetry in their overall grating structure which was not expected.

Further spectral simulations were performed by the integration of the Riccati equation [32], as was detailed in Chapter 2. These determined whether the asymmetry was apparent if the phase shift was inserted directly into the grating, rather than the phase shift being transferred from the phase mask to the grating. The results of such a simulation can be seen in Figure 5.19. These simulations provide similar results to those calculated incorporating the near field components (Figure 5.18) showing such components have only a little effect on the overall grating profile. Figure 5.19(c) clearly exhibits a symmetric structure, implying that the inclusion of the near field components increases the complexity of the grating thus providing the asymmetry witnessed in the simulated results of Figure 5.18. Figure 5.19(c) shows the case which corresponds to the quarter-wave phase shift for DFB semiconductor lasers, as was detailed earlier in this chapter.

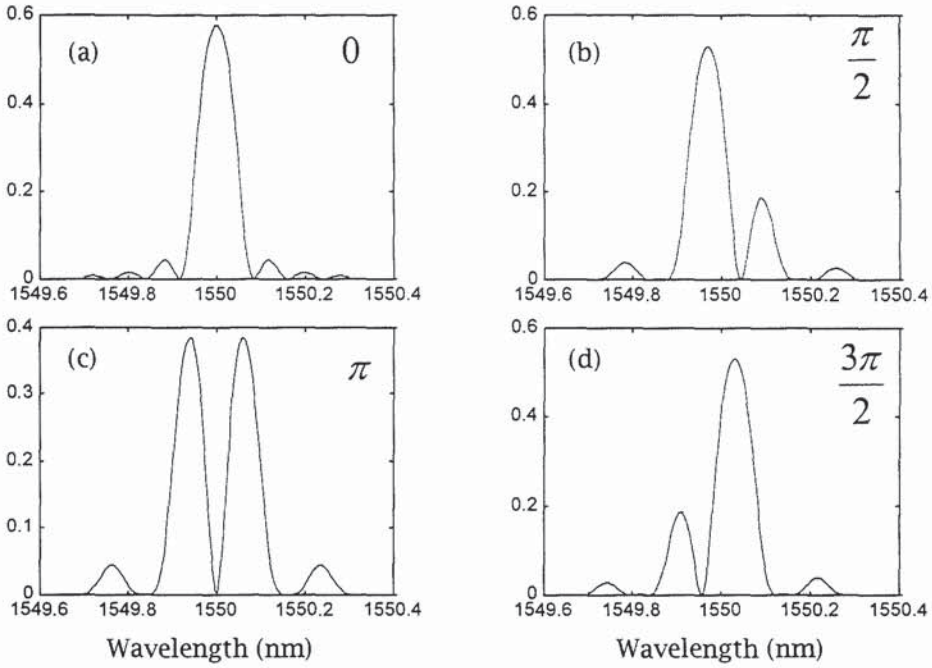

Figure 5.19: Simulated grating spectra having a single pure phase shift inserted into the profile, of size: (a) 0; (b) $\pi/2$; (c) π; (d) $3\pi/2$

5.3.5 Experimental Fabrication of Devices Containing a Single Phase Shift

In order to experimentally confirm the effect which a single phase shift has on the resulting Bragg grating a series of phase masks were produced, having varying sized phase shifts. These masks were of length 800μm which corresponded to two writing fields of the e-beam machine used in the phase mask fabrication. Thus the phase shift could be introduced in between these two fields, ensuring that there were no additional unintentional field stitching errors in the phase masks which would contribute to the final grating spectra. The experimental results clearly show the same asymmetry as was displayed in the simulated results (Figure 5.18) which included near-field components.

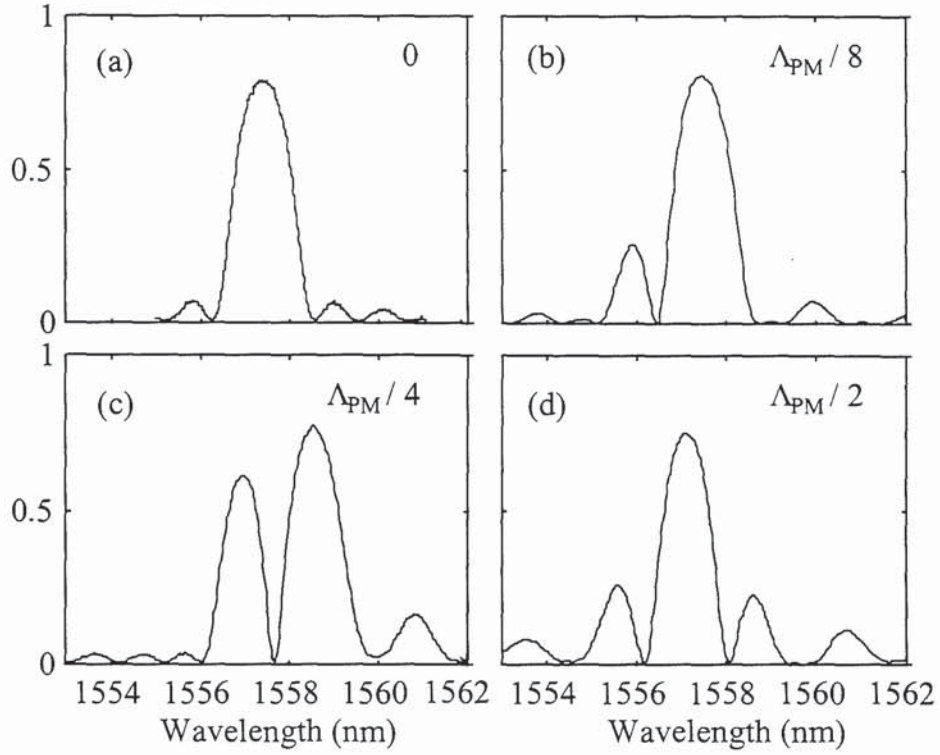

Figure 5.20: Experimental results showing Bragg grating reflection spectra fabricated using a phase mask containing a single shift of size: (a) 0; (b) $\Lambda_{PM}/8$ (c) $\Lambda_{PM}/4$; (d) $\Lambda_{PM}/2$

These results highlight the difference between the spectra simulated from a phase shift in the phase mask and those resulting from a discrete phase shift being introduced into the grating structure. The differences are significant enough to be of concern when designing a phase mask to produce a bandpass grating structure.

5.3.6 Multiple Phase Shift Gratings - Experimental and Theoretical Results

Numerical calculations were also performed for phase masks containing multiple phase steps within their structure. It is obvious that the introduction of multiple phase shifts would increase the complexity of the final grating structure. Figure 5.21 and Figure 5.22 show the results of numerical simulations for a set of masks containing two phase steps, both of size $\pi/2$, the phases of which vary relative to each other. Figure 5.21(a) shows the spectrum resulting from the introduction of two phase shifts placed at distances of one third and two thirds along the length of the mask. These shifts were of the same size and had the same sign, relative to one another. This can be compared to Figure 5.21(b), which again had two phase shifts at positions one third and two thirds along the length, but the signs of these shifts were opposite to one another. The difference in the resulting spectra can clearly be seen indicating

that the relative phases between the phase components are important for masks containing multiple shifts.

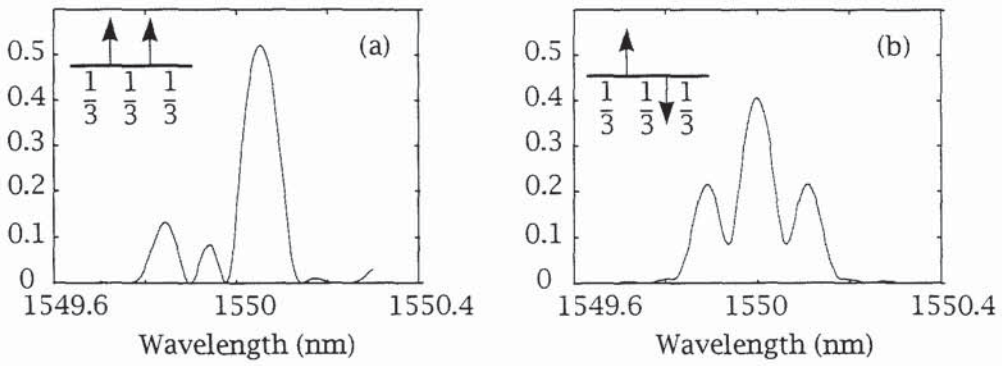

Figure 5.21: Simulated results for a phase mask containing two phase steps of size $\pi/2$ placed at a distance of one thirds and two thirds along the length of the grating

Figure 5.22 examines the effect which placing these two shifts at a different location has on the grating spectra. Figure 5.22(a) is the grating profile resulting from the two phase shifts having the same sign and being positioned at a distance of one quarter and three quarters along the length of the mask. Figure 5.22(b) shows the results of a grating having the same phase shift positions but having different signs. Again, a comparison of (a) and (b) shows that the variation of the relative sign between the two phases results in two different grating profiles. It is also clear when comparing Figure 5.21(a) and Figure 5.22(a) that not only is the relative phase an important parameter for the resulting grating, but the length positioning of these phase shifts greatly effects the profiles.

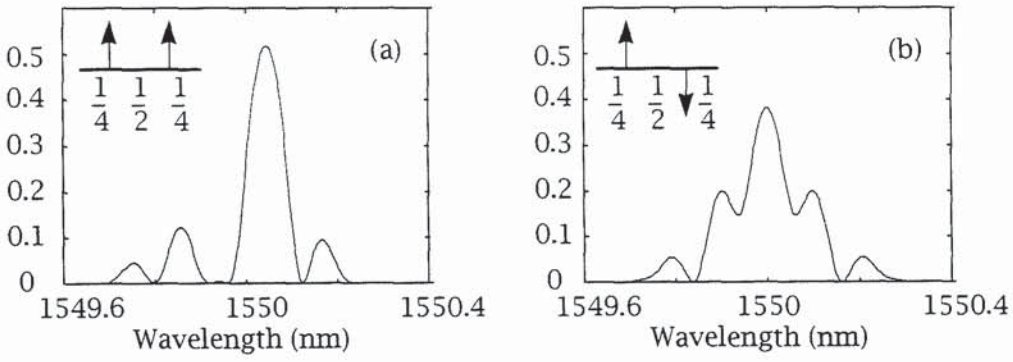

Figure 5.22: Simulated grating spectra for a phase mask having two $\pi/2$ phase shifts, placed at a length of one quarter and three quarters along the mask

In order to further examine the effect which multiple phase shifts have on grating profiles, a number of phase masks were produced. These were of length 2000μm, thus making it impossible to separate the grating features resulting from the introduction of the multiple phase shifts from those 'stitch errors' created when the numerous e-beam writing fields were stitched together. Figure 5.23 shows details of two gratings fabricated with masks containing two intentional phase shifts, of size $\Lambda_{PM}/4$, at varying locations. In (a) these shifts are positioned at ± 500μm and in (b) these shifts are placed at ± 333μm.

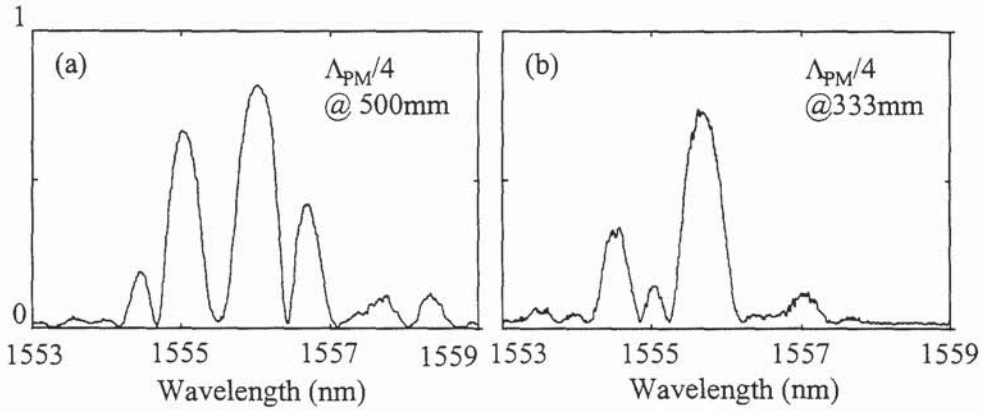

Figure 5.23: Actual grating spectra of multiple phase shifted gratings, total grating length 2000 μm: (a) two $\Lambda_{PM}/4$ phase shifts at ± 500μm; (b) two $\Lambda_{PM}/4$ phase shifts at ± 333 μm

As would be expected, the length of the phase mask has a direct effect on the resulting grating spectra. Shorter gratings generally have broader bandwidths and the features introduced by the phase stitch errors tend to broaden as well. This shown in Figure 5.24 where the two gratings both have a phase step of $\Lambda_{PM}/4$ but are of different lengths, (a) being of length 2000μm and (b) being of length 800μm.

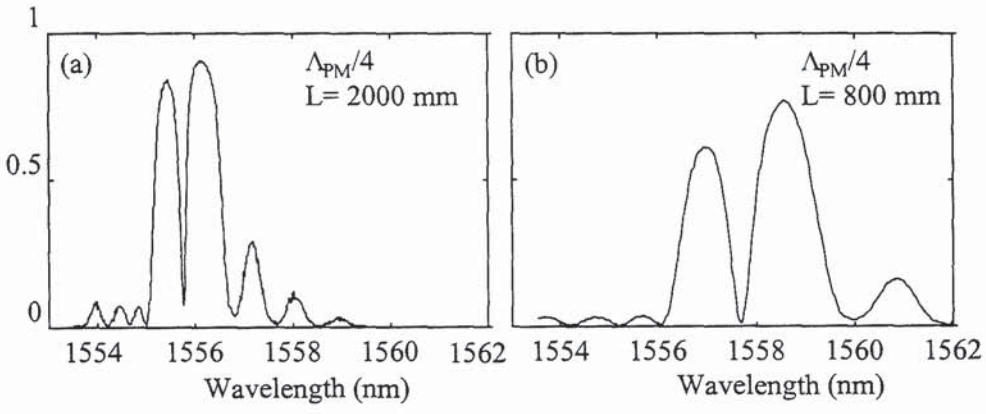

Figure 5.24: Single phase shifted gratings, having a phase shift of $\Lambda_{PM}/4$. (a) length 2000μm; (b) length 800μm

5.4 Multiple Wavelength Filters

An alternative - and arguably the most obvious - approach to the fabrication of multiple wavelength passband filters is to concatenate a number of single passband gratings [33] having different Bragg reflection wavelengths. This results in a grating array which can be used in conjunction with a circulator to obtain both the reflection and transmission data from the filter (Figure 5.25). Each grating is designed to pass one signal wavelength whilst rejecting the others.

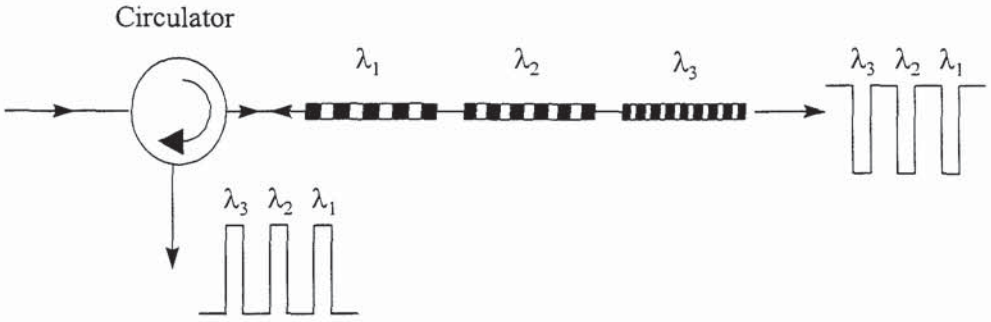

Figure 5.25: Multiple passband grating array configuration for measuring both reflection and transmission profiles

A similar concept was reported by Mizrahi *et al* [34] where four individual gratings were spliced on to an output port of a commercial fused 1 × 4 fibre splitter, where the device was designed to operate in transmission. Other research groups have demonstrated fibre grating transmission [35] and channel dropping filters [36] which employ a four port coupler for each filter. The problems these techniques encounter include high insertion loss and crosstalk, both of which degrade the signal transmission.

An advantage of using individual gratings is that it is possible to fabricate strong, apodised filters, with minimised out-of-band reflections which might otherwise interfere with the signal transmission.

This section describes the development and progression of ideas for the fabrication of multiple grating arrays, including both a holographic and phase mask method and the exploration of superposition and concatenation techniques. As explained at the start of this chapter, the applications for multiple wavelength filters include use in wavelength division multiplexed (WDM) and very high bit-rate TDM systems. This section includes work carried out under the PHOTOS project. The aim of which is to exploit new and significant technology to develop key fibre components written directly into photosensitive optical fibre, for the future photonics network.

5.4.1 Holographic Grating Arrays

The first technique adapted to fabricate multi-wavelength filters was that using the holographic interferometer. Here, the length of each grating is determined by the two UV beams at their point of interference. Typically, this length is a few millimetres and, consequently, this restricts the minimum achievable grating bandwidth. A single grating is fabricated; then the fibre is translated by a grating length and the angle of the two-beam interference is adjusted so a grating at a different wavelength can be written. Figure 5.26 shows an array of evenly spaced uniform period gratings fabricated in this manner.

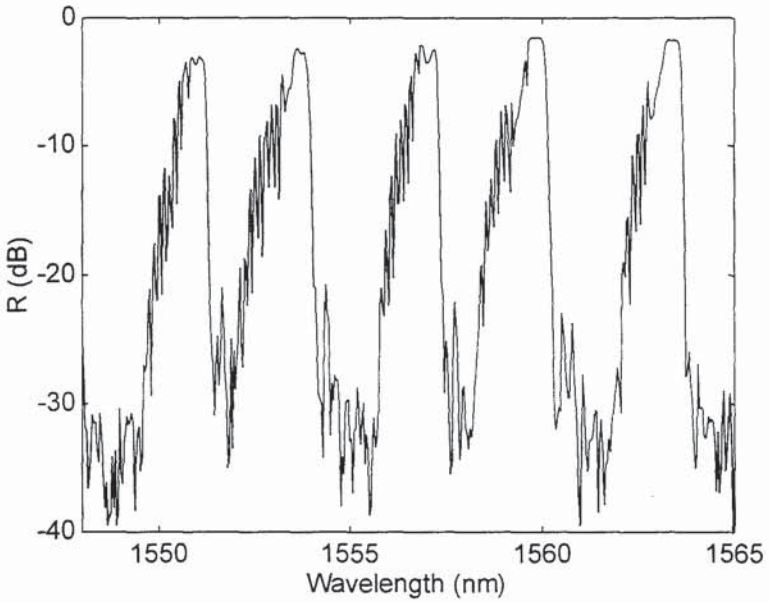

Figure 5.26: Reflection spectrum of an array of uniform period gratings fabricated using a holographic interferometer

Use of this method of fabrication renders it difficult to properly apodise each individual grating and, as mentioned previously, this results in a large number of unwanted spectral sidelobes. The UV beam used in the filter fabrication has a gaussian profile, which does in fact provide some degree of apodisation. The gaussian profile provides a non-uniform average refractive index in the fibre core, thereby 'apodising' each grating. Unfortunately, a consequence of using such a spatial profile is the production of further unwanted structure within the stopband. The Bragg wavelength is proportional to the effective refractive index of the grating (Equation 2.2) so in this case the non-uniform refractive index induces a local Bragg wavelength which is longer in the centre than at the edges of the grating. The two ends then act as a Fabry-Perot resonator, producing resonances on the short wavelength side of the grating stopband. Again this will degrade the signal transmission.

5.4.2 Phase Mask Grating Arrays

The use of a phase mask in the grating writing process allows gratings of constant average refractive index to be produced, thus removing the unwanted 'self chirping' effect which the holographic technique has. The various channel wavelengths can be achieved by either using a different phase mask for each grating, or more simply by straining the fibre a particular amount prior to UV exposure. This reduces the period of the resulting grating once the fibre is relaxed, as was detailed in Chapter 2, leading to fabrication of a grating at a shorter wavelength. This 'wavelength tuning' is limited by the amount of strain which the fibre will withstand before breaking and can be up to 10nm, depending on the fibre type. An obvious advantage to the wavelength tuning technique is that, depending on the channel spacing requirements, only one phase mask is needed to fabricate the complete grating array. A typical phase mask written grating array is shown in Figure 5.27. This filter was fabricated in highly doped germania fibre, which had been hydrogenated for over 10 days. It consisted of 4 gratings, each of length 5mm and separated by a gap of 1mm, making the device a total length of 23mm.

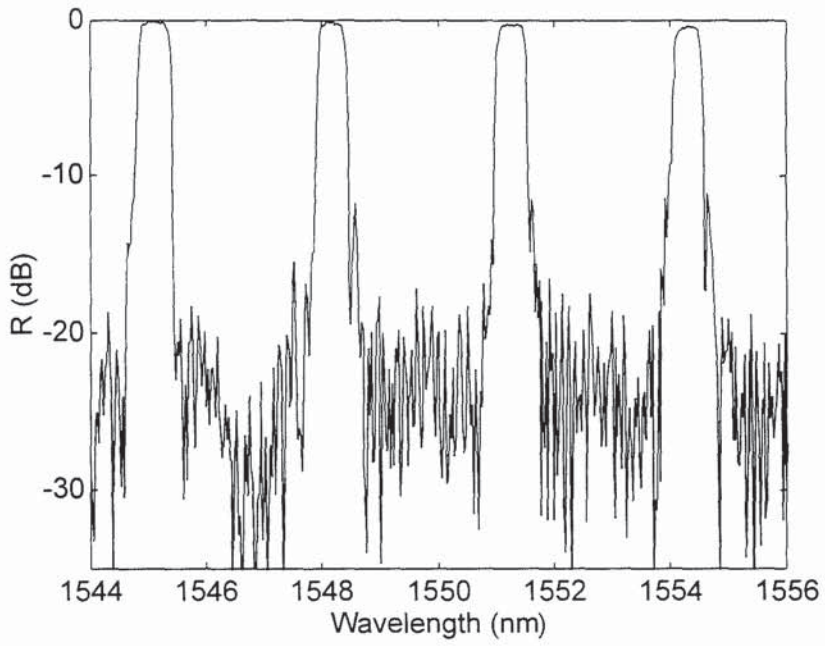

Figure 5.27: Reflection spectrum of an apodised array of gratings fabricated using 5cm uniform period phase mask

A possible limitation of this 'concatenation' technique is the length constraint which the packaging of such a device incurs. For commercial application, the device needs to be temperature and strain stabilised to ensure that the grating Bragg wavelengths do not change under the varying environmental conditions. This entails housing the

array in a packaging device, in which the gratings may need to be bonded to posts set a short distance apart. Obviously, this sets a maximum possible grating array length.

5.4.2.1 Multipassband Array by Superposition Technique

One method of minimising the total length of fibre required for the grating array is to write the gratings on top of one another. This means that the length of fibre used is only one grating long, rather than the more typical 5 or 6 lengths. Again, to reach the various channel spacings required, it is necessary to strain the fibre by varying amounts prior to exposure.

Although this fabrication technique optimises the length of fibre required, it highlights another problem, that of the non-linear refractive index growth for superimposed gratings. For the initial exposures, the induced refractive index change in the fibre core is large and strong gratings are written. As the overall refractive index change approaches saturation the rate of change decreases, as was illustrated in Figure 3.4 , thus fabricating weaker gratings for the same UV exposure. This leads to an uneven wavelength spacing between channels, as is observed in Figure 5.28.

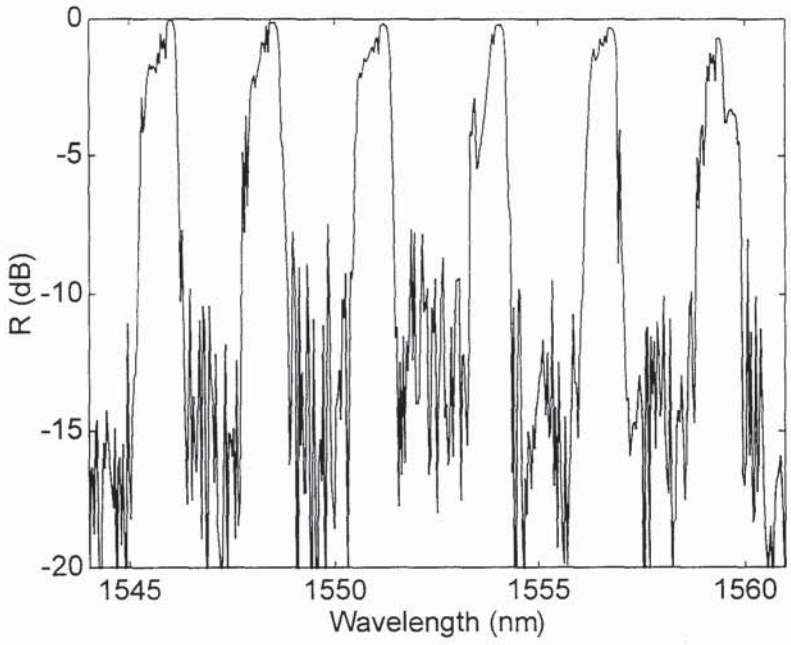

Figure 5.28: Reflection spectrum of a refractive index limited array fabricated by the grating overwriting technique

5.4.2.2 Multiple Wavelength Phase Mask Technique

The recent technical advances in the phase-mask fabrication process have resulted in the design and fabrication of more unusual phase mask patterns. For simplicity of fabrication and ease of mass production an apodised grating array is most easily

fabricated in a mask designed to write a number of adjacent gratings at various channel wavelengths.

For the final stage of this investigation, a five-wavelength mask was specifically designed to meet the PHOTOS project specification wavelengths. Initial tests revealed that the channel wavelengths of the mask did not meet the exact specifications and some strain tuning was still required. The stitch errors appeared to be less significant than for those observed using the 5cm uniform period mask. Using this mask, it was possible to fabricate a device 25mm long, consisting of 5 apodised gratings. This facilitated the inclusion of more channels in the fibre than by use of a single pattern and the stretch and write technique, due to the reduced fibre-strain required. As concluded in Chapter 3, a raised cosine apodisation profile appeared to offer a suitable compromise between maximum sidelobe suppression and maximum grating bandwidth for a grating of this length, therefore all the gratings in the array were apodised using this function.

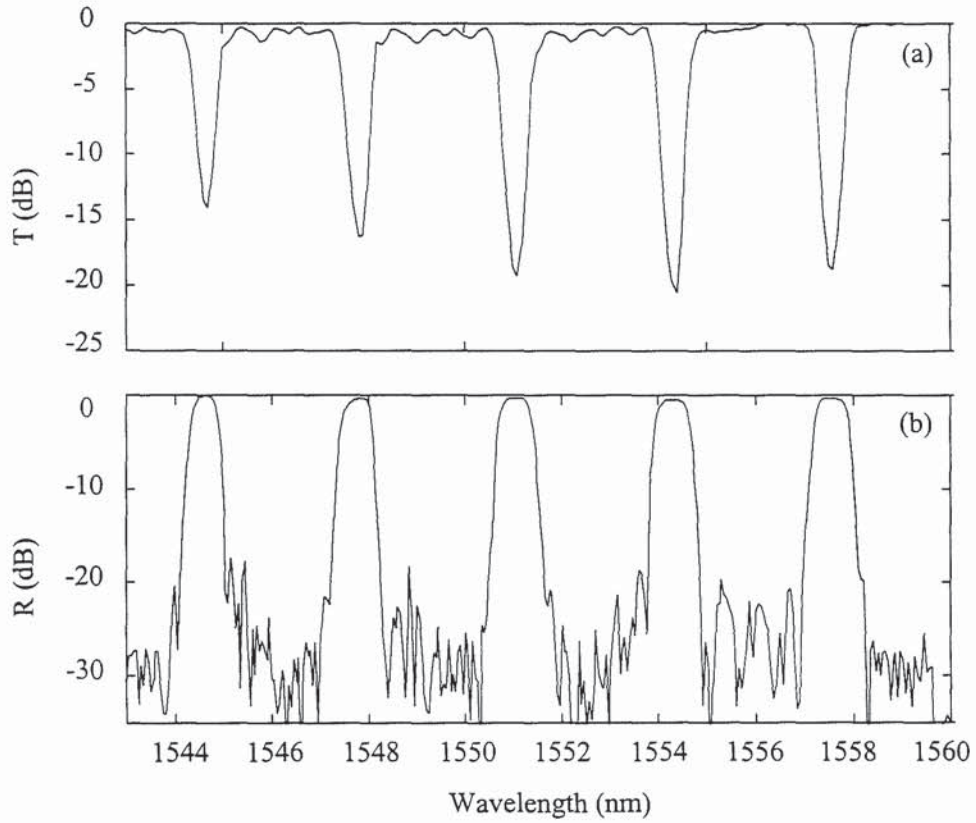

Figure 5.29: An apodised five-wavelength grating array made with a multi-wavelength phase mask (a) transmission spectrum (b) reflection spectrum

Figure 5.29 demonstrates one of the final multiwavelength devices fabricated using the previously described technique. Measurement of the transmission characteristics of the array revealed that, although the grating spacing was particularly uniform at

(3.20± 0.06)nm, the reflectivity ranged from 14dB to 20dB. The reflection measurement in Figure 5.29(b) shows an increased sidelobe suppression, down to a value of -20dB, with the overall noise floor at ~-30dB. The raised cosine apodisation function resulted in each of the five gratings having a 1dB bandwidth of 0.5nm and a 3dB bandwidth of 0.7nm.

5.4.3 Application of Multiple-Grating Arrays in WDM Systems - PHOTOS Project

As previously stated in this chapter, one of the main applications for multiple grating arrays is in wavelength division multiplexing systems [37]. This section details the work carried out by other partners within the PHOTOS project to package and field-test multi-wavelength filters for WDM applications. The five wavelength notch filter illustrated in Figure 5.29 was initially thermo-packaged by SIRTI and was subsequently characterised at Alcatel Alsthom Recherche (AAR).

5.4.3.1 Wavelength Division Multiplexing Device Specifications

Table 5-1 gives the specifications to which the multi-wavelength filters were to be made. The target of six channels, having 0.5nm 1-dB bandwidth and a 35nm stopband was rather ambitious and the number of channels fabricated was eventually limited by the packaging length constraints.

BANDPASS FILTER PARAMETER	GRATING SPECIFICATION
Channel Wavelengths	1542.94nm (194300 GHz) 1546.12nm (193900 GHz) 1549.31nm (193500 GHz) 1552.52nm (192700 GHz) 1555.75nm (192700 GHz) 1558.98nm (192300 GHz)
Channel Filter Bandwidth (1dB- b/w)	0.5nm
Insertion Loss	< 2dB
Spectral Rejection Rate	> 25dB
Stop-Band Width	> 35dB
Return Loss	> 35dB

Table 5-1:WDM specifications for multiwavelength filters

5.4.3.2 *Multiple Grating Array Packaging*

For the multi-wavelength arrays to be incorporated into real systems, they must be robust devices, with a high tolerance to transmitter wavelength drifts and temperature variations. The aim is to design a cost effective, compact and totally passive component which is able to operate within a temperature range of +5°C to +70°C. There are several solutions to the problem of wavelength stabilisation. One is to use temperature regulation based on the peltier effect, which involves bonding the grating to a peltier cell and gives good temperature control. It also presents the possibility of tuning the filter, although such an active solution is expensive, fairly complex and requires a power supply. Another solution is to design a specific package in order to stabilise all of the Bragg wavelengths. This second approach is more complex, but has the advantage that it is entirely passive. Under the temperature conditions previously stated this passive solution seemed more promising, and therefore this approach was used to design the packaging to house either a single or multiple-wavelength device. The final optimised packaging device is illustrated in Figure 5.30.

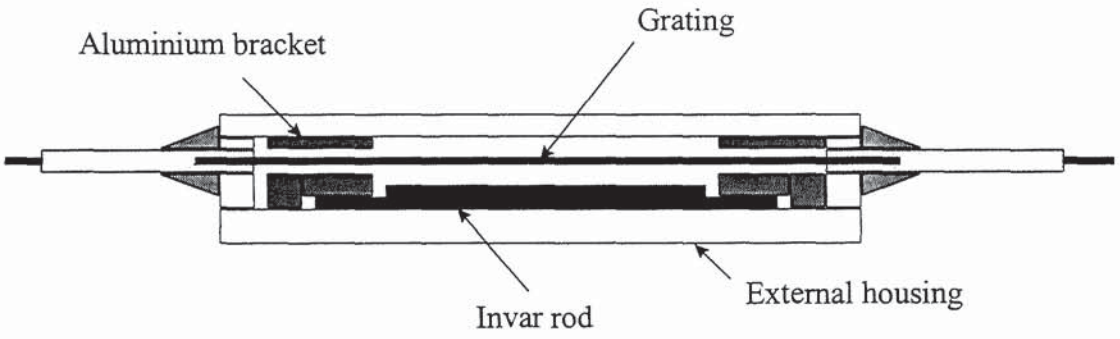

Figure 5.30: Passive packaging designed to temperature stabilise a multiple-wavelength grating array

The chosen passive packaging solution is based on a table-top mounted concept [38]. It consists of a rod, having two brackets screwed onto it. Two different metals are chosen for the rod and brackets, the brackets material having a greater thermal expansion coefficient than that of the rod. Here, the material chosen for the rod was invar, having a thermal coefficient of 1.6×10^{-6} °C^{-1}. The brackets were made from aluminium, with a thermal expansion coefficient of 23.8×10^{-6} °C^{-1}. As the temperature rises, the greater thermal coefficient of the aluminium causes the brackets to expand faster than the rod, thus decreasing the overall distance between the brackets. The grating is pre-tensioned within the packaging so that as the temperature increases and the blocks move closer together, the grating strain decreases. In this way the wavelength increase due to the rise in temperature is exactly counteracted by the

decrease in wavelength due to the reduced strain on the grating. From temperature and stress dependence theory it is possible to calculate the expected length variation of the two materials, allowing the required base and bracket length to be calculated. This leads to the maximum length of the device being restricted to the distance between the two brackets.

In order to hold the device within this packaging, there were a number requirements on the fibre grating. As explained above, the length constrains meant that the total length of the filter had to be less than 28mm and the plastic outer coating needed to be stripped back a length of between 44-46mm. To limit the mechanical degradation of the fibre, the coating was chemical stripped using dichloromethane. Prior to insertion into the packaging it was necessary to thermally anneal the filter, to ensure its wavelength stability during the packaging and temperature characterisation.

Once packaged, the filter was tested for its thermal stability by repeatedly changing the temperature, from 0°C to 80°C. Figure 5.31 shows the wavelength shift which each of the five channels experienced as the temperature of the surrounding environment was varied. The results show that all five channels experience a wavelength shift of less than 0.1nm for an operating temperature range of between 0°C and 80°C. The wavelength shift for one channel prior to the temperature compensation was monitored, and can be seen to be to shift as much as 0.7nm. These results highlight the importance of the effective thermal packaging of any type of device to minimise wavelength fluctuations caused by external influences.

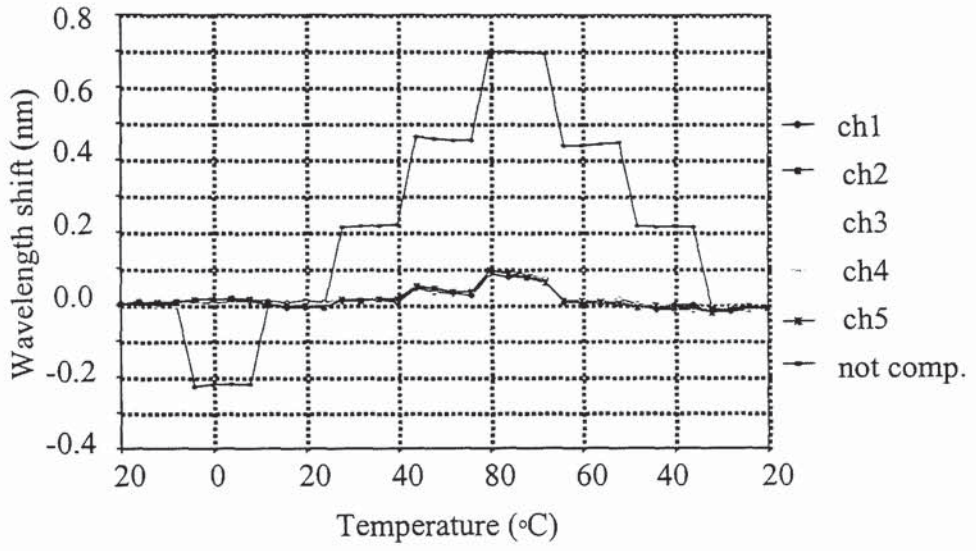

Figure 5.31: A graph showing the wavelength shift for each channel of a thermally stable five-wavelength WDM device when it is repeatedly heated and cooled

As well as monitoring the variation in wavelength for each channel when the device is subjected to changing environmental conditions, it is also necessary to ensure that

the reflectivity of each channel does not alter. Figure 5.32 shows the consistency of the reflectivity and wavelength separation results for all five gratings when the temperature is increased from 0°C up to 80°C.

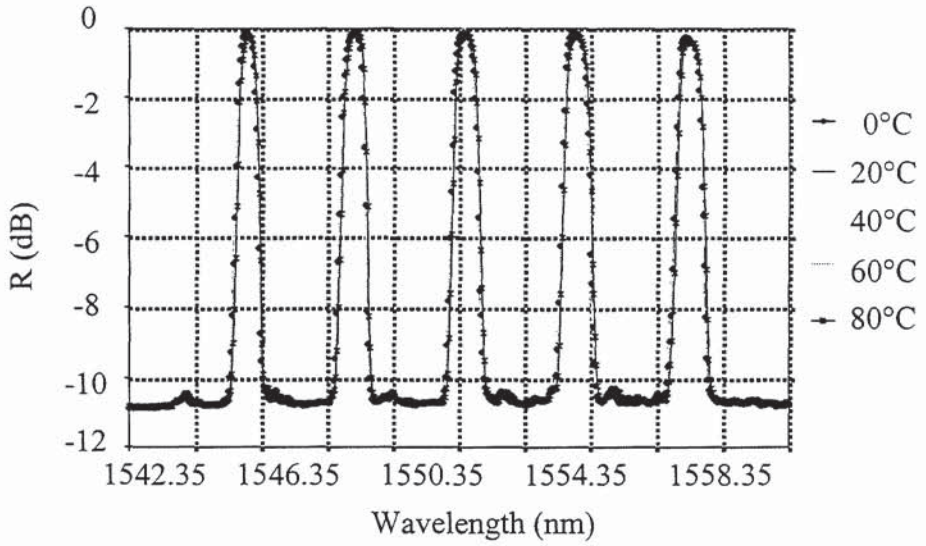

Figure 5.32: A graph showing the variation in reflectivity and wavelength when the temperature of a five channel WDM device is varied between 0°C and 80°C

5.4.3.3 System Tests on Multiple Wavelength Filters

Once the device was pre-strained in the thermally stabilised packaging, the channel wavelengths were found to match fairly closely with the ITU specifications given in Table 5-1 (1546.05, 1549.25, 1552.50, 1555.75 and 1559.05nm). As can be seen from the transmission spectrum shown in Figure 5.29, the reflectivity of the array ranges from 14dB to 20dB. The insertion loss of the device was measured to be about 7 dB and the isolation was about 20dB, measured using an optical spectrum analyser with 0.05nm resolution.

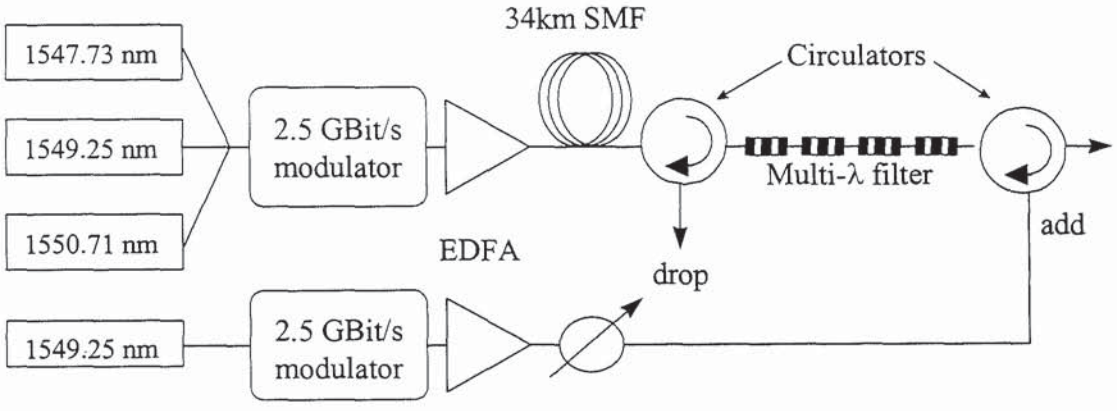

Figure 5.33: Experimental set-up used to characterise a multiple wavelength filter

Figure 5.33 shows the typical experimental arrangement used to characterise a multiple grating filter. This set-up consists of a source of three wavelengths modulated at 2.5 Gbit/s with a 200 GHz inter-channel spacing. The source at 1549.25nm corresponds to a wavelength of one of the gratings in the multiple grating filter and therefore can be dropped, once it is reflected by the filter and then can be added later by an additional wavelength source. The bit error rate can be measured on the drop port as a function of the received power.

A similar experimental set-up was used to characterise the five-wavelength notch filter illustrated in Figure 5.29. For the experimental trials, the gratings with the highest and lowest spectral rejection were each dropped in turn to see the resulting effect on the performance of the filter.

The lowest spectral rejection was for the grating at the lowest wavelength, 1546.05nm. Figure 5.34 shows the results for the sensitivity of the system when the channel at this wavelength was added. It was concluded that when no channel was added, the performance of the filter was the same as that observed using a 1nm commercial (JDS) filter, in terms of noise rejection. When a channel was added via the add-port a minimum penalty of 1dB was measured, as shown in Figure 5.34.

This minimum penalty of 1dB was constant over a 0.4nm (50 GHz) wavelength range, but once the wavelength of the added channel was tuned further away from the isolation peak of the grating, the performance of the filter could be seen to degrade abruptly.

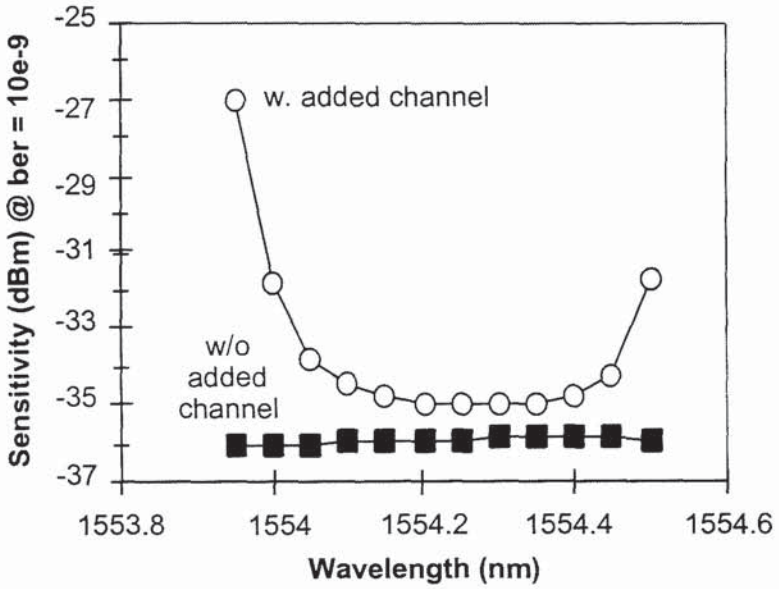

Figure 5.34: A graph showing the sensitivity at a bit error rate of 10^{-9} against wavelength for the channel added at 1546.05nm

The fourth channel of the multi-wavelength filter, situated at a wavelength of 1555.75nm and with a spectral isolation of 20dB, was then used as the channel to be dropped and subsequently added. The resulting changes to the sensitivity of the performance are shown in Figure 5.35. Again, the system experienced no penalty before the dropped channel was added.

Once the channel was added the minimum penalty at a bit-error-rate of 10^{-9} remained at a level of 0dB. As the 'add-port' source wavelength was tuned away from the wavelength of the dropped channel the performance of the filter degraded slightly. Figure 5.35 shows that, using this channel, the penalty of system was less than 1dB over a bandwidth of 0.8nm (100GHz).

The filter was only tested in the configuration shown in Figure 5.33, but from the tests which were carried out, it was concluded that the crosstalk of the system would increase if a different arrangement were used, e.g. if the drop port went directly to the add port.

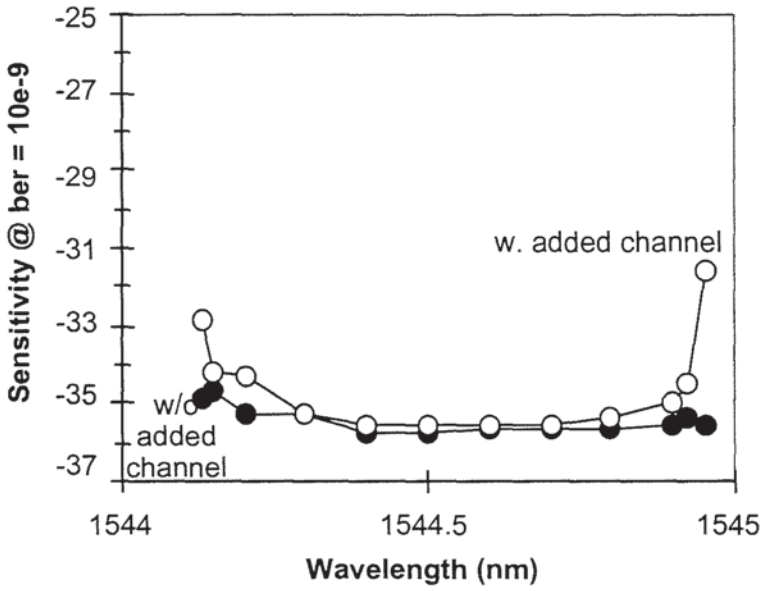

Figure 5.35: A graph showing the sensitivity at a bit error rate of 10^{-9} against the wavelength of the channel added

The results of these tests showed that the system experienced a lower penalty when the channel with the highest rejection ratio was used as the add/drop channel. Therefore, it can be concluded that, to achieve an improved performance from the filter, gratings with even higher spectral rejection are required. As discussed in Chapter 3, the increase in grating reflectivity will naturally lead to larger sidelobes for each grating in the array. So, as more channels are requested and the specification for each device is increased, then the optimisation of each grating profile, by apodisation, plays an increasingly important role in device fabrication.

5.5 Chapter Conclusions

This chapter has been concerned with the fabrication of bandpass filters for use in WDM and sensing systems. A number of different fabrication techniques were examined to test their flexibility and overall performance in meeting device specifications. Detailed in this chapter was the first published work on the use of a chirped phase mask in the fabrication of Moiré gratings. This technique enabled strong, highly reproducible broadband filters to be written, without the drawbacks of former fabrication techniques. The achieved flexibility in filter fabrication led to the possibility of designing multiple-passband devices at specific wavelengths for telecommunications applications. Using the Moiré technique it was possible to fabricate a filter with a single, extremely narrow passband (of bandwidth less than 0.001nm) within a 1nm stopband, useful for sensing applications.

A number of important conclusions could be drawn from the work concerning the design and fabrication of phase shifted gratings, including the fact that both the near and far-field components of the diffraction must considered in any numerical simulations performed.

The final section of this chapter was concerned with multiple-wavelength grating arrays and using a simple grating-concatenation technique an apodised five-wavelength grating array was written. Drawing on the conclusions from the apodisation work, detailed in Chapter 2, it was possible to optimise the array for the maximum possible sidelobe suppression achievable using the equipment available. The final device consisted of five gratings, each having a 1dB bandwidth of 0.5nm. The sidelobe suppression for each grating was greater than 20dB and at the wavelength of the next channel (±3.2nm) the sidelobe suppression was greater than 30dB. This work highlighted a number of key issues, including the importance of initial phase mask fabrication in order to minimise stitch errors and reduce the overall grating reflection noise floor to achieve maximum channel isolation. Although the final filter parameters were close to those requested in the initial device specifications within the PHOTOS project, the systems measurements carried out by other European research groups, proved that there are still improvements to be made in order for gratings to achieve their potential. There are several possible ways of improving the spectral characteristics of gratings. In terms of the phase mask, possible improvements lie with the employment of either a very high quality electron-beam written phase mask, having no significant stitching errors, or, as discussed in Chapter 3, a holographically-written phase mask which is intrinsically free from stitch errors due to the method of its manufacture. In order to reduce the overall noise floor of the reflection profile, the mask and fibre should be free from dust. Ideally, the

whole fabrication process should be carried out in a clean room to minimise this atmospheric 'pollution', which can produce defects in the resulting devices.

This work has highlighted the fact that grating apodisation is still an important issue which needs to be addressed further in order to achieve the high reflectivities combined with the level of sidelobe suppression which is required for WDM systems.

---

1 J.-M. Jouanno, J. Hubner, J.E. Pedersen, R. Kromann, T. Feuchter, M. Kristensen, 'Strong Bragg gratings for WDM devices in non-sensitised low-loss Ge-doped waveguides', *Electron. Lett.*, **32**, (23), 1996, pp.2151-2152

2 L.R. Chen, D.J.F. Cooper, P.W.E. Smith, 'Transmission filters with multiple flattened passbands based on chirped Moiré gratings', *IEEE Photon. Technol. Lett.*, **10**, (9), 1998, pp.1283-1285

3 A.D. Kersey, M.A. Davis, H.J. Patrick, M. LeBlanc, K.P. Koo, C.G. Askins, M.A. Putnam, E.J. Friebele, 'Fibre grating sensors', *J. Lightwave Technol.*, **15**, (8), 1997, pp.1442-1463

4 K.O. Hill, F. Bilodeau, B. Malo, D.C. .Johnson, J. Albert, 'Bragg gratings fabricated in monomode photosensitive optical fibre by UV exposure through a phase mask', *Appl. Phys. Lett.*, **62**, (10), 1993, pp.1035-1037

5 W.H. Loh, M.J. Cole, M.N. Zervas, S. Barcelos, R.I. Laming, 'Complex grating structures with uniform phase masks based on the moving fibre-scanning beam technique', *Opt. Lett.*, **20**, (20), 1995, pp.2051-2053

6 L.A. Everall, J.A.R. Williams, I. Bennion, X. Liu, R.M. De La Rue, 'The effects of phase steps in E-Beam written phase masks used for fibre grating fabrication by near-field holography', *European Conf. On Optic. Commun. (ECOC'97), IEE Conference Proceedings No.448*, 1, (MO4C) ,1997, pp187-190

7 L. Zhang, K. Sugden, I. Bennion, A. Molony, 'Wide stopband chirped fibre Moiré grating transmission filters', *Electron. Lett.*, **31**, (6), 1995, pp.477-479

8 L.A. Everall, K. Sugden, J.A.R. Williams, I. Bennion, X. Liu, J.S. Aitchison, S. Thoms, R.M. De La Rue, 'Fabrication of multipassband Moiré resonators in fibres by the dual-phase-mask exposure method', Opt. Lett., **22**, (19), 1997, pp.1473-1475

9 D.C.J. Reid, C.M. Ragdale, I. Bennion, D.J. Robbins, J. Buus, W.J. Stewart, 'Phase shifted Moiré grating fibre resonators', *Electron. Lett.*, **26**, (1), 1990, pp.10-12

10 S. Legoubin, E. Fertein, M. Douay, P. Bernage, P. Niay, 'Formation of Moiré gratings in core of germanosilicate fibre by a transverse holographic double exposure method', *Electron. Lett.*, **27**, (21), 1991, pp.1945-1947

11 F.R. Connor, *Introductory Topics in Electronics and Telecommunications: Modulation, 2nd Edn.*, (Arnold, London, UK, 1988)

12 J. Dunlop, D.G. Smith, *Telecommunications Engineering, 2nd Edn.*, (Chapman and Hall, London, UK, 1994)

13 S. Radic, N. George, G.P. Agrawal, 'Analysis of nonuniform distributed feedback structures: Generalized Transfer matrix method', *IEEE J. Quantum Electron.*, **31**, (7), 1995, pp.1326-1336

14 J. Hong, W. Huang, T. Makino, 'On the transfer matrix method for distributed feedback waveguide devices', *J. Lightwave Technol.*, **10**, 1992, pp.1860-1868

15 K. Sugden, L.A. Everall, J.A.R. Williams, I. Bennion, 'Single and multi-passband broadband Moiré filters from dual exposure of uniform-period and chirped phase masks', *SPIE Proc.*, **2998**, 1997, pp.29-34

16 K.O. Hill, D.C. Johnson, F. Bilodeau, S. Faucher, 'Narrow-bandwidth optical waveguide transmission filters: A new design concept and applications to optical fibre communications', *Electron. Lett.*, **23**, 1987, pp.465-466

17 R.C. Alferness, C.H. Joyner, M.D. Divino, M.J.R. Martyak, L.L. Buhl, 'Narrowband grating resonator filters in InGaAsP/InP waveguides', *Appl. Phys. Lett.*, **49**, (3), 1986, pp.125-127

18 J. Canning, M.G. Sceats, 'π- phase shifted periodic distributed structures in optical fibres by UV post processing', *Electron. Lett.*, **30**, (16), 1994, pp.1344-1345

19 R. Kashyap, P .F. McKee, D. Armes, 'UV written reflection grating structures in photosensitive optical fibres using phase shifted phase masks', *Electron. Lett.*, **30**, (23), 1994, pp.1977-1978

20 G.P. Agrawal, S. Radic, 'Phase-shifted fibre Bragg gratings and their applications for wavelength demultiplexing', *IEEE Photon. Technol. Lett.*, **6**, (8), 1994, pp.995-997

21 R. Zengerle, O. Leminger, 'Phase shifted Bragg grating filters with improved transmission characteristics', *J. Lightwave Technol.*, **13**, (12), 1995, pp.2354-2358

22 K. Utaka, S. Akiba, K. Sakai, Y. Matsushima, 'λ/4 - shifted InGaAsP/InP DFB Lasers', *IEEE J. Quantum Electron.*, **QE-22**, (7), 1986, pp.1042-1051

23 F. Bakhti, P. Sansonetti, 'Wide bandwidth, low loss and highly rejective doubly phase-shifted UV written fibre bandpass filter', *Electron. Lett.*, **32**, (6), 1996, pp.581-582

24 F. Bakhti, P. Sansonetti, 'Design and realization of multiple quarter -wave phase-shifts UV-written bandpass filters in optical fibres', *J. Lightwave Technol.*, **15**, (8), 1997, pp.1433-1437

25 X. Liu, J.S. Aitchison, R.M. De La Rue, P.Silva Marques, S. Thoms, L.A. Everall, J.A.R. Williams and I. Bennion, 'The influence of phase mask stitch errors on the performance of UV-written Bragg gratings', *Conf. on Bragg gratings, photosensitivity and poling in glass fibres and waveguides (BGPP '97),* Tech. Digest, 17, (BMG9), pp.210-212

26 D. Uttamchandani, A. Othonos, 'Phase shifted Bragg gratings formed in optical fibres by post-fabrication thermal processing', *Opt. Commun.*, **127**, 1996, pp200-204

27 G.E. Town, K. Sugden, J.A.R. Williams, I. Bennion, S.B. Poole, 'Wideband Fabry-Perot like filters in optical fiber', *IEEE Photon. Technol. Lett.*, **7**, (1), 1995, pp.78-80

28 M. Janos, J. Canning, 'Permanent and transient resonances thermally induced in optical fibre Bragg gratings', *Electron. Lett.*, **31**, (12), 1995, pp.1007-1009

29 X. Liu, R.M. De La Rue, T.F. Krauss, S. Thoms, S.E. Hick, J. S. Aitchison, L. Zhang, J.A.R. Williams, I. Bennion, 'Electron beam production of phase masks for direct writing of photosensitive gratings', CLEO/Europe-EQEC '96, Hamburg, Germany, 1996, pp.126

30 X. Liu, J. S. Aitchison, S. Thoms, R.M. De La Rue, L. Zhang, J.A.R. Williams, I. Bennion, 'E-beam lithography of phase mask gratings for near field holographic production of optical fibre gratings' *Microelectron. Eng.*, **35**, 1997, pp.345

31 T. Kjellberg, R. Schatz, The effect of stitching errors on the spectral characteristics of DFB Lasers fabricated using Electron Beam lithography', *J. Lightwave Technol.*, **10**, (9), 1992, pp.1256-1266

32 H. Kogelnik, 'Filter response of nonuniform almost-periodic structures', *Bell Syst. Tech. J.*, **55**, (1), 1976, pp.109-125

33 K. Sugden, L. Zhang, J.A.R. Wiliams, R.W. Fallon, L.A. Everall, K.E. Chisholm, I. Bennion, 'Fabrication and characterisation of bandpass filters based on concatenated chirped fibre gratings', *J. Lightwave Technol.*, **15**, (8), 1997, pp.1424-1432

34 V. Mizrahi, T. Erdogan, D.J. DiGiovanni, P.J. Lemaire, W.M. MacDonald, S.G. Kosinski, S. Cabot, J.E. Sipe, 'Four channel fibre grating demuliplexer', *Electron. Lett.*, **30**, (10), 1994, pp.780-781

35 F. Bilodeau, K.O. Hill, B. Malo, D.C. Johnson, J. Albert, 'High return-loss narrowband all-fibre bandpass Bragg transmission filter', *IEEE Photon. Technol. Lett.*, **6**, 1994, pp.80-82

36 J.-L. Archambault, P.St.J. Russell, S. Barcelos, P. Hua, L. Reekie, 'Grating frustrated coupler: A novel channel-dropping filter in single mode optical fibre', *Opt. Lett*, **19**, 1994, pp.180-182

37 F. Bilodeau, D.C. Johnson, S. Theriault, B. Malo, J. Albert, K.O. Hill, 'An all fibre dense-wavelength-division multiplexer/demultiplexer using photoimprinted Bragg gratings', *Photon. Tech. Lett.*, **7**, (4), 1995, pp.388-390

38 G.W. Yoffe, P.A. Krug, F. Ouellette, D. Thorncraft, 'Temperature-compensated optical fibre Bragg gratings', *Conf. Optic. Fibre Commun. (OFC '95), San Diego, California,* **8**, WI4, 1995, pp.134-135

6. LONG PERIOD GRATINGS

6.1 Chapter Overview

This chapter describes work on the fabrication and application of long period fibre gratings. It details work carried out to develop a simple experimental arrangement for the fabrication of long period gratings. Due to the fact that there are many commercial applications for long period fibre gratings it is important to ensure that low-cost, reproducible gratings can be fabricated to specification.

The fabrication technique detailed in this chapter can be easily adapted from the typical Bragg grating fabrication arrangement with minimal additional cost, thus making it an ideal fabrication technique. This approach has proved itself to be flexible and enabled a wide range of devices of varying periodicities to be produced. One such device has been incorporated into a novel interrogation system for strain or temperature sensing, highlighting the versatility of long period fibre gratings.

6.2 Introduction to Long Period Gratings

Interest in long period fibre gratings was renewed in 1996 by Vengsarkar *et al* [1]. Prior to this Hill *et al* had demonstrated the fabrication of gratings with large periods [2] for use as $LP_{01} \leftrightarrow LP_{11}$ or LP_{02} mode converters [3,4]. The fabrication principle for long period gratings is similar to that for Bragg gratings, whereby a refractive index change is induced in the fibre core as a result of the UV-exposure of a photosensitive fibre. The difference between a long period grating and a Bragg grating lies in the magnitude of the grating periodicity. Long period fibre gratings have periodicities of hundreds of microns, compared with Bragg gratings whose periodicities are usually less than one micron in size.

The principles of operation for a long period and a Bragg grating are completely different. In a single mode fibre, a long period grating couples light from the guided fundamental mode to forward propagating cladding modes. These forward propagating modes decay more rapidly as they propagate down the fibre due to the lossy cladding-outer coating interface and bends along the fibre. As detailed in Chapter 2, this differs from the operation of a Bragg grating where the coupling takes place between the forward and backward propagating modes. In the case of a long period grating the coupling that occurs is wavelength selective and thus the grating acts as a wavelength dependent loss element. The wavelength at which this coupling takes place depends on parameters such as the periodicity of the grating and the

differential refractive index change induced between the fibre core and cladding. The phase matching condition between the guided mode and the forward propagating cladding modes is given by

$$\Delta\beta = \beta_{01} - \beta_{cl}^{(m)} = \frac{2\pi}{\Lambda^{(m)}}$$

Equation 6-1

where β_{01} is the propagation constant of the fundamental mode LP_{01}, $\beta^{(m)}_{cl}$ is the propagation constant of the cladding modes and $\Lambda^{(m)}$ is the grating periodicity needed to couple the fundamental mode to the m^{th} cladding mode. The propagation constant is usually defined by $\beta = \frac{2\pi n_{eff}}{\lambda}$ where n_{eff} is the effective refractive index of the mode. Using this relationship the phase matching condition can be written as

$$\lambda = \left(n_{01} - n_{cl}^{(m)}\right)\Lambda^{(m)}$$

Equation 6-2

where n_{01} and $n^{(m)}_{cl}$ are the effective indices of the fundamental and m^{th} cladding modes, respectively. From Equation 6-2 it is possible to predict the wavelengths at which mode coupling will occur for a particular grating periodicity.

The spectral dependence of the long period grating transmission was derived in Appendix 8-1, using expressions from coupled mode theory, and is given by

$$\left|t_m(\lambda)\right|^2 = 1 - \frac{\sin^2\left[\kappa_m L\sqrt{1+\frac{(\Delta\beta\ 2)^2}{\kappa_m^2}}\right]}{1+\left(\frac{\Delta\beta\ 2}{\kappa_m}\right)^2}$$

Equation 6-3

where $\Delta\beta$ is the detuning parameter (or deviation from the phase matching condition) given by Equation 6-1, κ_m is the coupling strength of the grating and L is the grating length. κ_m is proportional to the UV induced index change. Figure 6.1 shows a typical transmission profile of an experimentally fabricated long period grating. This grating has a period of 500μm and a total length of 1.1cm, which results in three clear transmission peaks over the broad wavelength range illuminated by the light source.

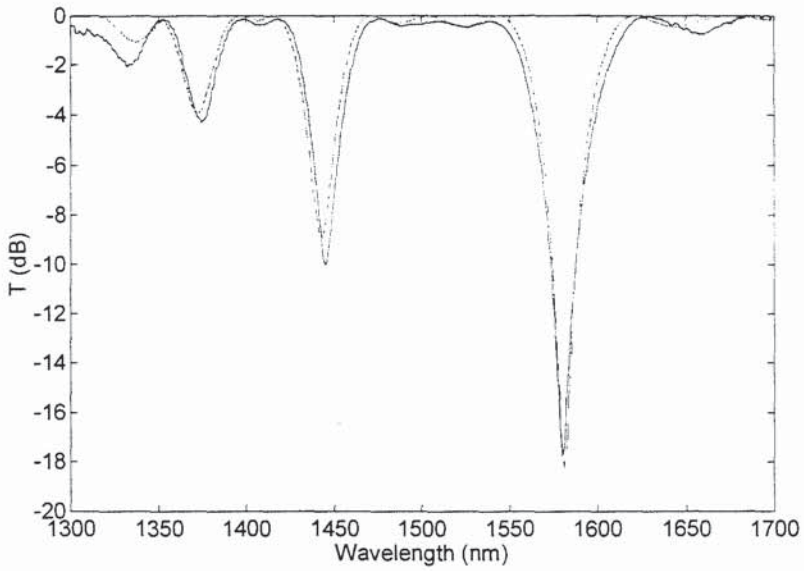

Figure 6.1: A typical transmission profile of a long period grating (— experimental profile; --- modelled profile)

Long period gratings have been proposed for a multitude of applications in recent years, partially due to the relative ease with which they can be fabricated compared to Bragg gratings and partially due to their spectral properties, such as low backreflections and broadband transmission peaks. These factors brought about reports of the use of long period gratings as band rejection filters [1] to remove unnecessary Stokes orders in a cascaded Raman amplifier/laser [5] and as wavelength stabilisers in 980nm pump diodes [6].

A useful application of long period gratings is in the gain flattening of erbium-doped fibre amplifiers (EDFA) [7]. A limitation of the EDFA is the non-uniform gain spectrum which limits the bandwidth over which a constant gain can be achieved [8]. Much work has been done on methods of flattening out this spectrum, including the use of a 3mm long blazed fibre Bragg grating [9]. This grating was written with a blaze angle of 8°, which allowed the guided mode to be coupled to the radiation field, flattening the ASE spectrum (±0.5dB) over a bandwidth of 35nm. The disadvantages of such a device include the large backreflection which occurs at a wavelength only a few nanometers longer than that of the radiation-coupled wavelength and the precision of the blaze angle required to produce the desired spectral profile. Long period gratings solve these problems, since they have ultra-low backreflections and are simple to fabricate, as will be demonstrated later in this chapter. Using a carefully designed long period grating the spectrum of an EDFA has been flattened to within 1dB over a 40nm bandwidth [10].

Another useful characteristic of long period gratings is their sensitivity to external perturbations such as strain, temperature and bends in the fibre [11]. When the fibre

experiences a change in the environment, the propagation constants, β_{01} and $\beta^{(m)}_{cl}$ change by different amounts and therefore the difference, $\Delta\beta$, is altered [1]. For a fixed periodicity then this implies that that there will be a shift in the wavelength of the resonant coupling between the fundamental and cladding modes. This property is very desirable for sensing purposes and there have been numerous reports of long period gratings being used as both strain and temperature sensors [12,13,14].

The temperature dependence of long period gratings has been examined by a number of groups. Bhatia *et al* [12] wrote similar gratings into five different types of fibre and studied the change in wavelength of the transmission peak due to a change in temperature. For each grating the peak wavelength was found to vary linearly with temperature and the variation in fibre type produced a temperature dependence ranging from 0.062 nm/°C to 0.154 nm/°C. For comparison, the peak wavelength of a Bragg grating has a temperature variation of ~0.01nm/°C, and so long period gratings have a higher temperature sensitivity than Bragg gratings, potentially making them a more attractive option for temperature sensing applications. Vengsarkar *et al* [1] examined the temperature sensitivity in a number of gratings of different lengths, ranging from 1.5cm to 2.5cm. Real-time monitoring of the transmission spectrum enabled the variation in peak wavelength with temperature to be measured for different length gratings. This was found to vary slightly between 0.04-0.05 nm/°C. The study concluded that neither the length of the grating nor the peak wavelength affected the temperature sensitivity greatly, implying that the predominant factor responsible for the temperature dependence was the difference in mode propagation constant.

There are two factors that change the effective indices of the fibre, and subsequently change the temperature sensitivity of a long period grating [15]. These are the temperature dependence of the refractive index of the material, dn/dT and the temperature dependence of the grating periodicity, $d\lambda/dT$. If the temperature dependence of the refractive index throughout the waveguide is approximated to that of pure silica, i.e. $dn_r/dT = dn_{si}/dT$, then the temperature sensitivity can be characterised by

$$\frac{d\lambda}{dT} = \frac{d\lambda}{dn_{si}}\frac{dn_{si}}{dT} + \frac{d\lambda}{d\Lambda}\frac{d\Lambda}{dT}$$

Equation 6-4

where the first term represents the material contribution and the second term represents the waveguide contribution.

From this equation and knowledge of the fibre parameters it is possible to fabricate long period gratings having a reduced temperature sensitivity [16] which can be used for strain or refractive index sensing.

Research into the strain sensitivity of long period gratings has concluded that the strain sensitive effect is more dependent on the type of fibre used than the temperature sensitivity effect [1]. Different fibres were found to have strain sensitivities ranging from -7.27 nm/‰ε to +15.21 nm/‰ε [12], which is about half that of a Bragg grating. This work highlighted the effect which the optical fibre parameters have on the resulting long period grating.

6.3 Long Period Grating Fabrication Techniques

As has been demonstrated, in-fibre gratings have huge potential for applications ranging from telecommunications to structural health monitoring. For gratings to be accepted in a commercial environment, there are a number of issues which need to be addressed, including the ability to fabricate highly reproducible gratings at minimal cost. Commercially available phase masks are still costly to buy and, as previously discussed, are restrictive in the number of different gratings that a single pattern can produce.

There have been numerous novel and interesting techniques reported for the fabrication of long period gratings. These include the point-by-point technique [2] and that using an amplitude mask [17]. Several more recent papers have reported the use of a heat source, such as a fusion splicer, to periodically release the residual stress of the core of specially designed fibre to fabricate a long period grating [18,19]. There have also been reports on the fabrication of long period gratings by periodically exposing the fibre to pulses from a CO_2 laser [20,21]. The most widely used of these techniques are still the point-by-point and amplitude mask methods, which have already proved their reliability. Both of these approaches will be introduced in this section and full details of the successful implementation of the point-by-point technique will be given.

6.3.1 Amplitude Mask Fabrication Technique

The majority of papers concerning the fabrication of long period gratings describe the use of an amplitude mask. This is similar to a phase mask in that it consists of a plate onto which a periodic pattern is etched and this pattern defines the periodicity of the resulting grating, which is typically greater than 100μm and few centimetres in length. The plate is usually covered with a photoresist, such as chrome, and a periodic pattern is imprinted onto its surface. After development, some of the surface of the

plate remains unetched and this periodically masks the fibre from the exposing beam, hence writing a grating. The difference between an amplitude and a phase mask is that an amplitude mask produces a modulation in the refractive index of the fibre by the periodic exposure of the fibre to the beam, whereas a phase mask induces a far smaller periodic modulation in the refractive index of the fibre core by the interference of the ±1 diffraction orders.

In practice, the fabrication procedure for long period gratings is identical to that for standard Bragg gratings, as may be seen in Figure 6.2. The core of the fibre is exposed to a UV laser, through the amplitude mask, which is placed in close proximity to the fibre allowing a periodic modulation of the refractive index in the core of the fibre. The UV beam can be translated along the length of the mask enabling long gratings to be written.

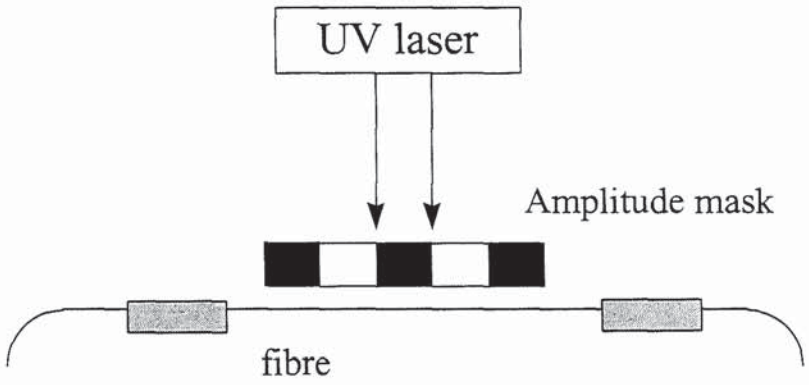

Figure 6.2: Experimental set-up for fabricating long period gratings using an amplitude mask

An amplitude mask has all the advantages of a phase mask, in that it is simple to fabricate numerous gratings with identical periodicity, but a different pattern is also required for each grating periodicity. Although amplitude masks are cheaper than phase masks, it is still true that if many gratings of varying periodicity are required then this method becomes costly.

6.3.2 Pulsed Exposure Fabrication Technique

The fabrication technique employed in the work detailed in this section is based on the point-by-point technique reported on by Malo *et al* [2]. The technique used here is a very simple one which involves the pulsed UV exposure of the fibre. A diagram of the experimental set-up used to fabricate long period gratings is shown in Figure 6.3.

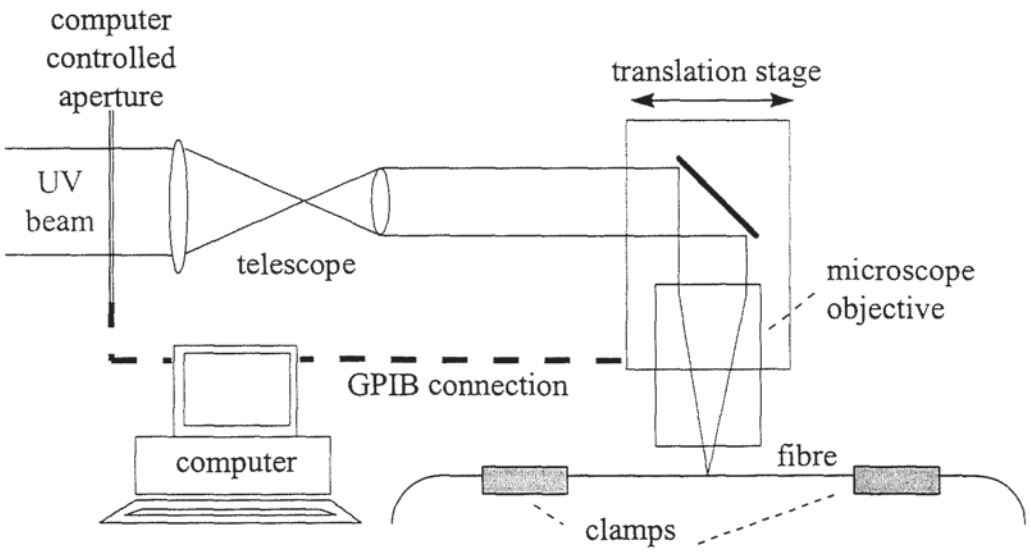

Figure 6.3: Experimental set-up for the fabrication of long period gratings

To write a long period grating a UV beam from a frequency doubled Argon ion laser is reduced eight-fold by a telescope arrangement and then focused onto the optical fibre via a microscope objective. The CW UV beam provides the high level of controllability and repeatability required when fabricating long period gratings. The microscope objective has a magnification of ×10 and, when correctly placed into the set-up, reduces the beam to a size of less than 30μm. Both the 45° reflecting mirror and the microscope objective are fixed on a motorised translation stage which allows the beam to be scanned along the length of the fibre thus writing long length gratings. The maximum possible length of the device is only limited by the total movement of this translation stage, which in this case is 15cm. As the beam is scanned along the length of the fibre, the periodic exposure is provided by a computer controlled aperture. This aperture was programmed to open and close at a rate dependent on the periodicity required. The aperture can either be operated at a fixed frequency or can be triggered to change its state (either open or closed) at particular positional points along the translation stage's movement. After experimental tests it was decided that the later method provided the most accurate results, since using the position of the translation stage to trigger the aperture eliminates any problems associated with variations in the velocity of the stage which would result in a varying periodicity of the device. Using this allowed the grating periodicity to be specified to a precision of <0.1μm.

This technique is very flexible since a grating of any periodicity and any length (up to a maximum of 15cm) can readily be written by programming the aperture and translation stage correctly. This technique has minimal additional fabrication costs compared to the standard Bragg grating fabrication set-up and has the added benefit that no masks are required, making it a low-cost fabrication technique.

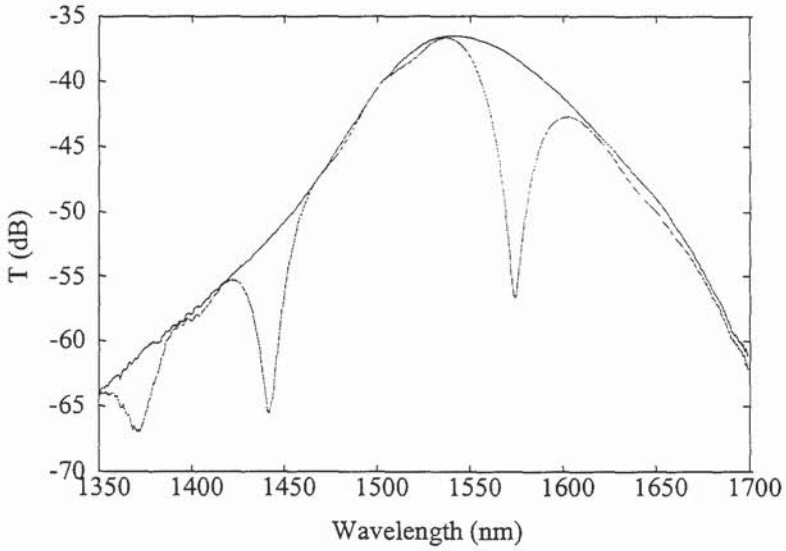

Figure 6.4: Optical spectrum analyser traces showing the light transmitted from a broadband source before and after grating fabrication

A broadband light source, spanning a wavelength range from 1300nm to 1700nm, was used to examine the gratings both during and after the UV exposure. The light source was connected to one end of the fibre in which the grating was written and the transmitted spectrum was observed on an optical spectrum analyser at the other end. The maximum wavelength resolution that can be achieved using an optical spectrum analyser is 0.01nm, but here the wavelength range needs to be as broad as possible and this subsequently reduces the resolution of the obtained trace. Figure 6.4 shows the transmission spectrum from the light source used throughout these experiments before and after a grating had been written into the fibre. The trace obtained prior to the grating being written allows the long period grating transmission spectrum to be normalised by simply subtracting one trace from the other, when the transmission data has been measured on a logarithmic scale.

A typical long period grating fabricated using this pulsed exposure technique is shown in Figure 6.5. The trace has been normalised to account for the non-uniformity in the intensity of the illuminated source, as described above. The grating was of total length 1cm with a periodicity of 600μm. The UV exposure produced a grating having three clear transmission peaks over a wavelength range of between 1300nm and 1700nm. The noise at the low wavelength end of the spectrum is generated by the illuminating light source and is not a real feature of the grating. The source can be seen to be at its lowest intensity at the short wavelength end of the spectrum, as illustrated in Figure 6.4. Therefore, when the grating spectrum is normalised, the signal-to-noise ratio is lowest in this wavelength region which results in noise on the normalised transmission profile.

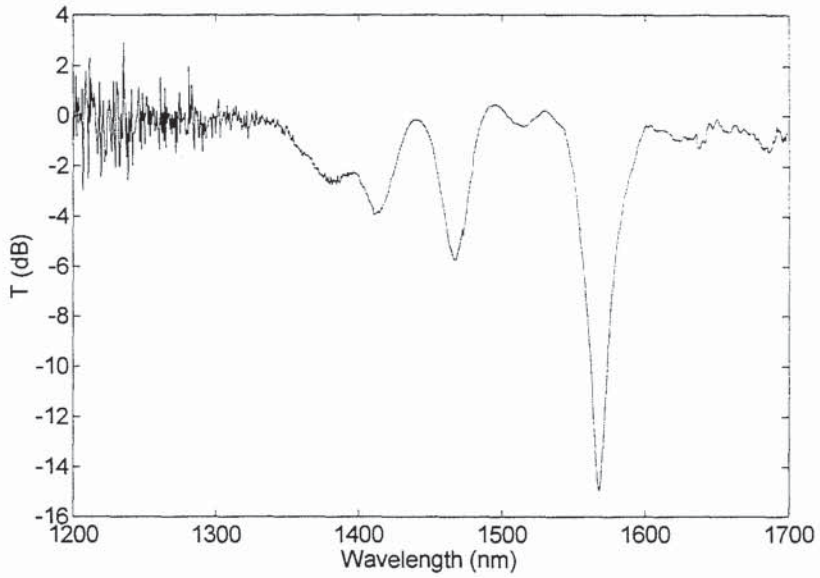

Figure 6.5: A long period grating fabricated using the pulsed exposure technique

The grating shown in Figure 6.5 was fabricated in boron-germanium co-doped fibre, without hydrogenation. Despite the absence of hydrogen, the main peak of the grating, occurring at a wavelength of 1568.9nm, had a reflectivity of 14.7dB. Using non-hydrogenated fibre, long period gratings of up to 19dB have been realised, showing that hydrogenation is not necessary in order to fabricate fairly strong long period gratings.

6.4 Long Period Gratings using Pulsed Exposure Method

The following section contains experimental and theoretical results for several long period gratings fabricated with various fibre and exposure parameters. From these results the sensitivity to small changes in the grating design parameters is illustrated.

Figure 6.6 shows a long period grating, of length 1.1cm, written in boron-germanium fibre using the pulsed exposure technique described in the previous section. The UV exposure produced a long period grating, of periodicity 500μm, with three large transmission loss peaks over the wavelength range 1300-1700nm. These peaks were situated at 1371.0nm, 1441.8nm and 1575.1nm, respectively. The grating was then modelled using a commercial package (Integrated Fibre Optics v.2) to confirm that the resulting transmission profile was as expected from theoretical calculations. In the experimental work the fibre parameters, such as core and cladding radii, were not known exactly and therefore some approximations were made. The refractive index of the core of the fibre was taken to be 1.46 and that of the cladding was taken to be 1.45, and the outer layer was presumed to have a refractive index of 1. The radius of the core was estimated to be 2μm and the cladding radius was estimated to be

62.5μm. The grating variables were set to a periodicity of 500μm, a length of 1.1cm and an induced refractive index change of 7.46×10^{-4}. From these values the various effective indices for the core (LP_{01}) and cladding ($LP_{0,1+m}$) modes could be calculated, using the weakly guiding approximation [22]. The resulting structure for coupling to the cladding modes LP_{03}, LP_{04} and LP_{05} can be seen in Figure 6.6. This result shows good agreement between the theoretical and the experimental result, although the slight discrepancies are probably due to the estimated values for the fibre parameters.

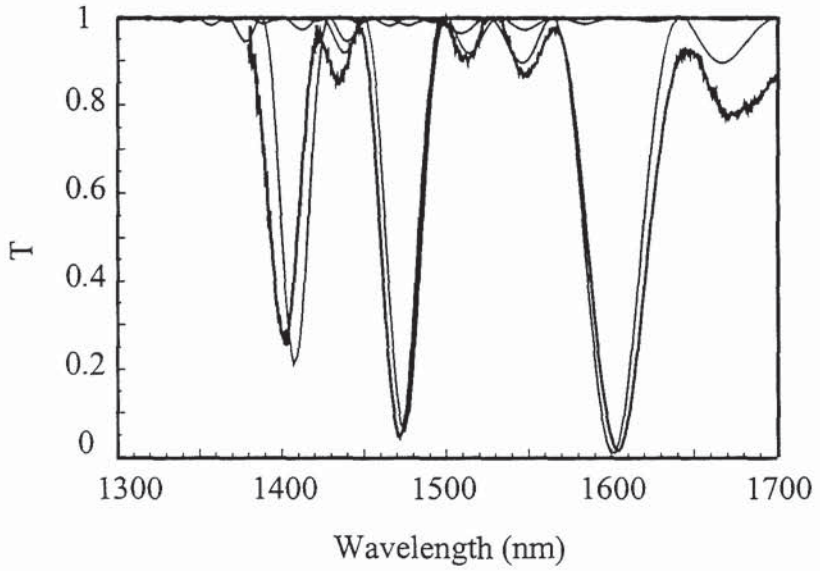

Figure 6.6: A comparison of the modelled and experimental results for a long period grating of length 1.1cm and periodicity 500μm (— experimental spectrum; — modelled spectrum)

The sensitivity of the resulting grating to these parameters is illustrated in Figure 6.7, showing theoretical transmission profiles of gratings produced as a result of altering the fibre core and cladding radii. Figure 6.7(a) shows the theoretical results of a long period grating having length 1cm and periodicity 500μm. The fibre core radius was given a value of 2.8μm and the cladding radius 62.5μm. Figure 6.7(b) shows the grating which would result if the fibre core radius was 5μm and the cladding radii was 64μm. The difference resulting from this fractional change in fibre dimensions clearly shows that if specific filters are to be realised, it is of great importance to know the parameters of the fibre into which the long period grating is being written.

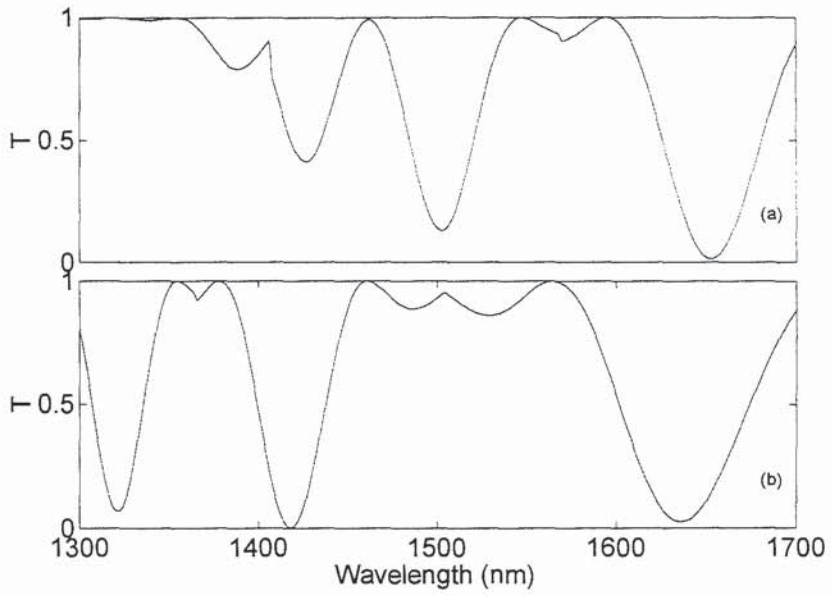

Figure 6.7: Theoretical results showing the effect on the grating when the radii of the fibre core and cladding are varied: (a) core radius 2.8μm, cladding radius 62.5μm; (b) core radius 5μm, cladding radius 64μm

An experimental investigation was undertaken into the effect which changing the grating periodicity has on the resulting grating profile. Several gratings were fabricated in the same fibre, all of the same length, but with periodicities of 300μm, 450μm and 600μm, respectively. The resulting grating structures are shown in Figure 6.8. Again, the noise at the low wavelength end of the spectrum is generated by the illuminating light source and is not a real feature of the grating. It can be seen that as the periodicity of the structure increases so does the coupling wavelength of each cladding mode. These experimental results agree very well with those theoretically calculated, as can be seen from a comparison of Figure 6.8 and Figure 6.9.

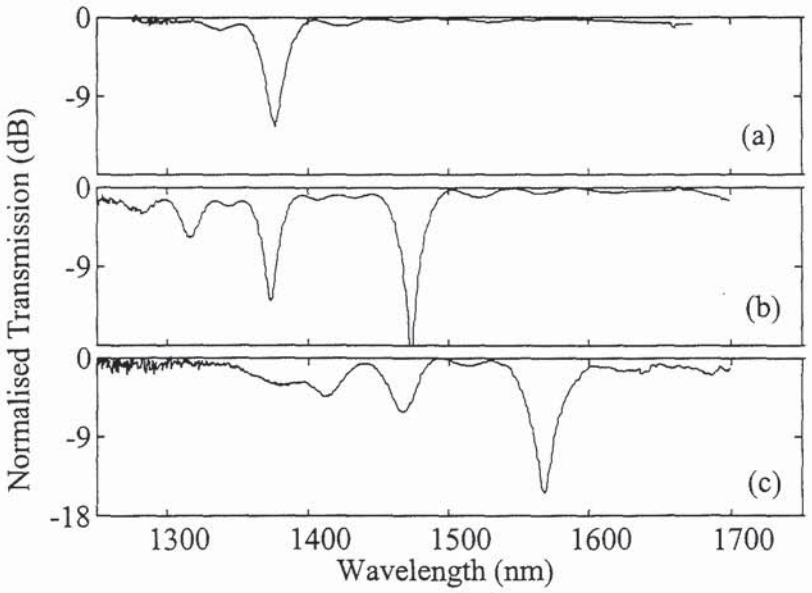

Figure 6.8: Experimentally achieved results showing the effect of increasing the periodicity of a long period grating: (a) period 300μm; (b) period 450μm; (c) period 600μm

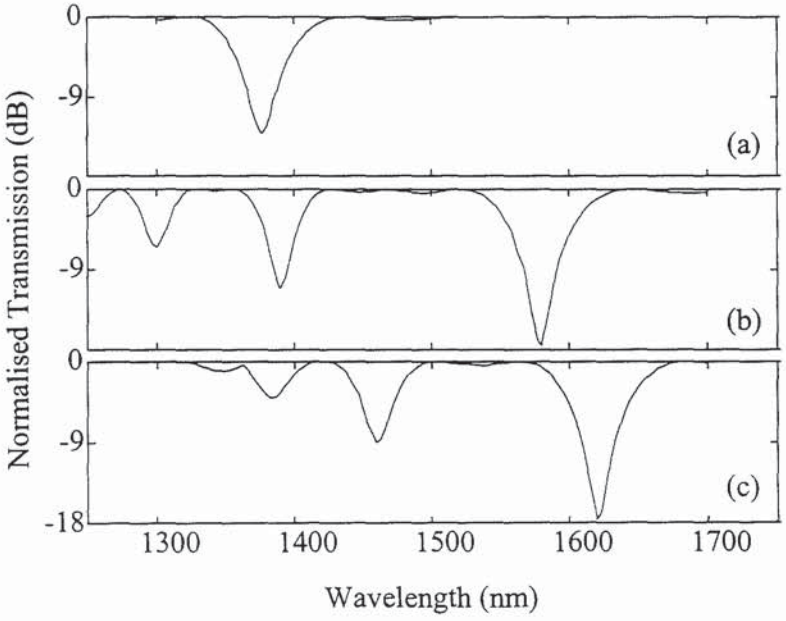

Figure 6.9: Theoretically calculated results showing the expected effect of increasing the periodicity of a long period grating: (a) period 300μm; (b) period 450μm; (c) period 600μm

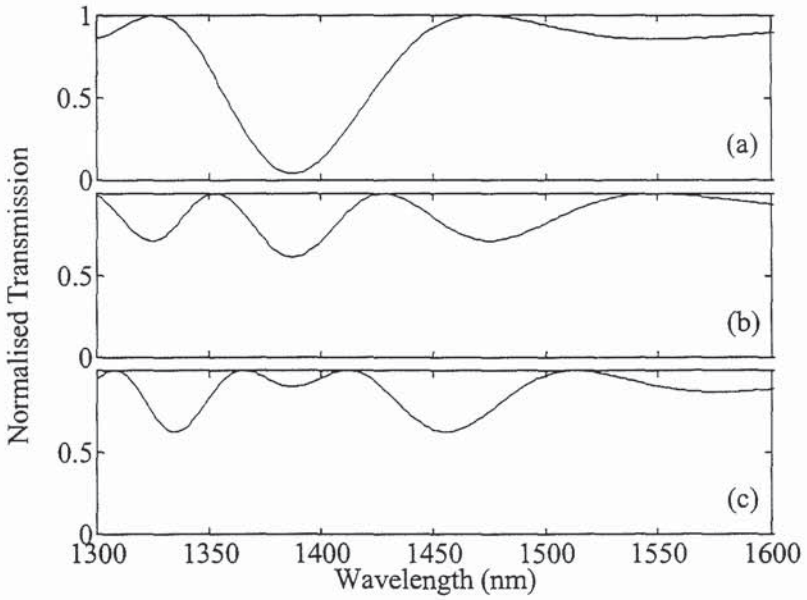

Figure 6.10: Theoretical results showing the effect of increasing the length of a long period grating: (a) length 10mm; (b) length 14mm; (c) length 16mm

In addition to changing the aforementioned parameters, an increase in length has a greater effect on a long period grating than it does on a Bragg grating. Figure 6.10 shows the theoretical transmission spectra from a grating of periodicity 500μm, with a change in refractive index of 7.5×10^{-4}. The fibre core and cladding radii were given values of 2.9μm and 64μm respectively. Illustrated is the change in the transmission spectra of a grating where the length increases from 10mm to 16mm. Again it is clear to see that the fabrication of a specifically shaped filter needs careful design prior to fabrication.

6.5 Long Period Grating Applications

As has been discussed earlier, there are a number of situations in which long period gratings have potential applications, including use in the gain flattening of erbium-doped fibre amplifiers and as band rejection filters. More recently long period gratings have been investigated in several sensing applications, detecting changes in parameters such as temperature, strain and refractive index [23].

A number of systems have incorporated both long period and standard Bragg gratings in order to discriminate between strain and temperature [13,24]. Patrick *et al* [13] demonstrated an approach using two fibre Bragg gratings and a single long period grating which utilised the fact that a long period grating has a much large temperature response than the Bragg grating, but a smaller strain response. By

monitoring the induced wavelength shifts, temperature and strain could simultaneously be measured to ±1.5°C and ±9με respectively.

In addition to this, Bhatia *et al* reported on the simultaneous measurement of strain and temperature using a single long period grating written in standard fibre [14]. This is exceedingly useful in systems that are sensitive to more than one external perturbation.

6.5.1 Strain Sensing System using a Long Period Grating

The following section describes the employment of a long period grating, fabricated by the pulsed exposure technique, and also a Bragg grating in a strain interrogation system. The system has a moderate resolution and offers a large sensing range. The sensor characterisation was carried out by R.W. Fallon at Aston University.

There have been many reported systems involving different types of gratings to interrogate a fibre Bragg grating sensor or array of sensors. These include the use of chirped gratings to act as the sensing and interrogation gratings [25] and the employment of an asymmetric grating to act as a wavelength-to-amplitude converter for linear sensing structures [26]. Both of these techniques have their disadvantages - the former system requires twice the bandwidth than for other techniques and the later system requires a more complex grating fabrication procedure. The inclusion of a long period grating into the sensing system, as the receiving grating, removes both of these disadvantages. Using the pulsed exposure fabrication technique a long period grating is very simple to fabricate and requires only a fraction of the bandwidth which the chirped grating system requires.

The principle of the long period grating interrogation system to monitor Bragg grating strain or temperature is based on the strain/temperature related optical power measurement. Figure 6.11 shows a typical long period grating transmission and Bragg grating reflection spectrum for use in such a system. The system is set up (as can be seen in Figure 6.12) such that the light reflected by the Bragg grating is then transmitted by the long period grating. The intensity of the transmitted light is dependent on the wavelength of the backreflected light from the Bragg grating and therefore, as the Bragg grating is strain/temperature tuned, the long period grating will act as a filter for direct wavelength-to-amplitude conversion.

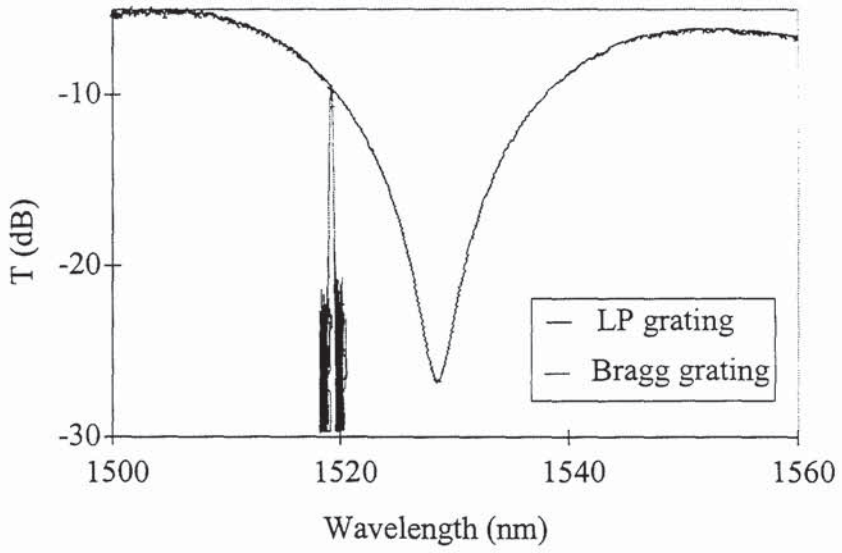

Figure 6.11: Typical long period and Bragg gratings used in the strain/temperature interrogation system

The long period grating shown in Figure 6.11 had a periodicity of 500μm and a total length of 1.1cm. The resulting transmission spectrum contained a peak of 27dB at a wavelength of 1529nm. Using such a grating it is possible to produce a near linear response of ~1.1dB/nm over a 10nm tuning range, from 1519nm to 1529nm. The sensing Bragg grating was written at a wavelength of 1519nm to allow the full 10nm range to be used for sensing purposes, thus allowing for up to ~10 000με. The fibre Bragg grating was 5mm in length and had a bandwidth of 0.5nm.

Figure 6.12 gives the schematic diagram of the low-cost all-fibre interrogation system developed to incorporate these gratings. The system consists of a broadband light source, the output of which is coupled to the sensing Bragg grating under interrogation. The backreflected light is then coupled to the long period receiving grating and detected by a photodiode after transmission through this grating. The reference arm of the coupler detects light reflected back from the Bragg grating alone and this measurement can then be used to remove general intensity fluctuations in the system and also to account for the non-uniformity of the broadband light source. In order to strain the Bragg grating it was secured between two steel blocks, held 277mm apart. One of the blocks was mounted onto a translation stage in order to strain the fibre, whilst the other was mounted onto a load cell, to monitor the tension of the fibre during the experiment.

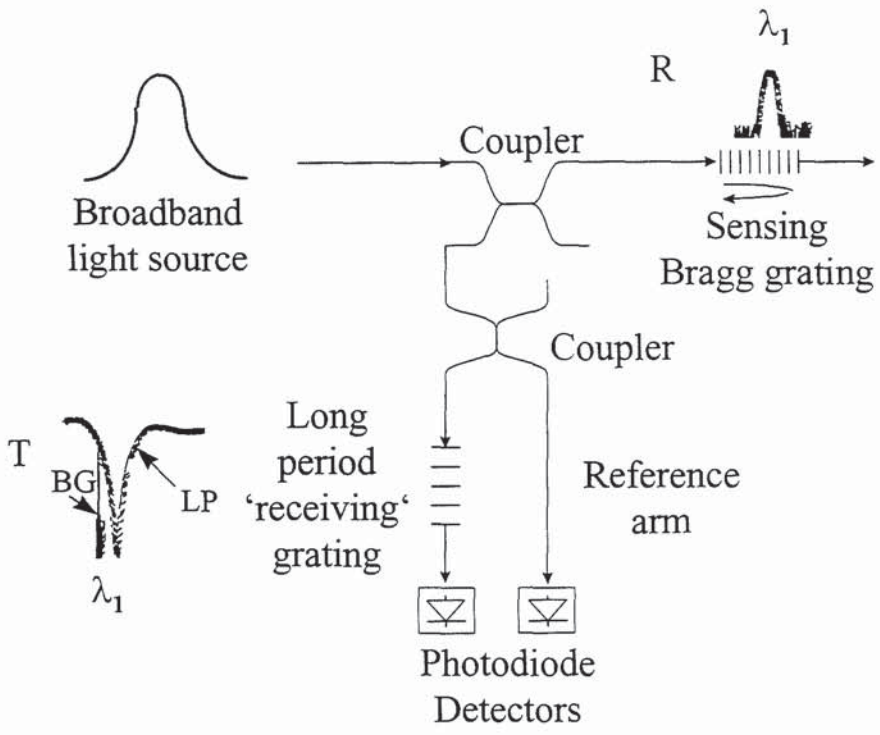

Figure 6.12: Schematic diagram of the experimental arrangement for strain or temperature interrogation employing both a Bragg and a long period grating

Initially the fibre Bragg grating was stretched in steps of ~550με up to a total strain of 7500με. The normalised power response of the system was achieved by dividing the transmitted signal from the long period grating by that received in the reference arm. The load cell indicated a linear increase in strain which proved that the fibre experienced no slippage whilst being held under strain. The results of the intensity variation with increasing strain can be seen in Figure 6.13.

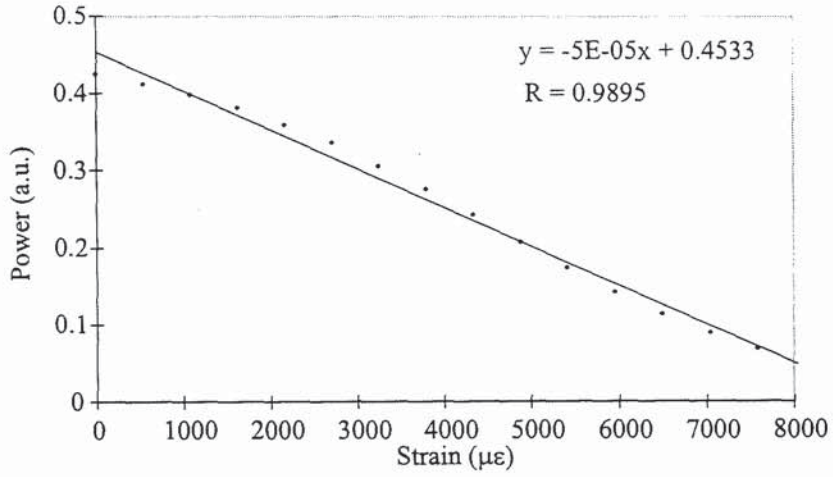

Figure 6.13: A graph showing the normalised power response for the interrogation of a Bragg grating

These results exhibit a linear relationship, although there appears to be some slight deviation from perfect linearity. The resolution of the system was calculated to be 2.4με.

The resolution of the system has been improved by utilising a modulated lock-in detection technique which reduces the extraneous 1/f noise [27]. The required modulation was placed onto the source output by a lithium niobate modulator. A function generator emitting a sine wave was used to control the modulator. The Bragg grating could then be stretched and the transmitted light output from both the long period grating and the reference arm were measured by a dual-channel lock-in amplifier. Using such a technique resulted in a static-strain resolution of ~0.5με.

Both the modulated and unmodulated systems are simple to implement in order to interrogate a fibre Bragg grating strain sensor. The incorporation of a long period grating as the receiver provides a simple wavelength-to-amplitude converter for strain sensing and, as has been shown, the fabrication arrangement for Bragg gratings can be easily adapted to fabricate long period gratings. The main disadvantage of long period gratings in strain sensing systems is that they are both strain and temperature sensitive. The strain sensing work detailed in this section was performed in a laboratory, where the thermal environment remained constant. Real strain sensing systems will be placed in more unstable environments and obviously the set-up previously detailed will produce inaccurate strain-sensing results. Possible solutions to this problem include placing the grating on a Peltier in order to regulate the temperature at which the grating is held, or by using a long period grating that has been specially designed to have reduced temperature sensitivity [16].

6.6 Chapter Summary

This chapter has described work carried out to obtain a flexible experimental arrangement for the fabrication of long period fibre gratings. Such a set-up is important in order to mass-produce a multitude of devices of different periodicity at minimum cost.

The fabrication technique chosen was that using the pulsed exposure of the fibre to a UV-beam. This method required no additional masks, which made it a cheap yet flexible approach to long period grating fabrication.

A long period grating fabricated using this technique was employed as a wavelength - to-amplitude converter in a strain sensing system. Such gratings are useful in sensing systems because they are simple to fabricate and usually require less bandwidth than other structures which have been tested, such as chirped gratings.

1 A.M. Vengsarkar, P.J. Lemaire, J.B. Judkins, V. Bhatia, T. Erdogan, J.E. Sipe, 'Long-period fibre gratings as band rejection filters', *J. Lightwave Technol.,* **14**, (1), 1996, pp.58-65

2 B. Malo, K.O. Hill, F. Bilodeau, D.C. Johnson, J. Albert, 'Point by point fabrication of micro Bragg gratings in photosensitive fibre using single excimer pulse refractive index modification techniques', *Electron. Lett.*, **29**, (18), 1993, pp.1668-1669

3 K.O. Hill, B. Malo, K.A. Vineberg, F. Bilodeau, D.C. Johnson, I. Skinner, 'Efficient mode conversion in telecommunication fibre using externally written gratings', *Electron. Lett.,* **26**, (16), 1990, pp.1270-1271

4 F. Bilodeau, K.O. Hill, B. Malo, D.C. Johnson, I. Skinner, 'Efficient narrowband $LP_{01} \leftrightarrow LP_{02}$ mode convertors fabricated in photosensitive fiber: Spectral response', *Electron. Lett.,* **27**, 1991, pp.682-684

5 S. Grubb, 'High power diode-pumped fibre lasers and amplifiers', *Conf. Optic. Fibre Commun. (OFC '95), Tech. Digest,* **8**, (TuJ1), 1995, pp.41-42

6 C.R. Giles, T. Erdogan, V. Mizrahi, 'Reflection-induced changes in the optical spectra of 980nm CW lasers', *J. Appl. Phys.*, **75**, 1994, pp.73-80

7 A.M. Vengsarkar, J.R. Pedrazzani, J.B. Judkins, P.J. Lemaire, N.S. Bergano, C.R. Davidson, 'Long period fibre grating based gain equalizers', *Opt. Lett.,* **21**, (5), 1996, pp.336-338

8 B.J. Ainslie, S.P. Craig-Ryan, S.T. Davey, J.R. Armitage, C.G. Atkins, J.F. Marricott, R. Wyatt, 'Erbium fibres for efficient optical amplifiers', *IEE Proc. J. Optoelectronics,* **137**, (4), 1990, pp.205-208

9 R. Kashyap, R. Wyatt, R.J. Campbell, 'Wideband gain flattened erbium fibre amplifier using a photosensitive fibre blazed grating', *Electron. Lett.,* **29**, (2), 1993, pp.154-156

10 P.F. Wysocki, J. Judkins, R. Espindola, M. Andrejco, A. Vengsarkar, K. Walker, 'Erbium-doped fibre amplifier flattened beyond 40nm using long-period grating', *Conf. Optic. Fibre Commun., (OFC '97), Tech. Digest*, postdeadline paper PD2, 1997

11 M.G. Xu, R. Maaskant, M.M. Ohn, A.T. Alavie, 'Independent tuning of cascaded long period fibre gratings for spectral shaping', *Electron. Lett.*, **33**, (22), 1997, pp.1893-1894

12 V. Bhatia, A.M. Vensarkar, 'Optical fibre long-period grating sensors', *Opt. Lett.,* **21**, (9), 1996, pp.692-694

13 H.J. Patrick, G.M. Williams, A.D. Kersey, J.R. Pedrazzani, A.M. Vengsarkar, 'Hybrid fiber Bragg grating/ long period fiber grating sensor for strain/temperature discrimination', *IEEE Photon. Tech. Lett.*, **8**, (9), 1996, pp.1223-1225

14 V. Bhatia, D. Campbell, R.O. Claus, A.M. Vengsarkar, 'Simultaneous strain and temperature measurement with long-period grating', *Opt. Lett.*, **22**, (9), 1997, pp.648-650

15 J.B. Judkins, J.R. Pedranzzani, D.J. DiGiovanni, A.M. Vengsarkar, 'Temperature-insensitive long-period fibre gratings', *Conf. Optic. Fibre Commun. (OFC '96), Tech. Digest*, postdeadline paper PD1, 1996

16 V. Bhatia, D.K.Campbell, T. D'Alberto, G.A. Ten Eycy, D. Sherr, K.A. Murphy, R.O. Claus, 'Standard optical fibre long-period gratings reduced temperature sensitivity for strain and refractive-index sensing', *Conf. Optic. Fibre Commun. (OFC '97), Tech. Digest*, FB1, 1997, pp.346-347

17 H.J. Patrick, C.G. Askins, R.W. McElhanon, E.J. Friebele, 'Amplitude mask patterned on an excimer laser mirror for high intensity writing of long period fibre gratings', *Electron. Lett.*, **33**, (13), 1997, pp. 1167-1168

18 M. Akiyama, K. Nishide, K. Shima, A. Wada, R. Yamauchi, 'A novel long-period fibre grating using periodically released residual stress of pure silica core fibre', *Conf. Optic. Fibre Commun. (OFC '98), Tech. Digest*, ThG1, 1998, pp.276-277

19 S.G. Kosinski, A.M. Vengsarkar, 'Splicer-based long-period fibre gratings', *Conf. Optic. Fibre Commun. (OFC '98), Tech. Digest*, ThG3, 1998, pp.278-279

20 E.M. Dianov, V.I. Karpov, K.M. Grekov, K.M. Golant, S.A. Vasiliev, O.I. Medvedkov, R.R. Khapko, 'Thermo-induced long-period fibre gratings', *European Conf. On Optic. Commun. (ECOC '97), Tech. Digest*, (448), 1997, pp.53-56

21 D.D. Davis, T.K. Gaylord, E.N. Glytsis, S.G. Kosinski, S.C. Mettler, A.M. Vengsarkar, 'Long-period fibre grating fabrication with focused CO_2 laser pulses', *Electron. Lett.*, **34**, (3), 1998, pp.302-303

22 M. Monerie, 'Propagation in doubly clad single-mode fibres', *IEEE J. Quantum Electron.*, **QE-18**, (4), 1982, pp.535-542

23 H.J. Patrick, A.D. Kersey, F. Bucholtz, K.J. Ewing, J.B. Judkins, A.M. Vengsarkar, 'Chemical sensor based on long period fibre grating response to index of refraction', *Conf. on Lasers and Electro-Optics (CLEO '97), Tech. Digest*, CThQ5, 1997.

24 A.J. Rogers, V.A. Handerek, S.E. Kanellopoulos, J. Zhang, 'New ideas in nonlinear distributed optical-fibre sensing', *Proc. Soc. Photo-Opt. Instrum. Eng. (SPIE)*, **2507**, 1995, pp.162-174

25 R.W. Fallon, L. Zhang, A. Gloag, I. Bennion, 'Multiplexed identical broadband chirped grating interrogation system for large strain sensing applications', *IEEE Photon. Technol. Lett.*, **9**, 1997, pp.1626-2628

26 R.W. Fallon, L.A. Everall, L. Zhang, I. Bennion, 'Multiple strain sensor interrogation with an asymmetric grating', *Conf. on Lasers and Electro-Optics (CLEO '98), Tech. Digest*, CThO53, 1998

27 R.W. Fallon, L. Zhang, L.A. Everall, J.A.R. Williams, I. Bennion, 'All-fibre optical sensing system: Bragg grating sensor interrogated by a long-period grating', *Meas. Sci. Technol,* **9**, (12), 1998, pp.1969-1973

7. CONCLUSIONS

This thesis has been concerned with the fabrication and characterisation of in-fibre gratings, for a wide range of applications. A number of different grating fabrication techniques were considered, the majority of which were based on the phase mask scanning technique. Where possible, the various techniques were compared and the advantages and disadvantages discussed. Final optimised devices were fabricated using the most appropriate method and these devices were then incorporated in a 'real' application in order to assess their potential. This highlighted the strengths and weaknesses of each device, and the feedback enabled further improvements to be made to future devices.

The work on the general characterisation of gratings produced a number of important results. The study on the maximum achievable refractive index change, induced when a photosensitive fibre is UV-exposed, confirmed that hydrogen-loaded fibre induces a larger index change than unhydrogenated fibre. For a sample of boron-germanium co-doped fibre, the hydrogenated index change was evaluated to be 1.5×10^{-2}, in comparison with the unhydrogenated index change which was only 2.2×10^{-4}. Further experiments were carried out, examining the effect of increasing the temperature at which the gratings were written. Following on from work presented by other research groups, it was hypothesised that an increase in the temperature of a grating during fabrication would lead to an increase in the maximum induced refractive index change. The results for this investigation proved inconclusive, since although there was a slight increase in the induced refractive index for the heated fibre, it was not as large as was expected. One proposed reason for this was that the fibre did not absorb the wavelength of the radiation that the heater supplied. This would mean that, despite the heater producing a temperature of up to 400°C, the fibre only reached a temperature equal to that of the air which surrounded it and therefore did not get hot enough to observe any significant increase in refractive index change. It is unclear as to whether this technique for increasing the achievable refractive index is feasible, since fibre alignment during fabrication becomes more of an issue with increasing environmental temperature. If fibre with a greater photosensitivity is required, then future work should include a study on other methods of increasing the fibre photosensitivity, or possibly examining some of the new types of fibre which are currently being fabricated.

For many grating applications, including WDM and sensing systems, it is important to spectrally shape the filter in order to achieve a more desirable filter spectrum. This includes suppressing the grating sidelobes and obtaining a sharper drop-off at the edges of the main reflection peak. Using a novel apodisation technique, which

involved dithering the phase mask to produce the desired apodisation profile, a detailed study was carried out on the optimisation of Bragg gratings for use in applications where there are restrictions placed on the maximum length of the filter. In these length-restricted cases it was concluded that there is no single apodisation function which produces optimised filters for every case. Instead, there are a number of fabrication trade-offs which must be considered. The optimum apodisation function depends on the order of priority placed on a number of grating parameters, including the required filter bandwidth and sidelobe suppression. Therefore, each case must be evaluated separately, by examining the individual filter requirements and deciding on the importance of each of the specified parameters.

A comparison of the experimental and theoretical apodised grating results showed a difference between the anticipated and produced noise floor of the most apodised devices and also some discrepancy between the bandwidths of the gratings. The bandwidth difference was greatest for the gaussian apodisation profile, where, for a particular level of sidelobe suppression, the actual bandwidth of each grating was consistently larger than that of the modelled one. The cause of this difference is still unknown. One suggestion is that it could be due to the combined effect of a gaussian shaped beam with the apodisation profile, producing slightly different results than expected. Since apodisation is proving a crucial factor in many applications, further investigation should be carried out to determine, and eliminate, the cause of this bandwidth discrepancy.

Chirped Bragg gratings are a source of much research interest at present, due to their potential as dispersion compensating elements in high-bit-rate communications systems. In the work on dispersion compensation, a number of fabrication techniques were presented. It was found that the use of a chirped phase mask produced the best and most consistent results, due to the inherent reproducibility of the technique. Such a device was incorporated as a dispersion compensating element in a re-circulating loop in order to assess its quality. This experiment highlighted one problem which needs to be addressed if Bragg gratings are to be seriously considered as the choice method for dispersion compensation; the problem of polarisation mode dispersion. It was concluded that polarisation mode dispersion can be minimised if care is taken during the fabrication process to ensure that the state of polarisation of the UV writing beam is parallel to the axis of the fibre. Current research is in the fabrication of ultra-long Bragg gratings for dispersion compensation. Typically, such gratings will provide dispersion equivalent to hundreds of kilometres of standard telecommunications fibre and be broad enough to allow for slight variations in the transmitter wavelength. Once such systems are established, fundamental grating problems, such as PMD and dispersion ripple, need to be pursued further. Despite the extensive research effort which has been devoted to such devices, the problem of

ripple on the dispersion characteristic has yet to be completely solved. It remains to be seen as to whether chirped Bragg gratings will actually attain high enough specifications to be accepted as the choice method of compensation in dispersion managed systems.

Many in-fibre gratings applications require bandpass structures, to provide broad stopbands, narrow passbands and high rejection levels, for uses such as wavelength selectivity and noise filtering. A number of different types of resonator were fabricated, each grating type having particular advantages and disadvantages. The first results on chirped Moiré resonators, fabricated using phase masks, were presented. Although it was shown that the use of a phase mask greatly simplifies the fabrication process, this work highlighted other issues which arose as a result. In order to reach the high rejection levels required in WDM networks, for the minimisation of channel-crosstalk, the phase mask pattern must be free from dirt and have minimised stitch errors. If either of these requirements are not met then the overall noise floor of the grating reflection spectrum increases dramatically. Systems measurements carried out on a 5-channel grating array also concluded that a smaller system penalty resulted from gratings which had higher rejection ratios. It was speculated that rejection ratios in the order of ~30dB are required to minimise penalties in WDM systems. The potential which gratings have shown should ensure that research continues into ways of reaching these increased device specifications. This work ties in with that detailed in Chapter 3, on the apodisation of short gratings. The results of this study show that it is theoretically possible to achieve a rejection ratio of greater than 30dB. Therefore, it is important to continue the work on the apodisation of filters in order to push the noise floor of the reflection spectrum of a grating down to a level which exceeds 30dB. This work will also prove important for future ultra-long devices, which will also required some apodisation. Future work in the area of wavelength division multiplexing should also include an investigation into ways of increasing the number of channels which can be incorporated into a certain length of fibre can be increased.

If grating fabrication is to progress from a research laboratory into industry then it is important to ensure that the resulting system is simple yet stable to operate, whilst the overall cost is kept to a minimum. The fabrication system developed to write long period gratings fulfilled all those criteria. The pulsed exposure technique required no expensive masks and yet could generate a long period grating of potentially any required period. The gratings fabricated using this system were highly reproducible and could be designed to any given specification. One such device proved itself to be an excellent amplitude-to-wavelength converter in a novel strain and temperature interrogation system. Long period gratings have great potential, due to their minimal reflection and broad transmission peaks. Also the increased sensitivity to the

environmental conditions opens up a number of potential applications. It should be possible to flatten the gain of an erbium-doped fibre amplifier with a single grating, if enough is known about the fibre into which the grating is being written.

As the in-fibre grating research field becomes better established, it is envisaged that future work will shift from the fundamental issues of gratings to topics concerning the integration of the technology into the commercial environment. A significant amount of work is necessary to improve the systems for grating fabrication so that they can be operated by less specialised engineers. From a commercial point of view, the ideal situation is that the whole fabrication process is completely automated, thus removing the element of human error which can led to inconsistent grating fabrication. Such automation is necessary for the mass-production of identical gratings.

Other issues will arise as gratings are transferred from the research laboratory into real systems. The increasing number of applications will all have slightly different device requirements and so the packaging of each device will become an issue. Work is still to be done on the best method of temperature and strain compensation of devices to ensure high wavelength stability is maintained. This becomes more important with the development of longer and more complex devices.

Industry is showing the same level of confidence in the success of Bragg gratings as the research community is, with at least 18 companies commercially producing gratings, world-wide. With the increased flexibility in grating fabrication it is inevitable that gratings with more complex spectral responses will emerge; ultra-long gratings having the potential to allow arbitrary fringe profiles to be generated. This flexibility should extend the application of gratings to many new and exciting areas. The use of in-fibre gratings as sensing elements seems particularly promising, with the recent incorporation of grating arrays into structures such as aircraft, boats and bridges for quasi-distributed strain monitoring. The advancement of related technology, for both the phase mask and grating fabrication, should enable in-fibre devices to achieve higher specifications than other competing technologies, ensuring that they are the choice component in any system.

With this in mind, it seems that the future for Bragg gratings is very promising indeed.

8. APPENDICES

8.1 Appendix : Coupled Mode Theory for Codirectional Coupling

In the case of codirectional coupling, the fundamental guided forward propagating mode is coupled to the forward propagating cladding modes. Taking $A_{01}^{(+)}(z)$ to be the amplitude of the L_{01} guided mode and $A_m^{(cl)}(z)$ to be the amplitude of the m^{th} cladding mode, then the forward propagating guided mode can be described by

$$\frac{dA_{01}^{(+)}}{dz} = i\kappa_m \exp\left(-i\Delta\beta z\right) A_m^{(cl)}$$

Equation 8.1.1

and the forward propagating cladding modes can be described by

$$\frac{dA_m^{(cl)}}{dz} = i\kappa_m \exp\left(i\Delta\beta z\right) A_{01}^{(+)}$$

Equation 8.1.2

where κ_m is the coupling coefficient, given by $\kappa_m = \frac{\pi\Delta n}{\lambda} C_m$, for a refractive index change of Δn and an overlap coefficient of C_m. The phase matching condition, $\Delta\beta$ is defined as $\Delta\beta = \beta_{01} - \beta_m^{cl} = \frac{2\pi}{\Lambda}$, where β_{01} is the propagation constant of the guided mode and β_m^{cl} is the propagation constant of the m^{th} cladding mode.

Taking the boundary condition that at z=0 all the light is in the guided mode and none has been coupled to the cladding modes, then $A_{01}^{(+)}\big|_{z=0} = 1$ and $A_m^{(cl)}\big|_{z=0} = 0$.

Substituting these into Equation 8.1.1 and Equation 8.1.2 respectively gives

$$\left.\frac{dA_{01}^{+}}{dz}\right|_{z=0} = 0$$

Equation 8.1.3

and

$$\left.\frac{dA_m^{(cl)}}{dz}\right|_{z=0} = i\kappa_m$$

Equation 8.1.4

Solution for $A_m^{(cl)}$

Rearranging Equation 8.1.2 gives

$$A_{01}^{(+)} = \frac{1}{i\kappa_m \exp\left[iz\left(\Delta\beta/2\right)\right]}\frac{dA_m^{(cl)}}{dz}$$

Equation 8.1.5

Differentiating Equation 8.1.5 with respect to z gives

$$\frac{dA_{01}^{(+)}}{dz} = \frac{1}{i\kappa_m}\left\{\frac{i\left(\Delta\beta/2\right)}{\exp\left[iz\left(\Delta\beta/2\right)\right]}\frac{dA_m^{(cl)}}{dz} + \frac{1}{\exp\left[iz\left(\Delta\beta/2\right)\right]}\frac{d^2A_m^{(cl)}}{dz^2}\right\}$$

Equation 8.1.6

Equating Equation 8.1.1 and Equation 8.1.6

$$i\kappa_m \exp\left[-iz\left(\Delta\beta/2\right)\right]A_m^{(cl)} = \frac{1}{i\kappa_m}\left\{\frac{i\left(\Delta\beta/2\right)}{\exp\left[iz\left(\Delta\beta/2\right)\right]}\frac{dA_m^{(cl)}}{dz} + \frac{1}{\exp\left[iz\left(\Delta\beta/2\right)\right]}\frac{d^2A_m^{(cl)}}{dz^2}\right\}$$

Equation 8.1.7

Multiplying Equation 8.1.7 by $\exp\left[iz\left(\Delta\beta/2\right)\right]$:

$$\frac{d^2A_m^{(cl)}}{dz^2} + i\frac{\Delta\beta}{2}\frac{dA_m^{(cl)}}{dz} + \kappa_m^2 A_m^{(cl)} = 0$$

Equation 8.1.8

Using the general solution for a second order differential equation, of $A_m^{(cl)} = C_1\exp(-bz)\sin(\delta z + \gamma_1)$ where $b = i\frac{\Delta\beta}{2}$ and

$\delta = \sqrt{\kappa_m^2 - (i\,\Delta\beta/2)^2} = \sqrt{\kappa_m^2 + \left(\Delta\beta/2\right)^2} = S_m$ then

$$A_m^{(cl)} = C_1\exp\left(-iz(\Delta\beta/2)\right)\sin(S_m z + \gamma_1)$$

Equation 8.1.9

where C and γ are unknown coefficients.

Differentiating Equation 8.1.9 with respect to z gives

$$\frac{dA_m^{(cl)}}{dz} = C_1\left\{\exp\left[-iz(\Delta\beta/2)\right]S_m\cos(S_m z+\gamma_1) - i\left(\Delta\beta/2\right)\exp\left[-iz(\Delta\beta/2)\right]\sin(S_m z+\gamma_1)\right\}$$

Equation 8.1.10

Using the initial boundary condition that $A_m^{(cl)}\big|_{z=0} = 0$, then the general solution, Equation 8.1.9, becomes

$$C_1\sin(\gamma_1) = 0$$

Equation 8.1.11

and using the condition given by Equation 8.1.4, that $\left.\frac{dA_m^{(cl)}}{dz}\right|_{z=0} = i\kappa_m$ then Equation 8.1.10 becomes

$$C_1\left[\Delta\beta\cos(\gamma_1) - \frac{i\Delta\beta}{2}\sin(\gamma_1)\right] = i\kappa_m$$

Equation 8.1.12

From the initial boundary condition then either $\gamma_1 \equiv 0$ or $C_1 \equiv 0$ but from Equation 8.1.12 it can be seen that $C_1 \neq 0$ which means that $\gamma_1 \equiv 0$. Equation 8.1.12 therefore becomes $C_1 = \frac{i\kappa_m}{S_m}$.

Substituting this into Equation 8.1.9 gives the solution

$$A_m^{(cl)} = \frac{i\kappa_m}{S_m}\exp\left[-iz(\Delta\beta/2)\right]\sin(S_m z)$$

Equation 8.1.13

The transmissivity can thus be defined as $\left|t_m(\lambda)\right|^2 = 1 - \left|A_m^{(cl)}(L)\right|^2$. Using the fact that $\left|A_m^{(cl)}(L)\right|^2 = \left[A_m^{(cl)}(L)\right]\left[A_m^{(cl)}(L)\right]^*$, then from Equation 8.1.13

$$\left|A_m^{(cl)}(L)\right|^2 = \left[i\frac{\kappa_m}{S_m}\exp\left[-iL(\Delta\beta/2)\right]\sin(S_m L)\right]\left[-i\frac{\kappa_m}{S_m}\exp\left[iL(\Delta\beta/2)\right]\sin(S_m L)\right]$$

$$\left|A_m^{(cl)}(L)\right|^2 = \frac{\kappa_m^2}{S_m^2}\sin^2(S_m L)$$

Substituting in S_m and dividing by κ_m^2 gives the final solution

$$\left|t_m(\lambda)\right|^2 = 1 - \frac{\sin^2\left[\kappa_m L\sqrt{1+\frac{(\Delta\beta\ 2)^2}{\kappa_m^2}}\right]}{1+\left(\frac{(\Delta\beta\ 2)}{\kappa_m}\right)^2}$$

Equation 8.1.14

8.2 Appendix: Kirchhoff's Scalar Diffraction Theory

Kirchhoff's scalar diffraction theory deals with the scalar optical disturbances and their derivatives over an arbitrary closed surface surrounding point, P, rather than evaluating the optical disturbance as the superposition of individual waves, as Huygen's did.

It is assumed that Fourier analysis will separate the constituent frequencies, such that only one frequency need be considered at a time. The monochromic optical disturbance, E is the solution of the differential wave equation

$$\nabla^2 E = \frac{1}{c^2}\frac{\partial^2 E}{\partial t^2}.$$

Equation 8.2.1

Thus the wave can be written as

$$E = \xi \exp[-kct]$$

Equation 8.2.2

where ε represents the complex-space part of the disturbance. Substituting this into the wave equation, Equation 8.2.1, gives

$$\nabla^2 \xi + k^2 \xi = 0$$

Equation 8.2.3

which is know as *Helmholtz equation* and can be solved using Green's theorem, which states that for two scalar functions, U_1 and U_2 then

$$\iiint_V \left(U_1 \nabla^2 U_2 - U_2 \nabla^2 U_1\right) dV = \oiint_S \left(U_1 \nabla U_2 - U_2 \nabla U_1\right) \cdot dS$$

Equation 8.2.4

If U_1 and U_2 are solutions of Helmholtz equation, i.e. if $\nabla^2 U_1 + k^2 U_1 = 0$ and $\nabla^2 U_2 + k^2 U_2 = 0$ then

$$\oiint_S \left(U_1 \nabla U_2 - U_2 \nabla U_1\right) \cdot dS = 0$$

Equation 8.2.5

Let $U_1 = \xi$ (from Equation 5-3) and $U_2 = \dfrac{\exp(ikr)}{r}$, where r is some distance from point P. Point P is a singularity at the position where r=0 and is enclosed in a small sphere, S' which excludes P from the region enclose by S, such that Equation 8.2.5 becomes

$$\oiint_S \left[\xi \nabla\left(\frac{\exp(ikr)}{r}\right) - \frac{\exp(ikr)}{r}\nabla\xi \right]\cdot dS + \oiint_{S'} \left[\xi \nabla\left(\frac{\exp(ikr)}{r}\right) - \frac{\exp(ikr)}{r}\nabla\xi \right]\cdot dS = 0$$

Equation 8.2.6

Expanding out the part of the integral concerned with the small sphere S' gives

$$\nabla\left(\frac{\exp(ikr)}{r}\right) = \left(\frac{1}{r^2} - \frac{ik}{r}\right)\exp(ikr)\,\hat{n}$$

where $\hat{n}$ is the unit normal, directed towards point P. In terms of the solid angle ($dS = r^2 d\Omega$) then the integral over S' becomes

$$\oiint_{S'} \left(\xi - ik\xi r + \frac{\partial\xi}{\partial r}\right)\exp(ikr)\,d\Omega$$

Equation 8.2.7

where $\nabla\xi\cdot dS = -\left(\partial\xi/\partial r\right)r^2\,d\Omega$. As S' shrinks, $r\to 0$ and $exp(ikr) \to 1$. The value of ξ approaches its value at P, ξ_p so that the last two terms of Equation 8.2.7 become zero and the integral evaluates to $4\pi\xi_p$. Equation 8.2.6 them becomes

$$\xi_P = \frac{1}{4\pi}\left[\oiint_S \frac{\exp(ikr)}{r}\nabla\xi\cdot dS - \oiint_S \xi\nabla\left(\frac{\exp(ikr)}{r}\right)\cdot dS \right]$$

Equation 8.2.8

which is know as the Kirchhoff integral theorem.

Applying this theorem to the particular case where an unobstructed spherical wave originates at a point source s then the disturbance can be thought of as taking the form $E(\rho,t) = \dfrac{\varepsilon_o}{\rho}\exp\left[i\left(k\rho - \omega t\right)\right]$, thus the complex-space part is $\xi(\rho) = \dfrac{\varepsilon_0}{\rho}\exp(ik\rho)$.

Substituting this into Equation 8.2.8 gives

$$\xi_P = \frac{1}{4\pi}\left[\oiint_S \frac{\exp(ikr)}{r}\frac{\partial}{\partial\rho}\left(\frac{\varepsilon_0}{\rho}\exp(ik\rho)\right)\cos(\hat{n},\hat{\rho})\,dS - \oiint_S \frac{\varepsilon_0}{\rho}\exp(ik\rho)\frac{\partial}{\partial r}\left(\frac{\exp(ikr)}{r}\right)\cos(\hat{n},\hat{r})\,dS \right]$$

Equation 8.2.9

where $dS = \hat{n}\,dS$, $\hat{n}, \hat{r}$ and $\hat{\rho}$ are unit vectors, $\nabla\left(\frac{\exp(ikr)}{r}\right) = \hat{r}\frac{\partial}{\partial r}\left(\frac{\exp(ikr)}{r}\right)$ and $\nabla\xi(\rho) = \hat{\rho}\,\xi\varepsilon/\partial\rho$.

The differentials can be evaluated as $\frac{\partial}{\partial\rho}\left(\frac{\exp(ik\rho)}{\rho}\right) = \exp(ik\rho)\left(\frac{ik}{\rho} - \frac{1}{\rho^2}\right)$ and $\frac{\partial}{\partial r}\left(\frac{\exp(ikr)}{r}\right) = \exp(ikr)\left(\frac{ik}{r} - \frac{1}{r^2}\right)$.

As $\rho \rangle\rangle \lambda$ and $r \rangle\rangle \lambda$ then the $1/\rho^2$ and $1/r^2$ terms can be neglected.

Thus Equation 8.2.9 becomes

$$\xi_P = -\frac{\varepsilon_0 i}{\lambda}\oiint_S \frac{\exp\left[ik(\rho + r)\right]}{\rho r}\left[\frac{\cos(\hat{n},\hat{r}) - \cos(\hat{n},\hat{\rho})}{2}\right]dS$$

Equation 8.2.10

This is known as the *Fresnel-Kirchhoff diffraction formula.*

9. PUBLICATIONS

1. L.A. Everall, J.A.R. Williams, I. Bennion, 'The fabrication of Bragg gratings for third-order dispersion', *IOP 'In-fibre Bragg Gratings and Special Fibres' meeting*, London, 1996

2. J.A.R. Williams, L.A. Everall, I. Bennion, N.J. Doran, 'Fibre Bragg Grating fabrication for dispersion slope compensation', *IEEE Photon. Technol. Lett.*, **8**, (9), 1996, pp1187-1189

3. K. Sugden, L.A Everall, J.A.R Williams, I. Bennion , 'Single and multi-passband Moiré filters fabricated by dual exposure of a uniform-period phase mask followed by a post-exposure refractive index profiling scan', *Optoelectronics '97 symposium on Photosensitive Optical Materials and Devices, San Jose, California*, SPIE Proc., **2998**, 1997, pp29-34

4. K. Sugden, L. Zhang, L.A. Everall, I. Bennion , 'Fabrication of high rejection, low loss, filters by the concatenation of broadly chirped fibre Bragg gratings', *Optoelectronics '97 symposium on Photosensitive Optical Materials and Devices, San Jose, California*, SPIE Proc., **2998**, 1997, pp22-28

5. X. Liu, J.S. Aitchison, J.A.R. Williams, L.A. Everall, I. Bennion, 'Realisation of specific responses in photosensitive fibre gratings produced by UV exposure through holographic phase masks', *Conf. Lasers and Electro Optics (CLEO '97), Baltimore, Tech. Digest*, CThL57, 1997

6. K. Sugden, L. Zhang, J.A.R. Williams R. Fallon, LA. Everall, K. Chisholm I. Bennion, 'Fabrication and characterisation of bandpass filters based on concatenated chirped fibre gratings', *J. Lightwave Technol.*, **8**, (15), 1997, pp1424-1432

7. L.A. Everall, J.A.R. Williams, I. Bennion, X. Liu, R.M. De La Rue, 'The effects of phase steps in e-beam written phase masks used for fibre grating fabrication by near-field holography', *European Conf. Optic. Commun. (ECOC '97), Edinburgh, UK, IEE Conference Proceedings No.448*, **1**, (MO4C), 1997, pp187-190

8. L.A. Everall, K. Sudgen, J.A.R. Williams, X. Liu, J.S. Aitchison, I. Bennion, R.M. De La Rue, 'Multiple passband In-fibre Moiré resonators fabricated using near field holography with a chirped phase mask' *European Conf. Optic. Commun. (ECOC '97), Edinburgh, UK, IEE Conference Proceedings No.448*, 2, (TU1C), 1997, pp 41-44

9. L.A. Everall, K. Sugden, J.A.R. Williams, I. Bennion, X. Liu, J.S. Aitchison, S. Thoms, R.M. De La Rue, 'Fabrication of multi-passband Moiré resonators in fibres by dual phase mask exposure method', *Opt. Lett.*, **22**, (19), 1997, pp1473-1475

10. L.A. Everall, K. Sugden, J.A.R. Williams, I. Bennion, X. Liu, J.S. Aitchison, R.M. De La Rue, 'Fabrication of in-fibre Moiré filters using a 5cm non-dedicated chirped phase mask', *Conf. On Bragg gratings, photosensitivity and poling (BGPP '97), OSA Conference Proceedings,* **17**, (BMG15), 1997, pp 228-230

11. X. Liu, J.S. Aitchison, R.M. De La Rue, P.Silva Marques, S. Thoms, L.A. Everall, J.A.R. Williams, I. Bennion, 'The influence of phase mask stitch errors on the performance of UV-written Bragg gratings', *Conf. On Bragg gratings, photosensitivity and poling (BGPP '97), OSA Conference Proceedings*, **17**, (BMG9), 1997, pp 210-212

12. X. Liu, S. Thoms, J.S. Aitchison, R.M. De La Rue, L.A. Everall, J.A.R. Williams, I. Bennion, 'Surface roughness reduction and diffraction efficiency optimisation for e-beam written phase masks', *Microelectronic Eng.*, **41/42**, 1998, pp.199-202

13. L.A. Everall, R.W. Fallon, J.A.R. Williams, L. Zhang, I. Bennion, 'Flexible Fabrication of Long Period In-Fibre Gratings', *Conf. Lasers and Electro Optics (CLEO '98), San Francisco, Tech. Digest*, (CFE2), 1998

14. R.W. Fallon, L.A. Everall, L. Zhang, I. Bennion, 'Multiple Strain Sensor Interrogation with an Asymmetric Grating', *Conf. Lasers and Electro Optics (CLEO '98), San Francisco, Tech. Digest*, (CTh053), 1998

15. X. Liu, J.S. Aitchison, R.M. De La Rue, J.A.R. Williams, L.A. Everall I. Bennion, 'Realisation of geometrically apodised phase masks for the production of apodised fibre gratings by UV exposure', *Conf. Lasers and Electro Optics (CLEO '98), San Francisco, Tech. Digest*, (CFE3), 1998

16. K.E. Chisholm, L.A. Everall, J.A.R. Williams, I. Bennion, 'Comparison of the performance of uniform period fibre Bragg gratings with different apodisation functions', *IOP 'In-Fibre Bragg Gratings and special fibres' meeting, London, Conf. Proceedings*, 1998

17. X. Liu, J.S. Aitchison, S. Thoms, R.M. De La Rue, L.A. Everall, J.A.R. Williams, I. Bennion, 'Characteristics of linearly chirped and functionally apodised phase masks and reflection spectra of UV written fibre gratings', *European Conf. Lasers and Electro Optics (ECLEO '98), Glasgow, Scotland,* (CWB3), 1998

18. K.E. Chisholm, L.A. Everall, J.A.R. Willams, I. Bennion, X. Liu, R.M. De La Rue, J.S. Aitchison, 'Apodised fibre Bragg grating design subject to length constraints', *24th European Conf. Optic. Commun. (ECOC '98), Madrid, Spain, Tech. Digest*, **1**, (WdA02) 1998, pp.385-386

19. W. Zhang, J.A.R. Williams, L.A. Everall, I. Bennion, 'Tuneable radio frequency filtering using linearly chirped fibre grating', *24th European Conf. Optic. Commun. (ECOC '98), Madrid, Spain, Tech. Digest*, **1**, 1998, pp.611-612

20. L. Zhang, R.W. Fallon, L.A. Everall, J.A.R. Williams, I. Bennion, 'Large-dynamic-range and high-resolution from a strain sensing system using long -period grating interrogating FBG strain sensor', *24th European Conf. Optic. Commun. (ECOC '98), Madrid, Spain, Tech. Digest*, **1**, (WdD22), 1998, pp.609-610

21. A. Iocco, H.G. Limberger, R.P. Salathé, L.A. Everall, I. Bennion, 'Compression and traction tuned tunable wavelength filters', *Summer School on Photosensitivity in Optical Waveguides and Glasses, Lausanne, Switzerland*, (P6), 1998

22. K.E. Chisholm, L.A. Everall, J.A.R. Williams, I. Bennion, 'Comparison of theoretical and experimental performance of uniform period fibre Bragg grating apodisation functions', *Summer School on Photosensitivity in Optical Waveguides and Glasses, Lausanne, Switzerland*, (P2), 1998

23. R.W. Fallon, L. Zhang, L.A. Everall, J.A.R. Williams, I. Bennion, 'All-fibre optical sensing system: Bragg grating sensor interrogated by a long-period grating', *Meas. Sci. Technol*, **9**, (12), 1998, pp.1969-1973

24. W. Zhang, J.A.R. Williams, L.A. Everall, I. Bennion, 'Fibre optic radio frequency notch filter with linear and continuous tuning by using a chirped fibre grating', *Electron. Lett.*, **34**, (18), 1998, pp.1770-1771

25. K.E. Chisholm, L.A. Everall, J.A.R. Williams, L. Zhang, I. Bennion, 'Apodised Fibre Bragg Grating Arrays for Quasi-distributed Strain Sensing', *IEEE Lasers and Electro-Optics Soc. (LEOS '98), 11th Annual meeting*, (WEE2), 1998

26. A. Iocco, H.G. Limberger, R.P. Salathé L.A. Everall, K.E. Chisholm, I. Bennion, 'Fast and widely tunable Bragg grating reflection filter', *Conf. on Optic. Fibre Commun. (OFC '99), San Diego, USA*, 1999

27. A. Iocco, H.G. Limberger, R.P. Salathé, L.A. Everall, K.E. Chisholm, I. Bennion, 'Bragg Grating Fast Tunable Filter Prototype', *Submitted to J. Lightwave Technol.*